LIDAR FOR MAINTENANCE OF PAVEMENT REFLECTIVE MARKINGS AND RETROREFLECTIVE SIGNS

VOL I: REFLECTIVE PAVEMENT MARKINGS

Final Report Draft

PROJECT SPR-799

Oregon Department of Transportation

LIDAR FOR MAINTENANCE OF PAVEMENT REFLECTIVE MARKINGS AND RETROREFLECTIVE SIGNS

VOL I: REFLECTIVE PAVEMENT MARKINGS

Final Report

PROJECT SPR799

by

Michael J. Olsen
Christopher Parrish
Erzhuo Che
Jaehoon Jung, and
Joseph Greenwood

for

Oregon Department of Transportation
Research Section
555 13th Street NE, Suite 1
Salem OR 97301

and

Federal Highway Administration
1200 New Jersey Ave, SE
Washington, DC 20590-0003

August 2018

Technical Report Documentation Page

1. Report No. FHWA-OR-RD-19-01	2. Government Accession No.	3. Recipient's Catalog No.
4. Title and Subtitle LIDAR FOR MAINTENANCE OF PAVEMENT REFLECTIVE MARKINGS AND RETROREFLECTIVE SIGNS VOL I. REFLECTIVE PAVEMENT MARKINGS		5. Report Date August 2018 6. Performing Organization Code
7. Author(s) Michael J. Olsen, Christopher E. Parrish, Erzhuo Che, Jaehoon Jung, and Joseph Greenwood		8. Performing Organization Report No.
9. Performing Organization Name and Address Oregon Department of Transportation Research Section 555 13th Street NE, Suite 1 Salem, OR 97301		10. Work Unit No. (TRAIS) 11. Contract or Grant No.
12. Sponsoring Agency Name and Address Oregon Dept. of Transportation Research Section and 555 13th Street NE, Suite 1 Salem, OR 97301 Federal Highway Admin. 1200 New Jersey Ave, SE Washington, DC 20590-0003		13. Type of Report and Period Covered Final Report 14. Sponsoring Agency Code

15. Supplementary Notes

16. Abstract:

Pavement markings and signs are important traffic control devices used to guide and regulate traffic movement through visual information presented to motorists. Signs and markings are made with retroreflective materials to enhance visibility for motorists, particularly at night. Retroreflectivity evaluation of an extensive highway network for maintenance and asset management purposes is a critical, yet challenging task for DOTs. Visual evaluation can often be subjective while field measurement techniques can be time-consuming and dangerous. This project investigated the effectiveness of evaluating pavement marking and sign retroreflectivity with mobile lidar data. Oregon DOT currently captures mobile lidar surveys of the entire highway network within a two-year cycle for other purposes of asset management, utility location, engineering surveys, and more. The study found that mobile lidar point clouds can be used to additionally extract quantitative, accurate estimates of retroreflectivity for pavement markings, providing a safe, cost-effective, and reliable solution. Software was also produced to extract the pavement markings and perform the evaluation. Reliable retroreflectivity measurements of signs, however, was not possible due to sensor intensity saturation effects.

17. Key Words Mobile lidar, retroreflectivity, pavement markings	18. Distribution Statement Copies available from NTIS, and online at www.oregon.gov/ODOT/Programs/Pages/Research-Publications.aspx

19. Security Classification (of this report) Unclassified	20. Security Classification (of this page) Unclassified	21. No. of Pages 200	22. Price

SI* (MODERN METRIC) CONVERSION FACTORS

APPROXIMATE CONVERSIONS TO SI UNITS

Symbol	When You Know	Multiply By	To Find	Symbol
		LENGTH		
in	inches	25.4	millimeters	mm
ft	feet	0.305	meters	m
yd	yards	0.914	meters	m
mi	miles	1.61	kilometers	km
		AREA		
in^2	square inches	645.2	millimeters squared	mm^2
ft^2	square feet	0.093	meters squared	m^2
yd^2	square yards	0.836	meters squared	m^2
ac	acres	0.405	hectares	ha
mi^2	square miles	2.59	kilometers squared	km^2
		VOLUME		
fl oz	fluid ounces	29.57	milliliters	ml
gal	gallons	3.785	liters	L
ft^3	cubic feet	0.028	meters cubed	m^3
yd^3	cubic yards	0.765	meters cubed	m^3
NOTE: Volumes greater than 1000 L shall be shown in m^3.				
		MASS		
oz	ounces	28.35	grams	g
lb	pounds	0.454	kilograms	kg
T	short tons (2000 lb)	0.907	megagrams	Mg
		TEMPERATURE (exact)		
°F	Fahrenheit	(F-32)/1.8	Celsius	°C

APPROXIMATE CONVERSIONS FROM SI UNITS

Symbol	When You Know	Multiply By	To Find	Symbol
		LENGTH		
mm	millimeters	0.039	inches	in
m	meters	3.28	feet	ft
m	meters	1.09	yards	yd
km	kilometers	0.621	miles	mi
		AREA		
mm^2	millimeters squared	0.0016	square inches	in^2
m^2	meters squared	10.764	square feet	ft^2
m^2	meters squared	1.196	square yards	yd^2
ha	hectares	2.47	acres	ac
km^2	kilometers squared	0.386	square miles	mi^2
		VOLUME		
ml	milliliters	0.034	fluid ounces	fl oz
L	liters	0.264	gallons	gal
m^3	meters cubed	35.315	cubic feet	ft^3
m^3	meters cubed	1.308	cubic yards	yd^3
		MASS		
g	grams	0.035	ounces	oz
kg	kilograms	2.205	pounds	lb
Mg	megagrams	1.102	short tons (2000 lb)	T
		TEMPERATURE (exact)		
°C	Celsius	1.8C+32	Fahrenheit	°F

*SI is the symbol for the International System of Measurement

ACKNOWLEDGEMENTS

The authors thank the Oregon DOT Technical Advisory Committee for their assistance and valuable insight throughout this project. In particular, Jon Lazarus coordinated the overall research effort, Joel Fry helped facilitate and implement the logistics associated with the field work, Lloyd Bledstoe acquired the mobile lidar data, and Dan Wright processed the mobile lidar data. Eric Leaming, Dennis Hackney, Nick Fortey, and Jason Motley also contributed feedback and insights throughout the project. We appreciate the assistance of Steve Barner, Meghan Jorgenson, and Shawn McKnight with the sign tests at the Oregon DOT maintenance yard. OSU students Nick Wilson, Nick Forfinski, Kory Kellum, Chase Simpson, Marian Jamieson, Katherine Shaefer, and Richie Slocum assisted with portions of the field work. Leica Geosystems and David Evans and Associates provided equipment and software used in this research. Maptek I-Site provided software that was also used for this research. The authors also appreciate the efforts of Daniel Girardeau-Montaut and others in developing the open-source CloudCompare software used in this research.

DISCLAIMER

TABLE OF CONTENTS

LIST OF TABLES

LIST OF FIGURES

LIST OF ABBREVIATIONS

AASHTO	American Association of State Highway and Transportation Officials
AC	Asphalt Concrete
ASPRS	American Society for Photogrammetry and Remote Sensing
ASTM	American Society for Testing and Materials
ATV	All-Terrain Vehicle
Avg.	Average
CCW	Counterclockwise
CP	Control Point
CPU	Central Processing Unit
CW	Clockwise
DCC	Data Collection Categories
DOT	Department of Transportation
EM	Expectation-Maximization
ETA	Engineering Technology Advancement
FHWA	Federal Highway Administration
GCP	Ground Control Points
GIS	Geographic Information System
GNSS	Global Navigation Satellite System
GPS	Global Positioning System
GUI	Graphical User Interface
HDR	High Dynamic Ranging
ID	Identifier
IDW	Inverse Distance Weighting
IMU	Inertial Measurement Unit
Int.	Intensity
Lidar	Light Detection and Ranging
Max.	Maximum
ME	Mean Error
Min.	Minimum
ML	Mobile Lidar
MLS	Mobile Laser Scanning
MMA	Methyl Methcrylate
MR	Minimum Retroreflectivity
MTLS	Mobile Terrestrial Laser Scanning
MUTCD	Manual on Uniform Traffic Control Devices
NAD83	North American Datum 1983
NCHRP	National Cooperative Highway Research Program
OCRS	Oregon Coordinate Reference System
OSU	Oregon State University
PCC	Portland Cement Concrete
PMM	Pavement Marking Materials
Preformed	Preformed Thermoplastic
RAM	Random Access Memory
RANSAC	Random Sample Consensus

RGB	Red-Green-Blue
R_L	Retroreflected Luminance
RoME	Road Marking Extractor
RMS	Root mean square
RMSE	Root-Mean-Square Error
ROI	Region of Interest
RSD	Relative Standard Deviation
RTK	Real-Time Kinematic
SAE	Society for Automotive Engineering
Std. Dev.	Standard Deviation
SUV	Sport Utility Vehicle
Thermo	Thermoplastic
TRB	Transportation Research Board
USB	Universal Serial Bus
Δ	Section Length
s	Pixel Size
θ	Angle Threshold
v	Vehicle Speed

EXECUTIVE SUMMARY

Pavement markings and signs are important traffic control devices, used to guide and regulate traffic movement through visual information presented to motorists. Retroreflectivity evaluation of the extensive highway network for maintenance and asset management purposes is a critical, yet challenging task. Visual evaluation can often be subjective and inconsistent, while field measurement techniques can be time-consuming and dangerous as a result of having to restrict traffic during measurement.

The Oregon Department of Transportation (Oregon DOT) has been a national leader at the forefront of geospatial technologies, such as mobile lidar. Oregon DOT Geometronics scans Oregon DOT's highway network on a two-year cycle to provide high-quality geometric information along the highways to support a wide range of applications, particularly asset management. This project investigated the effectiveness of evaluating marking and sign retroreflectivity with mobile lidar data to provide a safe, cost-effective, and reliable method compared to the current procedures.

After rigorous analysis of sample datasets collected at the Oregon DOT Testdeck site and validation performed on additional datasets (collected on US 20, Interstate-5, and local roads in Salem – all with variable degrees of wear) this project developed an empirical radiometric calibration model that can convert the lidar point cloud intensity to retroreflectivity measurements. A detailed evaluation was performed to investigate the impact of a range of operational parameters, including vehicle speed, lane of travel during data collection, direction of travel, and acquisition parameters.

The project resulted in a number of important findings, including:

1. Mobile lidar retroreflectivity evaluation works successfully to tell Oregon DOT if the pavement markings passed or failed and is comparable with the existing method of testing, which consist of a handheld device and mobile retroreflectometer units.

2. For lower ranges of retroreflectivity values, the mobile lidar system outperforms these other approaches in terms of reproducibility; in other words, when a pavement marking is worn, the lidar scan data and process to determine pass/fail has less variability.

3. The mobile lidar data enables a higher resolution of measurement to cover a large area much more efficiently and completely than operating existing handheld tools, which only evaluate a limited number of discrete sample points. Although not quantified in this study, use of the mobile lidar data is clearly a positive safety and efficiency benefit to Oregon DOT.

4. Retroreflectivity measurements from mobile lidar are significantly affected by wet surfaces. Fortunately, current Oregon DOT practice by Geometronics is to collect data under dry conditions; and

5. The mobile lidar unit was not successful in evaluating the retroreflectivity of signs.

A number of useful tools were developed in this research project and are currently being integrated into Oregon DOT's business processes, including:

1. A Road Marking Extraction (RoME) Tool software which identifies and extracts the pavement markings from the lidar data, as well as extracts useful attributes and metrics; and

2. Scripts to create detailed GIS layers that can be used on Oregon DOT's ArcGIS mapping software and TransGIS platform. These GIS mapping layers have detailed evaluations of specific sites, as well as generalized retroreflectivity condition layers along 1/100th mile increments.

The outcomes of this project provide significant benefits to Oregon DOT, including: safer data acquisition through reduction of roadside data collection; higher level of service of retroreflective markings for the public; decreased cost resulting from improved time efficiency of data collection by leveraging existing mobile lidar data acquired routinely by Oregon DOT; improved QA/QC for markings by enabling spatially continuous measurements at more frequent time intervals; enhanced asset management by improving user interaction with the data as well as improving the success of automated feature extraction algorithms; quantitative data for warranty disputes; and informative geospatial data layers that support informed decision making by supervisors. These benefits and associated increase in information will help Oregon DOT improve MAP-21 compliance through enabling performance-based procedures for evaluating pavement marking quality.

This research further enables Oregon DOT to obtain additional value from its current mobile lidar system. The mobile lidar has already shown solid performance, ROI, and many other benefits to Oregon DOT. Use of this lidar data, which is already collected every two years for other purposes, to support pavement marking evaluations helps reduce duplicative travel and fieldwork, which can result in significant cost savings and efficiencies, particularly in remote areas.

1.0 INTRODUCTION

Pavement markings and signs are important traffic control devices used to guide and regulate traffic movement through visual information presented to motorists. Signs and markings are made with retroreflective materials to enhance visibility for motorists, particularly at night. Retroreflectivity evaluation of an extensive highway network for maintenance and asset management purposes is a critical, yet challenging task for DOTs. Visual evaluation can often be subjective, while field measurement techniques can be time-consuming and dangerous. This project investigated whether mobile lidar datasets (georeferenced point clouds) could be used to extract quantitative, accurate estimates of retroreflectivity for pavement markings, in order to provide a safe, cost-effective, and reliable method of performing these required evaluations.

Oregon DOT currently tracks several metrics for compliance of pavement markings, including appearance and retroreflectivity. The Maintenance & Operations Branch own a vehicle with a Laserlux 6 system, which travels the state every summer, to capture retroreflectivity values on lane markings. These readings are analyzed and used in creating a plan of action for maintenance (e.g., vendor replacement if covered under warranty, or in house or contracted maintenance). Unfortunately, issues arise due to the timing and frequency of the data acquisition. Often, individual hand-held reflectometer readings are required after winter months to recheck compliance, which may be risky (due to roadside work) and staff time intensive. Sign retroreflectivity evaluations suffer from similar limitations and are more cumbersome for crews.

Oregon DOT has been a national leader at the forefront of geospatial technologies such as mobile lidar. This technology supports a wide range of transportation applications (Olsen et al. 2013) within a single dataset that is acquired more safely and efficiently than conventional methods. Oregon DOT Geometronics is a unit within Oregon DOT and currently owns and operates a Leica Pegasus:Two, which is a survey-grade mobile lidar unit with two profilers to produce high-resolution point clouds. Oregon DOT Geometronics routinely scans Oregon DOT's highway network (on a two year cycle in dry conditions) to provide high quality geometric information along the highways to support a wide range of applications, particularly asset management. Mobile lidar systems provide intensity (return signal strength) data as a point attribute in georeferenced point clouds. These intensity values may be used in estimating retroreflectivity of pavement markings, which can be used for quality control purposes after construction or maintenance at a site or for statewide asset management to help meet performance goals by using the data that are already being collected and used by Oregon DOT for other purposes.

Recent research has investigated the potential use of mobile lidar for retroreflectivity evaluation (Olsen et al. 2013; Ai and Tsai 2016), primarily focused on signs. While the results of this work are promising, detailed studies were needed to assess the operational feasibility of these methods for state DOTs and to develop production-ready procedures. Research was performed to: a) develop and test operational procedures for generating retroreflectivity data from Oregon DOT's mobile scanner, and b) evaluate the effects of challenging conditions, including precipitation, which are commonly encountered in the winter/spring seasons when crews evaluate lines for

summer work. Since some aspects of the lidar radiometric (intensity) calibration are specific to a particular system and configuration, it was critical to modify and test these procedures using data directly from Oregon DOT's system.

1.1 OBJECTIVES

SPR799 Lidar for Maintenance of Pavement Reflective Markings and Retroreflective Signs Vol. I. Reflective Pavement Markings, hereafter referred to SPR 799 has the following research overarching objectives:

- Develop a model for retroreflectivity and radiometric calibration for Oregon DOT's mobile lidar system.
- Generate a set of quality control metrics for pavement marking and sign retroreflectivity based on information derived from mobile lidar data.
- Establish procedures for extracting road markings from lidar data and creating GIS data layers from the output of the above steps to support decision making by supervisors and integrate analysis results into Oregon DOT's overall workflows.

This final report summarizes several research tasks performed to accomplish these research objectives, including describing the field experiments, the radiometric calibration procedure, the validation process, development of striping and sign quality control metrics, and ultimately, integration of the results into an efficient GIS tool.

1.2 ORGANIZATION OF REPORT

This report is divided into two volumes. Volume I explores and develops the capabilities of using mobile lidar for evaluating reflective pavement markings, while Volume II explores the feasibility of using mobile lidar for evaluating retroreflective signs.

The remainder of Volume I is organized as follows:

Chapter 2 provides a detailed, comprehensive literature review, which evaluates the current state-of-the-art methodologies for retroreflectivity measurements for pavements with their associated advantages and disadvantages. In particular, the review focuses on the utility of mobile lidar systems for extracting retroreflective measurements.

Chapter 3 presents a novel, efficient road marking extraction algorithm developed for this research with example results.

Chapters 4 through 6 describe three experiments completed at the Oregon DOT Testdeck site located near Stayton, OR. Every other year at the Testdeck, a series of transverse pavement markings from different vendors and materials are placed transversely across the lane to evaluate their performance as they are exposed to traffic and weather. For this research, a series of mobile lidar scans were captured at the Testdeck in different scanning configurations, lanes, and speeds in order to provide a comprehensive dataset to develop a radiometric calibration.

Chapters 7 and 8 then explore the sensitivity of retroreflective readings to wet conditions. In the first test (Chapter 7), a series of scanners were used to capture a scene with a variety of markings after rainfall and to quantify the degradation in laser intensity. The second test involved using Oregon DOT's mobile lidar system to capture a pavement marking after wetting to quantify the degradation.

Chapter 9 develops a radiometric calibration equation specific to Oregon DOT's mobile scanner configuration. In the development of this equation, a variety of geometric configurations are evaluated.

Chapter 10 evaluates the ability of the mobile lidar to measure degradation in retroreflectivity using repeat surveys collected on the Testdeck.

Chapter 11 describes additional tests conducted at a field site in Philomath, OR used to validate the radiometric calibration equation as well as evaluate the repeatability of the system.

Chapter 12 presents a software tool with supporting GIS python scripts developed for implementation of this research. First, Matlab code was compiled into an executable to extract linear pavement markings from the lidar point clouds and perform retroreflective evaluations. A python script then converts the output of this program into feature classes within a geodatabase. The output is designed to have layers to support both detailed analyses for a project or highway as well as aggregated results to support performance-based analyses in a regional or statewide asset management framework.

Chapter 13 provides an example implementation of the proposed framework using data collected on Interstate-5 and smaller roads in Salem.

Chapter 14 contains the overall conclusions, summarizing key findings of this research. It also discusses the limitations to the work, recommendations for implementation, and possibilities for future research.

The report also includes two appendices:

- Appendix A contains the input parameter text file (in meters and international feet) for the Road Marking Extractor (RoME) program.

- Appendix B contains the ArcGIS python scripts used to convert the output csv files from the RoME program into a geodatabase.

Additional products, including the RoME software and associated python scripts were delivered to Oregon DOT in conjunction with this report.

2.0 LITERATURE REVIEW

2.1 OVERVIEW

This chapter presents a comprehensive literature review to evaluate the current state-of-the-art methodologies for retroreflectivity measurements for pavement markings and signs with their associated advantages and disadvantages. In particular, the review will focus on the utility of mobile lidar systems for extracting these measurements.

The literature review commences with a brief physics background on retroreflectivity to highlight important concepts to consider. Next, it describes current procedures and reference manuals for obtaining reliable retroreflectivity readings. The review will then describe mobile lidar technology and a brief history of mobile lidar usage within Oregon DOT. Following this background, the review will cover critical concepts related to lidar intensity (return signal strength) and radiometric calibration principles. For more detailed insights on radiometric calibration procedures, a recently published review of current radiometric calibration procedures has been published in Kashani et al. (2015). The following two subsections discuss current research utilizing mobile lidar data for retroreflective readings as well as pavement marking and sign feature extraction techniques. Finally, the chapter closes with a description of challenges and possibilities, which were helpful to guide the work completed on SPR-799.

2.2 RETROREFLECTIVITY BASICS

When propagating electromagnetic radiation (such as the light from a vehicle's headlights) encounters a surface, it can be reflected, absorbed, and/or transmitted in varying proportion. From the law of conservation of energy, the fractions of the light transmitted, absorbed and reflected must sum to one, or:

$$\boldsymbol{\tau + \alpha + \rho = 1} \tag{2-1}$$

Where:

$$\boldsymbol{\tau = \frac{E_t}{E_i};\ \alpha = \frac{E_a}{E_i}\ ;\ \rho = \frac{E_r}{E_i}} \tag{2-2}$$

In Eq. 2-2, E_i is the incident energy, and E_t, E_a, and E_r, are, respectively, the transmitted, absorbed and reflected energies. The quantity, ρ, is referred to as reflectance, a measure of how well a surface reflects incident radiant energy. More specifically, it is the so-called "bi-hemispherical" reflectance, as it assumes diffuse illumination and reflection over all viewing angles. In the more general case, it is of interest to model reflectance as a function of the

viewing and illuminating geometries. This can be achieved using a bidirectional reflectance distribution function (BRDF), which is a function of four variables: two describing the direction of the illumination source relative to the surface normal, and two describing the direction of the viewer (*i.e.*, the person, camera or sensor receiving the reflected light) (Jensen 2005; Schaepman-Strub et al. 2006).

Three special, or ideal, cases of reflection can be defined (Austin and Schultz 2009):

- Perfect specular reflection
- Perfect diffuse reflection
- Retro-reflection

Specular reflection arises from a very smooth surface (relative to the wavelength of the light), and results in light being reflected away from the illumination source, with the angle of reflection being equal and opposite the angle of incidence (Figure 2.1a). Mirror-like and metal surfaces (often described as being "shiny" in appearance) exhibit specular reflection. Diffuse reflection is the opposite case from specular, and involves a surface reflecting light equally well in all directions (Figure 2.1b). Rough surfaces, which are often described as appearing "flat or matte," are diffuse reflectors. The third special case is retro-reflection, in which light is reflected back in the direction of the illumination source (Figure 2.1c). This type of reflection is typically achieved through corner cube reflectors or glass beads, which are specifically designed for this purpose (Lloyd 2008; Burns et al, 2008).

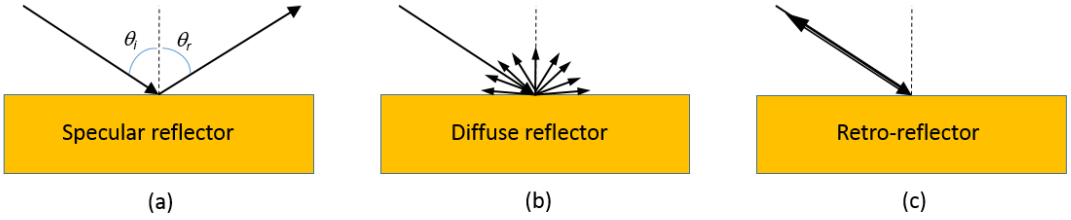

Figure 2.1: Three special cases of reflection: (a) specular, (b) diffuse, and (c) retro-reflection.

Retro-reflection plays an important role in increasing nighttime visibility of traffic signs and pavement markings. Specifically, if signs and pavement markings are designed to reflect light from a vehicle's headlights back to the driver, this increases the distances from which the pavement markings and signs can be seen at night and improves clarity (Austin and Schultz 2009). Statistics on the significantly higher fatal crash rates at nighttime, as compared with daytime, are frequently cited as an indication of the importance of retroreflectivity (Carlson and Picha 2009). At least as far back as the 1930s and the publication of the first version of the Manual on Uniform Traffic Control Devices (MUTCD), it was recognized that sign retroreflectivity was important to highway safety and efficiency (Carlson and Hawkins 2003). The late 1930s also saw the release of the first commercial enclosed bead sheeting (Lloyd 2008).

The 1993 Department of Transportation Appropriations Act (Public Law 102-388) mandated that the MUTCD be revised to establish minimum maintained levels for retroreflectivity for signs (McGee and Taori 1998; Carlson et al. 2003), and these minimum retroreflectivity (MR) levels are specified in Table 2A–3 of the current MUTCD.

Luminance is the photometric quantity describing the amount of light reflected, emitted or traveling through a given area and within a given solid angle, and is given in units of candela per square meter (cd/m^2). Loosely, luminance is a measure of how bright a surface appears to an observer viewing the surface from a particular angle. The ratio of luminous intensity to illuminance (the luminous flux incident on a surface per unit area in units of lux) provides a measure of retroreflectivity. In particular, retroreflectivity is typically reported in terms of retro-reflected luminance, R_L, in units of candelas per square meter per lux ($cd/m^2/lux$) or millicandelas per square meter per lux (mcd/m^2lux) (Migletz et al. 1999). Minimum retroreflectivity levels specified in MUTCD Table 2A-3 are given in $cd/lx/m^2$ measured at an observation angle of 0.2° and an entrance angle of ~4.0°.

Retroreflective sheeting used on traffic signs is classified into various types, which are specified in the American Society for Testing and Materials (ASTM) specification D4956: "Standard Specification for Retroreflective Sheeting for Traffic Control." Types I through II are beaded sheeting, while III through X are prismatic sheeting. Some of the types are also referred to by other terms: for example, Type I is referred to as "engineering grade," while Type V is "super high-intensity."

In addition to signs, pavement markings are another type of traffic control device that make use of retroreflectivity. In the case of pavement marking materials (PMM), retroreflectivity is typically achieved through the use of glass beads or microspheres embedded in the paint (Austin and Schultz 2009). Other types of marking materials include waterborne paint, epoxy, polyester, thermoplastic, and tape (Migletz et al. 1999). Advanced types of PMM have been shown to enable savings in pavement marking budgets in various state DOTs (Saetern 2016).

Unfortunately, the retroreflectivity of traffic control devices degrade over time, as a function of traffic, maintenance activities, weather, orientation, and precipitation, among other variables (Kirk et al. 2001; Migletz et al. 1999). It is for this reason that policies and procedures are in place to assess and maintain retroreflectivity over time. The specific wording in the MUTCD is that "Public agencies or officials having jurisdiction shall use an assessment or management method that is designed to maintain sign retroreflectivity at or above the minimum levels in Table 2A-3." Since degraded retroreflectivity can adversely affect safety, while premature replacement of signs and pavement markings can unnecessarily increase costs, effective inspection and maintenance procedures are critical to state DOTs. Current inspection methodologies fall into two general types: 1) a visual nighttime inspection using human inspectors, and 2) quantitative measurements made with retroreflectometers (Figure 2.2). Policies of blanket replacement on a set schedule may also be followed, but the disadvantage is wasted cost of unnecessary replacement of some signs (Austin and Schultz 2009).

Figure 2.2: Retroreflectometer being used to measure retroreflectance of pavement markings on the Oregon Department of Transportation Testdeck.

2.2.1 Degradation of retroreflectivity in wet conditions

Retroreflectivity can be significantly reduced when the surface is wet, such as during or just after a period of rainfall (Schnell et al. 2003; Lundkvist and Isacsson 2007; Carlson et al. 2007). One of the primary causes of this reduction in retroreflectivity is specular or "mirror-like" reflection (see Figure 2.1a) from a surface covered by a film of water, which leads to light from the headlights being reflected off in a direction away from the driver, rather than back towards the driver (Schnell et al. 2003; Pike et al. 2007). Refraction (bending) of the light rays at the air-water interface alters the optical path and can also lead to a reduction in retroreflectivity (Pike et al., 2007; Carlson et al. 2007; Burns et al. 2008). The effect of a layer of water on a bead can be modeled as an effective change in the refractive index of the bead (Burns et al. 2008). In pooled water, light can be scattered and/or absorbed within the water column, further reducing the proportion of incident light reflected back toward the driver.

There is some evidence to suggest that it may be possible to establish simple mathematical relationships between retroreflectivity under wet and dry conditions (Lundkvist and Isacsson 2007), suggesting the potential to predict retroreflectivity under wet conditions from measurements in dry conditions, or vice versa. However, additional research is needed to

develop and test such prediction methods and to determine the ranges of conditions and marking types under which they will hold.

2.2.2 Factors influencing visibility of pavement markings

Oregon DOT conducted prior research (van Schalkwyk 2010), which summarizes several factors that influence pavement marking visibility as well as provides detailed references. Some of these factors include:

- Driver – age, vision quality, eye location, human factors, driver attention, driver workload
- Vehicle – type, headlamps, windshield, speed
- Environment – glare, atmosphere, weather (wet/dry, snow)
- Roadway – geometry (e.g., curves, weaving), cross-slope, volume, overhead lighting, highway type, number of lanes, overhead roadway, pavement surface age, material and condition
- Pavement marking – location (center, left, right), placement quality, usage, material type, color, contrast with road surface, edge lines vs center line only, degree of obliteration, centerline configuration, lateral separation between double lines, width, style (e.g. solid or dashed), age, retroreflectivity, raised markers
- Policies – winter snow removal practices, studded tire usage

2.2.3 Pavement marking materials

Table 2.1 summarizes different types of pavement markings, including their advantages and disadvantages. The Oregon DOT Pavement Markings Design Guidelines (Oregon Department of Transportation 2015b) and Ceifetz et al. (2017) provide a detailed review of different marking materials and their application. Oregon DOT has released a document in 2016 entitled "Pavement Marking Approval Process for Permanent Markings for use on Oregon Department of Transportation (Oregon DOT) Highways," which summarizes the testing procedures required for acceptable pavement marking materials for the Qualified Products List (QPL) as well as warranty information. Permanent pavement markings are classified as: waterborne paint, high performance pavement markings, durable pavement markings, and pavement markers.

Table 2.1: Comparison of Pavement Marking Types from Oregon DOT's Pavement Marking Design Guidelines (Oregon 2015b)

MATERIAL AND APPLICATION CHOICES						PERFORMANCE FEATURE CHOICES							
Specification Section	Specification Method	Material	Surface Application Type	Application Method	Line Characteristics	Basic Performance (line presence & retro-reflectivity)	Short Life Span	Mid-length Life span	Long Life Span	Audible/Tactile	Wet Weather Retro-reflectivity	Protection from infrequent snow plowing	Protection from frequent snow plowing & increased durability under heavy traffic volumes
00855	N/A	Raised Pavement Markers	Surface Mounted	N/A	N/A	x*		x		x	x		
			Recessed			x*		x		x	x	x	x
00860	N/A	Paint	Surface Installed	Spray	Non-Profiled	x	x						
00865	Method A	Methyl Methacrylate (MMA)	Surface Installed	Extruded	Profiled	x			x	x			
		Thermoplastic				x			x	x			
	Method B	Methyl Methacrylate (MMA)	Surface Installed	Extruded	Non-Profiled	x			x				
		Thermoplastic				x			x				
	Method C	Methyl Methacrylate (MMA)	Protected Inlaid	Extruded	Non-Profiled	x			x			x	x
					Wet Weather	x			x		x	x	x
		Thermoplastic	Protected Inlaid	Extruded	Non-Profiled	x			x			x	x
					Wet Weather	x			x		x	x	x
	Method D	Methyl Methacrylate (MMA)	Surface Installed	Extruded	Profiled Wet Weather	x			x	x	x		
		Thermoplastic			Profiled Wet Weather	x			x	x	x		
	Method E	Methyl Methacrylate (MMA)	Surface Installed	Extruded	Wet Weather	x			x		x		
		Thermoplastic			Wet Weather	x			x		x		
	Method F	Methyl Methacrylate (MMA)	Surface Installed	Spray	Non-Profiled	x			x			x	
		Thermoplastic			Non-Profiled	x			x			x	
	Method G	Tape	Hot-laid	N/A	Non-Patterned	x			x			x	
			Hot-laid		Patterned	x			x			x	
			Hot-laid		Wet Weather	x			x		x	x	
			Grooved		Non-Patterned	x			x			x	x
			Grooved		Patterned	x			x			x	x
			Grooved		Wet Weather	x			x		x	x	x
	Method BF	Methyl Methacrylate (MMA)	Surface Installed	Spray or extruded	Non-Profiled	x			x				
		Thermoplastic	Surface Installed		Non-Profiled	x			x				
00866	N/A	Modified Urethane	Surface Installed	Spray	Non-Profiled	x		x				x	
			Protected Inlaid		Non-Profiled	x		x				x	x
		Hi-Build Paint	Surface Installed		Non-Profiled	x		x				x	
		Polyurea	Surface Installed		Non-Profiled	x		x				x	
00867	Type A	Thermoplastic	Surface Installed	Spray or extruded	Non-Profiled	x			x				
	Type B	Thermoplastic	Surface Installed	Pre-formed	Non-Profiled	x			x				
	Type B-HS	Thermoplastic	Surface Installed	Pre-formed	Non-Profiled - high skid resistance	x			x				
	Type AB	Thermoplastic	Surface Installed	Spray, extruded, or pre-formed	Non-Profiled	x			x				

*Only to be used in conjunction with other marking materials (paint, MMA, thermoplastic, modified urethane, etc.)

2.3 NATIONAL STANDARDS OR METHODOLOGIES

A variety of standards and specifications have been developed by FHWA, ASTM, AASHTO, DOTs, TRB, and other organizations for evaluating pavement retroreflectivity. This section will briefly summarize the most relevant procedures to SPR799.

2.3.1 FHWA guidance

The FHWA has a placeholder section (3A.03) for guidance on retroreflectivity in the 2009 Manual for Uniform Transportation Control Devices (MUTCD) Revision 2 pending future rule

making processes through FHWA-SA-10-015, *Summary of MUTCD Pavement Marking Retroreflectivity Standard.* This document provides proposed revisions to the 2009 MUTCD related to pavement marking retroreflectivity and the establishment of minimum levels. It summarizes where these minimum levels of retroreflectivity should be required, as well as methods for evaluating retroreflectivity and marking quality.

Additional documents of relevance to support this effort to establish minimum retroreflectivity values have been provided by the FHWA and include the following:

- FHWA-HRT-07-059. (Deballion et al. 2007). Updates to Research on Recommended Minimum Levels for Pavement Marking Retroreflectivity to Meet Driver Night Visibility Needs. This research identified factors important to the visibility of pavement markings and provided recommended minimum in-service retroreflectivity values for longitudinal stripes. The minimum values recommended increase with increasing speed on the roadway.

- FHWA-SA-08-010. (Hawkins et al. 2008). Preliminary Economic Impacts of Implementing Minimum Levels of Pavement Marking Retroreflectivity. This document outlines a methodology with an accompanying spreadsheet for performing economic analyses of different pavement marking strategies (e.g., using a more durable material).

- FHWA–2009–0139. Maintaining Minimum Retroreflectivity of Longitudinal Pavement Markings. This document contains proposed updates to the MUTCD and rulemaking associated with minimum retroreflectivity standards based on recent research efforts and workshop findings.

Van Schalkwyk (2010) provide a more detailed discussion of the development of federal retroreflectivity values.

2.3.2 Basic portable retroreflectivity evaluation approaches

Two primary ASTM Standards exist for obtaining retroreflective readings. These documents cover protocols such as calibration procedures to obtain consistent readings.

- ASTM D7585-10 Standard Practice for Evaluating Retroreflective Pavement Markings Using Portable Hand-Operated Instruments

- ASTM E1710-11 Standard Test Method for Measurement of Retroreflective Pavement Marking Materials with CEN-Prescribed Geometry using a Portable Retroreflectometer

2.3.3 Mobile platform for retroreflectometer readings

ASTM also has a working group developing a specification for using a mobile pavement marking system, which consists of a portable retroreflectometer attached to a vehicle such that it can follow a pavement stripe and collect periodic measurements.

- ASTM WK3833 Test Method for Mobile Pavement Marking Retroreflectivity Measurements. When completed, this method will cover the measurement of pavement marking materials from a mobile platform, including geometric and equipment requirements.

2.3.4 Wetting

Due to the known differences in retroreflectivity between wet and dry conditions, ASTM standards cover separate test methods for measurement of retroreflective properties of pavement markings under different conditions of wetness:

- ASTM E1710-11 Standard Test Method for Measurement of Retroreflective Pavement Marking Materials with CEN-Prescribed Geometry Using a Portable Retroreflectometer

- ASTM E2177-18 Standard Test Method for Measuring the Coefficient of Retroreflected Luminance (R_L) of Pavement Markings in a Standard Condition of Wetness

- ASTM E2832-12 Standard Test Method for Measuring the Coefficient of Retroreflected Luminance of Pavement Markings in a Standard Condition of Continuous Wetting ($R_{L\text{-}2}$)

The method for measuring retroreflectance under a standard condition of wetness described in ASTM E2177-18 requires pouring 3.0 liters of clean water from a bucket within 3-5 seconds and waiting 45 seconds before taking readings (ASTM, 2018). Meanwhile, ASTM E2832-12 describes a more sophisticated approach utilizing a wetting device for simulating rainfall and takes readings during the wetting process (ASTM 2012).

2.3.5 Rumble Stripes

MnDOT Report 2016-13 (Hawkins et al. 2016) evaluate the installation of rumble stipes, which is a combination of the rumble strip and pavement stripe. Rumble stripes offer advantages for improved durability in areas requiring frequent snow removal. It is important to note that the combination of rumble strips with pavement markings to produce “rumble stripes” is not a requirement for pavement markings per MUTCD Chapter 3J, although it is a good option for decreasing lane departures through the inclusion of sound and vibration (Hawkins et al. 2016).

2.4 OREGON DOT PROCEDURES

Oregon DOT has developed internal procedures and policies for pavement marking and sign maintenance and replacement. Note that these procedures are updated regularly and one of the purposes of SPR-799 is to inform future updates to these procedures. This section will briefly summarize relevant documents.

2.4.1 Design manuals

Pavement marking requirements for Oregon DOT are outlined in the following:

- *Traffic Line Manual* (Oregon Department of Transportation 2018). This manual establishes a guide for uniform traffic lines and pavement markings. It is based on MUTCD guidelines, the Oregon MUTCD supplement, and Oregon DOT policy and guidelines. The manual details the development of striping plans for all projects and maintenance activities where existing striping will be modified. It also covers the approval process for non-standard markings.

- *Pavement Marking Design Guidelines* (Oregon Department of Transportation 2015b) covers planning, survey requirements, drawing details, material selections, specifications, estimating, bidding, and drafting standards for roadway designers to develop pavement marking plans.

2.4.2 Maintenance protocols

Maintenance protocols related to pavement markings can be found in:

- *Desired Conditions of Maintenance Features on State Highways* (Oregon Department of Transportation 2002). This document provides objective descriptions of desired conditions for highway features to optimize use of tax dollars. It provides a system of five level-of-service ratings (A-E) to describe the feature's condition. In the case of pavement marking, desired conditions for each road category are specified in terms of the percentage of lane miles with each rating.

Table 2.2 summarizes the desired condition for level of service of pavement markings. Note that Oregon DOT is in the process of updating these requirements and in 2015 increased the minimum retroreflectivity values to 250 and 200 mcd/m^2/lux for newly installed white and yellow stripes, respectively.

Table 2.2: Oregon DOT Desired Conditions Level of Service Requirements for Pavement Markings

Level of Service	Centerline Condition	Fog stripe Condition	% Pavement markers in place	% Retrace present	Average Retroreflectivity (White, mcd/m^2/lux)	Average Retroreflectivity (Yellow, mcd/m^2/lux)
A	Like new	Like new	90-100%	<10%	150	125
B	Like new	Some wear	80-90%	<20%	120	90
C	Some wear	Some wear	70-80%	<40%	80	60
D	Some wear	Significant wear	50-70%	<60%	40	10
E	Significant wear	Nearly gone	<50%	<80%	0	0

2.4.3 Pavement marking specifications

Section 00850, Common Provisions for Pavement Markings, Part 00800, Permanent Traffic Safety and Guidance Devices, in the Oregon Standard Specifications for Construction, (Oregon Department of Transportation 2015a) covers specifications for pavement markers, paint, longitudinal durable markings, high-performance markings, and transverse bars and legends).

2.4.4 Pavement marking warranties

General Oregon DOT warranty specifications are covered in:

- Section 00170.85(c) (1), Responsibility for Defective Work of Part 00100, General Conditions, in the Oregon Standard Specifications for Construction (Oregon Department of Transportation 2015a).

2.4.5 Testdeck and Prior Research on Pavement Markings

Van Schalkwyk (2010), outlines Oregon DOT's protocol for performance and durability testing of pavement marking materials. This research was the foundation for the Testdeck, where pavement marking products are evaluated for two years at regular intervals to determine their suitability as Qualified Products. Oregon DOT's Testdeck site, which is on the westbound right travel lane of Highway OR-22 between mileposts 12.25 and 12.5 (44°49'32.4" N, 122°48'48.8 W), outside of Salem heading toward Stayton. The Testdeck is placed strategically to start on a joint where asphalt ends and concrete pavement starts. Vendors place two lines on each pavement type for each product they want evaluated. Tests include: thickness of marking material, dry weather retroreflectivity, and subjective evaluations of appearance and durability. The research provided several recommendations to Oregon DOT, many of which have been implemented in the current Testdeck procedures. This report also describes several other Testdecks throughout the U.S.

These procedures have been developed into Oregon DOT TM 777: *Method of Test for Evaluation of Retroreflectivity of Durable and High Performance Pavement Markings Using Portable Hand-Operated Instrument,* in the Manual of Field Test Procedures, (Oregon State Highway Division, Construction Section, 2015). This test method is based on ASTM E1710-05 and covers the testing of retroreflectivity for evaluating as-constructed conditions. Retroreflectivity readings are taken at 300 ft. intervals along longitudinal stripes and at 25% of the transverse bars, selected randomly. Measurements are taken in alternate directions for yellow lines and crosswalk bars, but in the direction of traffic for all other lines.

2.5 PRACTICES OF OTHER DOTS

2.5.1 Replacement strategies and Retroreflectivity readings.

Caltrans (Saetern 2016) recently performed a preliminary investigation of commercial pavement marking management systems. Caltrans itself relies on visual inspections as the primary means for determining when to replace pavement markings, but hopes to move to a more objective/systematic approach. As part of this report, they interviewed several state DOTs to

determine their requirements for minimum retroreflectivity levels and use of pavement marking management systems. The report indicates that several states have significantly reduced costs by using retroreflectivity readings rather than blanket replacements. Of note, several DOTs identified challenges in maintaining logs of quantities and locations of durable pavement markings and retroreflectivity readings.

Table 2.3 summarizes practices and minimum retroreflectivity values implemented by DOTs, as well as those obtained from other reports (e.g. CTC & Associates 2016). Some DOTs base their decisions off of minimum values, others consider a higher threshold to ensure adequate performance through the winter, and some specify minimum values for new striping.

Table 2.3: Summary of Findings of Saetern (2016) Describing Practices of Several State DOTs

Organization	Devices for readings	NEW		Existing – Required to withstand winter		Failure Point	
		White	Yellow	White	Yellow	White	Yellow
Caltrans	Visual assessment	-	-	-	-	-	-
Indiana DOT	-	-	-	130	Replaced annually	100	Replaced annually
NC DOT	-	-	-	-	-	150	100
Missouri DOT	Contractor with mobile retroreflectivity unit	300	225	200	175	150	125
Kansas DOT	-	-	-	-	-	150	100
Michigan DOT	Contractors	-	-	-	-	Replaced annually	Replaced annually
Florida DOT	Mobile Retroreflectivity	-	-	-	-	-	-
Iowa DOT	Lazerlux van, handheld LTX, and contractors	-	-	-	-	-	-
ASTM1710-11	-	-	-	-	-	90-150	90-100

**Retroreflectivity Values are in Units of mcd/m^2/lux. Note that not all DOTs provided values.*

Below is a summary of some of the practices implemented by DOTs:

- Indiana DOT repaints center lines annually, but uses readings to determine if edge lines need repainting. They use a requirement > 130 mcd/m^2/lux to account for degradation in the winter and ensure the MUTC 100 mcd/m^2/lux will be met.

- North Carolina DOT utilizes retroreflectivity readings since 2000 and recommends 150 mcd/m^2/lux for thermoplastic white markings and 100 mcd/m^2/lux for thermoplastic yellow markings.

- Missouri DOT restriped every minor route annually and every major route 2-3 times per year; however, due to budget cuts they have switched to a retroreflectivity

approach and recommend 150 mcd/m^2/lux for thermoplastic white markings and 125 mcd/m^2/lux for thermoplastic yellow markings. Different requirements are implemented for new versus existing pavement markings.

- ASTM 1710-11 performs calculations to determine retroreflectivity requirements of 90-150 mcd/m^2/lux for white markings and 90-100 mcd/m^2/lux for yellow markings.

2.5.2 Warranties

Caltrans also recently conducted a preliminary investigation of the usage of warranties by DOTs through two state of practice surveys (CTC & Associates 2016). The first survey focused on warranty information and minimum values for the warranty and the second focused on pavement markings outside of a warranty period. They found that of the states surveyed, there was relatively little consensus among the respondents in structuring or administering of pavement marking warranty programs as well as retroreflectivity requirements (Table 2.4). The timing of the initial readings also varies substantially from immediately after installation to within 45 days across the DOTs surveyed. NCHRP Synthesis 408 (Markow 2010) also provides more information on state warranty practices; however, practices have changed significantly in the last 6 years.

Table 2.4: Minimum Initial Retroreflectivity Values from State DOTs Based on Material Types (Modified from CTC & Associates, 2016)

State	White(mcd/m^2/lux)	Yellow(mcd/m^2/lux)
Unspecified Product		
Alabama	130	130
Iowa (wet)	150	100
Oregon	250*	200*
New Hampshire	200	150
Kentucky, Missouri	300	225
Delaware	450	375
Iowa (Regular)	550	325
Epoxy		
Pennsylvania	250	200
Minnesota	300	200
Kansas(epoxy/multicomponent)	325	250
Thermoplastic		
Minnesota (enhanced skid resistance)	250	150
Pennsylvania (cold)	250	200
Kansas	300	225
Pennsylvania (preformed)	300	250
Pennsylvania (hot)	300	250
Iowa (preformed)	325	150
North Carolina	375	250
Minnesota (preformed)	400	250
Nebraska (dry)	400	325
North Carolina (highly reflective elements)	700	700
Durable Markings		
Kansas (high-durability tape)	225	175
Iowa	300	200
South Dakota	331	206
Preformed Tape		
Georgia	600	400
Minnesota	600	500
Polyurea		
Nebraska (dry)	500	350
Georgia (longitudinal)	600	400
North Carolina	700	700
Waterborne		
Pennsylvania	250	165
Iowa (high-build)	300	225
Paint		
Minnesota	275	180
South Dakota (high-grade polymer)	350	275
Other		
Iowa (intersection)	150	100
Kansas (cold plastic)	250	175
Kansas (pattern cold plastic)	500	300
Iowa (profiled)	700	350

**Note that CTC & Associates (2016) reported minimum values of 150 and 125 for white and yellow stripes, respectively. However, these values have been updated to 250 and 200, respectively per the 2015 Oregon DOT Boilerplate Special Provisions Section SP00860.*

2.6 MOBILE LIDAR TECHNOLOGY

Mobile lidar (ML, also called Mobile Laser Scanning, MLS, or Mobile Terrestrial Laser Scanning, MTLS), hereafter referred to as MTLS, systems can acquire detailed 3D data efficiently from a moving vehicle at highway speeds with traffic. Georeferencing (i.e., the assignment of precise, 3D spatial coordinates in a defined coordinate system to each point in a lidar point cloud) can be completed directly with the combination of components included on the scanner (e.g., GNSS-aided inertial measurement systems); however, for highest accuracy applications, rigorous survey control points are often established. In addition to a wealth of geometric information across the roadway and surrounding area, a key benefit to mobile lidar data is its intensity information, which is related to the reflectivity of the objects.

Lidar provides several benefits and, as a result, is being widely adopted by DOTs across the country (*NCHRP Report 748* and *NCHRP Synthesis 446*). One of the key benefits of lidar is the fact that the same lidar dataset can be used by multiple people for a wide variety of applications, minimizing the need for multiple data collects. This versatility has resulted in the phrase, "Collect once, use many times" when discussing lidar. Figure 2.3 presents a sampling of these applications in transportation.

Additionally, one can remotely survey a site from safe locations, minimizing the danger to field crews and the travelling public. Lidar also enables a much more efficient and thorough field survey, minimizing the need for costly repeat visits to the site to collect information. The reduction in field time and ability to acquire data from the sides of the road with static lidar or at traffic speeds with mobile lidar provides significant safety benefits over typical surveying.

The comprehensive information provided by lidar greatly improves the detail in models used throughout the design process and, hence, reduces uncertainty in decision-making. The additional information that is resolvable in lidar data enables topography and other features to be modeled at a higher level of detail and accuracy over traditional techniques. This detailed, 3D virtual world provides personnel in the transportation agency with a much better understanding of the field conditions and variability throughout the site.

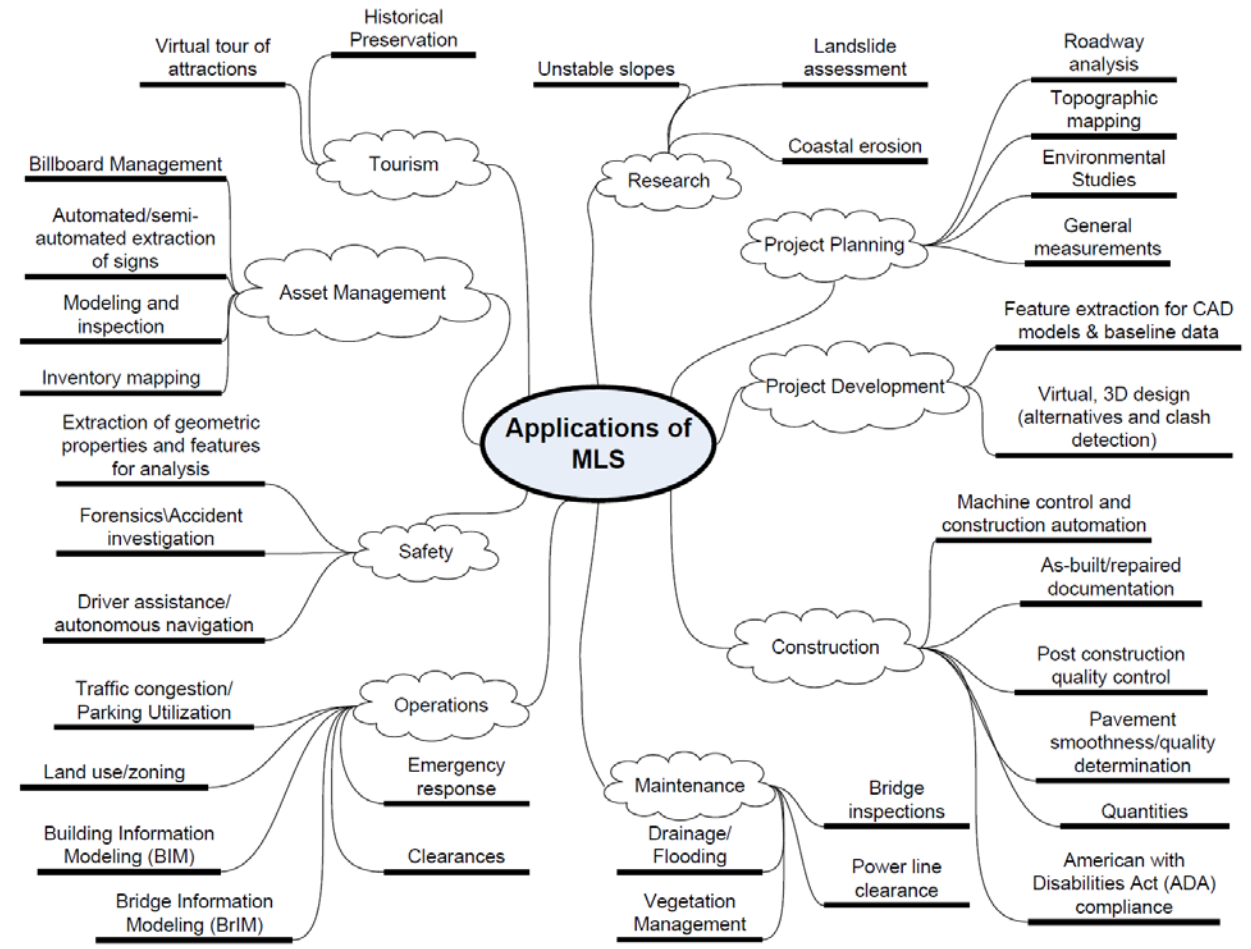

Figure 2.3: Sample applications using mobile lidar technology in transportation. From NCHRP Report 748 (Olsen et al. 2013).

Another key benefit of mobile lidar is the ability to integrate other sensors onto a single mobile platform (*NCHRP Synthesis 446*). This enables the collection of a wide variety of important metrics needed for various applications from a single data collection effort.

A wide range of MTLS systems exist depending on the scope of the survey. Puente et al. (2013) describes and compares configurations of a variety of MTLS. Systems can be designed to be specialized for certain applications such as pavement analysis or configured for general data acquisition. Lower cost asset management & mapping systems (~$400k) can achieve sub-meter (<3.3 ft) accuracies at the network level and decimeter (several inches) accuracies at the local level. Survey grade systems (~$1 million) can achieve centimeter (<1in) level accuracies at both the network and local level. While highest accuracy has required the use of dense targets, higher accuracy and more reliable results can be obtained by performing multiple passes of a section, enabling improved verification of Global Navigation Satellite System (GNSS) quality as well as trajectory enhancements by averaging multiple passes (Nolan et al. 2015a; 2015b).

One of the first DOTs to develop formal specifications was Caltrans (Chapter 15 California Survey Manual). These specifications have been modified and adopted by other DOTs such as Florida DOT. Caltrans has continued to develop best practices, workflow, and training documentation for mobile laser scanning data collection (Yen et al. 2014).

NCHRP Report 748 provides performance-based guidelines for the use of mobile lidar in transportation applications (Olsen et al. 2013c). Based on interviews with state DOTs and service providers, the report indicates that transportation agencies have a strong interest in mobile lidar going forward, but there are very few examples of best practices and/or in-depth discussions of results. This guideline establishes nine data collection categories (DCC) that are appropriate for the specific transportation applications based on resolution and accuracy requirements. The guidelines also provide general recommendations concerning the critical issue of data management. It is divided into two main sections: Management and Technical. The management portion contains a discussion of applications, workflows, data mining, procurement process, decision making, an implementation plan, and currently available guidelines. The technical section describes the components of MTLS, error sources, calibration and correction, accuracy and resolution requirements and specification, quality control methods, considerations for common applications, information management, deliverable specification, and future trends. Appendices also contain sample calibration reports and templates for developing scopes of work. This work was developed into an e-learning website (learnmobilelidar.com), which includes online, interactive learning modules, a detailed and searchable reference list, and user forums to help educate about mobile lidar usage to support transportation applications.

2.6.1 Mobile lidar at Oregon DOT

Oregon DOT has been an early adopter of mobile lidar technology. When the technology first became available, Oregon DOT contracted its use on several highway projects. In 2011, Oregon DOT purchased at TopCon IPS2 mobile lidar system primarily for asset management purposes. To the authors' knowledge, Oregon DOT was the first state DOT to own a mobile lidar system in 2011. Data from mobile lidar surveys were used to extract features to update asset management databases. As more people within Oregon DOT started utilizing the data, additional applications were identified, such as the use of the mobile lidar scans to measure drive approaches.

After several years working with and becoming more comfortable with the technology, Oregon DOT purchased a survey-grade system, the Leica Pegasus: Two (Figure 2.4). The higher quality of the data enables it to be used for a broader range of applications. This system also is a versatile system that can be mounted on additional vehicles aside from a truck or SUV such as ATVs or boats for more difficult to reach locales. The system also includes 8 cameras (7 providing a panoramic view and one focused on the pavement), enabling it to provide a detailed video log of the highway in addition to the geometric information provided by the scanner.

Figure 2.4: Oregon DOT's current mobile lidar system, Leica Pegasus:Two.

Oregon DOT's Engineering Technology Advancement (ETA) group is currently exploring additional opportunities to utilize the mobile lidar system throughout Oregon DOT to either complement or replace current data collection procedures. Current activities with mobile lidar at Oregon DOT are described on their webpage: (https://www.oregon.gov/ODOT/HWY/ETA/Pages/Mobile-LiDAR-Applicaitons.aspx). Oregon DOT's mobile lidar system is being utilized for acquiring survey data for project development, measuring vertical clearances, asset management, pavement evaluation, slope stability monitoring, accident reconstruction, and many more.

Recently, Oregon raised the speed limit on the state Highways in central and eastern Oregon. This project required Oregon DOT to evaluate sight distance as well as passing zone striping with the increased speed to ensure that they would be compliant with safety regulations. Mobile lidar data already collected from Oregon DOT's routine mapping were extensively used in the supporting passing distance studies. These data ensured that Oregon DOT could complete the necessary remediation quickly to meet strict timelines (Oregon DOT, 2015).

Oregon DOTs vision is to utilize mobile lidar and other technologies to provide a real-time, digital transportation system (Singh et al. 2009). When construction projects or maintenance are completed, the data would be updated to reflect those changes.

2.6.2 Intensity and Radiometric Calibration

Intensity values are often provided with lidar data sets as an additional attribute to accompany the X, Y, Z spatial coordinates of points and color information (Figure 2.5). These intensity values are a measure of backscattered signal strength and contain information on surface characteristics, including reflectance (Figure 2.5). However, the raw intensity values are generally provided as un-calibrated digital numbers, and, in addition to surface reflectance at the laser wavelength, they are also a function of several extraneous variables related to the environment, system and acquisition parameters (Höfle and Pfeifer, 2007; Wagner et al., 2008; Kaasalainen et al., 2009; Jutzi and Gross, 2009; Vain et al., 2009). Examples of these extraneous variables include laser range, incidence angle, receiver aperture, system transmittance, atmospheric transmittance, beam divergence, and transmitted laser power.

A great number of lidar intensity correction and radiometric calibration procedures have been developed with the goal of removing the effects of these environmental and system variables to provide values that better represent surface reflectance. (As a side note on terminology, while some authors draw a distinction between reflectance and reflectivity based on surface type, the terms are used interchangeably here.) Depending on the level and type of correction, the output may be referred to as calibrated intensity, pseudo-reflectance, relative-reflectance, reflectance factor, or true surface reflectance.

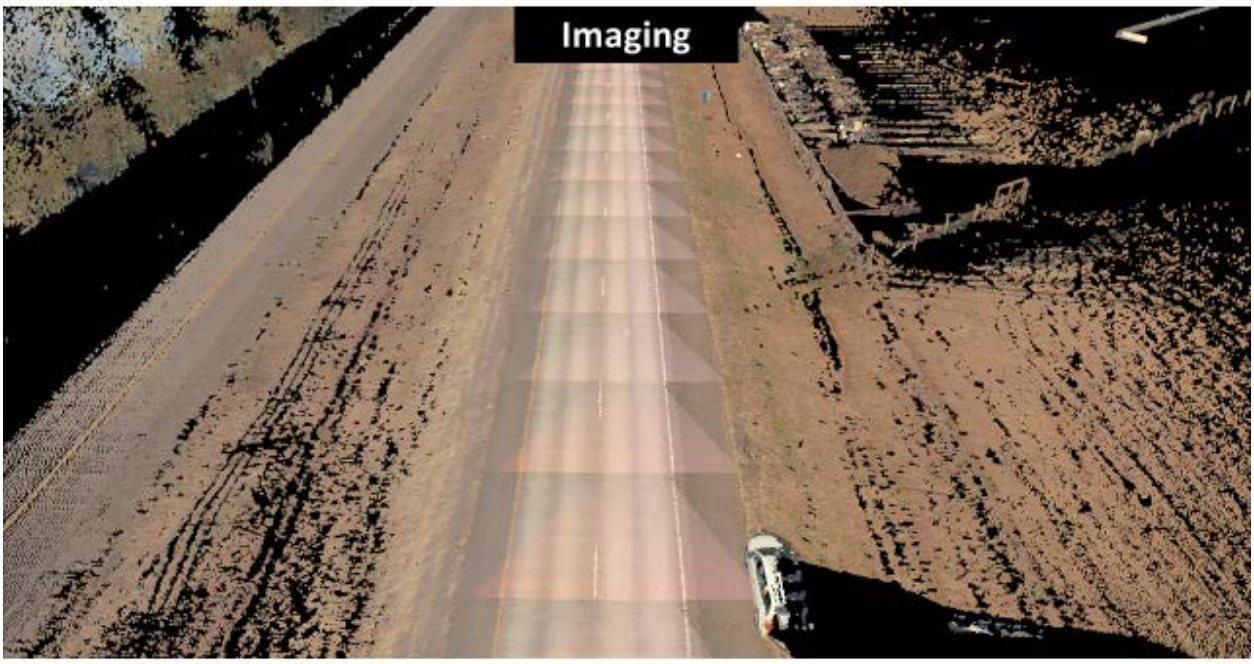

(a)

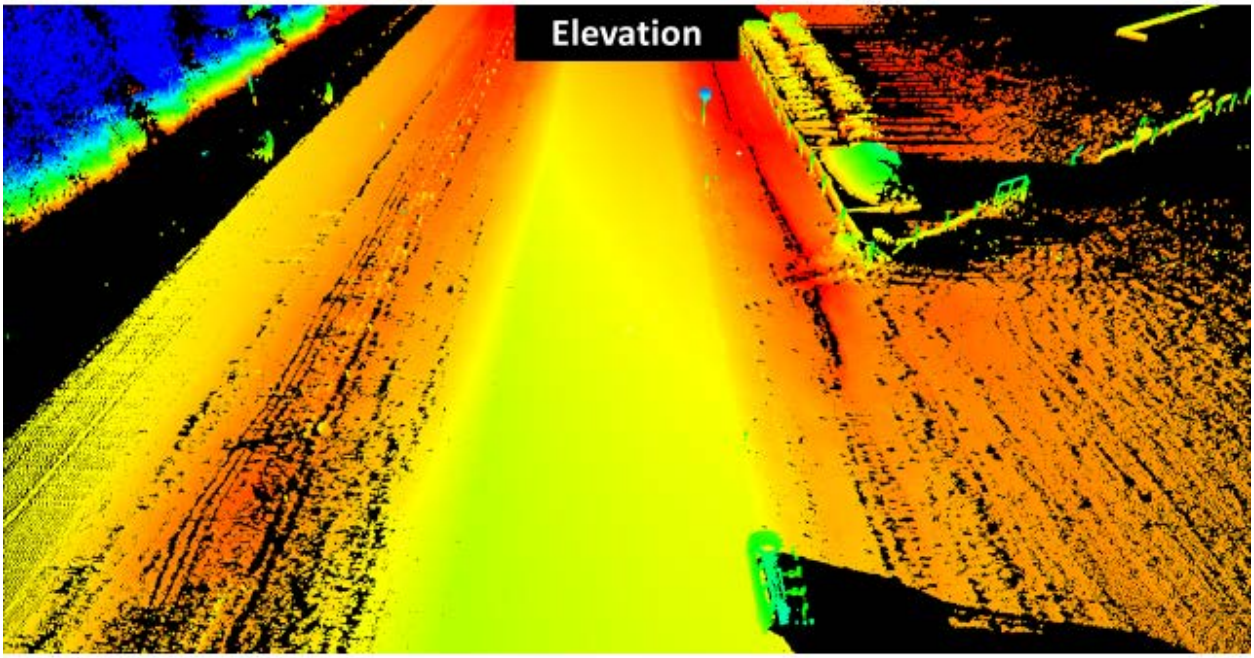

(b)

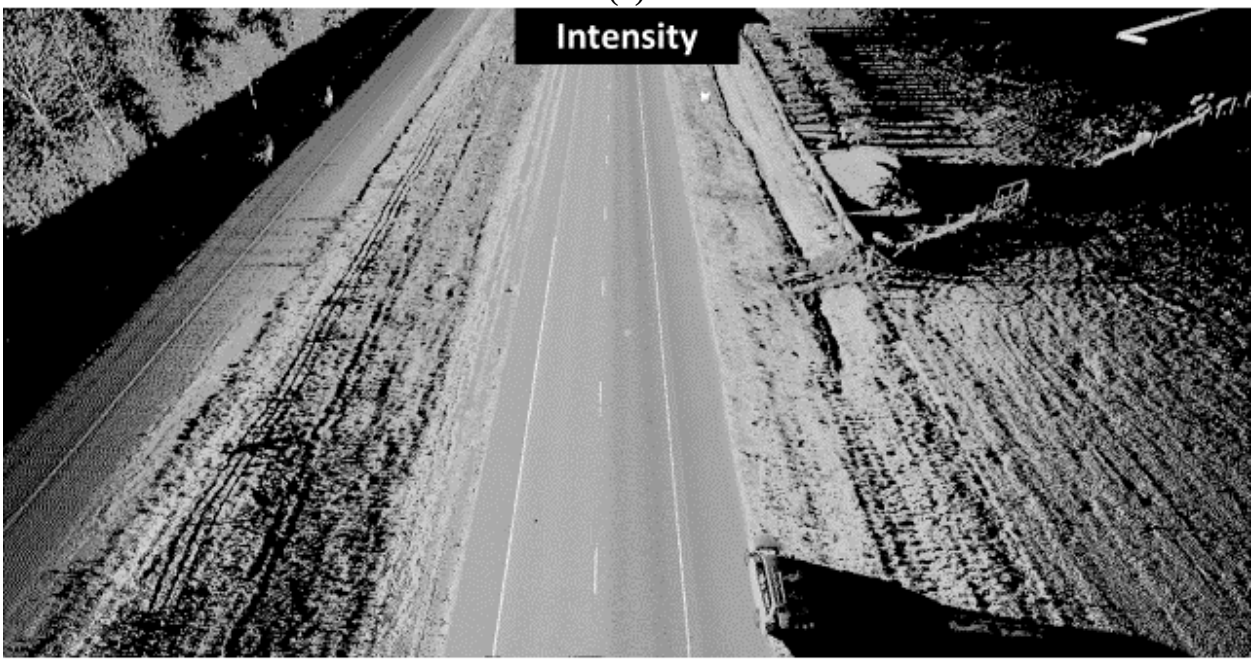

(c)

Figure 2.5: Mobile lidar data collected by Oregon DOT on Highway OR-22, near milepost 13. (a) the lidar data are colored using the imagery collected from the camera integrated in the mobile lidar system. (b) shows the point cloud color-coded by elevation, with a red-yellow-green-blue color ramp where red represents lower elevation while blue represents high elevation. (c) the same point cloud is shown displayed by intensity. Although the intensities shown here are un-calibrated, pavement markings and other features are clearly distinguishable.

Kashani et al. (2015) provide a comprehensive overview of different types of radiometric calibration and correction routines, which can be broken into the following general processing levels:

- Level 0: Raw intensity (no correction)
- Level 1: Intensity correction
- Level 2: Intensity normalization
- Level 3: Rigorous radiometric calibration

Based on the Kashani et al. (2015) classification of intensity correction/calibration, examples of work using Level 1 processing include Luzum et al. (2004), Jutzi and Gross (2009), and Korpela et al. (2010) while Level 3 processing is discussed in Ahokas et al. (2006), Kaasalainen et al. (2009), and Briese et al. (2012).

Another method of classifying radiometric processing strategies discussed in Kashani et al. (2015) is to separate them into: 1) theoretical or model-driven approaches, and 2) empirical approaches. Those in the first category generally involve inverting the laser range equation to obtain surface reflectance as a function of (known, modeled, or assumed) system, acquisition and environmental variables. Although many different forms of the laser range equation have been published (e.g., Jelalian 1992; Baltsavias 1999; Höfle and Pfeifer 2007; Wagner et al. 2008; Mallet and Bretar 2009; Kaasalainen et al. 2011), a common form—under the assumption of a Lambertian, area target—is:

$$\boldsymbol{P_r = \frac{P_t D_r^2 \eta_{atm} \eta_{sys} \rho}{4R^2} \cos \theta_i} \qquad \textbf{(2-3)}$$

Where P_r = received optical power (watts), P_t = transmitted power (watts), D_r = receiver aperture diameter (meters), η_{atm} = atmospheric transmission factor (dimensionless), η_{sys} = system transmission factor (dimensionless), ρ = target reflectance at the laser wavelength (dimensionless), R = range (meters), and θ_i = incidence angle. Empirical approaches are generally similar, but rely to a greater extent on experimentally-estimated parameters, rather than mathematical models.

Because the transmitter and receiver in a lidar system are collocated as closely as possible, lidar intensity inherently measures something akin to retroreflectivity (i.e., the amount of laser light reflected *back in the direction of the source*.) In fact, if lidar intensity data can be appropriately corrected—using, as a basis, the methods presented in the work referenced here—they can provide good estimates of surface retroreflectivity. It is this observation that forms the theoretical basis for this work.

2.6.3 Quality control measurements from lidar

Several studies evaluate the geometric state of traffic signs (e.g., flatness, inclination) from lidar data, which can be directly calculated after extracting the signs from the point cloud (Gonzalez-Jorge et al. 2013; Wen et al. 2016). However, few studies take advantage of intensity readings from mobile lidar to assess the retroreflectivity condition of the traffic signs or pavement markings.

2.6.4 Automated feature extraction based on intensity/intensity contrast

A variety of approaches have been proposed to extract road markings from lidar datasets. Often, to simplify the extraction of road markings from mobile lidar data, the road surface is extracted first. Guan et al. (2016) reviews a number of methods that have been proposed for road pavement extraction, many of which are summarized in Table 2.5. Most of these methods use the geometric or material characteristics of the road surface including: local elevation, local intensity, and line or planar features from road edges (curbs). Other methods fuse the mobile lidar data with other data sources such as video camera logs, airborne lidar data, road network map, and so on.

Table 2.5: Summary of Road Marking Extraction Techniques from Lidar Data

		Reference	Intensity Correction	Image processing	Road marking categories in classification	Curb extraction
Projected Image	Fixed thresholding	Jaakkola et al. (2008)	Curve fitting, mean filtering	Morphological operation	Zebra crossings, parking space lines.	Yes
		Smadja et al. (2010)	N/A	N/A	N/A	N/A
		Yang et al. (2012)	N/A	N/A	N/A	N/A
		Guan et al. (2013, 2014, 2015a)	Gaussian normal distribution	Morphological operation	N/A	Yes
		Yao and Hu (2014)	N/A	Morphological operation, Hough Transform	N/A	N/A
		Guo et al. (2015)	N/A	Morphological operation	Lane line, zebra crossing, straight ahead arrow, left (right) -turn arrow, straight ahead or left (right) -turn arrow	Yes
		Riveiro et al. (2015)	N/A	Canny operator, Hough Transformation	Zebra crossings	N/A
		Zhang et al. (2016)	Linear model with cosine of the scan angle rank	Region grow	16 types of road markings	Yes
	Dynamic thresholding	Kumar et al. (2014)	N/A	Morphological operation	N/A	N/A
		Yu et al. (2015)	N/A	N/A	Boundary line, Stop line, rectangular marking, pedestrian warning, Arrow marking	Yes
		Guan et al. (2015)	N/A	Tensor voting	Rectangular marking, Arrow marking, written information, zebra crossing	Yes
		Soilan et al. (2017)	N/A	Morphological operation	Rectangular marking, Arrow marking, Chevron marking, written information	Yes
Scanline Profile	Fixed thresholding	Yan et al. (2016)	Median filtering	N/A	N/A	N/A
		Chen et al. (2009)	N/A	Hough Transform, RANSAC	Solid and dashed lane marking	Yes
		Yang et al. (2017)	N/A	N/A	Lane line, zebra crossing	Yes

Once the road surface is extracted from the mobile lidar data, the road markings can be extracted based on high radiometric contrast (e.g., color, intensity) against the road pavement through either a 2D projection or a profile scanline. By projecting the data onto a 2D image, a binary image can be generated by setting a threshold of intensity to extract the road markings (Yang et al., 2012; Riveiro et al., 2015; Guo et al., 2015; Yao and Hu, 2014; Smadja et al., 2010; Toth et al., 2008). However, in addition to the material, the scanning geometry including range and incidence angle and many other factors will also affect the intensity reading from the lidar sensor (e.g., Kashani et al. 2015). For example, due to a larger range and incidence angle, the intensity of a point at the edge of the road can be lower than one acquired at the center due to energy loss with range and often a more oblique angle. To solve this problem, normalizing the intensity value based on the range and incidence angle from the trajectory can be performed, since the scan geometry is relatively consistent along a roadway with mobile lidar sensors following the roadway (Vosselman, 2009; Yan et al., 2016; Jaakkola et al., 2008; Guan et al., 2015a; Zhang et al., 2016). Another approach to eliminate this change in intensity is to set dynamic intensity thresholds instead of correcting the intensity itself (Kumar et al., 2014; Yu et al., 2015; Solian et al., 2017). Then, in the binary image, morphological operators are usually used to connect and cluster the pixels (Riveiro et al., 2015; Guo et al., 2015; Kumar et al., 2014; Yao and Hu, 2014; Jaakkola et al., 2008). Some of these methods also include a refinement or classification by recognizing different types of road markings by considering some other characteristics such as shape, size, and orientation (Yang et al., 2012; Riveiro et al., 2015; Guo et al., 2015; Zhang et al., 2016; Yu et al., 2015; Chen et al., 2009; Kumar et al., 2014; Jaakkola et al., 2008).

As an alternative to the aforementioned projection method, some methods (Chen et al., 2009; Yan et al., 2016; Yang et al. 2017) directly extract the road markings from the point clouds themselves. In this way, they could avoid the loss of precision that occurs transforming point clouds into images; nevertheless, issues arise due to the high computational cost, i.e., processing time.

2.7 ONGOING AND FUTURE RESEARCH

Predominately, pavement markings and signs have been designed as visual cues to humans for safe driving. However, computer/machine vision technologies employed in driver-assisted or autonomous vehicles also rely on these markings for their advanced navigations (Hadi 2007). These require high contrast between the marking and the pavement for efficient and reliable extraction. NCHRP 20-102, *Impacts of Connected Vehicles and Automated Vehicles on State and Local Transportation Agencies*, currently has a task (Task 6, research in progress) devoted to the following objectives:

- Define and describe the performance characteristics of pavement markings that influence the recognition ability of machine vision systems
- Provide data and recommendations to help the AASTHO/SAE working group in the development of guidelines and criteria.

Ongoing testing to support this NCHRP research project will include the evaluation of high contrast markings (e.g., black painted behind white stripes) for daytime navigation and

retroreflectivity and roadway illumination at night. The tests will also cover wet and dry conditions.

2.8 LIMITATIONS OF CURRENT LITERATURE

Several gaps and limitations were found in this review of current literature, which will be summarized in this section and used to guide much of the future work in SPR-799.

For retroreflectivity, the physics are being modeled or simulated in the systems with great effort; however, a key limitation is that measurements are done at few, discrete locations to be manageable. Given the high level of uncertainty and variability of the measurements themselves, is this modeling necessary, or can a device such as mobile lidar relatively accurately acquire that information at higher spatial resolution without following the exact geometry? Further, researchers such as Kopf (2004), Carlson (2007), and van Schalkwyk (2010) discuss several challenges with accurate retroreflectivity measurements including inaccuracies in the geometric modeling, varying conditions during data collection, difficultly in calibration, variability in the units themselves, and influence of cross slope, directionality affects, application thickness, and variability in the operator skill level.

Saetern (2016) mentions that information regarding pavement marking effectiveness is scarce. This is compounded by the fact that many DOTs and organizations historically have used approaches such as blanket replacement of pavement markings due to challenges in data collection and management for information where markings are installed, as well as for retroreflectivity data. Mobile lidar can help with both of these situations. Repeated scans can be geospatially linked so that assets can be tracked through time. This information can ultimately be used for proactive management where life of assets can be predicted.

Unfortunately, there is minimal research on calibrating mobile lidar for retroreflective readings. Most studies in radiometric calibration are focused on a single device and focus on specific object types of interest to its application. Few DOTs have mobile lidar units and no DOTs currently have a method in place to use this information for radiometric calibration of their system. Radiometric calibration is highly dependent on the device itself. Hence, the relationships observed and findings of one system do not directly transfer over to another.

Several approaches exist for extracting the markings from the intensity information in the point cloud data. One notable limitation observed in existing approaches is that many of them require a curb extraction to segment the desirable road surface. Curb extraction would be available only for specific areas, primarily roads in high density urban locations, thereby limiting the versatility of using the approach in other regions (e.g., rural). Furthermore, some methods have been developed on small or idealized datasets with minimal noise and may not scale to work effectively with larger, nosier datasets as are often collected in real-world applications. Lastly, the majority of existing approaches have focused on extraction for road asset inventory by limiting their search thresholds to only detect road markings in good condition. However, to effectively evaluate the retroreflectivity and condition of the road markings, it is desirable to extract the worn portions of the markings that are missing; otherwise, one would skew the results to indicate better retroreflectivity than reality since worn portions in poor condition would be

screened from the analysis. Chapter 3 presents an approach to extract pavement markings that overcomes many of these limitations.

3.0 ROAD MARKING EXTRACTION ALGORITHM

3.1 OBJECTIVES

Automated extraction of lane markings from the MTLS data remains an open challenge, due to variable noise and road conditions. Several approaches have been developed and are summarized in Table 2.5; however, these approaches are designed for new markings with minimal wear rather than existing markings and they also are employed for short test sections with minimal variance in highway geometry. This research addresses these challenges presenting a novel approach for efficient, reliable extraction of pavement markings, including those that have been significantly worn. Specifically, the following objectives are achieved:

1. Developing an efficient framework to automatically extract lane markings from 3D mobile lidar data that can handle a wide ran-*ge of road geometries and sensor orientations,

2. Proposing a constrained RANSAC segmentation that extracts a road surface in the absence of curb structure and can account for road curvature and grade changes,

3. Proposing a line association to consider poorly-worn lane markings such that the data can help agencies assess the marking condition,

4. Presenting a filtering method for noise using statistical analysis of the intensity distribution, and

5. Evaluating the approach under a variety of road conditions, including urban, rural, and a specifically-designed Testdeck.

3.2 ALGORITHM

3.2.1 Road surface extraction

Typically, MTLS systems collect a substantial number of laser points along the roadway. Road discretization is therefore a necessary step to reduce the computational complexity while also enabling the proposed algorithm to extract curved lane markings over a localized area. Before discretizing the road into smaller sections, the lidar data further than a distance of 10.8 m (35.4 ft) from the trajectory line are removed. This value was selected as a threshold based on typical, three-lane roadways in the U.S. Where lane widths range between 2.7 m (9 ft.) and 3.6 m (12 ft.) (USDOT, 2018). Then the remaining data are divided into smaller sections with a constant, user defined section length,Δ.

Each discretized road surface is translated and rotated to the local coordinate system such that the travel path is aligned with the y direction and then rotated by arctangent of the slope along the MTLS system travel path such that the section is more or less horizontal. To extract the road

surface, RANSAC segmentation is adopted due to its robustness against outliers (Boulaassal et al. 2007). Since the road surface is not truly planar due to the cross slope as part of the drainage design, a 2nd-order polynomial fitting, which is reported as the best approximate for the cross section of road surface data (Smadja et al., 2010), is applied based on the x and z values.

This RANSAC segmentation approach is advantageous because it enables the road surface to be extracted even in the absence of curbs; however, it can fail when the selected polynomial opens upwards (Figure 3.1-a). Hence, to remedy this problem, a constrained RANSAC segmentation is used only to select a polynomial with a negative leading coefficient. In addition, the search space is limited for finding the seed points to the x range of ± 3 m (10 ft.) from the trajectory to ensure that these points fall within the roadway. However, in some cases, due to the limited search space or complex road geometry, a single polynomial may not be properly fit with the entire road surface. Therefore, all points are divided into the left and right groups based on the extreme point to represent the crown of the road and then the RANSAC segmentation is performed separately for each group. Figure 3.1-b shows an example of the extracted road surface using the proposed segmentation.

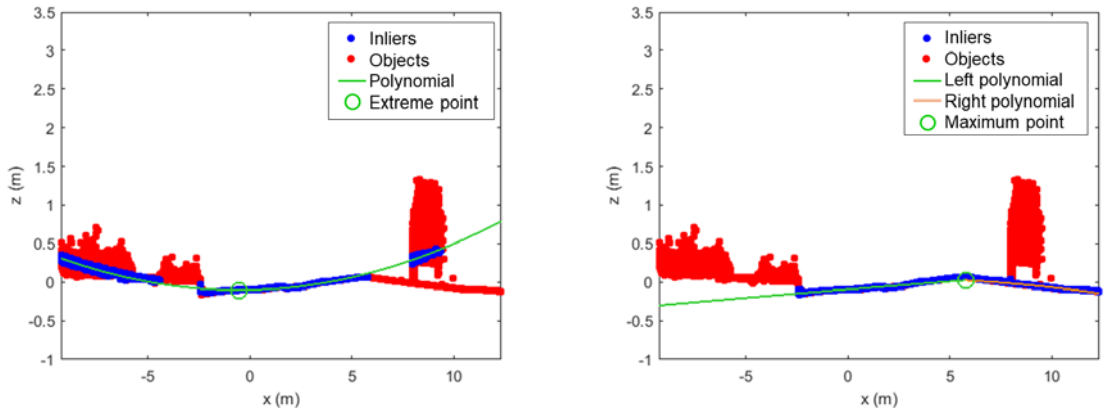

(a) (b)

Figure 3.1: Road surface extraction using RANSAC segmentation: (a) incorrect polynomial fitting and (b) double-polynomial fitting with constraints.

3.2.2 Image processing

Because the immense size of lidar point cloud often leads to time-consuming processing due to intensive computation, this study adopts a 2D projection approach to reduce the computation complexity. In this approach, the points constituting the road surface are projected onto a 2D image, which represents occupied pixels (i.e., the pixels contain at least one projected point) as mean intensity in a range from 0 to 1 and the unoccupied points as 0. It should be noted that only the intensity values are considered in the rasterization because the RGB values are very sensitive to changes in the lighting conditions such as shadows. Figure 3.2 (a) provides an example rasterized intensity images using mobile lidar data.

Subsequently, the intensity image is used to extract the road markings through image segmentation. Based on the high radiometric contrast between road markings and road

pavements, it is reasonable to assume that the intensity image is bimodal that can be segmented into two groups. The separation is achieved using the Expectation-Maximization (EM) algorithm, which determines the maximum likelihood parameters (mean and variance) of a mixture of two Gaussians (Dempster and Rubin, 1977; Zhang, 2001). Figure 3.2-b illustrates an example of the segmented image using the EM algorithm, where green and red segments indicate the high- and low-intensity groups, respectively. In this stage, areas with highly worn markings will have low contrast and may be lost with this process; fortunately, the line association process described in Section 3.2.3 will help recover many of these worn markings for extraction.

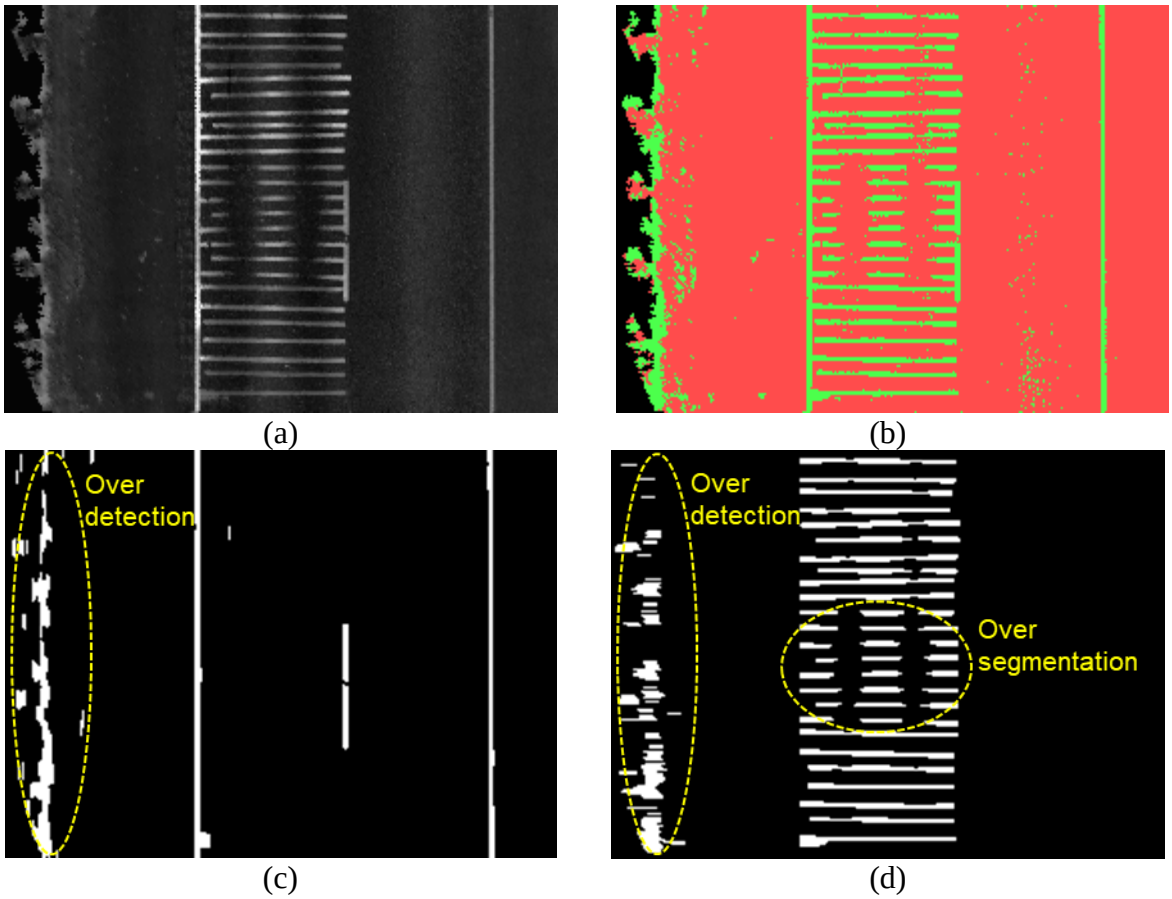

Figure 3.2: (a) Intensity image and (b) segmented image with low (red) and high (green) intensity groups; morphologically filtered (c) longitudinal and (d) transverse lane markings.

Following this step, a morphological opening operation (i.e., erosion followed by dilation) is performed to reduce noise present in the segmented image. Because properly placed lane markings are nearly linear in each discretized section, a linear-shaped structuring element is appropriate not only for filtering small noise objects but also enlarging the straight lane markings (Kumar et al. 2014). The opening operation is performed in two ways to separate the longitudinal and transverse lanes, which enables the later line-association and noise-filtering phases to be conducted independently and effectively. The morphologically filtered longitudinal and transverse lane markings, however, may suffer from over-detection (Figure 3.2-c and 3.2-d) or over-segmentation (Figure 3.2-d) due to noise in image segmentation or poorly worn

markings, respectively. The following steps include line association and gap filling, which are designed to achieve the correct segmentation. Noise filtering then identifies and filters the over-detected lane markings.

3.2.3 Line association and gap filling

The extracted lane markings may be over-segmented, principally from shadows created by moving vehicles between the scanner and the pavement marking or from worn portions created by moving vehicles passing over the markings. Line association is an important step to permit a proper segmentation by linking the segments which topologically lie on the same lane. First, a skeletonization yields a 1-pixel-wide line for each segment by iteratively reducing pixels composing a segment (Jung et al. 2017). A labeling process is then performed to determine which pixels are connected to other pixels based on the number of connected neighborhoods (Jung et al. 2014; Mozos et al. 2007) (Figure 3.3-a and 3.3-b). For each connected segment, the Hessian line model is computed as follows

$$\boldsymbol{x\cos\alpha + y\sin\alpha - r = 0} \qquad \textbf{(3-1)}$$

Where *x* and *y* are projected coordinates constituting the skeletons and line parameters α and r are orientation and distance from the origin, respectively. Figures 3.3-c and 3.3-d show an example of the estimated line model for each segment.

Next, the conditions of line association are evaluated in three ways: orientation, adjacency, and linearity. First, a symmetric matrix is computed to find the pair of lines with the minimum angular difference in orientations. Second, if the angular difference is less than the pre-defined threshold (θ), the condition for two candidate lines is further evaluated with their adjacency to see if the perpendicular feet of the shorter line on the longer one are less than the pre-defined minimum distance threshold (μ). If the two candidate lines satisfy the second condition, they are evaluated with the linearity criterion; by using all of the points constituting two lines, a new line model is computed to check whether the mean of the orthogonal distances is less than the predefined threshold (η). The two candidate lane markings satisfying the above three conditions are identified as the same marking (Figure 3.3-e and 3.3-f). After line association, any lines less than the minimum length (τ) are discarded as noise. The proposed line association requires 4 parameters for evaluations: those are, the angle (θ), orthogonal distance (η), minimum distance (μ), and minimum length (τ) thresholds. Among which, η, μ, and τ are available in specifications by transportation agencies, (e.g., Oregon DOT, 2011) corresponding to the orthogonal distance (0.1 m or 0.3 ft.) between two parallel double longitudinal markings, and the interval (1.8 m or 5.9 ft.) and the length (0.6 m of 2 ft.) of a series of dotted lane markings, respectively. In practice, however, the threshold μ and τ are loosely set to 1.5 and 0.5 m (4.9 and 1.6 ft.), respectively to avoid under-detection with the assumption that it is easier to clean out false detections than to digitize missing segments. Section 3.3 will evaluate the selection of the angle threshold (θ) in more detail.

As a consequence of line association, the topologies among the lane-marking segments are reconstructed. Therein, one can see that some lane markings, particularly the transverse

markings in Figure 3.3-b, are worn significantly in the predominant wheel paths of moving vehicles. Since the worn part is also an important indicator representing the conditions of appearance and retroreflectivity, gap filling connects fragmented segments on the topologically-same marking. Initially, a convex hull method is applied to find the smallest convex polygon that contains all the segmented pixels (Sonka et al. 2014). However, this approach often yields over- or under-estimates of the true areas. In order to provide the regularized lane markings, a skeletonization followed by a dilation operation is performed. The resulting markings (Figure 3.3-g and 3.3-h) may still include some noise that can be filtered in the following noise filtering phase.

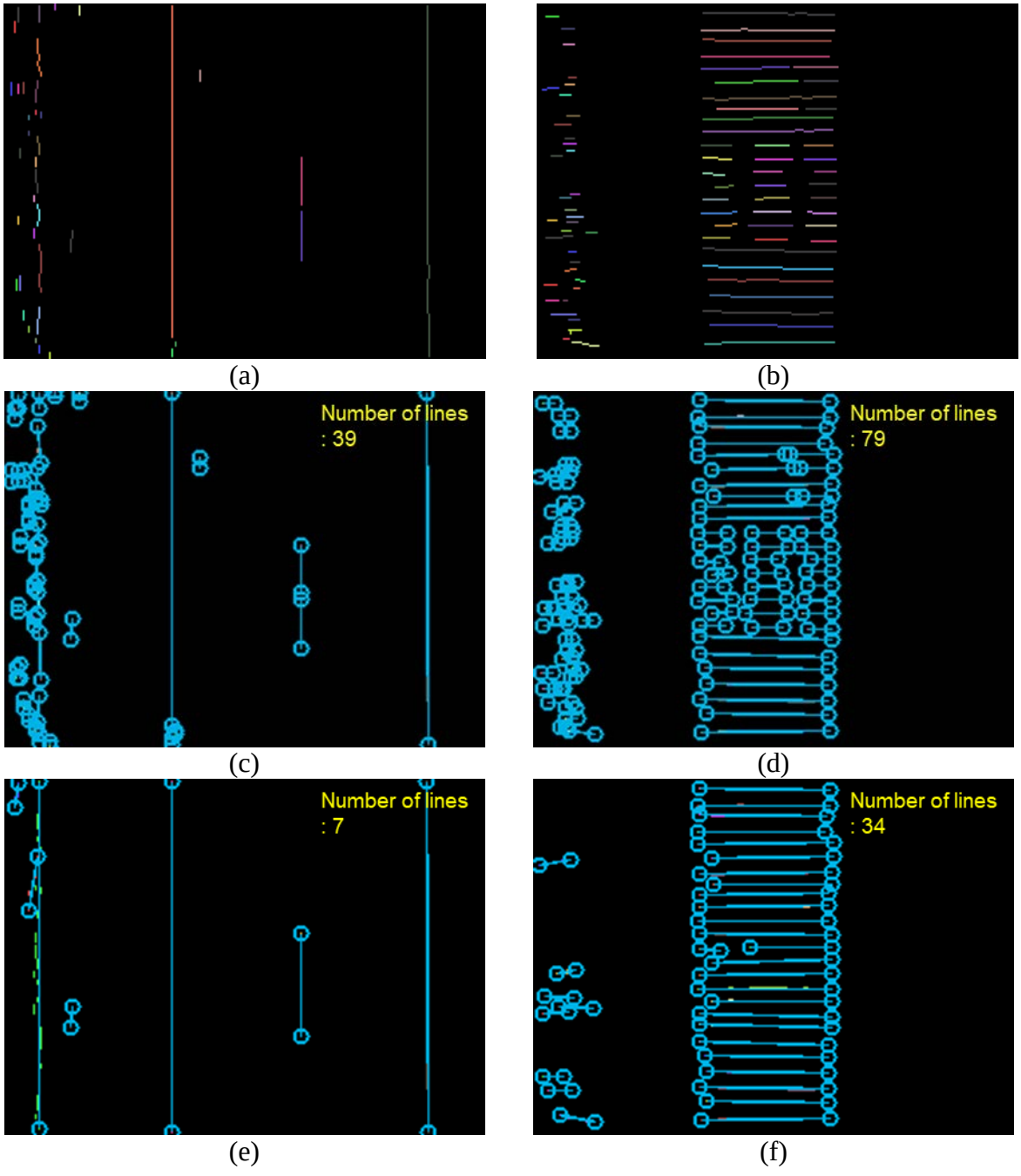

(a) (b)

(c) (d)

(e) (f)

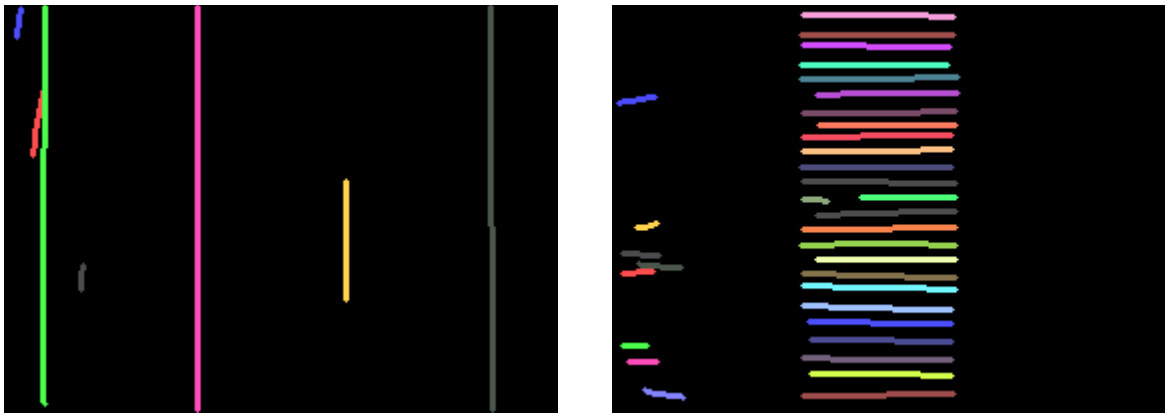

(g) (h)

Figure 3.3: Example of line association for longitudinal (a, c, e, g) and transverse (b, d, f, h) lane markings: (a) and (b) are skeletonized lane markings; (c) and (d) are estimated; (e) and (f) are associated line models; (g) and (h) are gap-filled lane markings.

3.2.4 Noise filtering and refinement

Image segmentation is sensitive to noise with high intensity, and thus may result in over-detection of lane markings. Because the lane marking and the surrounding pavement have a high contrast of intensity values, they tend to represent a bimodal distribution compared to the noise object, which lends itself particularly well as an indicator for detecting noise. The points composing a lane marking are readily extracted from the original lidar data according to their projected 2D locations on the marking image. In order to evaluate the intensity distribution of the extracted points, the dip test statistic is adopted (Hartigan and Hartigan, 1985), where the dip is a measure to determine if a distribution follows a unimodal or bimodal pattern; a higher dip value is more likely to be bimodal and vice versa. To assess significance levels for the dip test, bootstrapping creates a sampling distribution from the uniform distribution. Bootstrapping is often regarded as the optimal choice for null distribution (Hartigan and Hartigan, 1985). The lane markings with the number of points over the range are evaluated with a maximum bootstrap samples of 10,000. An input distribution with the dip value greater than the p-value (0.05) is considered a noise within the unimodal distribution (Figure 3.4-a). In other words, the p-value is used to confirm that a pavement marking exists within 95% confidence.

Subsequently, the points corresponding to lane markings from the original 3D point cloud can be extracted using the noise-filtered image. Nevertheless, the extracted marking may still include pavement points within the area that it covers on the road because of the laser footprint which may slightly overlap with the stripe and result in a higher intensity value. In order to remove the unwanted points while preserving its worn portions, a least-squares line-fitting refinement is conducted as shown in Figure 3.4-b. First, assuming a bimodal distribution, the Gaussian mixture modeling with EM algorithm is performed for the intensity values on the stripe. The Hessian line model in Equation 3.1 is then fitted to a set of points in the high-intensity group. Next, the points closer to the line fit than half the estimated stripe width (0.05 m or 0.16 ft) are segmented and transformed back into their original coordinates to produce the refined lane markings (Figure 3.5) in a global coordinate system.

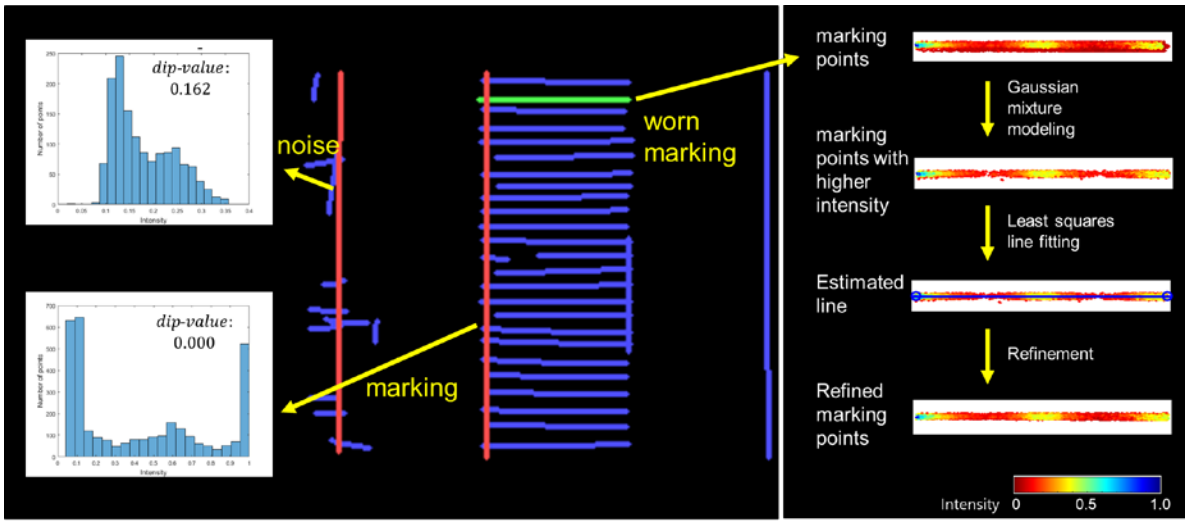

(a) (b)

Figure 3.4: (a) Noise filtering with the dip test and (b) refinement with the least-squares line fitting.

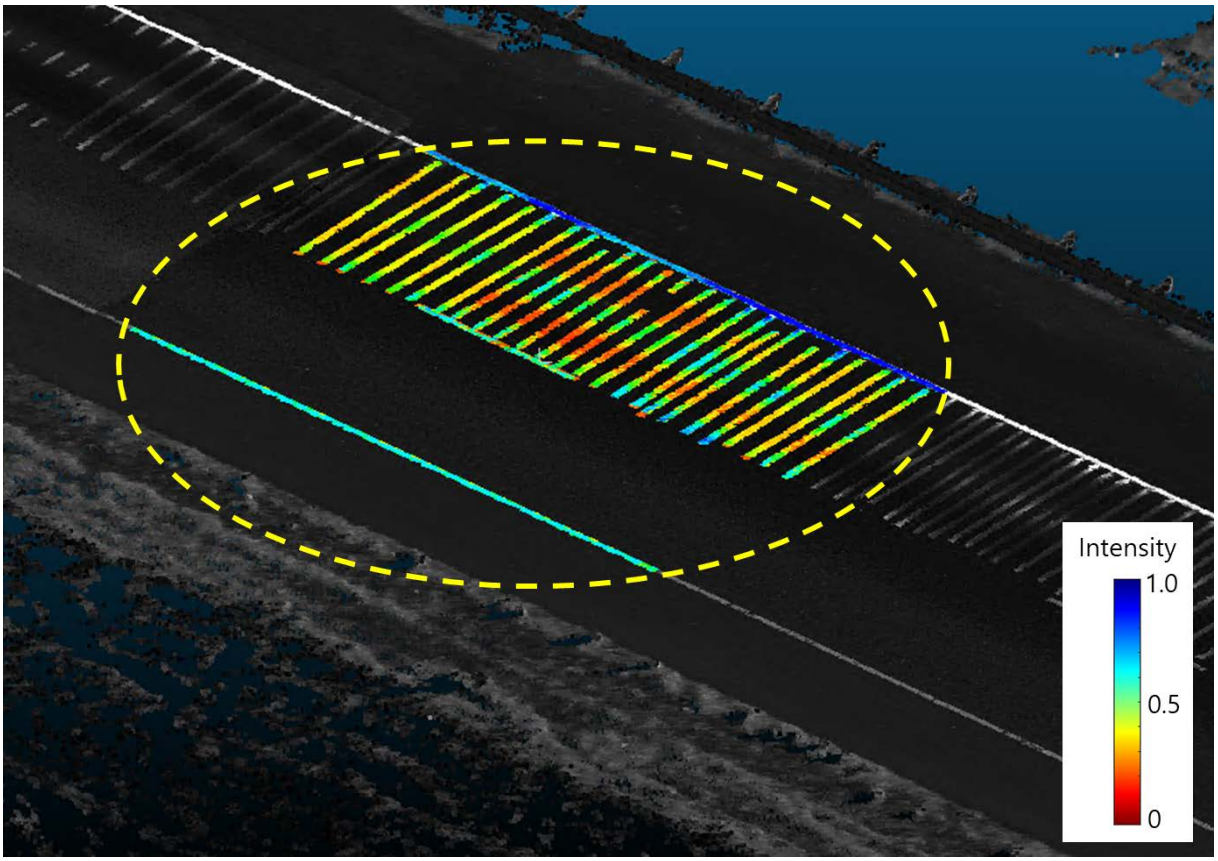

Figure 3.5: Filtered and Refined lane markings presented with a color scale based on intensity values overlain on road surface lidar data with a grayscale color scale based on intensity values.

3.3 EXTRACTION QUALITY EVALUATION

In order to check the sensibility of the results, the algorithm has been run with different values for the section length (Δ), pixel size (s), angle threshold (θ), noise filtering, and vehicle speed (v). Table 3.1 provides the result of a sensitivity analysis using two data sets acquired in Testdeck Experiment III (180 m or 590 ft.) and the Oregon DOT mobile lidar test course in Salem, OR (460 m or 1510 ft.). Chapter 6.0 will offer a detailed description of Testdeck Experiment III. The project team implemented the algorithm using MATLAB, and performed the experiment on a computer with Intel Xeon CPU (2.4 GHz, 24.0 GB of RAM). The time consumption shown in the test excludes the time loading the input files including the lidar and trajectory data in LAS1.2 and ASCII format, respectively. The extracted markings were validated with reference to the manually-detected ones. Some stripes, which are too faded to be distinguished or shadowed by passing vehicles, were excluded from the validation. In order to evaluate the performance of the proposed algorithm with employing different parameter combinations, the extracted lane markings are compared with manually detected markings (i.e., the ground truth). Two types of false detection can happen: false positives and false negatives. A false positive is a detected marking that is not in the ground truth (i.e., an over-detection). A false negative is a marking in the ground truth that is not detected (i.e., an under-detection). Based on these definitions, three metrics for quantitative evaluations are computed, as follows:

$$\boldsymbol{precision} = \frac{\boldsymbol{total\ number\ of\ true\ positives}}{\boldsymbol{sum\ of\ true\ positives\ and\ false\ positives}} \tag{3-2}$$

$$\boldsymbol{recall} = \frac{\boldsymbol{total\ number\ of\ true\ positives}}{\boldsymbol{sum\ of\ true\ positives\ and\ false\ negatives}} \tag{3-3}$$

$$\boldsymbol{F1\ score} = \boldsymbol{2} \times \frac{\boldsymbol{precision} \times \boldsymbol{recall}}{\boldsymbol{precision} + \boldsymbol{recall}} \tag{3-4}$$

3.3.1 Section length, Δ

The road data is discretized with a constant section length (Δ) along the direction of MTLS travel path. Table 3.1 indicates how the section length affects the processing time and the performance. A larger section length leads to more time consumption because it quadratically increases the computational complexity in the line association phase. In terms of the F1 score, the section length of 10 m (32.8 ft.) was found to be the best for both data sets. This is principally due to the fact that, compared to the section length of 5 m* (16.4 ft.) (The asterisks, *, indicate the cases using the control variables), some longitudinal noises are more likely to be aggregated and filtered in the noise filtering phase, thus resulting in the increase in precision. However, the recall rates gradually degraded with the increase of the section length because it increases both the computational complexity and failure rate in the line association phase. Compared to the

Testdeck, the Salem data are more susceptible to the increase in the section length; with the section length greater than 10 m (32.8 ft.), the Salem results rapidly degraded in both the precision and recall rates because the curved road data cannot hold the linear assumption as the section length increases. Therefore, it is recommended using the section length of 10 m (32.8 ft.), which permits the best performance for both data sets without requiring expensive computational loads.

3.3.2 Pixel size, s

Pixel size greatly influences the processing time because the image size quadratically increases with the decrease of pixel size. However, pixel size should not be greater than the minimum orthogonal distance between double markings (0.1 m or 0.32 ft. in Oregon Department of Transportation 2018); otherwise, part of double markings may be aggregated into one pixel. We investigated the processing time and the performance with the different pixel sizes of 0.025, 0.05*, and 0.1 m (0.08, 0.16, and 0.32 ft.). Notably, though at the cost of excessive time consumption with the smallest pixel size of 0.025 m (0.08 ft.), the performance of proposed approach was greatly degraded, particularly for the Salem data. This degradation occurs because a too-small pixel size can result in large data gaps in the scan data, which increase with distance from the scanner. These gaps cannot be reliably inpainted (interpolated) in the rasterization phase. Minimization of the processing time was achieved with the pixel size of 0.1 m (0.32 ft.) for both data sets, but the recall rates greatly degraded because a too-large pixel would contain intensity information from multiple objects. Therefore, the pixel size of 0.05 m (0.16 ft.) was recommended as the optimal value, which allows a balance between processing time and performance for road marking extraction.

3.3.3 Angle threshold, θ

The angle threshold impacts the success rate of line association: with a larger angle threshold, more line segments can be merged, but it also may result in the decrease in recall rate owing to the over-association. Basically, the different segments in the same lane marking have more or less the same orientations that can be associated with small angle difference. In practice, however, the angle threshold should be large enough to cover arbitrarily-oriented segments that could have some distortions due to worn portions. We investigated the influence of angle thresholds ranging from 5°* to 20° with an interval of 5°. In Table 3.1, it can be seen that changing the angle threshold (θ) had a nearly negligible impact on the processing time. In terms of the F1 score, however, the angle threshold of 15° proved to be the best fit for both data sets.

3.3.4 Noise filtering

The discretized road data may include other objects with high intensity on roadside, which can incur over-detections (false positives) in the image segmentation phase. To separate the false positives from the true lane markings, the intensity contrast between the lane marking and its surrounding pavements was evaluated using the dip test. Table 3.1 includes the test results with and without the dip-test noise filtering. The result indicates that, without the noise filtering, the performance is skewed toward higher recall rates for both data sets because the algorithm is directed toward tolerating false positives than false negatives. The improved F-1 score illustrates

that implementing this process to filter noise from the data effectively balances precision and recall through its quality check with a minor (or marginal) increase in processing time.

Table 3.1: Sensitivity Analysis of the Road Marking Extraction Algorithm

Data	Test variables		Time (sec)	Precision (%)	Recall (%)	F1 score (%)	Control variables				
							Section length	Pixel size	Angle threshold (°)	Noise filtering	Vehicle speed (mph)
Testdeck III	Control variables (*)	-	135.3	91.4	89.8	90.6	5 m (16 ft.)	0.05 m (2 in)	5	✓	25
Salem		-	216.3	89.5	88.6	89.0					
Testdeck III	Section length (Δ)	10	153.4	97.5	88.7	92.8	-	0.05 m (2 in)	5	✓	25
		15	181.2	94.6	87.5	90.9					
		20	205.1	94.7	85.6	89.9					
Salem		10	232.9	91.8	90.1	90.9					
		15	242.0	88.2	87.8	88.0					
		20	251.0	83.2	78.5	80.8					
Testdeck III	Pixel size (s)	0.025	335.2	92.6	85.3	88.8	5 m (16 ft.)	-	5	✓	25
		0.1	118.8	88.1	79.7	83.7					
Salem		0.025	479.6	78.5	56.3	65.5					
		0.1	179.5	90.1	76.8	82.9					
Testdeck III	Angle threshold (θ)	10	134.4	92.1	92.5	92.3	5 m (16 ft.)	0.05 m (2 in)	-	✓	25
		15	138.9	92.5	93.1	92.8					
		20	134.9	90.8	90.0	90.4					
Salem		10	217.1	91.5	88.4	89.9					
		15	216.7	93.6	88.8	91.2					
		20	216.4	91.8	87.5	89.6					
Testdeck III	Noise filtering	X	134.1	84.6	94.9	89.4	5 m (16 ft.)	0.05 m (2 in)	5	-	25
Salem		X	214.9	85.7	90.8	88.2					
Testdeck III	Vehicle speed (v)	35	91.7	91.3	89.0	90.1	5 m (16 ft.)	0.05 m (2 in)	5	✓	-
		45	89.8	86.7	74.4	80.0					
		55	108.2	79.7	70.0	74.5					
Testdeck III	Optimal variables	-	155.9	95.6	91.0	93.3	10 m (33 ft.)	0.05 m (2 in)	15	✓	25
Salem		-	231.8	95.1	95.5	95.3					

* indicates cases using the control variables.

3.3.5 Vehicle speed, v

The vehicle speed of mobile lidar scans can greatly affect the marking extractions. Typically, it is desirable to collect lidar data with low speed because high speed data collection can increase the space between scan lines, and thus cause loss of information. In order to evaluate the sensitivity of the algorithm to the vehicle speed, we compared Testdeck III data captured with different speeds of about 25*, 35, 45 and 55 mph. In Table 3.1, the test indicated that the performance degradation is not significant until the vehicle speed reached 35 mph while the processing time is reduced due to the reduced data size. With the vehicle speed equal to or greater than 45 mph, however, the performance radically degraded most likely because the gaps between scan lines are too large to be mitigated by the inpainting algorithm, thus increasing the probability of false positives (in case where the unoccupied pixels on the pavements are inpainted with the nearby markings) and false negatives (in case where the unoccupied pixels on the markings are inpainted with the nearby pavements). Extraction of the transverse markings is affected much more significantly than the longitudinal ones; hence, high speeds greater than 35 mph are clearly not preferable for detecting transverse markings. For longitudinal stripes, extractions were successful across the range of traffic speeds tested, which cover typical speed limits for most of Oregon's highway network.

For ordinary collection efforts, Oregon DOT's current practice is to follow speed limits and keep speeds as consistent as possible (e.g., cruise control) when collecting data. For specialized collections requiring the vehicle to travel slightly or significantly slower than posted speed limits, warning lights and traffic control are utilized, respectively. Vehicles in adjacent lanes that pass the MTLS system will result in some data dropouts. Usually, only small portions of the stripes will be blocked by a vehicle; however, larger trucks that take longer to pass will block the stripe for longer lengths. Potential mitigation strategies include additional passes or capturing data during lower traffic periods.

3.3.6 Optimal parameters

Finally, with the optimal parameters obtained in the sensitivity analysis, the precision and recall rates were computed for both data sets. Table 3.1 shows that the performance of the proposed method with the optimal parameters outperforms the other combinations. The optimal parameters discovered are: 10 m (32.8 ft.) for the section length (Δ), 0.05 m (0.16 ft.) for the pixel size (s), 15° for the angle threshold (θ), with noise filtering (O), and 25 mph for the vehicle speed (v).

4.0 TESTDECK EXPIREMENT I

4.1 TEST OBJECTIVES

The first data collection at the Testdeck was completed within weeks of the project start to serve as a preliminary experiment to guide the development of the main Testdeck experiment (Testdeck II). The experiment had the following objectives:

- Serve as a proof of concept that mobile lidar would provide meaningful results of differences in pavement marking retroreflectivity
- Evaluate data density obtained on striping based on vehicle speed and sensor orientation
- Correlate lidar intensity measurements with handheld retroreflectometer using measurement processes typically conducted on the Testdeck by Oregon DOT staff.
- Observe the Testdeck evaluation process performed by Oregon DOT.
- Perform a preliminary look at lidar intensity readings on signs
- Provide preliminary data to design the main Testdeck Experiment (II).

4.2 TEST DESCRIPTION

Collection of mobile lidar data from Oregon DOT's Testdeck site (Figure 4.1) using Oregon DOT's Pegasus:Two system with a Z+F profiler 9012 (Figure 4.2) was performed on July 28, 2016 starting at 8am. The Testdeck is located on the westbound right travel lane of Highway OR-22 between mileposts 12.25 and 12.5 (44˚ 49' 32" N, 122˚ 48' 49" W), outside of Salem and near Stayton. This roadway has two lanes travelling westbound with a large median dividing the eastbound traffic as well as a large shoulder (Figure 4.1). Testdeck is an area strategically chosen by Oregon DOT because it starts on a joint where concrete asphalt concrete (AC) ends and Portland Cement Concrete (PCC) pavement starts (van Schalkwyk, 2010). Testdeck trials are conducted every other year, where vendors are asked to place two lines for each product they want evaluated transversely on the right-most lane (known as the 'B' lane). A few control lines are also placed with the group to assist with grading. The transverse lines are evaluated over time to determine their resistance to depredation as traffic passes over the markings.

The first test captured mobile lidar and retroreflectivity information on transverse as well as longitudinal pavement markings. The pavement marking team, led by Joel Fry, performed retroreflective measurements (Figure 4.3) on all transverse stripes on the deck following their protocols. Five handheld retroreflectometer readings were collected per transverse line in the middle of the line, which is the lesser worn portion of the stripe, and averaged. The approximate

location was captured with RTK GNSS for comparison to the mobile lidar data. Preliminary correlations were developed from these data and showed reasonable agreement.

In addition to pavement markings, this first experiment provided data to evaluate the ability of the system to capture signs to plan for a future test on sign inventories (Volume II).

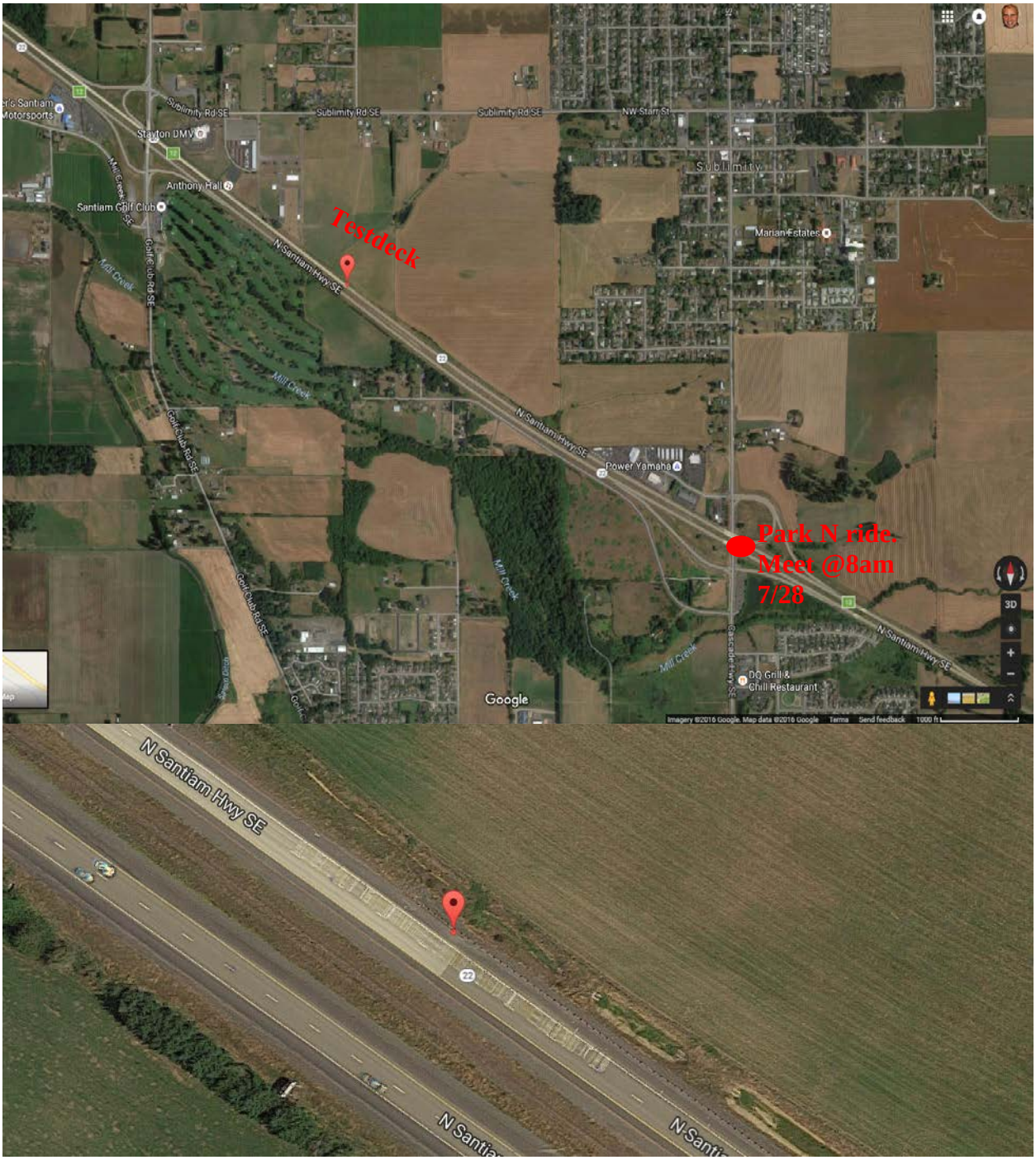

Figure 4.1: Location map (a) of Testdeck site and Park N'Ride on Highway 22 with close-up view (b)

Figure 4.2: Oregon DOT's Leica Pegasus:Two mobile lidar system collecting data on the Testdeck.

Figure 4.3: Acquisition of retroreflectivity readings with a Delta LTL-X Handheld retroreflectometer.

For this first evaluation, the project team obtained mobile lidar data using different truck speeds and sensor orientations using Oregon DOT's Leica Pegasus:Two (Figure 4.2). (Note that for this test, Oregon DOT was only operating with a single profiler solution on the mobile lidar unit). Data at each speed was collected twice: once with the sensor rotation of 0° and another one with -30°. At that time, Oregon DOT normally operated the MTLS system in 0° orientation, which provides profiles along the roadway perpendicular to the travel direction. However, the -30° orientation provides the ability to capture information on the front face of street signs in both directions in a single pass. Table 4.1 shows the scanning settings for each pass of the lidar data collection.

Table 4.1: Test Configurations and Schedule

Pass #	Start Time	Speed (mph)	Profiler unit rotation (°)	Oregon DOT traffic control required (Y/N)	Approximate time (mins)
0	8:00	N/A	Meet at site, onsite safety briefing, review MTLS procedure, and perform MTLS initial site calibration process	N	40
1	8:10	45	0 (normal orientation)	N	10
2	8:20	55	0 (normal orientation)	N	10
3	8:30	55	-30	N	10 + rotate scanner
4	8:40	45	-30	N	10
5	8:50	35	-30	Y	10 + placing traffic control
6	9:00	25	-30	Y	10
7	9:10	35	0 (normal orientation)	Y	10 + rotate scanner
8	9:20	25	0 (normal orientation)	Y	10
9*	9:30	25	0 (normal orientation)	Y	10

**Pass 9 was a repeat pass since the data were not recorded on Pass 8 due to a blunder.*

Considering the rotation speed of the Z+F profiler on the Pegasus system (200 revolutions per second), transverse orientation of the test stripes, and the width of pavement stripes, the project team collected data with lower truck speeds in order to obtain enough sample points on each stripe. Mobile lidar acquisition speeds greater than 25 mph were insufficient for detailed coverage at the 0° orientation for the transverse stripes, which are parallel to the scan lines. Stripes can be missed when the profile spacing exceeds the width of the stripe, which is generally 4 in. However, the -30° orientation provides adequate coverage on the transverse stripes because each scan line intersects the stripe at an angle, avoiding this problem. In order to evaluate data quality captured on longitude stripes in faster speeds, the project team also collected data with speeds of 45 and 55 mph; however, they have limited coverage on the transverse striping with the 0° orientation (Table 4.2).

Table 4.2: Calculated Profile Spacing for Several Vehicle Speeds with MTLS Configured in the 0° Orientation

Speed (mph)	Speed (m/s)	Profile Spacing	#Profiles per stripe
5	2.2	0.011 m (0.43 in)	13.6
10	4.5	0.022 m (0.87 in)	6.8
15	6.7	0.034 m (1.34 in)	4.5
20	8.9	0.045 m (1.77 in)	3.4
25	11.2	0.056 m (2.21 in)	2.7
30	13.4	0.067 m (2.64 in)	2.3
35	15.6	0.078 m (3.07 in)	1.9
40	17.9	0.089 m (3.50 in)	1.7
45	20.1	0.101 m (3.98 in)	1.5
50	22.4	0.112 m (4.41 in)	1.4
55	24.6	0.123 m (4.84 in)	1.2

The order of data collection passes was designed for efficiency. In order to avoid blocking a lane during morning traffic rush hours, the project team started with high-speed passes in the morning (approximately 9 am). Once the high speed data collections were completed, the project team ran low-speed paths which required traffic control to block the lane using signs and cones. Each pass took approximately 10-15 minutes to complete, including the time required for turning around. Only a few minutes were required to switch the sensor rotation from 0° to -30°.

In between each pass, the vehicle turned around at the next exit on the roadway, Exit 12, before returning to the Testdeck area. Scanning was continued to capture the data from the Eastbound return travel as well (at 55 mph each time) in an effort to provide additional data to support the analysis even though it was on the opposite side of the road. Ultimately, the view of the Testdeck area was too limited from the eastbound passes for the analysis.

After completion of the passes, the research team downloaded and commenced processing the MTLS data. The project team archived a copy of all source files (GPS, IMU, scanner data streams) from the collection as well as the processed (georeferenced) scans in ASPRS LAS 1.2 format that were later provided by Oregon DOT. For all Testdeck Experiments, the measurements were geo-referenced using the same coordinate system, OCRS Salem Zone NAD83 (2011) Epoch 2010.00 (Unit: Meters).

Upon completion of the MTLS surveys, the pavement marking team commenced their work on the test site of obtaining retroreflective and other quality metrics. While the pavement marking team collected their measurements, the project team captured RTK GNSS coordinates near the center of each stripe (10 second occupations). Note that given the speed at which the handheld retroreflectometer operated, the RTK GNSS was not able to keep up with the pace, so the project team had to estimate the measurement locations for reference. Each point was tagged with the ID of each stripe so that the data could be linked.

Multiple photographs clearly identifying the stripe and ID were captured along the entire segment of the Testdeck for reference and to aid with data interpretation.

4.3 TEST RESULTS AND ANALYSIS

Evaluations of signs captured during this test will be discussed in Volume II. Initial correlations were developed using the data from this experiment and presented to the Technical Advisory Committee (TAC); however, they were superseded by data from Testdeck II and Testdeck III for the radiometric calibration process described in Section 10.0 and are not included in this report to avoid confusion. The preliminary data in this test (Figures 4.4, 4.5, and 4.6) provided satisfactory qualitative results that the mobile lidar system could distinguish between sections of stripes with the range of lower (more wear) and higher reflectivity. In particular, typical intensity values for asphalt (~0.10) and concrete (~0.15) were determined (Figure 4.5). Table 4.3 summarizes range and incidence angle values for the test. In addition, the point density in the datasets obtained in different speeds (25 and 55 mph) and scanner orientations (0° and -30°) is compared to determine the optimal speed and orientation for the Testdeck II and Testdeck III (Figure 4.7). Georeferencing errors are shown in Figure 4.8.

Table 4.3: Summary of Range and Incidence Angle Values for Data Obtained on Pavement Markings for Different Mobile Lidar Configurations

Lane	Parameters	Scanner Orientation		
		30°	**0°**	**-30°**
Left	Range	4.39 – 9.29 m (14.4 – 30.5 ft.)	3.67 – 6.96 m (12.0 – 22.8 ft.)	3.54 – 6.53 m (11.6 – 21.4 ft.)
	Incidence Angle	55.3 – 74.4°	47.1 – 69.0°	45.0 – 67.5°
Right	Range	3.54 – 4.22 m (11.6 – 13.8 ft.)	3.54 – 4.06 m (11.6 – 13.3 ft.)	3.54 – 4.22 m (11.6 – 13.8 ft.)
	Incidence Angle	45.0 – 61.0°	45.0 – 52.0°	45.0 – 61.0°

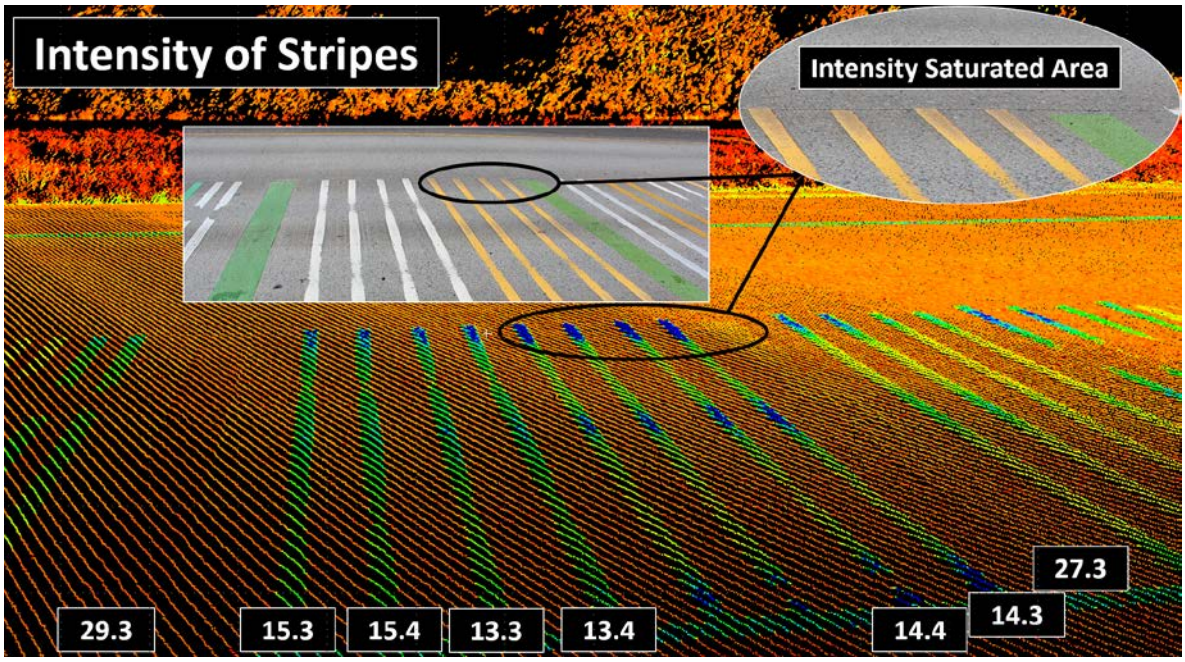

Figure 4.4: Example data colored by intensity values with Stripe IDs and photographs for comparison. Blue indicates high intensity while red indicates low intensity.

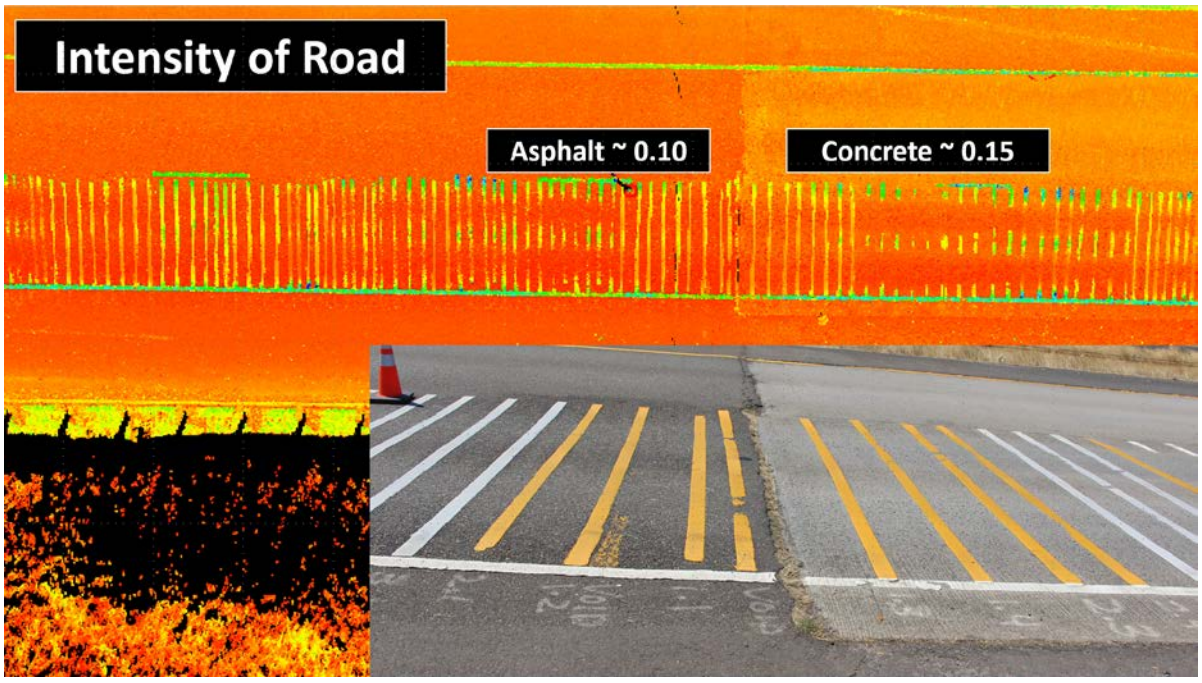

Figure 4.5: Example plan view of data at Testdeck at the asphalt/concrete interface colored by intensity values. Blue indicates high intensity while red indicates low intensity. An oblique photograph at the interface is included for reference purposes. The figure shows typical intensity values for asphalt (~0.10) and concrete (~0.15).

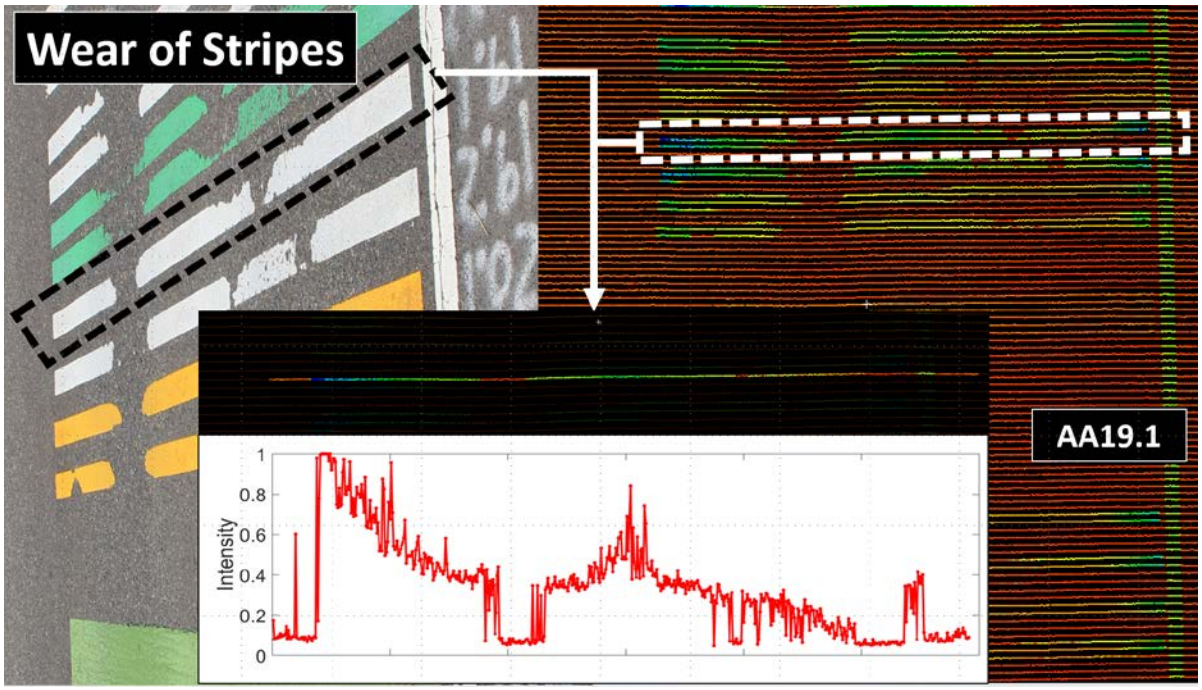

Figure 4.6: Example plan view of data at Testdeck near stripe 19.1 in the asphalt. Blue indicates high intensity while red indicates low intensity. An oblique photograph at the interface is included for reference purposes. Intensity values across a profile for stripe 19.1 are included showing higher wear at the locations of the wheel paths.

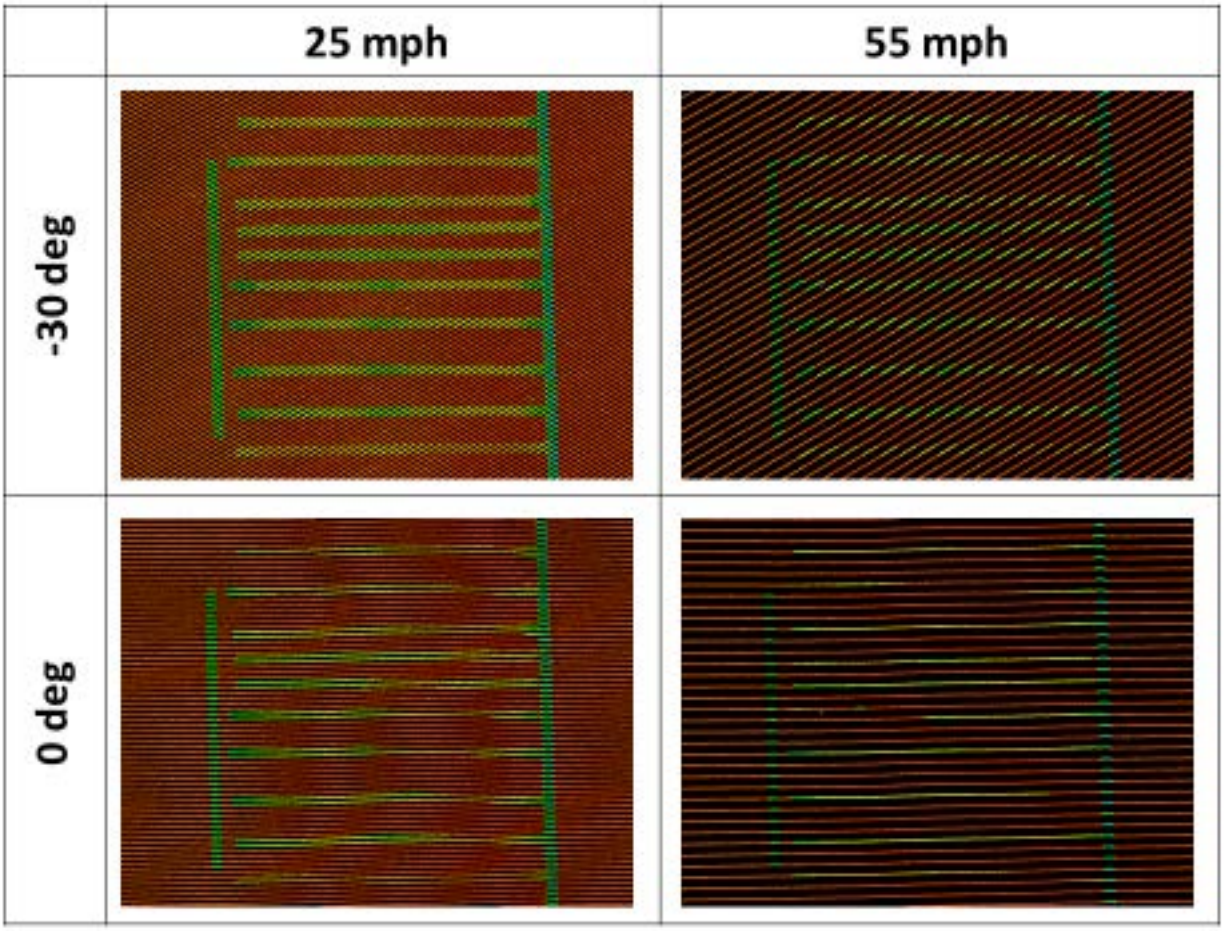

Figure 4.7: Comparison of point density in terms of speed and scanner orientation.

4.4 TEST LIMITATIONS

This test provided several insights that helped guide the subsequent future tests:

- It was difficult to for the RTK GNSS crew to keep up with the retroreflectometer crew, so locations of the retro reflectometer readings on the stripes were approximate.
- An approximately 5 cm vertical offset was observed between the MTLS and RTK GNSS data (Figure 4.8). Horizontally positioning was within 1-2 cm, as expected.
- Minor data loss from cones blocking stripes was observed.
- Visualization of the data was slightly affected by cars parked in the shoulder.

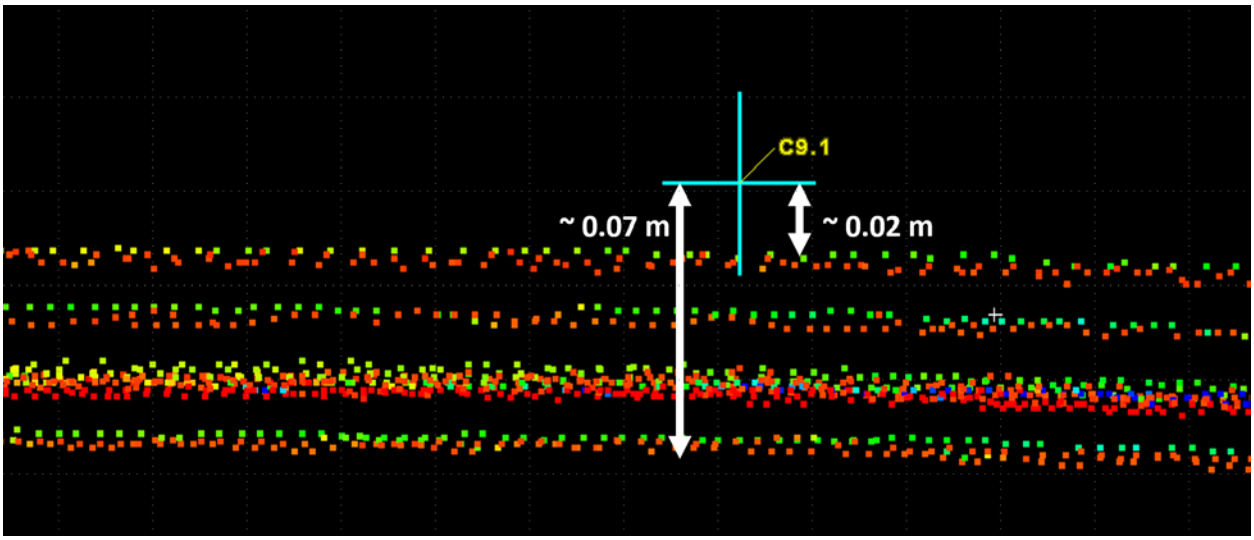

Figure 4.8: Example of the unconstrained (i.e., direct geo-referencing solution only) mobile lidar data for several passes compared with the RTK-GNSS coordinates.

Chapters 5 and 6 describe additional experiments completed on the Testdeck.

5.0 TESTDECK EXPIREMENT II

5.1 TEST OBJECTIVES

Testdeck II was designed based on lessons learned from Testdeck I. This experiment had the following objectives:

1. Test radiometric correction for MTLS data with different ranges and angles of incidence.

2. Demonstrate the possibility and limit of evaluating retroreflectivity using MTLS intensity.

3. Test the robustness of retroreflectivity measurements using the retroreflectometer.

4. Explore relationship between intensity value from MTLS data and retroreflectivity from retroreflectometer considering different colors and materials.

5. Set up control points on the site for the test for improved MTLS accuracy.

5.2 TEST DESCRIPTION

The second Testdeck test was completed on September 13, 2016. Based on lessons learned from Testdeck I, special considerations were implemented:

1. Traffic cones were not located directly over a stripe whenever possible.

2. Field crews avoided parking vehicles in the shoulder adjacent to the Testdeck during testing, whenever possible. Vehicles were parked east or west of the Testdeck in the area still protected by traffic control.

5.2.1 MTLS

For the lidar data acquisition in this second experiment (Table 5.1), the project team collected data on the Testdeck using the mobile lidar system (Leica Pegasus:Two) with Oregon DOT on both traffic lanes and the shoulder in different orientation settings (-60°, -30°, 0°, 30° , and 60°). In this way the project team covered the entire area of interest with different view angles for testing the radiometric calibration methods. For running mobile lidar on the left lane, the project team collected data at a slower but safe speed using hazard lights. After two passes on the left lane with -30°, and 30° orientation setting, the traffic control was setup to block the right lane where the Testdeck is located. Then the project team kept the Testdeck and the shoulder clear to run the two passes on the shoulder with the -30°, and 30° orientation setting at a speed of 25 mph. Next, five passes on the right lane with –60°, 30°, 0°, 30°, 60° orientation with a speed of 25 mph were performed. After confirming all 9 passes were collected properly, a copy of the

raw data was downloaded to a USB drive provided by OSU and another copy taken to Oregon DOT for subsequent processing (geo-referencing).

Table 5.1: Summary of Data Collection for Mobile Lidar System

Pass #	Lane	Orientation (°)	Speed (mph)
1	Left	+30	25
2	Left	-30	25
3	Right Shoulder	+30	25
4	Right Shoulder	-30	25
5*	Right	+60	25
6	Right	+30	25
7	Right	0	25
8	Right	-30	25
9	Right	-60	25

**Note that that a system exception occurred during the first pass on the right lane. It was resolved by restarting the system, creating a new mission and reinitializing the system and the pass was repeated.*

5.2.2 Control Points:

Because the mobile lidar system employs a direct geo-referencing solution, it can typically have about 5 cm of positional uncertainty, primarily in the vertical (confirmed in the Testdeck I Experiment). The project team set control points to improve the geo-referencing of the MTLS data to match the control used for obtaining the locations of the retroreflectivity measurements. The project team set up 9 control points (CP01 - CP09) for this test (Figure 5.1). CP03 and CP07 are temporary control points used to improve the geometry; however they are not visible from the scanner. The other control points are permanent markings and could be used for the following tests. CP01 and CP09 consist of painted chevrons from a template by Oregon DOT prior to the MTLS passes so that they could be observed by all the passes for merging the data. In the field, once the passes on the left lane was completed and the traffic control was set up, the project team set up the permanent control points (CP02, CP04, CP05, CP06, CP08) by using PK nails make sure they can be used in future tests. After the MTLS passes, the project team obtained static GNSS observations over these control points (Figure 5.2) and used these coordinates as constraints to register the data both from mobile lidar and the total station coordinates of the locations of retroreflectivity measurements. CP01, CP05, and CP09 were occupied for over 2 hours for static GPS observations, while the other control points were observed for 15 to 30 minutes for rapid static GPS observations (Table 5.2). CP02 and CP08 were set arbitrary with a reasonable distance from the stripes to be measured so that the project team could avoid the additional errors when targeting the prism at close range. All the control points were measured by the total station setup over CP02 and CP08 as well to connect the retroreflectivity measurements to the control network.

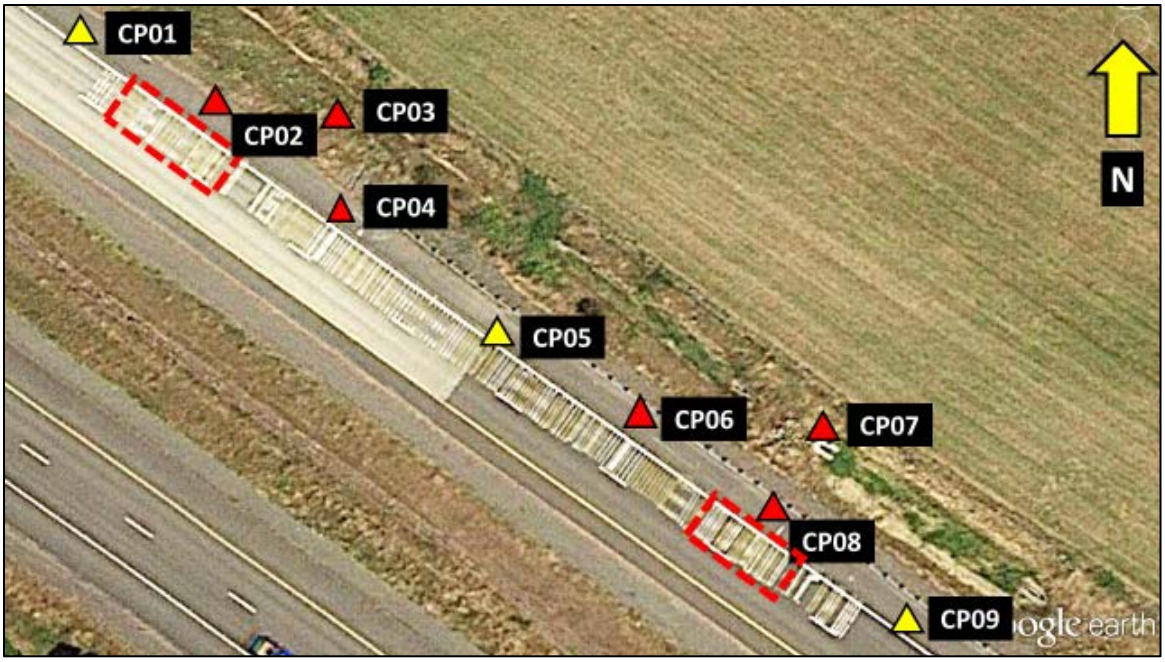

Figure 5.1: Control point setup on the site.

Table 5.2: Summary of Control Points

Control Point	Type of Setup	GPS Observation Type	Notes
CP01	Permanent - Chevron	Static	Included in MTLS scans
CP02	Permanent – PK nail	Rapid Static	Total Station set-up #1
CP03	Temporary- Wood stake with tac	Rapid Static	
CP04	Permanent– PK nail	Rapid Static	
CP05	Permanent– PK nail	Static	
CP06	Permanent– PK nail	Rapid Static	
CP07	Temporary- Wood stake with tac	Rapid Static	
CP08	Permanent– PK nail	Rapid Static	Total Station set-up #2
CP09	Permanent - Chevron	Static	Included in MTLS scans

Figure 5.2: Acquisition of GNSS survey control data, retroreflectivity readings, and total station coordinates on locations of retroreflectivity readings.

5.2.3 Detailed Retro Testing:

For the detailed retroreflectivity measurements, the project team obtained several measurements with the retroreflectometer:

- 10 measurements across each of the 12 selected stripes (6 AC, 6 PCC)
- 30 measurements on pavement at random locations (15 AC, 15 PCC)
- 30 measurements at random locations along the longitudinal stripe (15 PCC, 15 AC)
- For both AC and PCC, obtain 15 measurements without moving the retroreflectometer to evaluate repeatability. Complete these measurements at three different locations capturing worn sections of stripe in worn, fair, and good condition.

The position of each measurement was captured with the total station targeting on a prism positioned over the point. The project team selected a number of stripes painted in 2015 both on AC and PCC pavement with different colors and types of material (Table 5.3). The project team obtained retroreflectivity readings over 10 evenly-distributed points of interest on each selected

stripe and acquired total station prism measurements at the same points so that the retroreflectivity measurements could be geo-referenced to within a few centimeters of accuracy. Note that the stripe IDs shown on the site are not guaranteed to be unique, so the crews searched for the selected stripes from north end of the test-deck on PCC and south end on AC where the 2015 stripes are located. To mark the points of interest on each stripe, the project team started at 0.20 m (0.7 ft) the inward edge of the longitudinal stripe (the edge facing the centerline) and placed 10 marks along the stripe with an interval of 0.30 m (1.0 ft) between each (Table 5.4, Figure 5.3). Once the points of interest on the selected stripes were marked, the project team obtained measurements using both retroreflectometer and total station. After finishing all the measurements on the stripes at one total station set-up, the project team acquired another 15 measurements on the pavement at randomly selected locations, 15 measurements on the actual longitude stripe, followed by the repeatability measurements at 3 different locations with different retroreflectivities. Once finished with this process for the stripes in the asphalt concrete, the project team followed the same procedures in the Portland Concrete section.

Table 5.3: Summary of Selected Stripes for Testing

Stripe ID	Pavement	Color	Material
4.1 - 4.2	AC	Yellow	MMA
9.1 – 9.2	AC	White	MMA
13.1 – 13.2	AC	White	Thermo
14.1 – 14.2	AC	Yellow	Thermo
19.1 – 19.2	AC	White	Preformed
20.1 – 20.2	AC	Yellow	Preformed
4.3 - 4.4	PCC	Yellow	MMA
9.3 – 9.4	PCC	White	MMA
13.3 – 13.4	PCC	White	Thermo
14.3 – 14.4	PCC	Yellow	Thermo
19.3 – 19.4	PCC	White	Preformed
20.3 – 20.4	PCC	Yellow	Preformed

Table 5.4: Layout of Detailed Retroreflectivity Measurements on the Stripes in Table 5.3

Meas. ID	Distance to Mark from Inner Boundary of Longitudinal Stripe	Field of View of Retroreflectivity Measurement	
		Inner	Outer
1	0.20 m (0.7 ft.)	0.00 m (0.0 ft.)	0.60 m (2.0 ft.)
2	0.50 m (1.6 ft.)	0.30 m (1.0 ft.)	0.90 m (3.0 ft.)
3	0.80 m (2.6 ft.)	0.60 m (2.0 ft.)	1.20 m (3.9 ft.)
4	1.10 m (3.6 ft.)	0.90 m (3.0 ft.)	1.50 m (4.9 ft.)
5	1.40 m (4.6 ft.)	1.20 m (3.9 ft.)	1.80 m (5.9 ft.)
6	1.70 m (5.6 ft.)	1.50 m (4.9 ft.)	2.10 m (6.9 ft.)
7	2.00 m (6.6 ft.)	1.80 m (5.9 ft.)	2.40 m (7.9 ft.)
8	2.30 m (7.5 ft.)	2.10 m (6.9 ft.)	2.70 m (8.9 ft.)
9	2.60 m (8.5 ft.)	2.40 m (7.9 ft.)	3.00 m (9.8 ft.)
10	2.90 m (9.5 ft.)	2.70 m (8.9 ft.)	3.30 m (10.8 ft.)

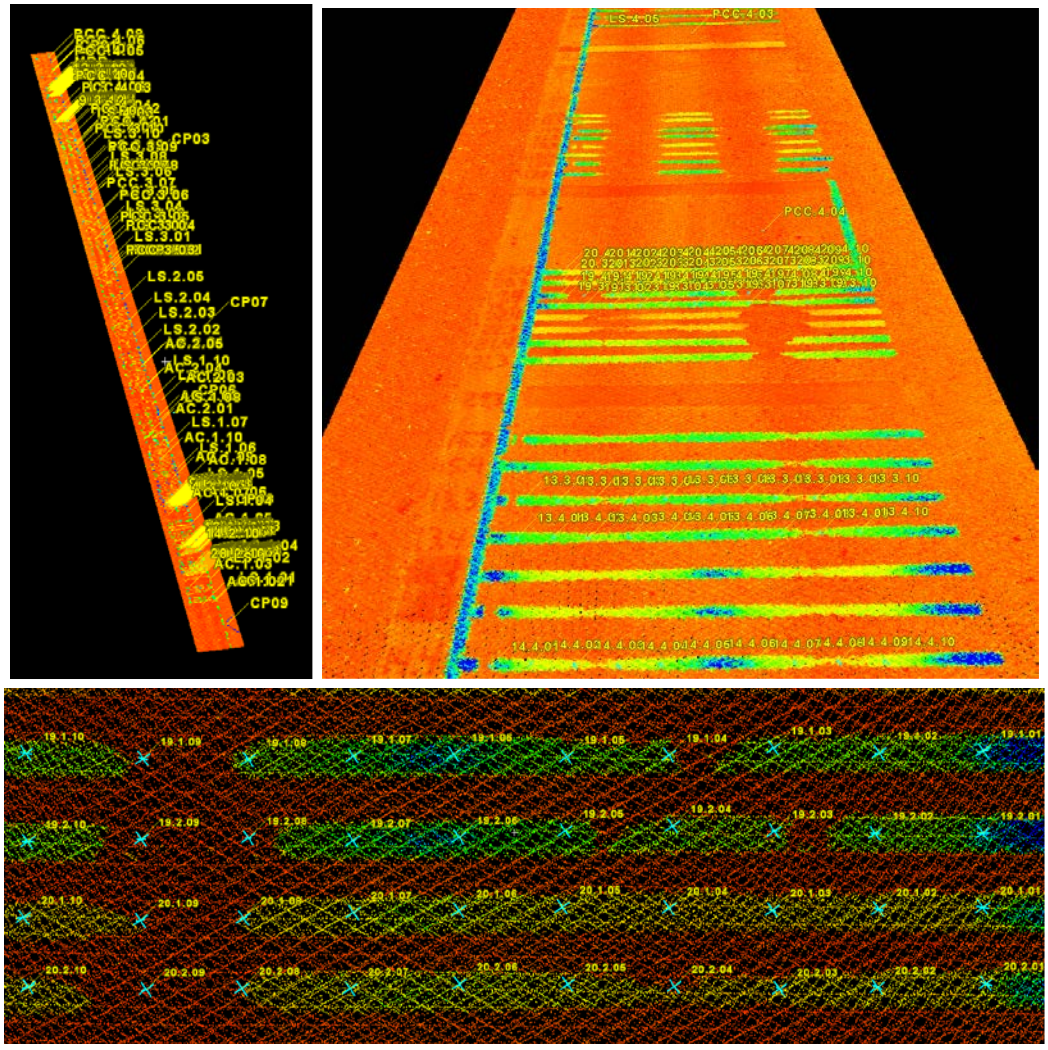

Figure 5.3: Mobile lidar point cloud with (a) labels of stripes across the Testdeck (b) View of locations of retroreflective readings (c) Close-up of retroreflective measurement locations on stripes.

5.3 TEST RESULTS AND ANALYSIS

The data from Testdeck Experiments II and III were used in the analysis to develop the radiometric calibration model. This analysis and model development is presented in Chapter 9. Table 5.5 summarizes the range and angle of incidence values on the stripes analyzed in this test.

Table 5.5: Summary of Range and Incidence Angle Values for Data Obtained on Pavement Markings for Different Mobile Lidar Configurations

Lane	Parameter	Scanner Orientation				
		60°	**30°**	**0°**	**-30°**	**-60°**
Left	Range	-	5.64 – 9.22 m (18.5 – 30.2 ft.)	-	3.88 – 6.10 m (12.7 – 20.0 ft.)	-
	Incidence Angle (°)	-	68.22 – 76.61	-	59.00 – 71.51	-
Right	Range	4.14 – 9.38 m (13.6 – 30.8 ft.)	3.75 – 5.36 m (12.3 – 17.6 ft.)	3.69 - 4.26 m (12.1 - 14.0 ft.)	3.74 – 5.42 m (12.3 – 17.8 ft.)	4.15 – 8.97 m (13.6 – 29.4 ft.)
	Incidence Angle (°)	59.76 – 75.82	55.34 – 67.80	55.16 – 61.72	55.47 – 67.51	59.41 – 74.48
Right Shoulder	Range	-	3.70 – 5.34 m (12.1 – 17.5 ft.)	-	5.03 – 8.22 m (16.5 – 27.0 ft.)	-
	Incidence Angle (°)	-	57.10 – 67.90	-	65.90 – 75.06	-

The evaluations of signs captured by mobile lidar in this test will be discussed in Volume II.

6.0 TESTDECK EXPIREMENT III

6.1 TEST OBJECTIVES

The third Testdeck experiment had the following objectives:

1. Testing radiometric correction for MTLS data with different ranges and angles of incidence.

2. Demonstrating the possibility and limit of evaluating retroreflectivity using MTLS intensity.

3. Testing the robustness of retroreflectivity measurements using the retroreflectometer.

4. Exploring relationship between intensity value from MTLS data and retroreflectivity from retroreflectometer considering different colors and materials.

5. Testing the radiometric correction for MTLS data to quantitatively evaluate the pavement marking degradation with respect to retroreflectivity.

6.2 TEST DESCRIPTION

Testdeck III was completed on July 25, 2017 with the same considerations as Testdeck II. However, between Testdeck II and Testdeck III, Oregon DOT Geometronics updated the system with a second profiler, which locked the sensor orientation into -30/+60°. This upgrade was completed in order to increase the density and coverage of point clouds acquired with Oregon DOT's MTLS system to improve the data quality for a variety of applications. The preliminary results from Testdeck Experiments I and II were considered in this decision process.

6.2.1 MTLS

For the lidar data acquisition in this test (Table 6.1), the project team collected data on the Testdeck using the mobile lidar system (Leica Pegasus:Two) with Oregon DOT on both traffic lanes and the shoulder in the fixed orientation (-30/+60 degrees). In this way, the project team can cover the entire area of interest with different view angle for testing the radiometric calibration methods. For the three passes of running mobile lidar on the left lane, the data were collected in a speed of 25, 35, and 45 mph respectively. The passes on the left lane were performed with a rolling slowdown to avoid the cones blocking the laser beams and creating shadows in the data. After three passes on the left lane, the traffic control was performed to block the right lane where the Testdeck is located. The shoulder was kept clear to run the two passes at speeds of 15 and 25 mph, respectively. Next, five passes on the right lane with a speed of 15, 25, 35, 45, and 55 mph were performed. After confirming all the 9 passes are collected properly, a copy of the raw data was downloaded to the USB drive provided by OSU and another copy taken to Oregon DOT for processing.

Table 6.1: Summary of Data Collection for Mobile Lidar System

Pass #	Lane	Orientation (°)	Speed (mph)
1	Left	-30/+60	25
2	Left	-30/+60	35
3	Left	-30/+60	45
4	Shoulder	-30/+60	15
5	Shoulder	-30/+60	25
6	Right	-30/+60	15
7	Right	-30/+60	25
8	Right	-30/+60	35
9	Right	-30/+60	45
10	Right	-30/+60	55

6.2.2 TLS

To capture the detailed information on the Testdeck for further analysis, the project team collected the data using Leica P40 on the Testdeck. The scan positions were set up every 20 meters to cover the Testdeck while a GPS receiver on top of the scanner collected ORGN data during the scan. The scans started from the west ends of the Testdeck and 12 scans were acquired with the scan settings listed as follows:

- Field of view: Horizontal: Target All = 0° - 360°, Vertical: -55 – 0°
- Scanning Resolution: 0.01m @ 30m
- Mode: Range, Sensitivity: Normal
- Imaging: Resolution: 1920 x 1920, HDR: No

6.2.3 Control Points

To add constraints for georeferencing all the data consistently, including data from prior tests, 9 control points (CP01 – CP09) were utilized for this test (Figure 6.1). CP03 and CP07 are temporary control points to improve the geometry of the control network, while the other control points are the same permanent ground control points from the prior field test, Testdeck II (Chapter 5). The project team revisited these control points to ensure they were still available and performed additional GNSS occupation. After the MTLS passes, the project team performed static GNSS observation over these control points with a similar process to Testdeck II (Table 6.2). In this test, at each point, the project team obtained an ORGN coordinate in addition to the static occupations. All the control points were measured by the total station from a single setup near CP05 (compared with two setups in Testdeck II) to connect the control points and the retroreflectivity measurements.

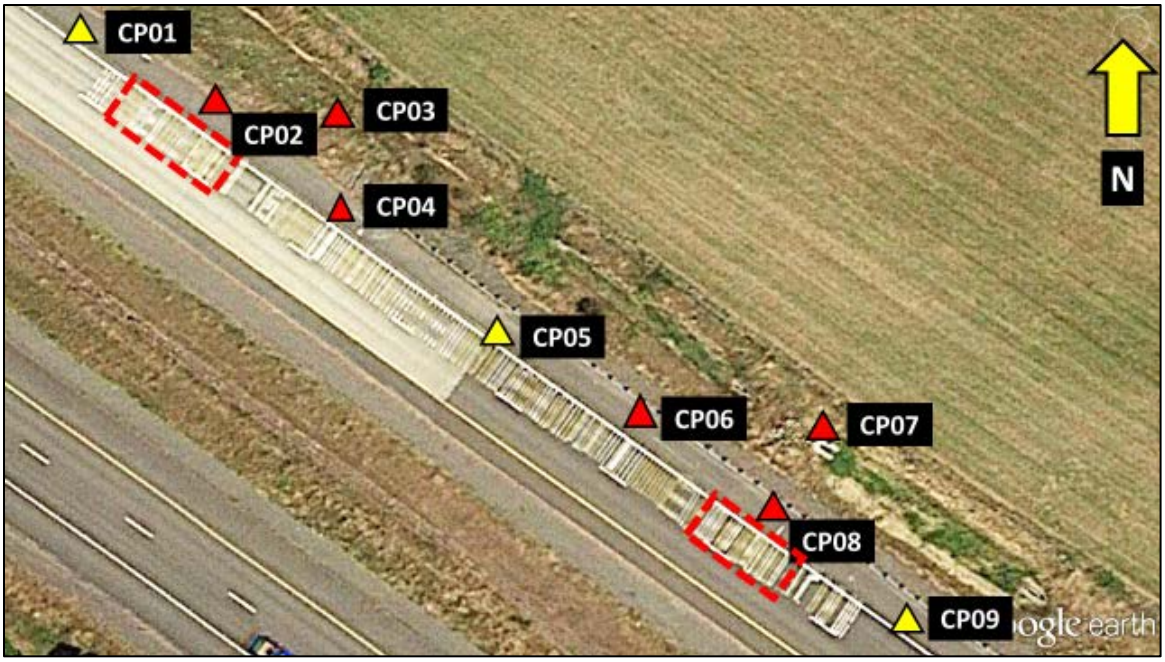

Figure 6.1: Control point setup on the site.

Table 6.2: Summary of Control Points

Control Point ID	Type of Setup	GNSS Observation Method
CP01	Permanent – Chevron	Static
CP02	Permanent – PK nail	Rapid Static
CP03	Temporary – Wood stake with tac	Rapid Static
CP04	Permanent – PK nail	Rapid Static
CP05	Permanent – PK nail	Static
CP06	Permanent – PK nail	Rapid Static
CP07	Temporary – Wood stake with tac	Rapid Static
CP08	Permanent – PK nail	Rapid Static
CP09	Permanent – Chevron	Static

6.2.4 Detailed Retro Testing:

For the detailed retroreflectivity measurements, the project team obtained the measurements with the retroreflectometer as follows. The position of each was also captured with the total station.

- 240 measurements across 24 selected stripes
- 20 measurements on pavement at random locations (10 AC, 10 PCC)
- 96 measurements along the longitudinal stripe (every 2 m or 6.6 ft, 41 AC, 49 PCC)
- 40 measurements at 4 spots on longitudinal stripe with a rough surface. (10 for each)

For the retroreflectivity measurements, the project team selected a number of stripes painted in 2015 both on AC and PCC pavement with different colors and types of material (Table 5.3), which are the same with the previous test. Note that the stripe IDs shown on the site are not guaranteed to be unique, so the crews were suggested to search for the selected stripes from north end of the test-deck on PCC and south end on AC where the 2015 stripes are located. Since the project team obtained retroreflectivity readings over 10 points of interest on each selected stripe systematically (Table 5.4) and acquired total station readings to geo-reference these points, the project team acquired 2 measurements on each stripe (Measurement IDs 1 and 10). Then both the retroreflectivity readings and geo-referenced coordinates are compared against the previous test.

The longitudinal stripe testing was performed starting from CP01 to CP09 (chevron templates). The project team took a retroreflectivity reading and total station shot every 2 meters (6.6 ft), totaling 96 measurements. Then the project team selected 4 test locations on the longitudinal stripe with cracking and obtained 10 readings for each spot to test the repeatability and reliability of the retroreflectometer on a rough surface.

6.3 TEST RESULTS AND ANALYSIS

The data from this test was used for developing the radiometric calibration model in combination with Testdeck II. The full analysis is presented in Chapter 9. Table 6.3 summarizes the range and angle of incidence values on the stripes in this test.

Table 6.3: Summary of Range and Incidence Angle Values to the -30° Profiler for Data Obtained on Pavement Markings for Different Mobile Lidar Configurations

Lane	Parameters	Scanner Orientation (-30°)
Left	Range	4.16 – 6.57 m (13.6 – 21.6 ft.)
	Incidence Angle (°)	59.81 – 72.06 degrees
Right	Range	3.74 – 5.05 m (12.3 – 16.6 ft.)
	Incidence Angle (°)	55.05 – 65.55 degrees
Right Shoulder	Range	5.08 – 7.84 m (16.7 – 25.7 ft.)
	Incidence Angle (°)	65.49 – 74.35 degrees

6.4 TEST LIMITATIONS

During the course of this research, Oregon DOT upgraded their mobile lidar system to support a dual-profiler configuration (-30°/+60°), which improves the data quality (*e.g.,* point density, coverage). However, this configuration no longer allows the flexibility of switching to the other configurations (e.g., 0° and +60°) as was conducted on the previous tests. Hence, the data acquisition strategy varied from Testdeck II.

7.0 WET VS DRY CONDITIONS EVALUATION #1

7.1 TEST OBJECTIVES

To evaluate the reduction of calibrated lidar intensity values when pavement markings are wet, a wet versus dry conditions test was conducted. The reduction in retroreflectivity between dry and wet conditions is a well-known phenomenon and is covered in two ASTM standards: 1) ASTM E2177-11 Standard Test Method for Measuring the Coefficient of Retroreflected Luminance (RL) of Pavement Markings in a Standard Condition of Wetness; and 2) ASTM E2832-12 Standard Test Method for Measuring the Coefficient of Retroreflected Luminance of Pavement Markings in a Standard Condition of Continuous Wetting ($R_{L\text{-}2}$). Reflectance of non-retroreflective surfaces also tends to decrease when wet. Figure 7.1 illustrates a ~20% decrease in the spectral reflectance of a surface under wet conditions, based on data acquired by the project team using an ASD FieldSpec Pro spectro-radiometer. The noisy data in the reflectance spectra between 1800 and 2000 nm result from a strong atmospheric water absorption band. It should be noted that the spectral reflectance in the plot is unit-less, as it is defined as the ratio of reflected radiant flux (W) to incident radiant flux (W), as opposed to retroreflectivity (or, more formally, the coefficient of retroreflection, RA), described elsewhere in this report, which has units of mcd/m^2/lux.

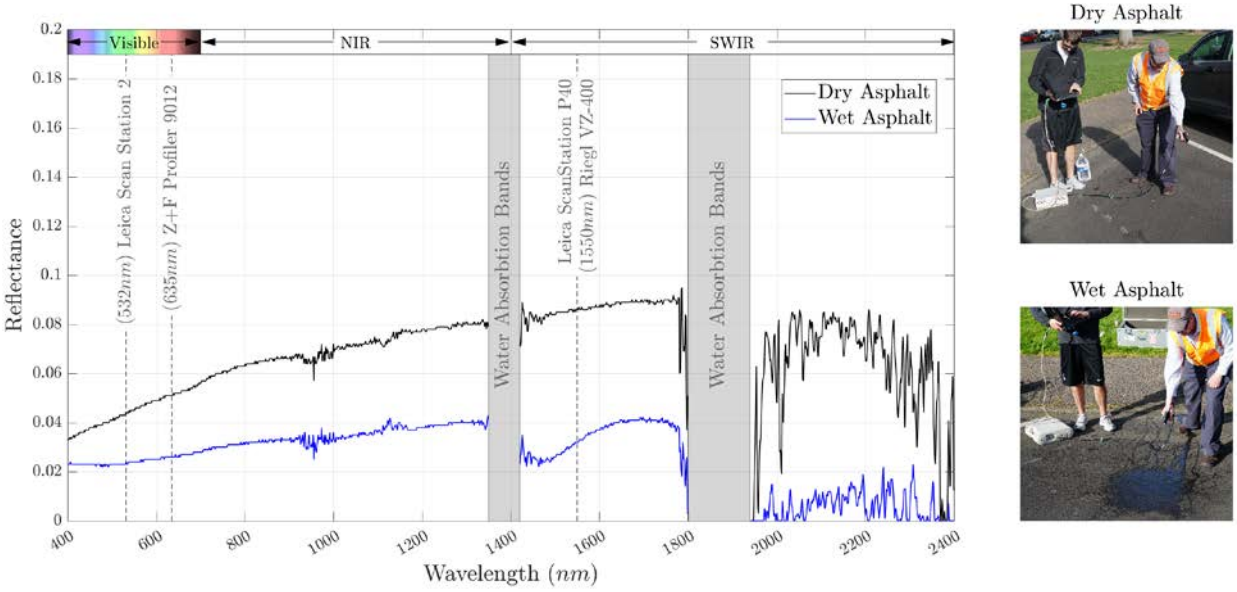

Figure 7.1: Spectral reflectance measurements using an ASD Field Spec Pro (depicted at right) on pavement. The spectral curves illustrate the drop in reflectance for the same surface under dry (black line) and wet (blue line) conditions.

7.3 TEST DESCRIPTION

To evaluate the effects of wetting from rain on our procedures for estimating retroreflectance from calibrated lidar intensity data, scans were collected before and after a rainstorm from the same location at a site with several retroreflective signs and pavement markings (e.g., parking lot or intersection). This test utilized three different terrestrial laser scanners (Table 7.1): 1) Riegl VZ-400, 2) Leica ScanStation 2, and 3) Leica P40. It is important to note that the ScanStation 2 has the closest wavelength to the Z+F scanner on the Leica Pegasus:Two, and that both the ScanStation 2 and Pegasus:Two operate at wavelengths visible to the human eye (i.e., within the visible light portion of the electromagnetic spectrum).

Table 7.1: Scanners Utilized in the Wet Vs Dry Evaluation and their Associated Wavelengths

Scanner	Wavelength	Comments
Z+F Profiler 9012 (Oregon DOT scanner on the Leica Pegasus:Two)	635nm (visible red/orange)	Reference
Leica ScanStation P40	1550nm (invisible, NIR)	Used in test
Riegl VZ-400	1550nm (invisible, NIR)	Used in test
Leica ScanStation 2	532 nm (visible/green)	Used in test

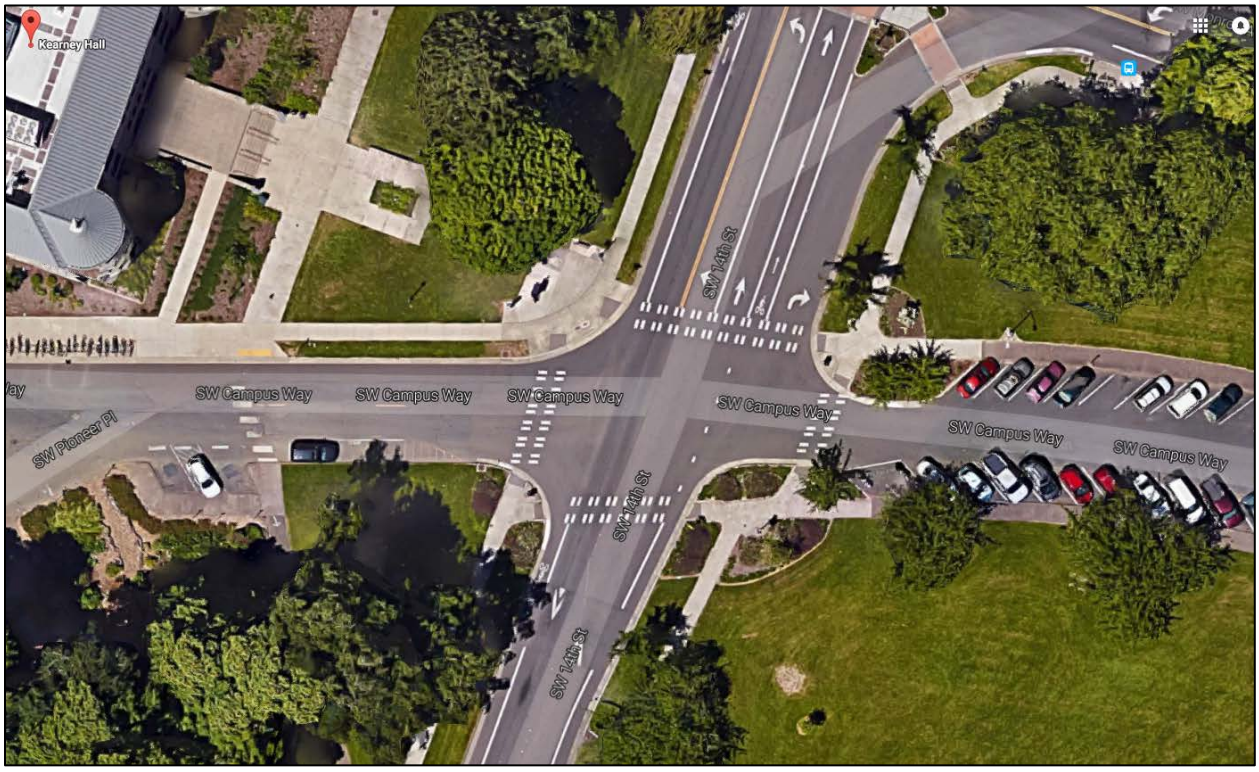

Figure 7.2: Aerial photograph of test site (intersection) for the wet-dry conditions field test. This site contains a variety of pavement markings in a variety of conditions.

Ideally, the wet/dry test would be timed for a day of heavy rainfall followed by bright sunshine and warm temperatures, such that data could be acquired at constant time intervals as the surface

dried. However, the logistical challenges associated with planning an experiment for such stringently-defined weather conditions proved impractical. Therefore, the project team first collected data for a site with all three scanners during dry conditions and then again on a different day during wet conditions. The data sets from these two days were then analyzed and used to design additional tests.

The team selected the intersection of SW 14th Street and SW Campus Way on the OSU campus as the test site (Figure 7.2). The data collection under dry and wet condition was performed on March 10, 2017 (Figure 7.3 left) and March 30, 2017 (Figure 7.3 right), respectively.

(a) (b)

Figure 7.3: Data collection under (a) dry and (b) wet conditions with three laser scanners.

7.4 TEST RESULTS AND ANALYSIS

All the scans were co-registered and transformed to a consistent coordinate system to enable investigation of the effects of a wet road surface on both the lidar positioning accuracy and intensity. It was found from viewing the point cloud of a road surface as a vertical slice along a horizontal profile (Figure 7.4) that the point cloud acquired by Leica ScanStation P40 under wet conditions (blue) has a vertical error up to 0.04 m (0.13 ft.) on a horizontal plane (road surface) and up to 0.01 m (0.03 ft.) on a vertical plane (curb). As shown in the result, the largest vertical errors under wet condition occurred in the areas close to the curb resulting in points located consistently under the actual ground surface. Such phenomenon of the positive errors in ranging was mainly caused by the specular reflection on the wet surface. In this case, the laser beam hit the wet road surface and subsequently reflected off of the curb, ultimately increasing the travel time of the pulse. Because the scanner cannot account for these reflections, it simply computes a larger range from the increased travel time, resulting in a reflection below the ground surface of the curb. For the other scanners (e.g., Reigl VZ-400), no noticeable errors were observed in positioning accuracy as a function of wetting condition of the surface.

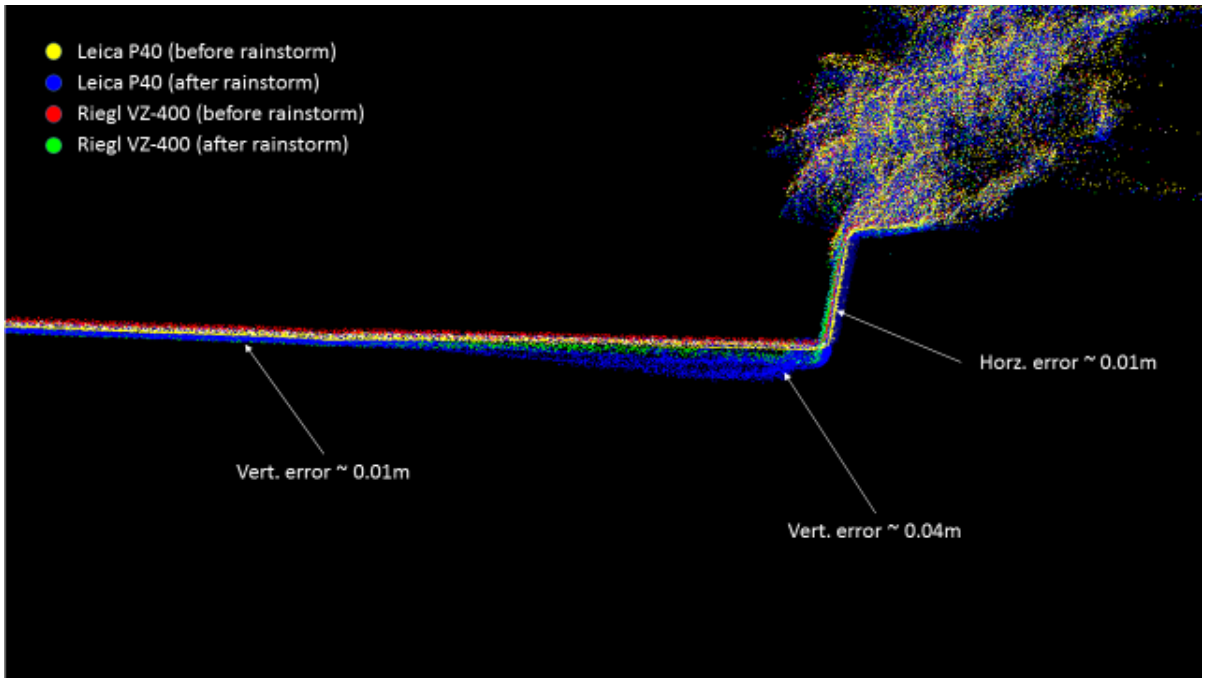

Figure 7.4: Example profiles showing erroneous geometric measurements obtained with terrestrial laser scans resulting from wet surfaces.

To compare and quality check intensity values, a small area containing both pavement and pavement markings was cropped out of the lidar point cloud, and histograms of intensity from dry and wet road surfaces were compared (Figure 7.5). Each scanner has its own built-in intensity scaling and correction approach. Therefore, the comparison focused on the distribution and relative difference of intensity. As shown in Figure 7.5, although the intensity values are consistently lower on a wet surface, as expected, the effects of surface wetness are variable across the different laser scanners. For the Riegl VZ-400, there is no significant difference in the decrease of intensity between the pavement and the pavement markings; hence, the histograms are similar in terms of their distribution. Due to the crown on the road surface, water will tend to flow to the edge, which is one reason why the intensity under wet conditions on the pavement shows greater variation. For Leica ScanStation P40, there are numerous drop-out points on the wet road surface. These are likely the result of the built-in scaling and intensity correction, as the ScanStation P40 uses a laser with the same wavelength as the Riegl VZ-400 (1550 nm). The intensity from the Leica ScanStation 2 is least affected by surface wetness, especially for the points lying on the pavement markings (depicted in red in Figure 7.5).

VZ400

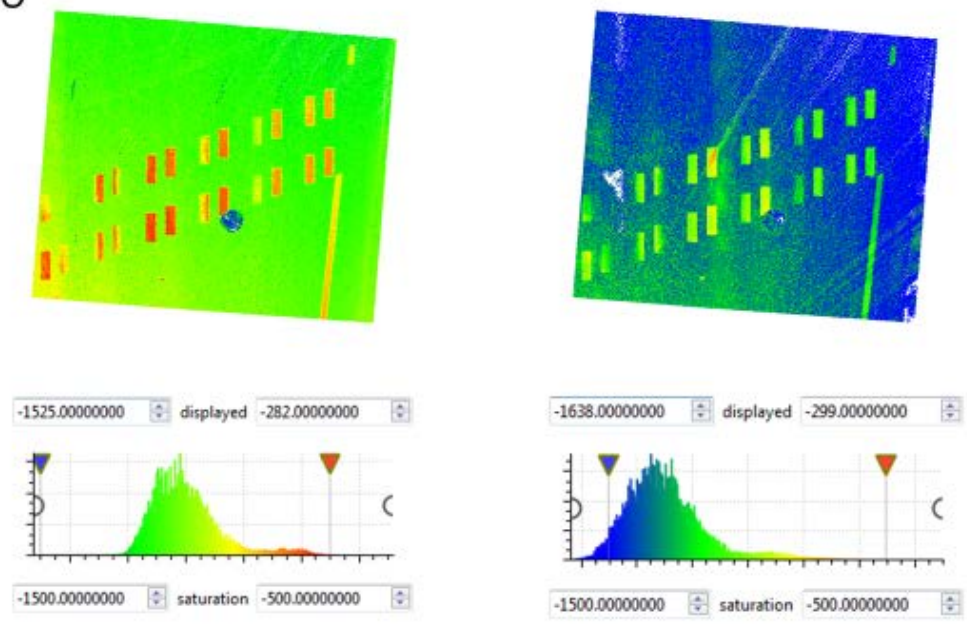
-1525.00000000
displayed
-282.00000000
-1500.00000000
saturation
-500.00000000
-1638.00000000
displayed
-299.00000000
-1500.00000000
saturation
-500.00000000

(a)

P40

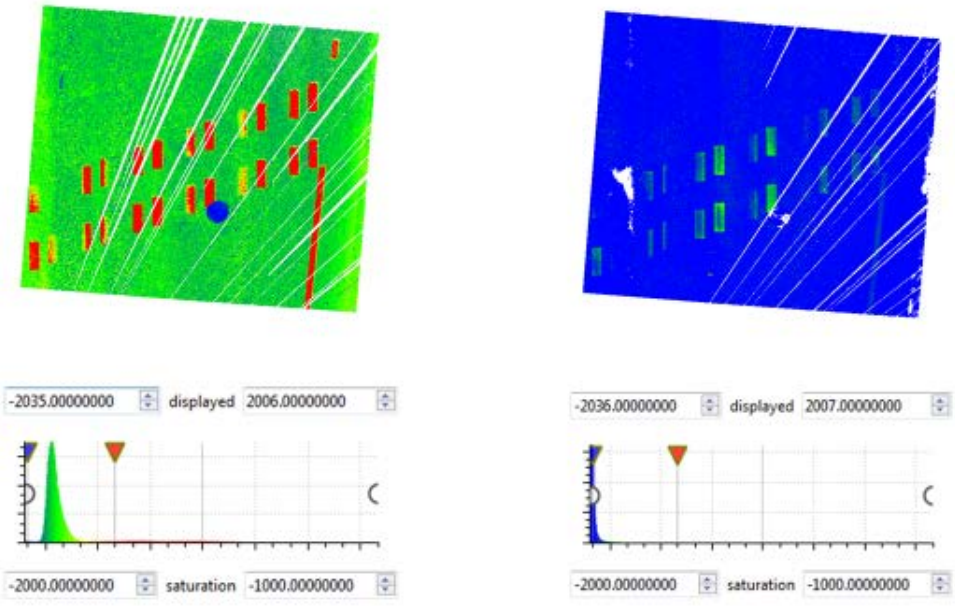
-2035.00000000
displayed
2006.00000000
-2000.00000000
saturation
-1000.00000000
-2036.00000000
displayed
2007.00000000
-2000.00000000
saturation
-1000.00000000

(b)

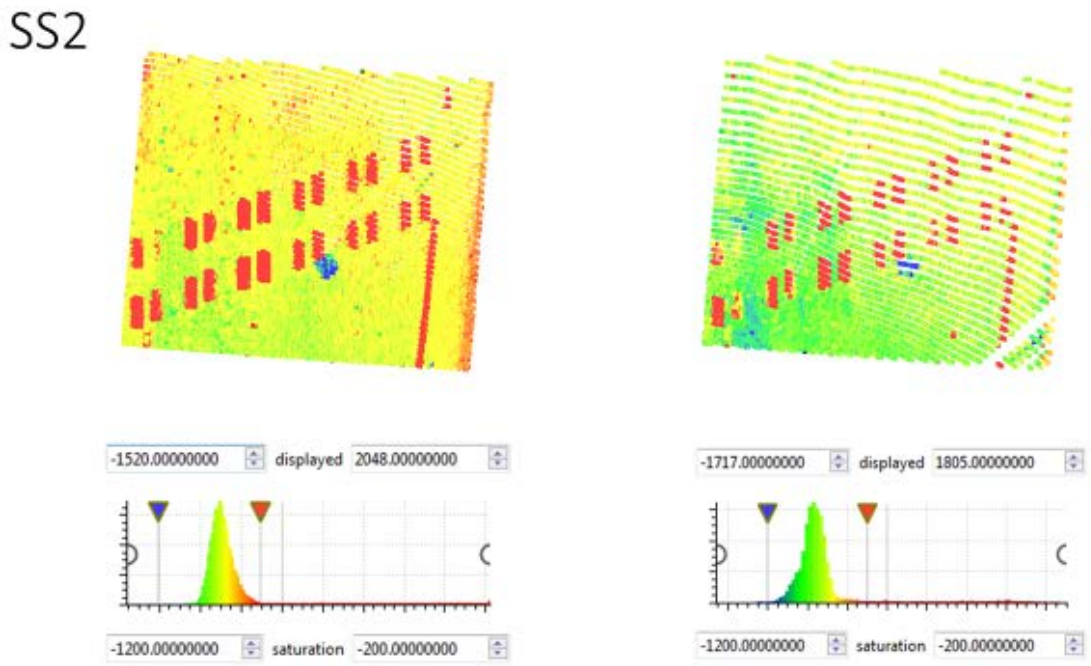

(c)

Figure 7.5: Comparison of intensity histograms before and after rainstorm with different terrestrial laser scanners: (a) Riegl VZ-400; (b) Leica ScanStation P40; (c) Leica ScanStation 2.

The primary conclusion from this test was that the intensity values of the scanners were significantly affected by the dry/wet condition in terms of both positioning accuracy and intensity values. Unfortunately, it is challenging to develop a mathematical model for intensity variation with surface wetness for several reasons. First, the results vary significantly across different scanner makes and models. For instance, although the Riegl VZ-400 and Leica ScanStation P40 operate at the same wavelength, both the absolute intensity values and the intensity variation before and after rainstorm are significantly different. Further, it is even more difficult to quantify the "degree of wetness" or set up the test condition according to ASTM testing standards for such a large area. For example, in ASTM E2177, 3.0 liters of clean water from a bucket needs to be poured within 3 to 5s to the measurement area (footprint of handheld retroreflectometer) and the retroreflectivity is measured 45s after.

7.5 TEST LIMITATIONS

The scanners were approximately positioned (within ~1 m, or ~3 ft) at the same locations for the wet and dry tests, rather than set up over a distinct mark. This results in a slightly different view of the scene between surveys. However, the view is close enough that differences in scanning geometry are minimal and would not likely affect the test results. This experiment also did not directly evaluate the capabilities of the Leica Pegasus:Two system used by Oregon DOT, which will be investigated in Chapter 8. Nevertheless, it still provides relevant information on how intensity degrades on wet surfaces using scanners operating at different wavelengths, including in the visible portion of the electromagnetic spectrum. Fortunately, Oregon DOT Geometronics

currently collects routine scans during dry conditions to ensure high geometric data quality and coverage. Hence, most of Oregon DOT's MTLS inventory would not suffer from these limitations resulting from wet conditions.

8.0 WET VS DRY CONDITIONS EVALUATION #2

8.1 TEST OBJECTIVES

As an extension of the experiment descripted in Chapter 7 to Oregon DOT's Leica Pegasus:Two mobile lidar system, a simple wetting test was conducted with the following objectives:

1. Evaluate the extent to which wet and dry conditions affect mobile lidar data, using data from Oregon DOT's Pegasus:Two, rather than relying on terrestrial laser scanners, as in the previous wet-dry test.

2. Investigate the deviation of intensity variation caused by wet road surfaces over multiple passes and lanes.

3. Provide recommendations for operating the mobile lidar system to collect data during wet conditions.

8.2 TEST DESCRIPTION

The fieldwork for this test was performed concurrently with the signs test (described Volume II) on June 19, 2017 at the Oregon DOT Maintenance Yard in Salem, Oregon. First, six passes were acquired of the road surface under dry condition. Then, the project team wet a selected pavement marking using a water bucket. This marking was kept wet (Figure 8.1) during the following passes, which repeated the speeds, lanes, and directions in the first 6 passes. Figure 8.2 shows the layout of the test and details of the passes.

Figure 8.1: A project team member wets pavement with bucket prior to pass T07.

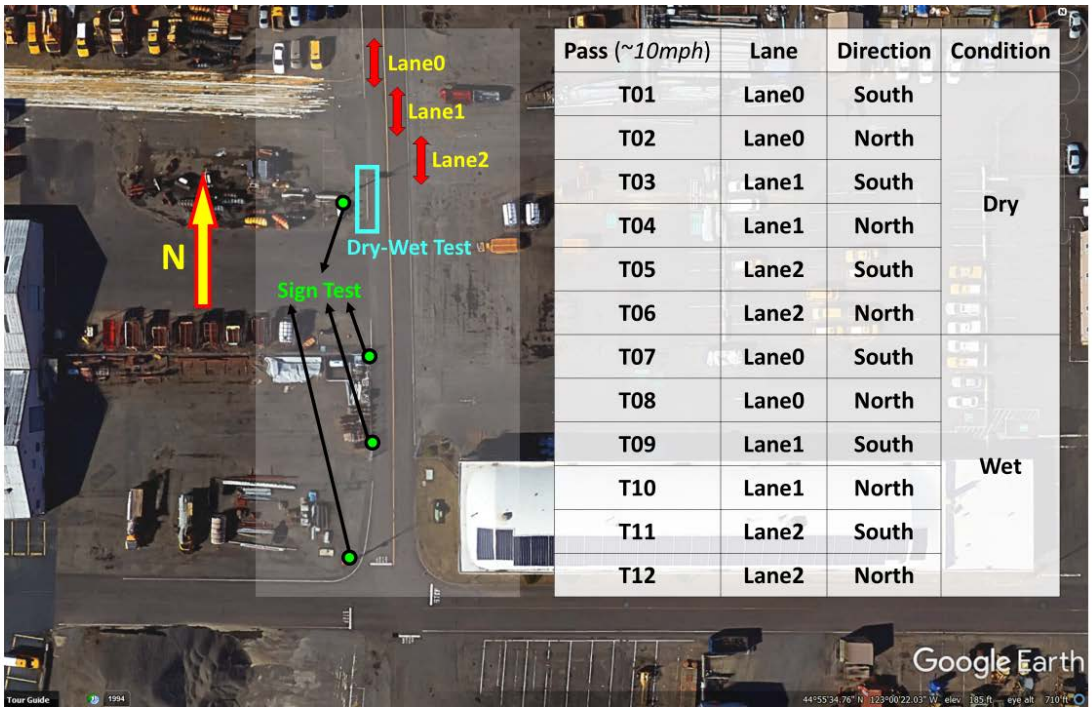

Pass (~10mph)	Lane	Direction	Condition
T01	Lane0	South	Dry
T02	Lane0	North	
T03	Lane1	South	
T04	Lane1	North	
T05	Lane2	South	
T06	Lane2	North	
T07	Lane0	South	Wet
T08	Lane0	North	
T09	Lane1	South	
T10	Lane1	North	
T11	Lane2	South	
T12	Lane2	North	

Figure 8.2: Layout of wet-dry conditions test with Oregon DOT's Pegasus:Two mobile laser scanner in the Maintenance Yard.

This test was intended to be an exploratory test to determine if more rigorous evaluation was necessary and as such is only loosely based on ASTM procedures.

8.3 TEST RESULTS AND ANALYSIS

The mobile lidar data at the pavement markings under dry and wet conditions were qualitatively compared by coloring the point clouds by intensity values (Figure 8.3). Some laser pulses incident on the wet pavement do not yield sufficient return signal strength for the scanner to measure a valid range, yet nevertheless provide an intensity value. These intensity values from the wet pavement are significantly lower than those from the adjacent pavement marking, as shown in Figure 8.3 by the dark areas surrounding the relatively bright stripe. In this test, there was no significant difference in range from the lidar to the points on the wet and dry surface. It is interesting to note that the areas surrounding the data gaps correspond to a transition from wet to dry surface conditions, and the intensities show a corresponding gradual increase.

Theoretically, this gradual change of intensity values could be mathematically modeled and used to determine a surface wetness correction. However, for such a model to provide reliable results, it would be necessary to conduct more tests, such that possible confounding variables, such as temperature, humidity, wind, slope, material, and traffic, could be controlled.

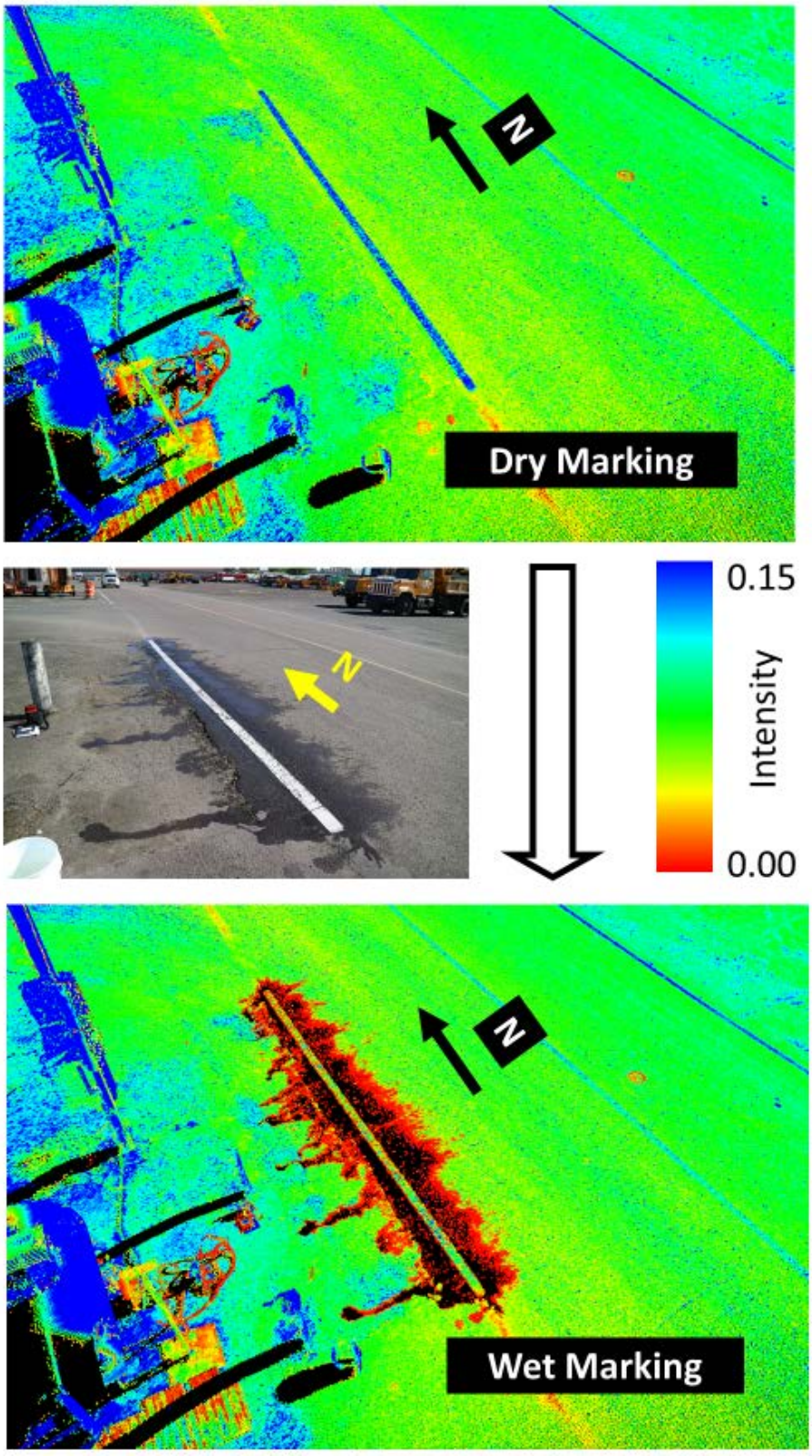

Figure 8.3: Comparison of (a) point cloud of pavement marking (dry), (b) photograph (wet), and (c) pavement marking (wet)

To further evaluate the change in intensity on the pavement marking quantitatively, points lying on the test stripe were extracted, and the mean, standard deviation, and relative standard deviation of the intensity were computed, and the difference between the passes in the same lane and direction were assessed (Table 8.1). It is important to note that the number of points is mainly affected by the scan geometry, and that surface wetness does not cause point drop-outs (i.e., data gaps), as it does on the bare pavement. However, the average value of the intensity for the wet stripe is consistently lower than when it is dry. The distribution of the intensity values for each pass (Table 8.2) shows that the intensity values on a dry stripe are more likely to follow a normal distribution than the wet stripe. As a result of the different distributions, it difficult to derive a simple, yet reliable mathematical model for the change in intensity with surface wetness. Possible causes of the differing distributions include irregularities in the surface pavement, which can lead to different quantities of water pooling on the surface, as well as the fact that water tends to drain quicker at locations with cracking.

Table 8.1: Summary of Intensity Readings Obtained for the Dry/Wet Test Stripe for Each Pass.

Pass	# of points	Int. Avg.	Int. Std. Dev.	Int. RSD
T01	3865	0.141	0.023	0.159
T02	2555	0.192	0.021	0.108
T03	2618	0.147	0.018	0.123
T04	736	0.156	0.017	0.111
T05	752	0.116	0.014	0.122
T06	394	0.098	0.011	0.107
T07	3983	0.063	0.032	0.515
T08	2260	0.098	0.037	0.377
T09	2067	0.046	0.024	0.529
T10	1102	0.049	0.023	0.461
T11	687	0.026	0.012	0.455
T12	330	0.026	0.011	0.406

Table 8.2: Dry-Wet Comparison of Intensity for each Pair of Passes with the Same Configuration

Pass	Difference between the passes			
	# of points	Int. Avg.	Int. Std. Dev	Int. RSD
T01 -> T07	118	-0.078	0.010	0.356
T02 -> T08	-295	-0.094	0.016	0.269
T03 -> T09	-551	-0.101	0.006	0.406
T04 -> T10	366	-0.107	0.005	0.349
T05 -> T11	-65	-0.091	-0.003	0.333
T06 -> T12	-64	-0.072	0.000	0.299

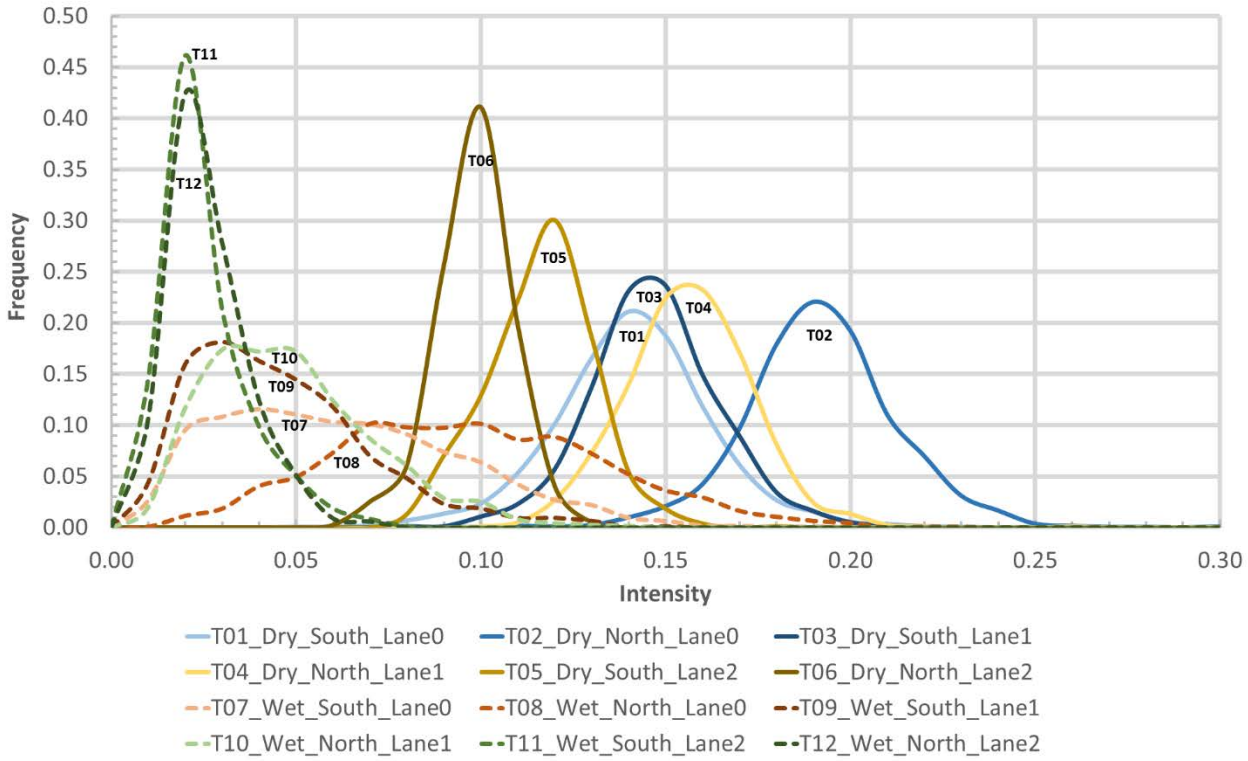

Figure 8.4: Distribution of intensity values extracted across the stripe of interest for each pass for wet and dry conditions. (Single profiler results)

8.4 TEST LIMITATIONS

Only one stripe was evaluated in this test to verify the degradation effect. Should Oregon DOT wish to pursue the idea of applying a wet-dry correction to the data, extensive data collection of the same area in wet and dry conditions as close together in time as possible would need to be completed to provide a variety of samples to have confidence in a mathematical correction. A key challenge that needs to be considered is the difficulty in quantifying wetness, not only during the test, but during subsequent mobile lidar data acquisition in wet conditions. Water will be thicker in some areas than others depending on the road condition and extent of pooling. Also, the wetness and drying time are functions of environmental conditions (e.g., temperature and humidity), and surface conditions. Further, although the intensity values on the test stripe showed similar amounts of degradation, the overall effect on retroreflectivity values will behave differently, given that the relationship between intensity and retroreflectivity is a power function. Finally, the relatively small variation observed in the differences in intensity values may result, in part, from factors such as differences in concentration of water across the stripe as well as differences in time intervals between application of the water to the stripe and acquisition of the mobile lidar data, which were not controlled in this experiment.

9.0 RADIOMETRIC CALIBRATION

9.1 TEST SITE "TESTDECK"

In order to develop a robust empirical model to calculate retroreflectivity from intensity values, the project team collected both mobile lidar data and retroreflectivity data at the Testdeck. This site is ideal for developing a radiometric calibration for striping because: (1) the transverse line were painted in different years with a wide range of materials, and colors (van Schalkwyk, 2010); and (2) the wear is highly variable (Figure 9.1) across the lines with the most significant wear occurring at the locations of the typical wheel paths for vehicles driving in the lane.

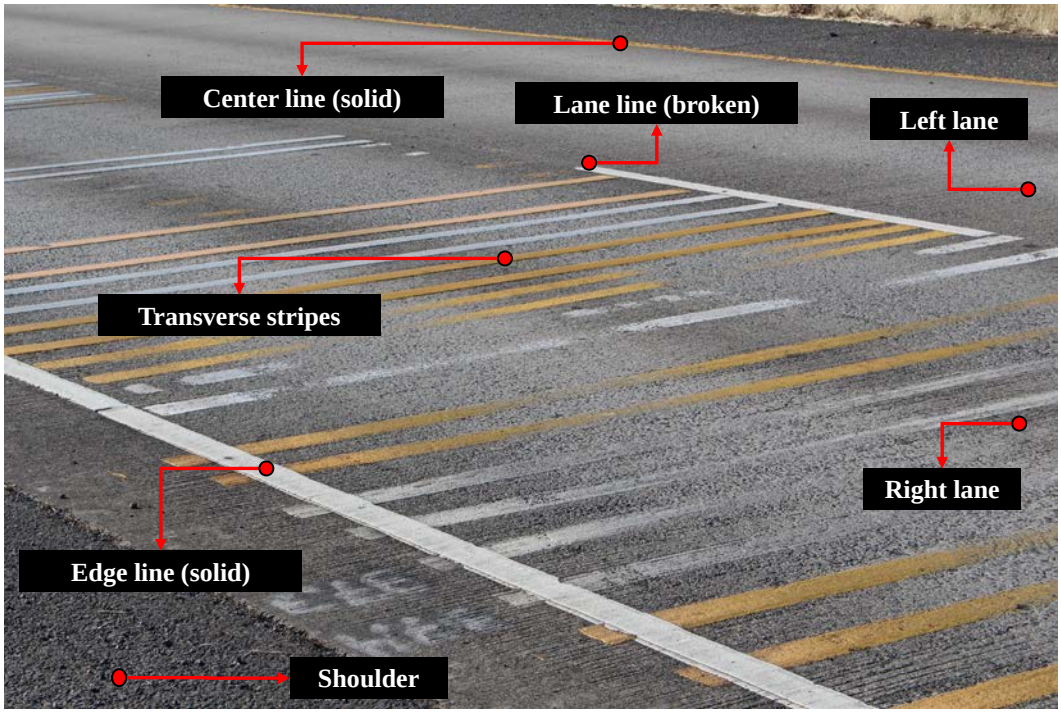

Figure 9.1: Photograph of the "Testdeck" site where detailed retroreflectivity measurements were obtained for the development of the radiometric calibration model

Data were captured for a total of 24 lines at this site for the calibration (Table 9.1). Half of these were located Asphalt Concrete (AC) and the other half on Portland Cement Concrete (PCC) pavement. These lines cover both yellow and white lines as well as three common types of marking materials (Table 2.1): Methyl Methcrylate (MMA), Thermoplastic (Thermo), and Preformed Thermoplastic (Preformed). For each line of interest, retroreflectometer measurements were sampled every 0.3m (10-12 per line) in order to systematically capture the wide range of wear conditions across the line. To further improve the coverage of lines in different conditions, the project team repeated the survey of these lines approximately one year after the first acquisition. In total, there were 245 samples from Testdeck II and 240 from Testdeck III.

Table 9.1: Summary of the Transverse Lines with Detailed Retroreflectivity Measurements.

Line ID	Pavement	Color	Material
01 – 02	AC	Yellow	MMA
03 – 04	AC	White	MMA
05 – 06	AC	White	Thermo
07 – 08	AC	Yellow	Thermo
09 – 10	AC	White	Preformed
11 – 12	AC	Yellow	Preformed
13 – 14	PCC	Yellow	MMA
15 – 16	PCC	White	MMA
17 – 18	PCC	White	Thermo
19 – 20	PCC	Yellow	Thermo
21 – 22	PCC	White	Preformed
23 – 24	PCC	Yellow	Preformed

9.2 MOBILE LIDAR ACQUISITION

The Leica Pegasus:Two mobile lidar system owned by Oregon DOT was used for the acquisition. In the first survey, the scanner was operated with a single laser profiler that could be adjusted to 5 operational configurations (+60°, +30°, 0°, -30°, -60°), referring to the orientation of the entire system with respect to the mounting platform. For example, with a 0° configuration, the point distribution of a scanline collected by the mobile lidar system is perpendicular to the driving direction. Prior to the second survey in July 2017, the scanner had been upgraded to include a second profiler. In this configuration, one scanner is mounted in the -30° configuration while the second is mounted in the +60° configuration. The key benefit of this dual profiler configuration is to increase the point density. In addition, because the profilers are equipped in a different orientation, an object can near-simultaneously be captured in two different incidence angles and ranges within a single pass. As a result, this configuration can potentially help balance the impact in the intensity caused by range and incidence angle when the project team sample the points within the search window to retrieve retroreflectivity.

By altering the orientation as well as the lane of travel, the road markings on the Testdeck (right lane) can be captured from a wide range of distances and incidence angles (Table 9.2). While more permutations are physically possible, only a select number of combinations were possible due to safety and traffic control requirements. For purposes of the calibration, only passes obtained at 25 mph were included. Higher speeds were used for the validation of the model. Note that the rationale for more passes at the -30° orientation was that it was the primary setting used in a variety of general applications. For example, this orientation enables the front faces of signs to be captured.

Table 9.2: Summary of Mobile Lidar Data Acquisition.

Year	Pass #	Lane	Orientation (°)	Speed (mph)
Testdeck II (2016)	01	Left	+30	25
	02	Left	-30	25
	03	Shoulder	+30	25
	04	Shoulder	-30	25
	05	Right	+60	25
	06	Right	+30	25
	07	Right	0	25
	08	Right	-30	25
	09	Right	-60	25
Testdeck III (2017)	10	Left	-30	25
	11	Shoulder	-30	25
	12	Right	-30	25

9.3 RETROREFLECTOMETER ACQUISITION AND SURVEY CONTROL

A Delta LTL-X Mark II handheld retroreflectometer was used to acquire the ground truth retroreflectivity values at all of the sample points on each line of interest. This system is Oregon DOT's current standard device to test and measure retroreflection quality for warranty disputes. Sample locations were pre-marked systematically using a tape so that all measurements could be obtained at the same location. To register these retroreflectivity readings to the point cloud data collected by the mobile lidar system, the project team surveyed the sample points and linked them to ground control points set up on the Testdeck using a Leica Viva TS15 total station. GNSS coordinates were obtained for the ground control points using a Leica GS14 GNSS receiver. Although the mobile lidar system employs direct geo-referencing from the onboard sensors, additional constraints through the use of ground control points (GCPs) improve the accuracy of the point cloud data, particularly relative to the total station measurements since the same GCPs were used. The typical accuracy (0.03 m, 0.1 ft. horizontal RMS) of the direct geo-referencing observed for this dataset can lead to additional errors in linking the retroreflectivity readings to the point cloud, most dramatically in locations with variable wear. Figure 9.2 shows examples of the data acquisition as well as an example of the registered point cloud with the sampling points correctly located along the centerline of the 0.1 m (0.32 ft.) wide line.

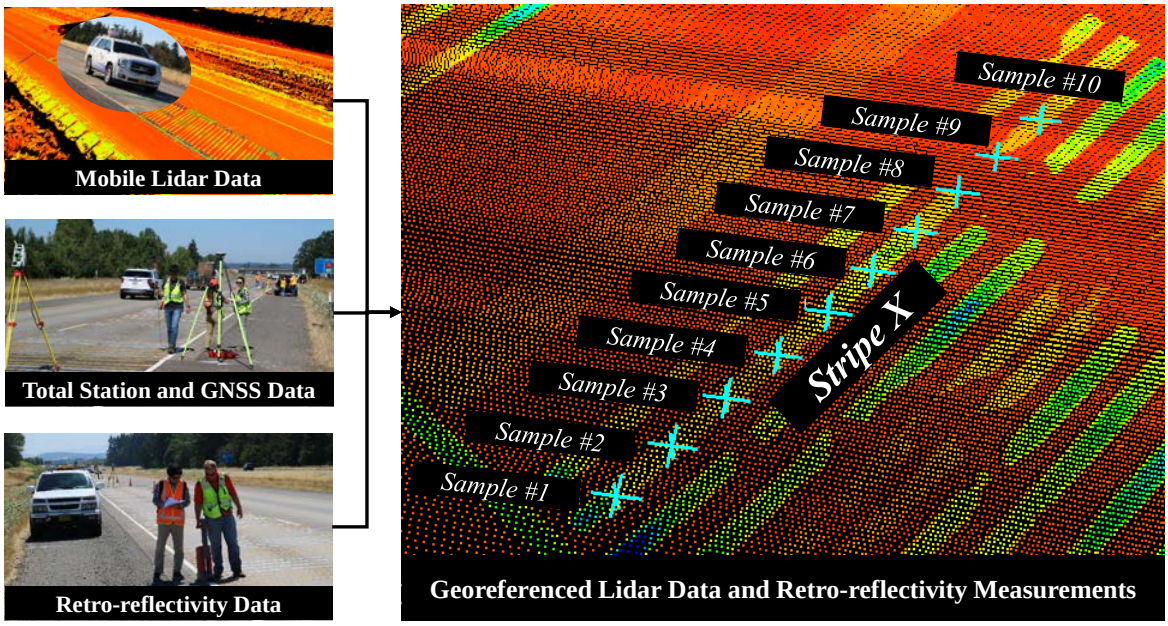

Figure 9.2: Data registration of mobile lidar data and retroreflectivity measurements.

9.4 LEAST SQUARES REGRESSION

9.4.1 Sampling Technique

The fundamental concept of a retroreflectometer for road markings is to illuminate a field (active window) at a certain angle and observe the illumination over another field (passive window) such that it can simulate the physics of how road markings reflect the light from the headlight of a vehicle to the driver's eyes (Figure 9.3).

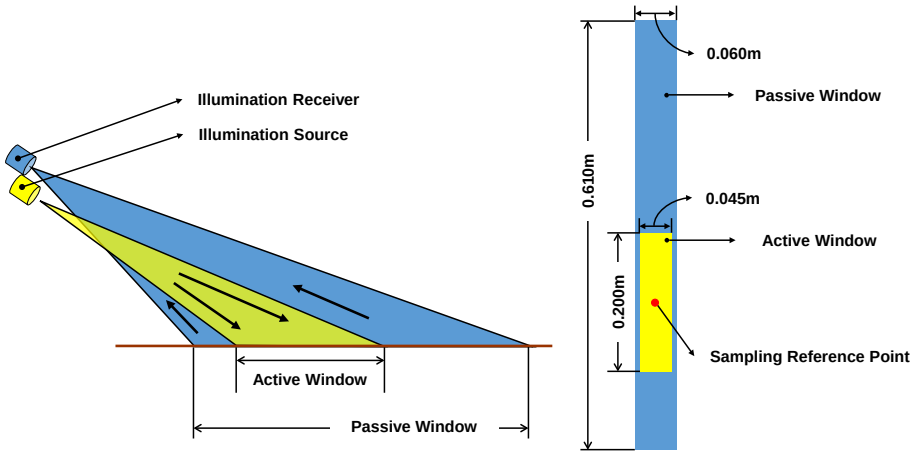

Figure 9.3: Schematic illustrating the operating principles of the handheld retroreflectometer for obtaining retroreflectivity measurements of road markings. Schematic is based on ASTM E1710-11 and the LTL-X Mark II User Manual.

Unlike the retroreflectometer using a fixed active window and passive window, the intensity value of a point in the mobile lidar data is collected by measuring the energy from a much smaller field (mm to a few cm in size), which is a function of the beam exit diameter, beam divergence, range, and incidence angle. Although a theoretical radiometric calibration model can be developed by converting the measurements of illumination and intensity to reflectance based on the mechanism of the instruments, the manufactures usually do not provide all the details of their products such as interpolation approach, internal corrections, calibration models, and so forth. Further, there are fundamental differences in terms of operating wavelengths and the window size of illumination between the mobile lidar data and retroreflectometer data. Given these challenges, the project team elected to develop an empirical model to find an effective, straightforward relationship between the two data sources rather than attempt to model the underlying physics given the amount of unknown variables. Hence, to develop this empirical model to simulate the retroreflectometer measurement with mobile lidar data, the project team tested and evaluated 21 different sampling techniques through regression analysis (Table 9.3).

Table 9.3: Summary of Sampling Approaches Tested in the Proposed Regression Analysis.

Search Window	Interpolation approach	Definition
N/A	Nearest Neighbor	The intensity of the nearest point to the sampling point to the sampling reference point of the retroreflectometer measurement.
Both Active & Passive Windows	Mean	Average intensity of all the points within the search window with an equal weight
	Inverse Distance Weighting (IDW, $1/d^i$)	Weighted average intensity of all points within the search window where each point is weighted by the inverse of the distance against the sampling point to the power of *i*.
	Percentile (j %)	The intensity value corresponding to the top *j* % of all the points within the search window.

9.4.2 Regression Analysis

Plots of the retroreflectivity measurements and the intensity values all sampling techniques tested show a correlation between retroreflectivity and intensity (Figure 9.4). Note that all of the intensity values were scaled to floating point values with a range from 0 to 1 whilst the retroreflectivity readings consist of integer values ranging from 0 to 2000 ($mcd/m^2/lux$), according to the specification of the retroreflectometer. From the distribution of the data points, this correlation tends to be stronger in for relatively low values of retroreflectivity and intensity compared with the higher values. The primary reason for such phenomena results from how pavement markings are made so that they can reflect the incoming light. Typically, glass beads are distributed in the material to provide the retroreflectivity of the road markings. When the road marking is worn, the material is less likely to be even-distributed such that it is impossible to estimate the portion of reflective and non-reflective part within the footprint of a measurement

for both lidar system and retroreflectometer. In addition, for the mobile lidar system, the intensity value can be saturated (more energy is received than can be recorded with the sensitivity of the sensor) on a road marking with high retroreflectivity. As a result of this information loss, it is impossible to convert these intensity values to reflectance using a radiometric calibration approach. Fortunately, these highly retroreflective markings are not as much of a concern to transportation agencies who are focused more on evaluating worn markings, which may require maintenance or replacement. Hence, it is most important to have a higher quality fit at the lower values of retroreflectivity.

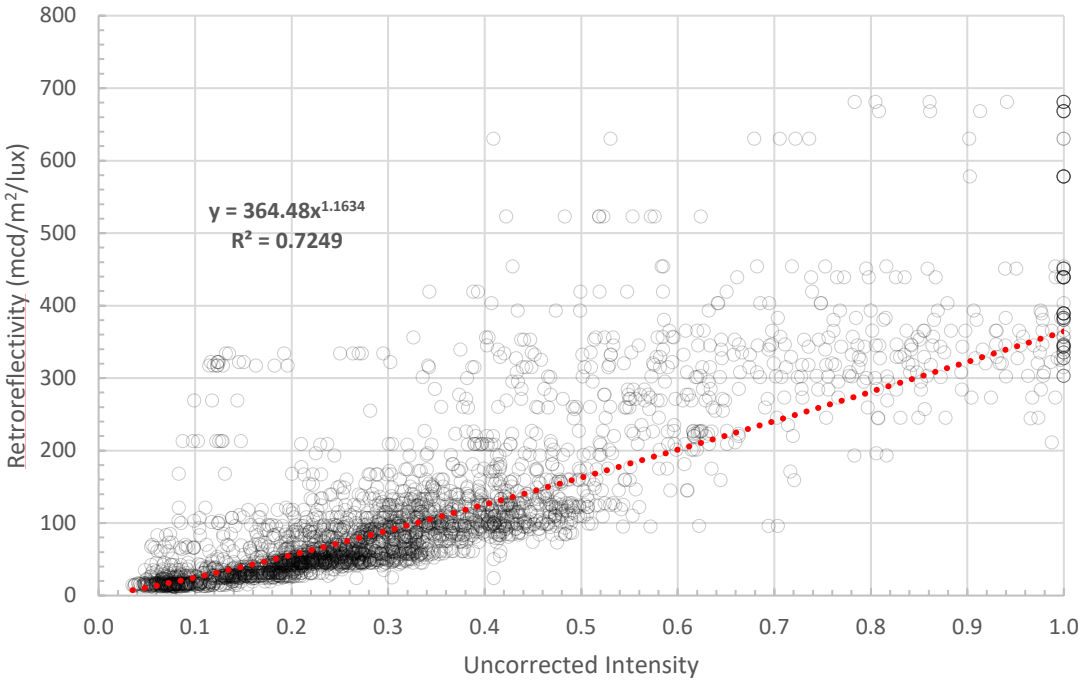

(a) Nearest Neighbor

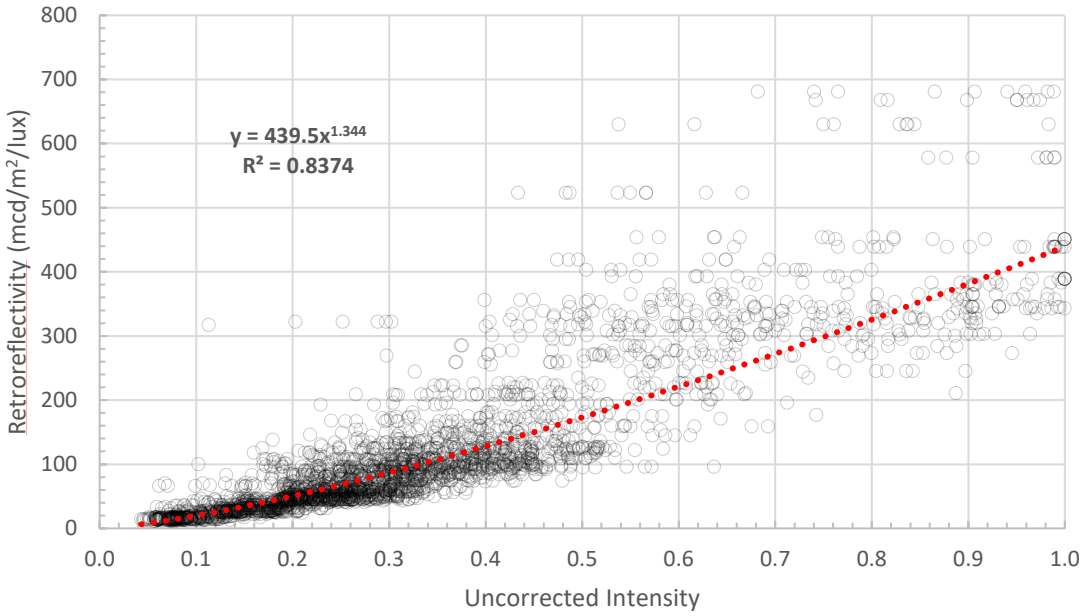

(b) Active Window Mean

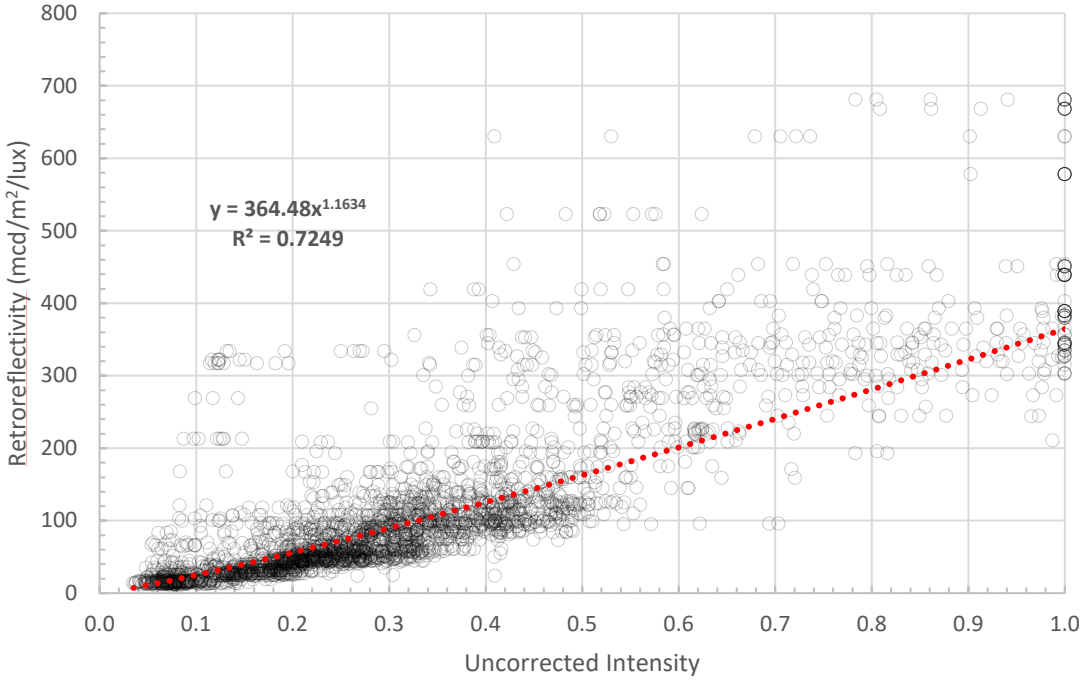

(c) Passive Window Mean

Figure 9.4: Example correlations between intensity values and retroreflectivity with different sampling approaches of (a) Nearest Neighbor, (b) Active Window Mean, and (c) Passive Window Mean.

Based on visual analysis of the distribution of the data points from the Testdeck II experiment, the project team explored a number of models such as power, linear, and exponential functions

for the least squares regression. The project team also explored a number of models correcting the intensity values for range and angle of incidence. The range to a point was obtained by matching each point to the corresponding point on the trajectory based on timestamp and then computing the distance. Given the limited possible geometric configurations of acquisition from the roadway, it was found that angle of incidence and range were highly correlated (Figure 9.5).

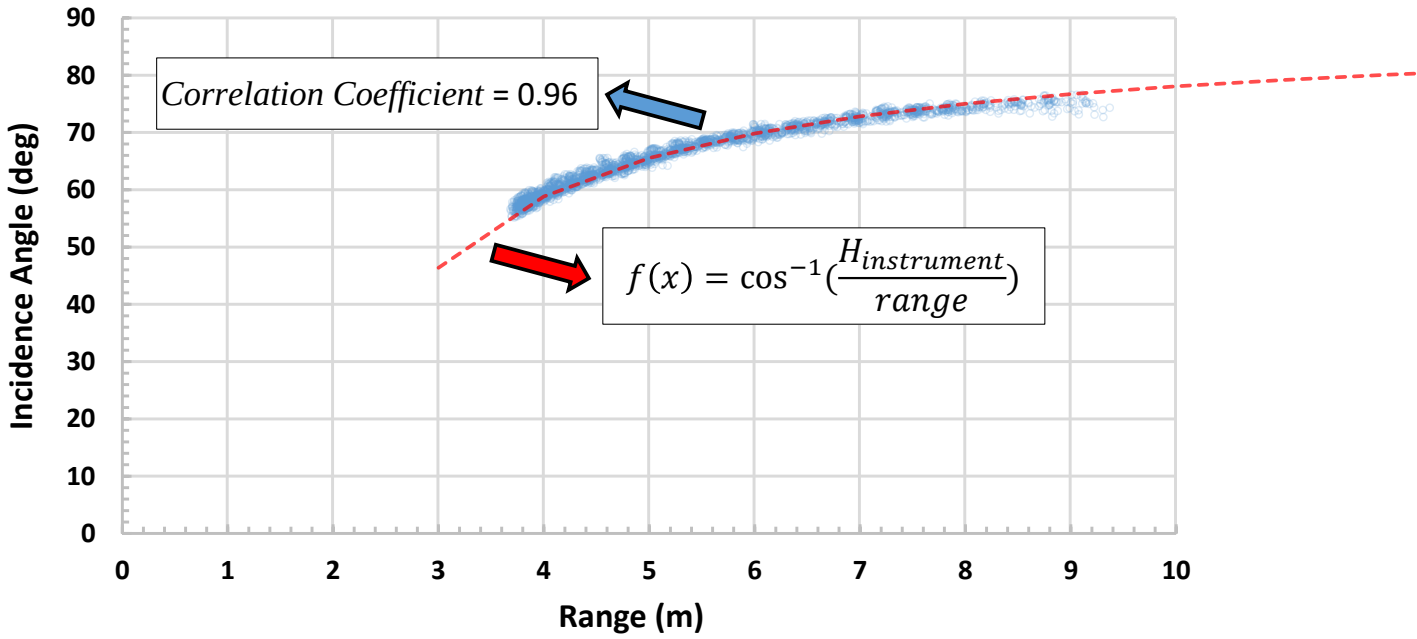

Figure 9.5: Correlation between the range and incidence angle at the sample points on the road surface.

Hence, the project team tested a model applying a range correction to the intensity models as a second order polynomial function, as is common in the literature (e.g., Kashani et al. 2015). To evaluate the performance of each sampling technique and model, the project team calculate not only the correlation coefficient (R2) showing the fitting quality in retrieving retroreflectivity (Table 9.4) but also the variance of intensity showing the uncertainty of the intensity value in the least squares regression quantitatively (Table 9.5). Both tables are color coded by the corresponding values where the color ramp from green to red represents the fitting quality from high to low. The variance of intensity from the regression analysis can serve as a reference to help with further analysis of the results in the experiment for validation and accuracy assessment by detecting a potential over-fitting problem, which is critical for a data-driven empirical model. For example, if a validation using an independent dataset is conducted with errors significantly larger than what the variance is shown in the least squares regression, there can be an overfitting problem during the model development, thus indicating that the model is invalid.

Table 9.4: Correlation Coefficients (R^2) from Least Squares Regression using Different Sampling Approaches and Models for Retrieving Retroreflectivity.

Model / Sampling tech.	$a \times Int.^b$	$a \times Int. + b$	$a^{b \times Int.}$	$a \times Int.^2 + b \times Int. + c$	$a \times Int.^b + c$	$(a \times range^2 + b \times range + c) \times Int.^d$
Nearest Neighbor	0.7002	0.6963	0.6361	0.6982	0.6930	0.7128
Active Window Mean	0.7798	0.7815	0.6899	0.7817	0.7597	0.7795
Active Window IDW^1	0.7670	0.7682	0.6802	0.7684	0.7500	0.7708
Active Window IDW^2	0.7479	0.7474	0.6680	0.7478	0.7340	0.7553
Active Window 05%	0.8357	0.8273	0.7980	0.8348	0.8006	0.8191
Active Window 10%	**0.8360**	0.8306	0.7870	0.8352	0.8009	0.8190
Active Window 15%	0.8277	0.8248	0.7694	0.8273	0.7933	0.8147
Active Window 20%	0.8186	0.8173	0.7526	0.8187	0.7870	0.8094
Active Window 30%	0.8043	0.8041	0.7275	0.8048	0.7777	0.8006
Active Window 40%	0.7779	0.7786	0.6940	0.7788	0.7555	0.7779
Active Window Median	0.7436	0.7438	0.6543	0.7439	0.7283	0.7484
Passive Window Mean	0.5913	0.5856	0.5422	0.5905	0.5536	0.5764
Passive Window IDW^1	0.7552	0.7537	0.6771	0.7556	0.7296	0.7516
Passive Window IDW^2	0.7527	0.7525	0.6714	0.7530	0.7351	0.7571
Passive Window 05%	0.5412	0.5388	0.5242	0.5411	0.5349	0.5583
Passive Window 10%	0.5598	0.5591	0.5333	0.5600	0.5549	0.5819
Passive Window 15%	0.5677	0.5675	0.5353	0.5680	0.5624	0.5919
Passive Window 20%	0.5797	0.5787	0.5457	0.5798	0.5701	0.5988
Passive Window 30%	0.5839	0.5825	0.5387	0.5836	0.5662	0.5882
Passive Window 40%	0.5674	0.5664	0.5105	0.5670	0.5324	0.5490
Passive Window Median	0.5219	0.5200	0.4593	0.5207	0.4691	0.4832

Table 9.5: Variance of Intensity Values in Least Squares Regression using Different Sampling Approaches and Empirical Models for Estimating Retroreflectivity.

Model / Sampling tech.	$a \times Int.^b$	$a \times Int. + b$	$a^{b \times Int.}$	$a \times Int.^2 + b \times Int. + c$	$a \times Int.^b + c$	$(a \times range^2 + b \times range + c) \times Int.^d$
Nearest Neighbor	0.0249	0.0265	0.0269	0.0316	0.0367	0.0355
Active Window Mean	0.0213	0.0226	0.0248	0.0269	0.0324	0.0311
Active Window IDW^1	0.0219	0.0232	0.0252	0.0277	0.0331	0.0317
Active Window IDW^2	0.0228	0.0242	0.0257	0.0289	0.0342	0.0328
Active Window 05%	0.0189	0.0203	0.0209	0.0241	0.0304	0.0287
Active Window 10%	**0.0188**	0.0200	0.0213	0.0239	0.0302	0.0286
Active Window 15%	0.0192	0.0203	0.0221	0.0244	0.0306	0.0289
Active Window 20%	0.0196	0.0207	0.0227	0.0249	0.0310	0.0292
Active Window 30%	0.0202	0.0214	0.0236	0.0257	0.0315	0.0297
Active Window 40%	0.0214	0.0227	0.0248	0.0272	0.0328	0.0313
Active Window Median	0.0229	0.0244	0.0261	0.0290	0.0344	0.0332
Passive Window Mean	0.0294	0.0314	0.0300	0.0366	0.0440	0.0448
Passive Window IDW^1	0.0224	0.0240	0.0252	0.0284	0.0344	0.0332
Passive Window IDW^2	0.0226	0.0240	0.0255	0.0286	0.0341	0.0327
Passive Window 05%	0.0330	0.0336	0.0333	0.0408	0.0472	0.0476
Passive Window 10%	0.0319	0.0327	0.0325	0.0396	0.0456	0.0456
Passive Window 15%	0.0313	0.0322	0.0320	0.0389	0.0449	0.0446
Passive Window 20%	0.0305	0.0317	0.0312	0.0380	0.0441	0.0438
Passive Window 30%	0.0298	0.0313	0.0307	0.0373	0.0436	0.0437
Passive Window 40%	0.0300	0.0317	0.0310	0.0374	0.0448	0.0457
Passive Window Median	0.0312	0.0333	0.0320	0.0389	0.0472	0.0492

From this rigorous analysis of model quality shown in Table 9.4 and Table 9.5, the power function with two coefficients using the 10th percentile of intensity in the active window

footprint fits the sampling data better than any other models tested in this work in terms of both R2 values and variance of intensity values. Because all the sampling points are evenly weighted in the regression process, the points concentrated at lower retroreflectivity and intensity may cause a bias in determining the coefficients of the retroreflectivity retrieval model. To compensate the bias in the sampling dataset, the project team weight each sampling point by its retroreflectivity value in the least squares regression. This weighting helps improve the fit at the higher retroreflectivity values where there is more scatter and less data. Then, the final coefficients of the power function for the radiometric calibration can be derived from a weighted least squares regression (Figure 9.6). The proposed empirical retroreflectivity prediction model is further validated and evaluated quantitatively in the Chapters 11 and 12 using independent data (US 20 in Philomath).

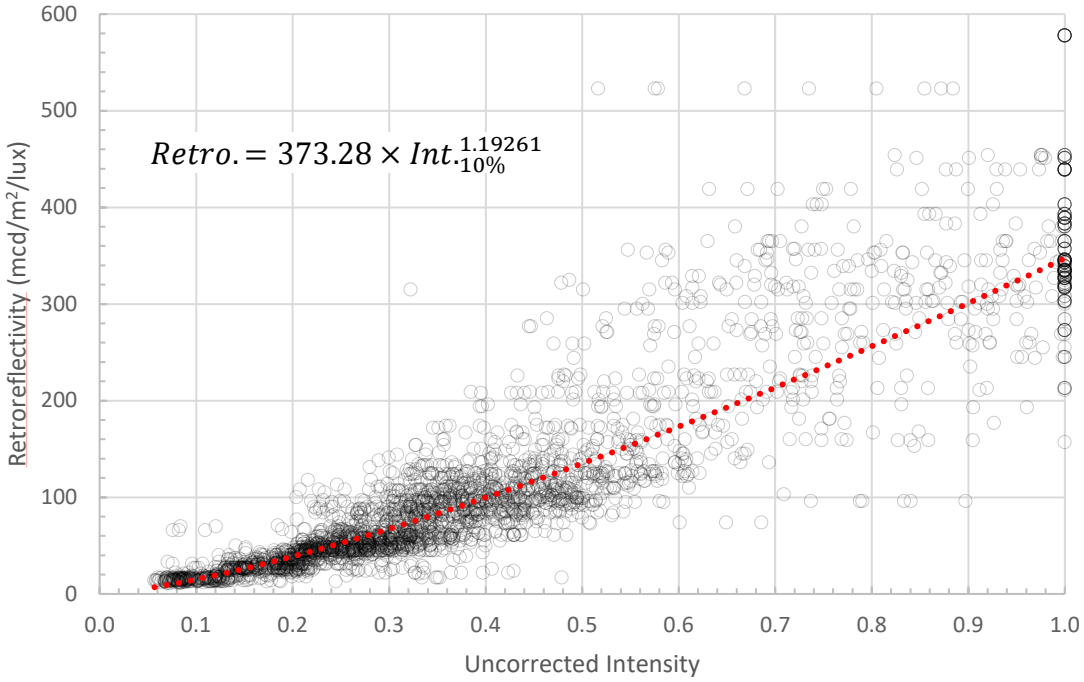

Figure 9.6: Final resulting retroreflectivity prediction model derived from the weighted least squares regression using the 10th percentile of intensity values within the active window. The equation shows the coefficients of the proposed empirical model and is plotted as a red line.

Table 9.6 provides a comparison of the Testdeck II dual profiler accuracies for different colors and types of pavement markings.

Table 9.6: Testdeck III Dual Profiler: Accuracy as a Function of Material Type and Color.

	Retroreflectivity measurement (mcd/m2/lux)					Estimation Results	
	Average	**Std. Dev.**	**Max**	**Min**	**Median**	**Mean Error**	**RMSE**
White	71.2	58.8	300	11	61	21.7	34.5
Yellow	56.4	56.4	325	12	36	16.2	29.6
MMA	89.2	70.8	325	25	63.5	21.8	36.8
Preformed	47.6	39.1	144	12	30	13.4	24.8
Thermo	54.4	51.1	255	11	27	21.6	33.6

In general, higher RMSE values are observed for the materials with the higher retroreflectivity. The same is true where the white samples had a higher RMSE compared with the yellow given the higher retroreflectivity values of the white stripe.

10.0 RETROREFLECTIVITY DEGRADATION AND MEASUREMENT REPEATABILITY EVALUATION

To demonstrate the effectiveness of the proposed model in detecting and quantifying the retroreflectivity degradation on the pavement markings, the project team computed the differences in retroreflectivity collected from MTLS and handheld retroreflectometer from the Testdeck II and Testdeck III surveys. These surveys were completed 10 months apart. A total of 239 sampling points from 24 transverse stripes on the Testdeck were suitable for the comparison.

10.1 POSITIONING ACCURACY ASSESSMENT

Prior to comparing retroreflectivity readings, the project team evaluated the local positioning accuracy of the sampling points by computing the distance of a sample point coordinates measured by the total station between the Testdeck II and Testdeck III surveys (Table 10.1). In order to maintain high accuracy for the local coordinates of the sampling points, the project team adjusted all of the points by holding the control points fixed with the same coordinates for both surveys so that the project team did not consider geo-referencing error. Hence, the primary source of error would be the error in marking sampling points while the errors associated with targeting the markings for retroreflectivity measurement are considered within the measures of repeatability and reproducibility of the retroreflectometer. The results show that overall the project team achieved an average local positioning accuracy within several centimeters for local positioning, which is significantly smaller than the retroreflectivity window.

Table 10.1: Summary of Local Positioning Errors at the Sampling Points (Units: Meters)

Error	Average	Max.	Min.	Median	Std. Dev.
1-D Error (Vertical)	-0.008	-0.005	-0.015	-0.008	0.002
2-D Error (Horizontal)	0.026	0.064	0.002	0.022	0.016
3-D Error	0.028	0.065	0.007	0.023	0.015

10.2 HANDHELD RETROREFLECTOMETER DEGREDATION

The project team summarized the results of retroreflectometer degradation using the handheld retroreflectometer observed between Testdeck II and Testdeck II (Table 10.2). These degradations are categorized by material type. From these readings, the MMA and preformed materials both performed well but the thermoplastic degraded much more significantly. The white stripes also showed more degradation compared with yellow stripes. However, a detailed analysis of the material performance is beyond the scope of this work since this work focuses on the ability of the mobile lidar to capture these differences compared with the handheld retroreflectometer. Future research efforts could use the mobile lidar data and GIS outputs of

this research to perform more detailed analysis of the retroreflectivity degradation of different materials to evaluate their overall performance.

Table 10.2: Summary of retroreflectivity degradation measured with the handheld retroreflectometer between the Testdeck II and III surveys, categorized by material type. Values are in units of mcd/m^2/lux.

Material/Color	Average	Max.	Min.	Median
MMA	-51.3	37	-274	-20
Preformed	-57.5	5	-287	-36
Thermo	-110.5	10	-560	-68
White	-80.6	37	-560	-68
Yellow	-65.3	22	-488	-32
All	-72.9	37	-560	-45

10.3 SPOT CHECK REPEATABILITY TEST

In Table 10.2, several sample points indicate a positive difference in retroreflectivity, which would be abnormal. These degradation estimates simply show the uncertainty in the retroreflectometer measurements because the retroreflectivity would be expected to degrade with time due to the continued wear on the stripe. For example, for the measurements on the MMA stripes, according to ASTM1710-11, the reproducibility standard deviation is 22.9 mcd/m2/lux while the repeatability standard deviation is 14.4 mcd/m2/lux. Because reproducibility considers the ability of independently achieving the same results with a different system, operator, calibration and conditions whereas repeatability considers the ability of achieving the same results with repeated measurements with the same device in similar conditions. If this uncertainty is propagated to the differences between two retroreflectivity readings to measure degradation, the reproducibility and repeatability are 32.4 and 20.4 mcd/m2/lux, respectively. In addition to the reported repeatability standard deviations provided by ASTM, the project team conducted a repeatability test by measuring the retroreflectivity 10 times at the same point located on a cracked portion of the longitudinal stripe, which resulted in some inconsistency in the readings (Figure 10.1).

The results (Table 10.3) of this repeatability test show the uncertainty in measuring retroreflectivity with a hand-held retroreflectometer, which should be considered when interpreting the results of the validation and analysis of the radiometric calibration in other sections of this report. The values in Table 10.3 are somewhat higher than those reported in ASTM given that the ASTM study was completed with an experimental setup with new painted markings in good shape rather than the worn and irregular cracked stripe used in our study. Such differences in reproducibility and repeatability can be caused by any or all of five error sources listed in ASTM 1710-11: (1) slight changes in position; (2) transverse lines yield less uniform readings than longitudinal lines due to the wear; (3) the readings are affected by the refractive index of the glass spheres and their depth of embedment and population on the pavement marking material; (4) the pigment loading of the binder, road films, dirt, dust, etc. will also affect the readings; and (5) the physical characteristics of the specimen (e.g., cracks on the stripe in this study) can affect the entrance angle with respect to the specimen plane.

Figure 10.1: Example section of the longitudinal stripe with cracks measured in repeatability test.

Table 10.3: Summary of repeatability test with the handheld retroreflectometer. 10 measurements were completed at each sample location.

Point #	Average	Max.	Min.	Median	Std. Dev
Sample 1	275.8	317	214	280.5	31.4
Sample 2	258.8	284	239	258	16.7
Sample 3	188.2	236	142	183.5	29.1
Sample 4	311.5	332	277	313.5	18.4

10.4 DEGRADATION RESULTS FROM MOBILE LIDAR

Using the model developed in Chapter 9.0, the project team estimated the retroreflectivity at the Testdeck samples and evaluated their degradation using mobile lidar data. These values were then compared with the degradation determined from the handheld retroreflectometer. For Testdeck II and III, the retroreflectivity degradation is evaluated by comparing the retroreflectivity estimation with the passes with the same lane (left, right, or shoulder), speed (25mph), and orientation (-30°) for consistency. As previously mentioned, the proposed radiometric calibration model has an intensity saturation limit (corresponding to 373 mcd/m2/lux) to estimate retroreflectivity. This threshold is substantially above the current requirements of 250 and 200 mcd/m2/lux for new installation of white and yellow stripes, respectively (Table 2.4). Hence, the project team only used the sample points with a retroreflectivity lower than this saturation limit of the lidar sensor for the following analysis.

Based on this comparison of the distribution of retroreflectivity degradation evaluated by the handheld retroreflectometer and mobile lidar (Figure 10.2), the right lane (the same lane as the Testdeck markings) provides the most similar distribution with the ground truth measurement while the results from the other two lanes show good similarity for a decrease in retroreflectivity more than 100 mcd/m2/lux. Higher discrepancies in the distributions of degradation are observed when the degradation is less than 100 mcd/m2/lux, which are more difficult to resolve given the reproducibility of the retroreflectometer on evaluating these worn stripes. Fortunately, the pavement markings with a larger degradation would be of interest in this case for determining the need for and extent of maintenance.

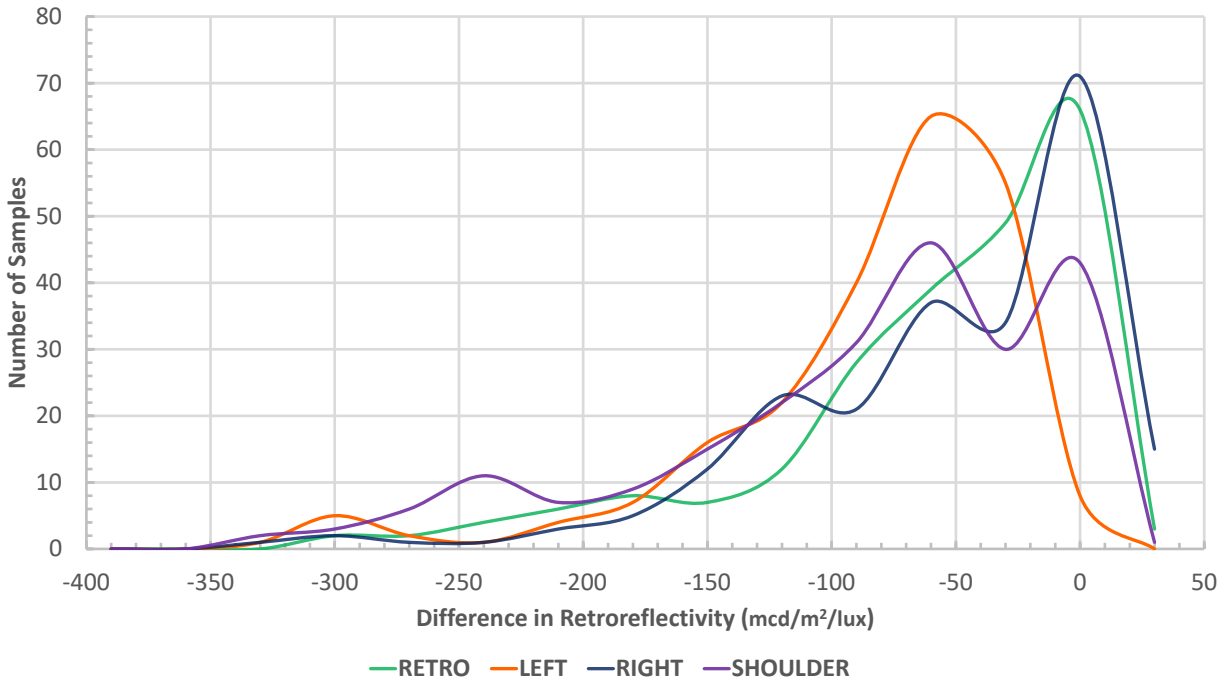

Figure 10.2: Distribution of retroreflectivity degradation determined with mobile lidar passes from several lanes and compared with the handheld retroreflectometer (RETRO) on the Testdeck obtained from Testdeck Experiments II and III

To further evaluate the effectiveness of the proposed model in detecting degradation quantitatively, the mean error (ME) and root mean squared error (RMSE) are computed for the passes on each lane (Table 10.4).

Table 10.4: Accuracy assessment for the proposed radiometric calibration model in evaluating the retroreflectivity degradation (mcd/m^2/lux)

Pass	Mean Error	RMSE
Left -30°	-26.2	50.5
Right -30°	4.7	40.5
Shoulder -30°	-31.9	47.8

The ME and RMSE values for the right lane show that the result is very accurate comparing with the reproducibility of the retroreflectivity measurement. Although the results on the shoulder and left lane are not as accurate as right lane, the ME values are negative, which indicates that the proposed model tends to over-estimate the retroreflectivity degradation, leading to a more conservative decision. Note that for this degradation study only single profiler data were used to be consistent between the Testdeck surveys since the dual profiler configuration was not available for the Testdeck II survey. Hence, these results of degradation evaluation would likely be significantly improved by using the dual profiler configuration because the dual profiler provides higher accuracy and precision in estimating retroreflectivity (as will be explored in the subsequent sections).

11.0 REPEATABILITY TESTING AND VALIDATION

11.1 TEST OBJECTIVES

A test site was selected in Philomath, Oregon for data capture for validation with the following objectives:

1. Validate the current radiometric calibration model for estimating the retroreflectivity using an independent data source from the Testdeck data used in development of the model.

2. Test the capabilities of the mobile lidar system for evaluating the retroreflectivity on a stripe with highly variable wear.

3. Explore the optimal driving lane of the mobile lidar system for retroreflectivity evaluation of the longitudinal stripe.

4. Evaluate the effects of using dual profiler versus single profiler data, and

5. Test the effectiveness of the marking extraction approach (Section 3.0) and its robustness to the data collected at different speeds.

11.2 TEST DESCRIPTION

The Philomath Validation Test was conducted on July 19, 2017 for a section (Figure 11.1) of the Corvallis-Newport Hwy (Westbound), east of N 20th St.

Figure 11.1: Validation test site in Philomath, Oregon (44°32'24.6" N 123°21'22.9" W).

11.2.1 Control points

In this field test, the point cloud data is geo-referenced through a direct geo-referencing solution using the GPS and IMU integrated on the mobile lidar system (Leica Pegasus:Two), which was determined to have a positioning uncertainty of approximately 5 cm based on the results of the Testdeck I survey. In order to geo-reference the retroreflectivity readings as well, 5 control points were set across the area of interest as a constraint for merging all the data together into a common coordinate system (Figure 11.2). CP1, CP3, and CP5 were created by painting a checkerboard template on the pavement around a PK nail while the project team used 4.5" black/white pattern targets for CP2 and CP4, which also could be extracted in the mobile lidar data and measured reflectorlessly with the total station. After the mobile lidar driving passes were complete, the project team performed rapid static GNSS observations over control points CP1, CP3, and CP5 using a Leica GS14 GNSS Receiver. The project team registered all the data using these coordinates as constraints. The coordinate system used for this work is the OCRS Salem Zone NAD83(2011) Epoch 2010.00 and Geoid 12B (Unit: Meters).

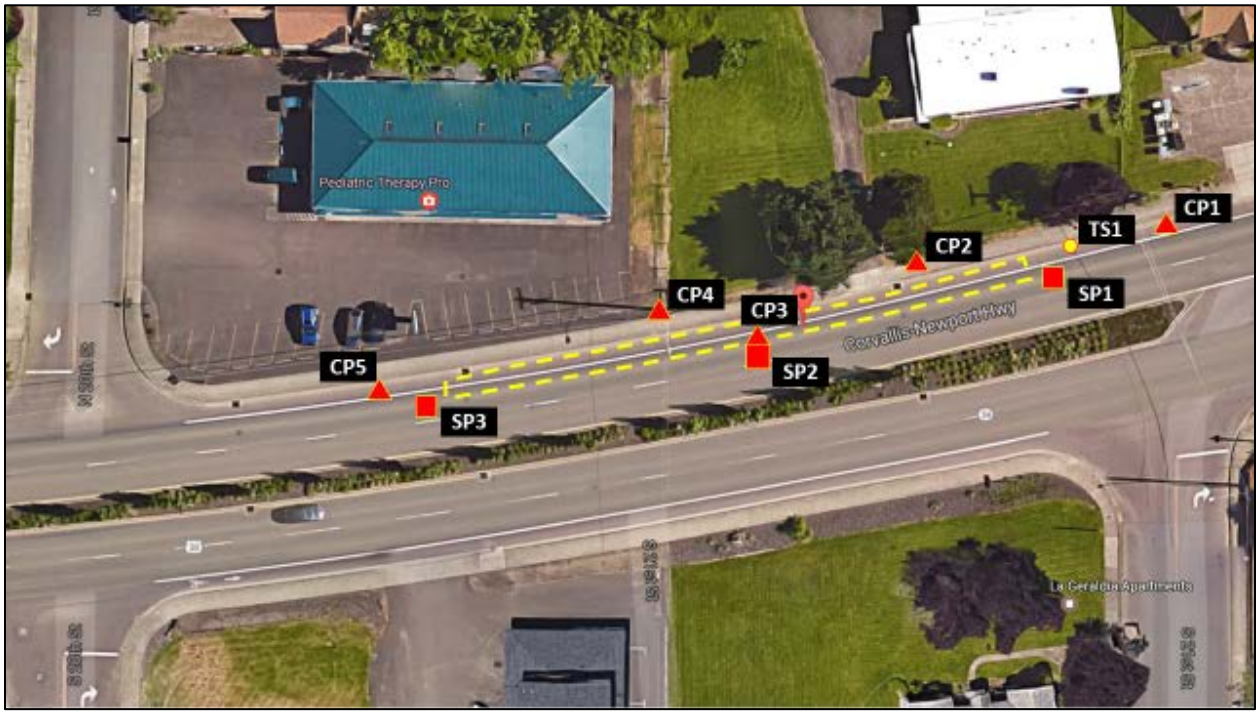

Figure 11.2: Control points (CP1 – CP5), total station set-up location (TS1), and scan setup position (SP1 – SP3).

11.2.2 MTLS passes

The lidar data was collected by Oregon DOT's Leica Pegasus:Two mobile lidar system from both traffic lanes in the fixed dual profiler orientation (-30/+60°) at speeds of 15 mph and 25 mph (Table 11.1). For each pass, the length of the stripe both before and after the worn section of the longitudinal stripe was captured to cover a wide range of retroreflectivity within a single location. Four passes were completed in both the left and right lanes at 25 mph respectively to test the repeatability of the derived retroreflectivity values from the MTLS system. After

confirming all the 10 passes are collected properly, a copy of the raw data was downloaded to a USB drive provided to Oregon DOT by OSU and another copy was taken to OSU for processing. Table 11.2 summarizes the range and angle of incidence values achieved on the pavement markings during this test.

Table 11.1: Summary of Data Collection for Mobile Lidar System.

Pass #	Lane	Orientation (°)	Speed (mph)
01	Left	-30/+60	15
02	Left	-30/+60	25
03	Left	-30/+60	25
04	Left	-30/+60	25
05	Left	-30/+60	25
06	Right	-30/+60	15
07	Right	-30/+60	25
08	Right	-30/+60	25
09	Right	-30/+60	25
10	Right	-30/+60	25

Table 11.2: Summary of range and incidence angle values to the -30° profiler for data obtained on pavement markings for different mobile lidar configurations.

Lane	Parameters	Scanner Orientation
		-30°
Left	Range	5.37 – 6.84 m (17.6 – 22.4 ft.)
	Incidence Angle	66.23 – 73.88°
Right	Range	3.78 – 4.27 m (12.4 – 14.0 ft.)
	Incidence Angle	56.02 – 59.28°

11.2.3 Retro reading:

Using the Delta LTL-X from Oregon DOT the project team measured the retroreflectivity every 0.5 meters (1.6 ft.) on the longitudinal stripe, resulting in a total of 155 retro readings. In addition, 22 retro readings on the pavement were acquired. The position of each reading was pre-marked and captured with the total station. During the data collection, the retroreflectometer was consistently oriented to the west.

11.2.4 TLS collection:

In this work, the project team also collected high resolution Terrestrial Laser Scanning (TLS) data using a Leica P40 to capture more detailed information and compare against the MTLS data. TLS units also operate over a larger range of distances and angles of incidence. A GPS receiver was mounted on top of the scanner to aid with geo-referencing. There are 9 scans in total collected with the settings below:

- Field of view: Horizontal: Target All, Vertical: -55 – 30°

- Scanning: Resolution: 0.01m @ 30m, Mode: Range, Sensitivity: Normal
- Imaging: Resolution: 1920 x 1920, HDR: No

Ultimately, analysis of the data was deemed unnecessary for this project. However, the data was collected to provide a TLS dataset should Oregon DOT desire to utilize their TLS units for spot checks or detailed retroreflectivity analyses at some point in the future.

11.3 TEST RESULTS AND ANALYSIS

11.3.1 Validation of the proposed radiometric calibration model

The calculated retroreflectivity values from the mobile lidar data are compared against the retroreflectometer measurements as ground truth (Table 11.3) to quantitatively validate the proposed radiometric calibration model. For each pass, the project team computed the mean error (ME) and root-mean-squared error (RMSE) for all of the retroreflectometer data points collected. The ME and the RMSE represent the accuracy and the precision of the proposed model, respectively, in estimating the retroreflectivity (mcd/m^2/lux). For each lane, the project team also combined all of the results of the passes in that lane to obtain an overall accuracy and precision for the lane.

Table 11.3: Summary of the accuracy assessment of the retroreflectivity estimation. (Unit: mcd/m^2/lux)

Lane & Pass #		Single profiler (-30°)		Dual profiler (-30°/+60°)	
		Mean Error	***RMSE***	***Mean Error***	***RMSE***
Left Lane	01	-0.1	22.9	-0.5	21.4
	02	-3.4	24.1	-4.0	23.0
	03	-3.3	25.5	-4.0	23.9
	04	-5.3	24.4	-4.6	23.4
	01 – 04	-3.0	24.2	-3.3	22.9
Right Lane	05	-21.8	35.8	-7.1	25.1
	06	-21.1	35.1	-8.1	25.2
	07	-20.9	35.2	-5.4	24.4
	08	-24.0	37.4	-9.1	25.4
	05 – 08	-22.0	35.9	-7.4	25.0
All Passes		-12.5	30.6	-5.4	24.0

The project team compared the ME and RMSE under different system configurations and lane selections. Table 11.4 shows the passes from the left lane consistently provided improved results compared to passes in the right lane with the same profiler configuration in terms of both ME and RMSE. This improvement likely occurs because the longitudinal stripe is closer to the mobile lidar system for the right lane passes compared with the left lane passes, resulting in larger incidence angles for the left lane passes. Because the retroreflectometer simulates retroreflectivity at a range of 30 meters (98,4 ft) with an incidence angle of 88.76° (ASTM1710-11), the scan geometry on the left lane is more similar to that being simulated by the handheld

retroreflectometer. As a result, the left lane provides a more accurate and precise result in estimating retroreflectivity of the longitudinal stripe with the proposed method. Fortunately, by utilizing the dual-profiler, the results on the right lane are significantly improved and similar to those obtained on the left lane. The primary reason for this improvement is that the +60° profiler collects data on the longitudinal stripe at a larger range and incidence angle. Hence, the dual configuration helps balance the effects of acquisition geometry when capturing information for stripes across the roadway.

Table 11.4: Accuracy comparison under different system configurations and lane selections. (Unit: mcd/m^2/lux)

Comparison	Lane & Pass	$d_{abs(ME)}$	d_{RMSE}
Single profiler → Dual profiler	Left 01 – 04	0.2	-1.3
	Right 05 – 08	-14.5	-10.9
	All passes	-7.1	-6.6
Right lane → Left lane	Single Profiler	-18.9	-11.6
	Dual Profiler	-4.2	-2.1

The project team further demonstrated the repeatability of the proposed model by plotting the average retroreflectivity values extracted from data acquired from the left and right lanes (Figure 11.3). Although both the single and dual profiler data show similar trends with the ground truth retroreflectivity measurements overall, the dual profiler provides a more robust result regardless of the lane driven. The dual profiler not only increases the point density, which may help improve the overall repeatability, but the acquisition of points at a different incidence angle helps provide additional data at a geometric configuration more consistent to the physics that are being modeled by the retroreflectometer. Thus, to some extent, it helps overcome the need for intensity corrections in the proposed model without compromising the overall accuracy and precision.

The results from the precision test of the handheld retroreflectometer (ASTM E1710-11) and the proposed model is comparable to the manual retroreflectivity precision test measurements in terms of repeatability and reproducibility. Additionally, the project team compared the result of the proposed radiometric calibration against the evaluation to the mobile pavement marking retroreflectivity measurement system reported by (Pike and Carlson, 2013). The results of percentage error (Table 11.5) show that the proposed method based on mobile lidar intensity is consistent, although slightly underestimating the retroreflectivity, which yields more conservative results. The proposed method shows higher accuracy (-5.89% ~ -0.3%) than mobile retroreflectometer measurement systems (-12.80% ~ +30.88%). However, the proposed radiometric calibration model is limited by the range of intensity values that can be captured by the sensor so that it can only estimate retroreflectivity equal to or lower than 373 mcd/m^2/lux (Section 9.4.2). Above that threshold, the intensity values saturate.

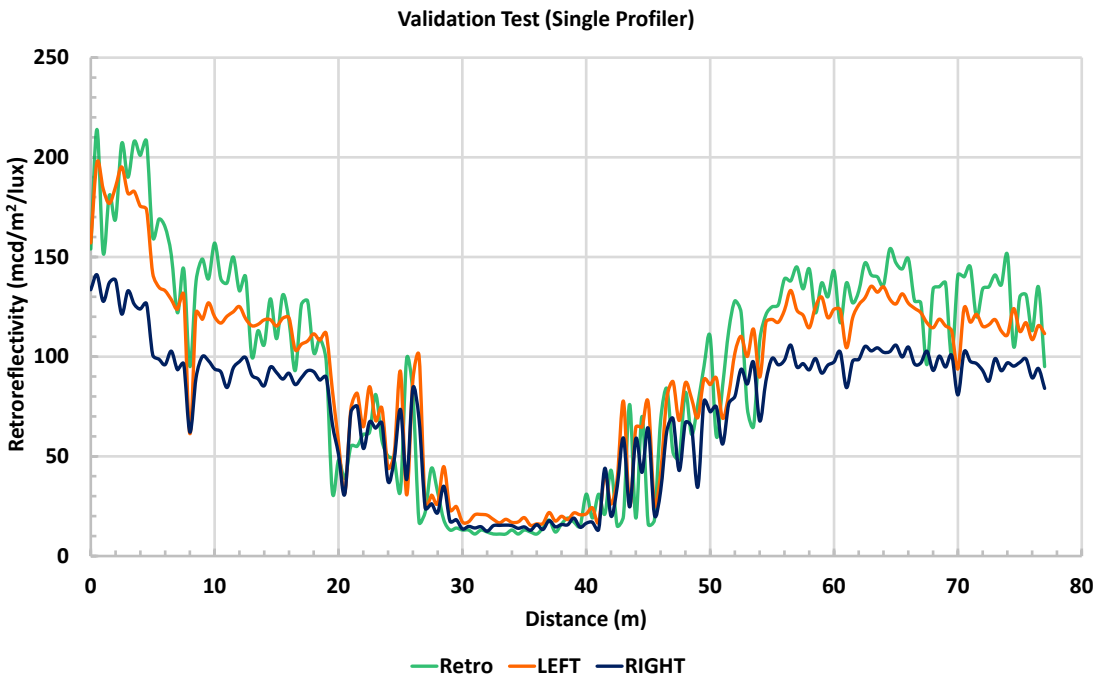

(a) Single profiler.

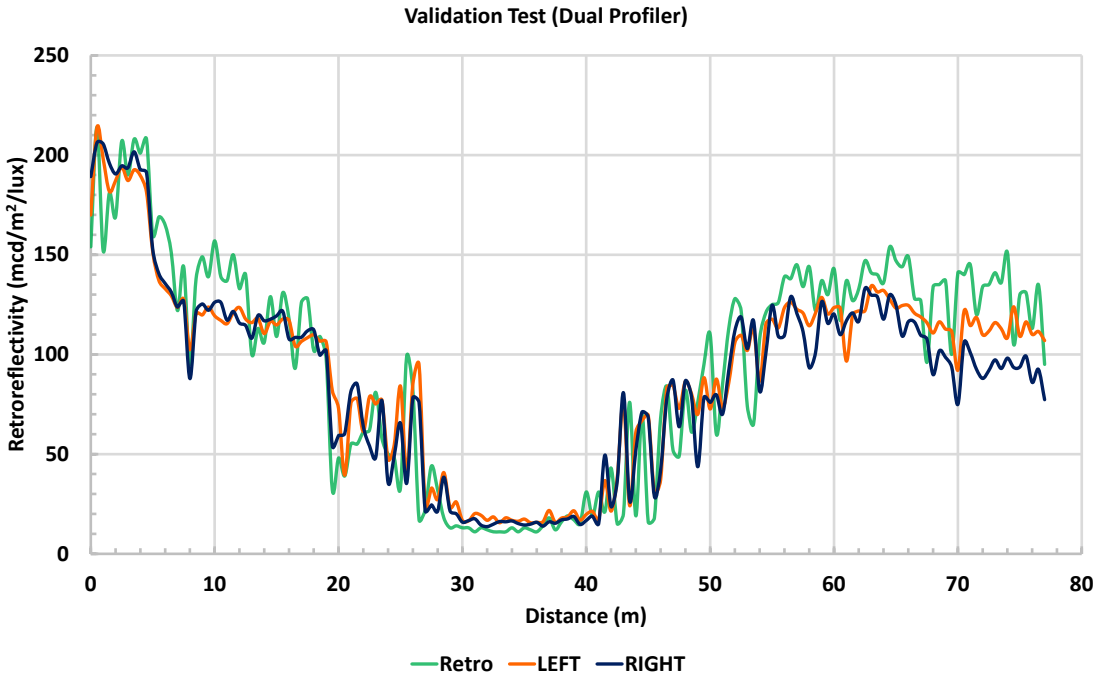

(b) Dual profiler

Figure 11.3: Lane sensitivity test of the proposed model for the single (a) and dual (b) profiler configurations: the averaged retrieved retroreflectivity on the left and right lanes are presented as orange and blue lines, respectively, while the green line represents the ground truth retroreflectivity readings.

Table 11.5: Summary of percent error for the single and dual profiler configurations for the left and right lanes.

Lane & Pass #		Single profiler (-30°)	Dual profiler (-30°/+60°)
		% Error	*% Error*
Left Lane	**01**	-0.04	-0.30
	02	-2.20	-2.63
	03	-2.17	-2.59
	04	-3.45	-2.97
	01 – 04	-14.14	-4.60
Right Lane	**05**	-13.71	-5.27
	06	-13.57	-3.53
	07	-15.59	-5.89
	08	-24.0	-9.1
	05 – 08	-22.0	-7.4
All Passes		-12.5	-5.4

The project team noticed that all of the mean errors are negative, which indicates that the proposed method tends to slightly under-predict the retroreflectivity. Hence, the next section will explore this influence on the determination of a pass/fail (compliance) rating for the pavement marking.

11.3.2 Validation of the road marking condition assessment

Oregon DOT's standard for minimum initial retroreflectivity is 250 mcd/m^2/lux for white and 200 mcd/m^2/lux for yellow, however, there is no requirement for minimum levels for worn pavement markings (see literature review for guidance from FHWA in Chapter 2) aside from the level of service guidance discussed in Section 2.4.2. Therefore, the project team selected a pass/fail threshold of 90 mcd/m^2/lux as recommended by Debaillon et al. (2007) to evaluate the retroreflectivity of a sampling point. This threshold separates the 155 ground-truth samples from the Philomath dataset into pass and fail categories with a proportion of 59% and 41%, respectively (Figure 11.4).

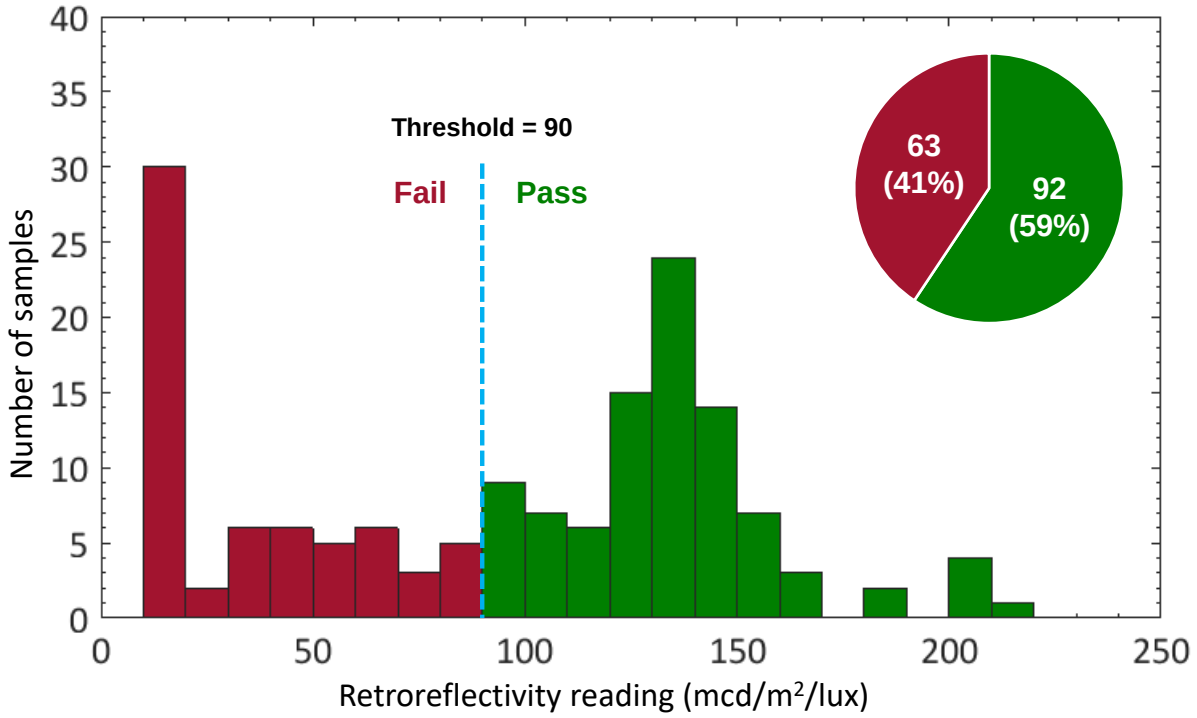

Figure 11.4: The distribution of the test data and the threshold of minimum retroreflectivity reading used in validation.

The precision, recall, and F1-score are then computed and compared to quantitatively evaluate the performance of the pass/fail decision and compact of lane selection and system configuration using the proposed method (Table 11.6 and Table 11.7).

Table 11.6: Evaluation of the proposed model for a pass-fail assessment of the retroreflectivity condition of the road marking.

Lane & Pass #		Single profiler (-30°)			Dual profiler (-30°/+60°)		
		Precision	***Recall***	***F1-score***	***Precision***	***Recall***	***F1-score***
Left Lane	01	91.84%	97.83%	94.74%	94.68%	96.74%	95.70%
	02	92.47%	93.48%	92.97%	94.51%	93.48%	93.99%
	03	94.57%	94.57%	94.57%	96.67%	94.57%	95.60%
	04	94.62%	95.65%	95.14%	95.65%	95.65%	95.65%
	01 – 04	93.35%	95.38%	94.35%	95.37%	95.11%	95.24%
Right Lane	05	97.18%	75.00%	84.66%	95.29%	88.04%	91.53%
	06	98.68%	81.52%	89.29%	97.62%	89.13%	93.18%
	07	98.70%	82.61%	89.94%	95.35%	89.13%	92.13%
	08	96.92%	68.48%	80.25%	96.34%	85.87%	90.80%
	05 – 08	97.92%	76.90%	86.15%	96.14%	88.04%	91.91%
All Passes		95.34%	86.14%	90.51%	95.74%	91.58%	93.61%

Table 11.7: Comparison of pass-fail accuracy under different system configurations and lane selections.

Comparison	Lane & Pass	$d_{precision}$	d_{recall}	$d_{f1\text{-}score}$
Single profiler vs. Dual profiler	Left 01 – 04	2.02%	-0.27%	0.89%
	Right 05 – 08	-1.78%	11.14%	5.76%
	All passes	0.40%	5.44%	3.10%
Right lane vs. Left lane	Single Profiler	-4.57%	18.48%	8.20%
	Dual Profiler	-0.77%	7.07%	3.33%

Irrespective of the various combinations of lane, pass, and configuration, the precision is consistently over 90%, which indicates that the proposed method is conservative in detecting a line in good condition. Further, these results agree with the analysis in the Section 11.3.1 that the proposed model exhibits better performance from the left lane compared with the right lane. Moreover, the precision percentage is generally more consistent and higher than the recall percentage, especially for the right lane with a single profiler. This proves that estimates from the proposed model are improved by using the dual profiler configuration. It also supports the finding that improved results can be achieved by collecting data from the adjacent lane (left in this example) next to the lane bounded by the stripe (right in this example). Lastly, the F1-score quantifies the accuracy of the proposed model by considering both precision and recall. Similarly, the F1-score indicates that the adjacent lane driving practice to collect data and utilizing the dual profiler configuration can improve the results.

12.0 GIS ANALYSIS TOOL DEVELOPMENT

12.1 OVERVIEW

This chapter describes the Road Marking Extractor (RoME) software and the supporting GIS python scripts for implementation of the research results. Figure 12.1 provides an overview of the various tasks required to implement the road marking process. The outputs of these tools are ultimately designed to support both detailed analyses of a specific corridor as well as summary layers to support regional or state-wide asset management efforts.

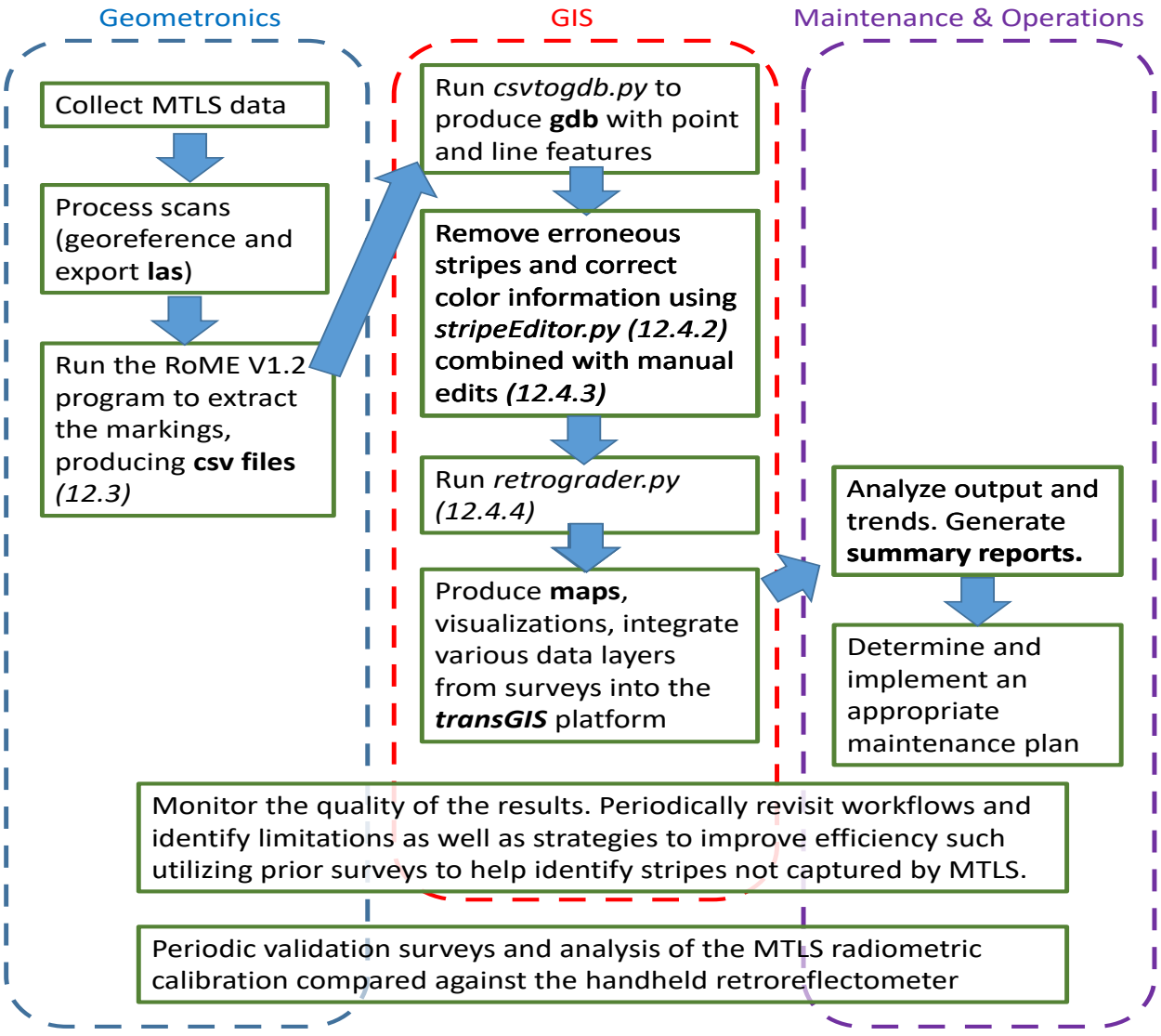

Figure 12.1: Potential execution plan of implementation tasks by Oregon DOT divisions.

12.2 DATA COLLECTION AND PROCESSING

Oregon DOT Geometronics has primary responsibility for acquisition and processing of mobile lidar data. In many cases, data they have already collected for other efforts can and should be utilized to build up a pavement marking GIS geodatabase. In some cases, specific MTLS surveys may be commissioned for pavement marking evaluation.

Geometronics exports ASRPS LAS 1.2 files with the point clouds as well as trajectory information (asciitrj) which serve as inputs to the RoME software described in the next section.

12.3 ROAD MARKING EXTRACTOR SOFTWARE

The RoME (Road Marking Extractor) program is a user-friendly, automated tool to extract and assess lane markings. This software was created by the OSU research team and is open source available for download at [*www.learnmobilelidar.com/software-tools*]. The inputs to the program are the point cloud (ASPRS LAS 1.2 format) and trajectory (asciitrj) data obtained by a mobile lidar unit. The outputs provide retroreflectivity evaluations that can be used for informed decision making for maintenance of road markings. The RoME tool contains a simple interface which does not require the user to have extensive knowledge of the program in order to successfully run it. Some of the material in this chapter has been packaged into a separate user guide document for simplicity as well.

At this time, road markings should be able to be extracted from most mobile lidar systems; however, the radiometric calibration applied for retroreflectivity evaluation is specific to Oregon DOT's current mobile lidar system (Leica Pegasus:Two) and will not produce correct results for other systems. Future releases may address these when radiometric calibrations have been completed and are integrated into the software. For mobile lidar systems with multiple profilers (i.e., scanners), the classification field should be provided to distinguish the data from each profiler; otherwise, the program needs two sets of las files: one set with data from a single profiler and a second corresponding set with the data from the other profilers combined. The data from the single profiler is used to extract the markings initially based on intensity and then used as a reference to extract the markings from the other profilers.

12.3.1 Tool features

Several features contained within the Graphical User Interface (GUI) of the RoME program are shown in Figure 12.2 and described in Table 12.1. Figure 12.3 shows the GUI for setting the user parameters, which are further described in Table 12.2. Figure 12.4 shows an example of final results of the extracted stripes.

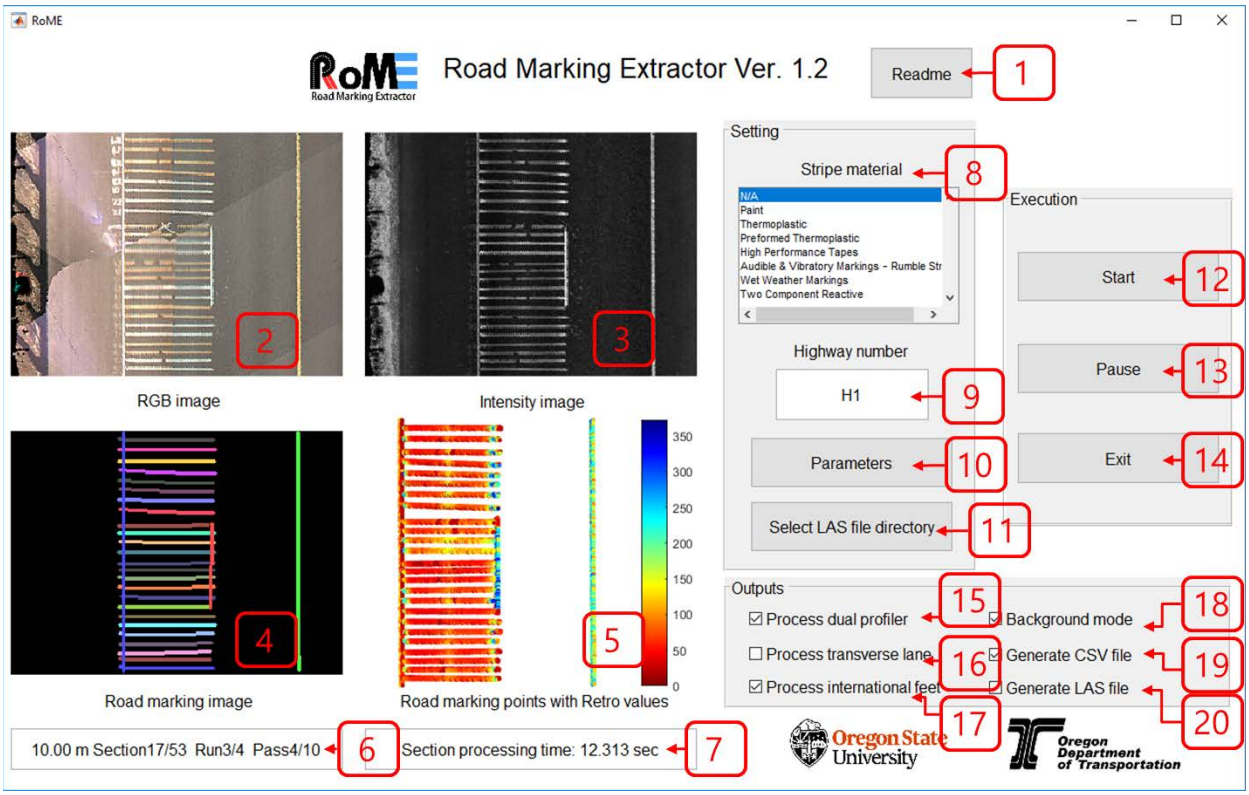

Figure 12.2: Main GUI of the RoME program (version 1.2).

Table 12.1: Description of the features in the main GUI shown in Figure 12.2.

No.	Description
1	Opens the user manual.
2	Displays the rasterized RGB image of each section from the input lidar data.
3	Displays the rasterized intensity image of each section from the input lidar data.
4	Displays the rasterized, extracted road markings of each section from the input lidar data.
5	Displays the point cloud corresponding to the extracted road markings of each section. The scale bar indicates the retroreflectivity estimates ranging from 0 to 373 mcd/m^2/lux.
6	Displays the progress (the discretized section length, the current section / the total number of sections included in the current run (LAS), the current run / the total number of runs included in the current pass (trajectory), the current pass / the total number of passes in the current directory).
7	Displays the processing time.
8	Enables the user to add the stripe material into the resulting *Stripe* CSV file. (All extracted stripes from that run will receive that attribute. The user may need to manually adjust those in GIS later).
9	This tool enables the user to enter the highway number into the resulting *Run* CSV file.
10	This tool enables the user to change the input parameters (See Figure 12.3 and Section 12.3.2).
11	This tool enables the user to browse the folder containing the mobile lidar data to be processed.
12	This tool enables the user to start the road marking extraction.
13	This tool enables the user to pause the road marking extraction process.
14	This tool enables the user to exit the program.
15	Select this checkbox to evaluate the road markings with using the dual profiler mobile lidar data. Note that the classification field should be provided to distinguish the data from each profiler (For the Leica Pegasus:Two Profiler 1 (-30°) is classified as 1 and Profiler 2 (+60°) is classified as 17); otherwise, the separate single profiler las files in addition to the dual profiler mobile lidar data are still required for the road marking extraction.
16	Select the checkbox to extract the transverse road markings in addition to longitudinal markings.
17	Select the checkbox to process the data in international feet rather than meters. Selecting this checkbox will also swap the parameter interface to appear in international feet. Note that the user should verify that they are consistent with using the same units throughout. If the input las file is in international feet, this box should be checked and the output will be international feet. However, if the user provides a las file in meters but then checks international feet, erroneous results will occur.
18	Select the checkbox to run the program in the background. In this mode, the program does not show the figures (Features 2-5) and the text (Features 6-7).
19	Select the checkbox to generate the CSV files. See the "Output files" section (Section 12.3.3) for detailed information about these files. Note that this option is required in order to run the python scripts to produce the GIS data layers.
20	Select the checkbox to export the extracted road marking points in LAS1.2 file format. See the "Output files" section (Section 12.3.3) for detailed information.

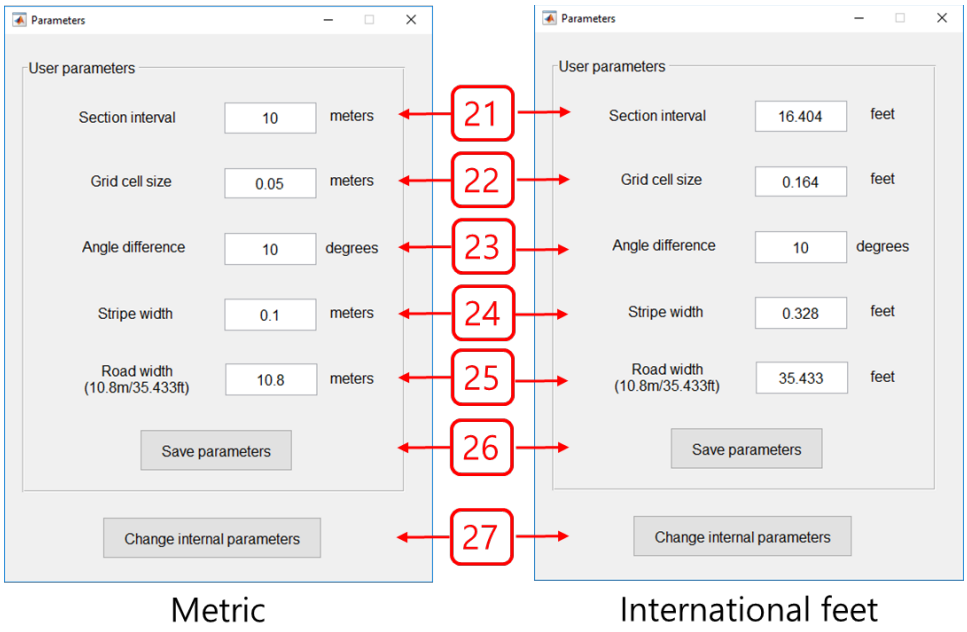

Figure 12.3: Parameter GUI with default settings in metric and international feet. These parameters are further described in detail in Table 12.2.

Table 12.2: Description of the parameter interface, shown in figure 12.3.

No.	Description
21	This is the interval value for dividing the road data into smaller sections. Dividing the road data will help reduce the computational complexity while allowing extension of the algorithm to reliably extract curved lane markings, which are more or less linear over a localized area.
22	This is the grid cell size for used for rasterization. The grid cell size is recommended to be smaller than the width of lane markings to be detected, but should not be too small to reduce processing time or result in substantial unoccupied grids on the rasterized image. It is also dependent on the resolution of the mobile lidar data, which is a function of vehicle speed. In general, 5 cm (0.164 ft.) has worked well.
23	This is the angle difference threshold to merge lane markings. The extracted lane markings may be over-segmented, primarily from moving vehicles. Line association is an important step to permit a proper segmentation by linking the segments which lie on the topologically-same lane. The conditions of line association are evaluated by this threshold value.
24	This is the stipe width used to extract the point cloud for the markings to be exported as LAS file format.
25	This is the estimated road width to be processed for road marking extraction. If the value is too large, more false positives will occur.
26	This tool enables the user to save the current parameter set to the file both for the run as well as the default.
27	This tool enables the user to access and modify the internal, advanced parameters used in the processing algorithms. ***Users should exercise caution in modifying these internal parameters, as changes could significantly affect the quality of the results.***

12.3.2 Input files

The RoME tool inputs mobile lidar data (LAS 1.2) collected by Oregon DOT's Leica Pegasus:Two system and the corresponding trajectory data (Table 12.3). *While other mobile lidar datasets should work provided the information is input in the same format, they have not yet been tested as of the published date of this report.*

Table 12.3: Example format for the trajectory data file (asciitrj)

TIME	X	Y	Z	PITCH
147179.190	57612.364	61356.273	73.863	1.860
147179.195	57612.363	61356.273	73.863	1.861
147179.200	57612.361	61356.273	73.863	1.863
147179.205	57612.360	61356.273	73.863	1.865
147179.210	57612.359	61356.273	73.863	1.866
147179.215	57612.358	61356.273	73.863	1.868

ROLL	HEADING	ST.DEV POS	ST.DEV. ANGLES	QUALITY
0.844	234.282	0	0	1
0.844	234.282	0	0	1
0.845	234.283	0	0	1
0.845	234.283	0	0	1
0.845	234.284	0	0	1

12.3.3 Output file

The final output consists of the *Run, Section, Stripe, Node, and Retro* tables in CSV (comma separated values) files (Select feature19 in Table 13.1 to generate the CSV files). These tables are linked through a set of IDs such that the attributes can be efficiently stored but still available throughout the various data layers. The generated CSV files can be imported into commercial GIS software or analyzed by themselves. A script is provided in section 12.4 to automate this conversion and reconstruction of the geometry as a GIS layer. *Note that the units of distance measurements are either meters or feet and are based on the user's setting in the RoME software.*

The *Run* table (Table 12.4) is generated as a summary of the data with a separate line for each LAS file. It contains the following attributes:

- *RunID* – A unique ID for each run.
- *HWYNumber* - The highway number, which is used to link the data to other databases by Oregon DOT.
- *Date* – The acquisition date, which is useful for tracking pavement marking degradation with time.

- *SectionIDStart, SectionIDEnd* – The starting and ending indices of the sections for each run (las file).

- *StripeIDStart, StripeIDEnd* – The starting and ending indices of the stripes extracted for each run.

- *NodeStart, NodeEnd* – The starting and ending indices of the nodes extracted for each run.

- Several user parameters, described earlier, are provided in the table as well for reference.

- *Software Version* – The current software version.

- *File Name* – Input LAS file name for each run.

Table 12.4: Example of fields and data in the *Run* table.

RunID	HWY Number	Date	Section IDStart	Section IDEnd	Stripe IDStart	Stripe IDEnd	Node Start
1	H1	20170725	1	2	1	6	1
2	H1	20170725	3	4	7	62	13

Node End	Section Interval	Grid CellSize	Angle DiffDeg	Stripe Width	Road Width	Software Version	File Name
12	10	0.05	15	0.1	7.2	1.2	T04…
124	10	0.05	15	0.1	7.2	1.2	T05...

The *Section* table (Table 12.5) is generated for each section where stripes are extracted. It contains the following attributes:

- *trajMidX, trajMidY, trajMidZ* - location of trajectory's mid spot (meters or feet),

- *StripeIDStart, StripeIDEnd* – The starting and ending indices of the stripes extracted for each section.

- *RunID* - the corresponding ID to link the section table to the *Run* table.

Table 12.5: Example of fields and data in the *Section* table.

SectionID	trajMidX	trajMidY	trajMidZ	StripeID Start	StripeID End	RunID
1	71521.710	54613.878	136.311	1	4	1
2	71513.559	54619.596	136.244	5	7	1
3	71505.359	54625.336	136.178	8	10	1
4	71497.208	54631.049	136.110	11	13	1
5	71489.012	54636.801	136.050	14	16	1
6	71480.813	54642.549	135.986	17	19	1

The *Stripe* table (Table 12.6) is generated for each extracted stripe and contains:

- *StripeID* – a unique identifier for each extracted stripe.
- *SectionID* - the corresponding section to link the *Stripe* table to the *Section* table.
- *NodeStart, NodeEnd* – The starting and ending indices of the nodes of the stripe.
- *Color* – The estimated color (white, yellow or green) of the stripe using the RGB colors mapped to the point cloud. Note that this field is not very reliable with the current system.
- *Material* – If the user provides a material type in the appropriate box in the GUI, this field will be populated with that value. This should be used if most of the stripes in the area are of a specific material type, but users should then edit this field later if using for analysis to ensure correctness.
- *Length* – The length of the extracted stripe (in meters or feet).
- *ConditionScore* – A Grade (A - F) assigned based on the median retroreflectivity value of the simulated retroreflectivity readings for the stripe.
- *RetroNumPts* – Number of the retro samples on the stripe.
- *RetroMin, RetroMax, RetroMedian, RetroAve, RetroStdDev* – summary statistics of the simulated retroreflectivity readings for the stripe extracted from the *Retro* table.
- *NumPtsPC* – The number of lidar points composing the stripe,
- *IntMin, IntMax, IntMedian, IntAve, intStdev* – summary statistics of the intensity values for the lidar points belonging to that stripe.
- *Width* – Width of the stripe based on the user input parameter. (This is not currently computed in the code but auto filled based on the parameter).
- *StripeType* – Indicates whether the stripe is Transverse (T) or Longitudinal (L).

Table 12.6: Example of fields and data provided in the *Stripe* table

StripeID	SectionID	Node Start	Node End	Color	Material	Length	Condition Score	Retro NumPts	Retro Min	Retro Max
1	1	1	2	White	N/A	10.06	D	20	84.5	121.6
2	1	3	4	White	N/A	3.24	A	7	339.8	373.2

Retro Median	Retro Ave	Retro StdDev	Num PtsPC	Int Min	Int Max	Int Median	Int Ave	Int StdDev	Width	Stripe type
101.2	103.4	10.5	2775	0.045	0.502	0.259	0.249	0.073	0.1	L
373.2	361.4	15.1	642	0.074	1.000	0.849	0.803	0.178	0.1	L

The *Node* table (Table 12.7) is generated for each node (start and end points for each stripe). It contains the following attributes:

- *NodeID* – Unique ID for each node.
- *X, Y, Z* – The X, Y, Z coordinates (meters or feet) for each node.
- *StripeID* – The corresponding *StripeID* to provide the link to the *Stripe* table.

Table 12.7: Example of fields and data provided in the *Node* table

NodeID	X	Y	Z	StripeID
1	71526.766	54612.320	134.245	1
2	71518.552	54618.135	134.179	1
3	71521.947	54611.244	134.295	2
4	71519.298	54613.112	134.270	2
5	71522.562	54606.341	134.399	3
6	71514.357	54612.146	134.334	3

Simulated retroreflectivity readings are generated at a fixed distance (user parameter: Default 2 feet) along each stripe. These readings are simulated by extracting the lidar points within a window size with the dimensions of the active window of the Delta LTX handheld retroreflectometer. The results are stored in the *Retro* table (Table 12.8), which contains:

- *RetroID* – Unique ID for each simulate retroreflectivity reading.
- *X, Y, Z* – The X, Y, and Z coordinates (meters or feet) for each simulated retroreflectivity reading.
- *StripeID* – A link to the corresponding stripe where the simulated retroreflectivity reading is obtained.
- *NumPtsPC* – The number of lidar points within the simulated retroreflectivity reading that were used for evaluation. This can also serve as a quality control metric.
- *Retro10* – The 10^{th} percentile retro value from the lidar points within that window.

Table 12.8: Example of the fields and data provided in the *Retro* table

RetroID	X	Y	Z	StripeID	NumPtsPC	Retro10
1	71526.685	54612.378	134.244	1	44	99.933
2	71526.276	54612.667	134.241	1	45	86.530
3	71525.868	54612.956	134.239	1	39	93.282
4	71525.460	54613.245	134.236	1	40	90.638
5	71525.052	54613.534	134.232	1	39	84.522
6	71524.644	54613.822	134.229	1	38	100.653

Users can also export just the points corresponding to the extracted road marking in LAS file format (v1.2) (See the feature20 in Figure 12.2 to generate LAS files) for additional quality control.

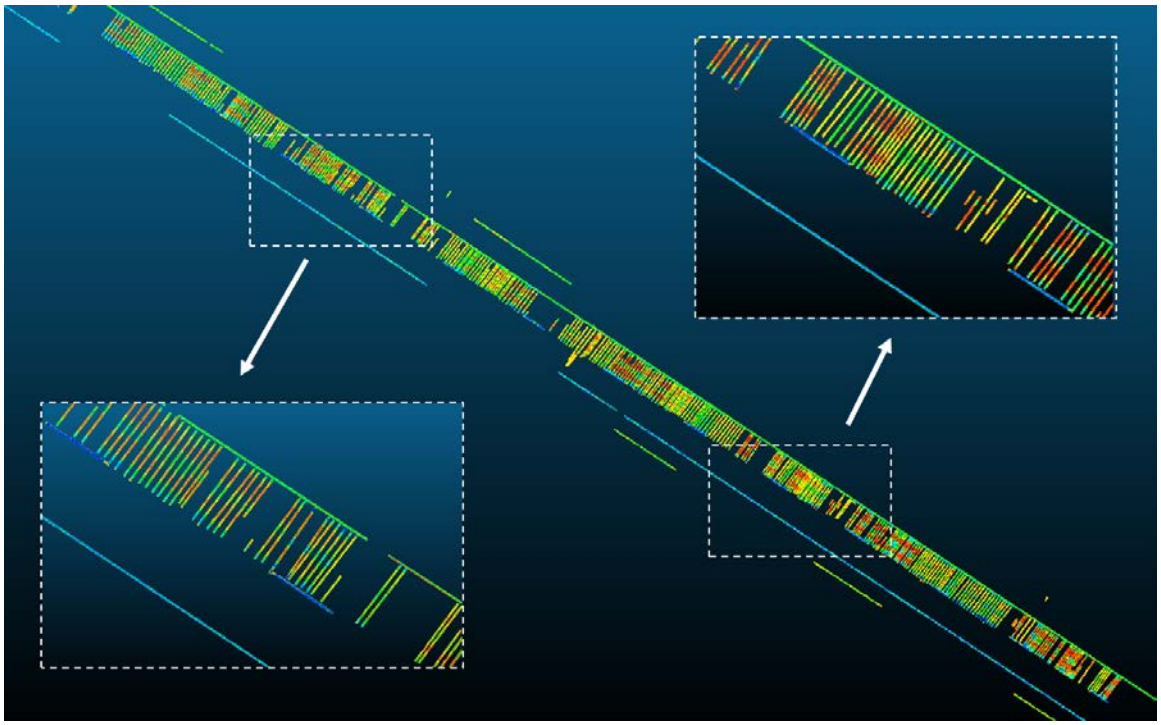

(a)

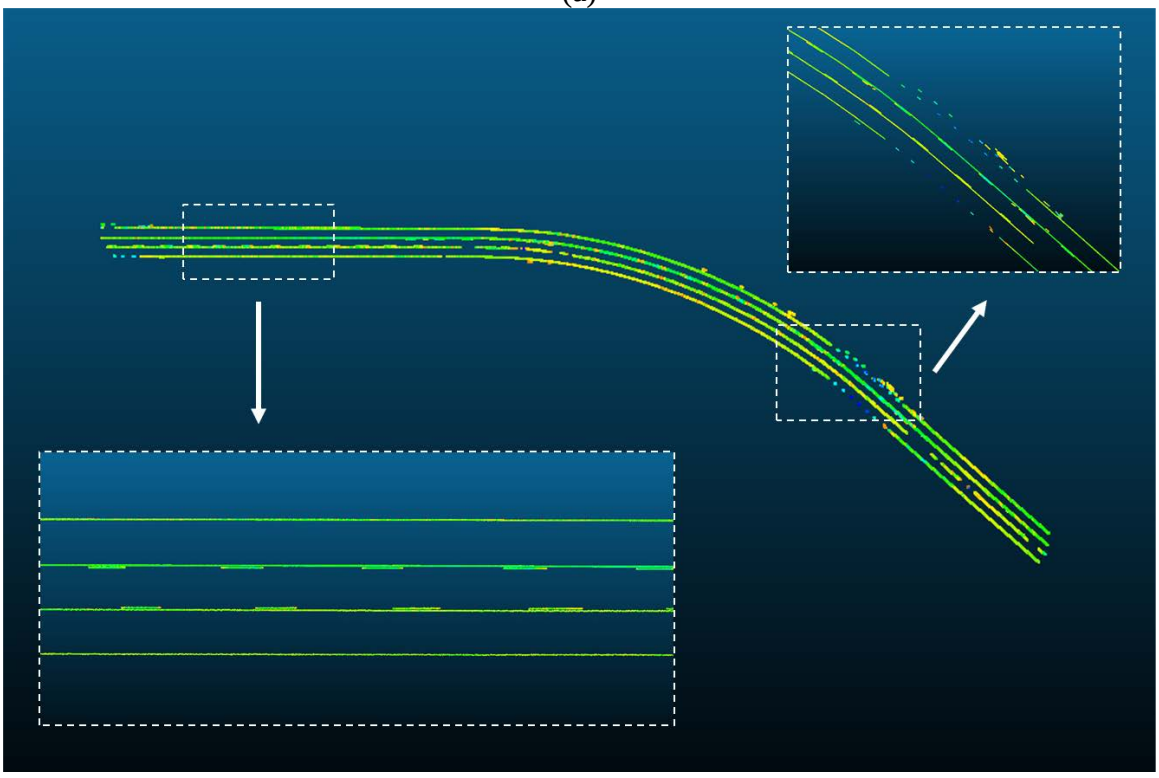

(b)

Figure 12.4: Example of the point cloud of the extracted road markings with closeups for detail: (a) Testdeck and (b) Salem data sets.

12.4 ARCGIS TOOL DEVELOPMENT AND USAGE

Three ArcGIS Python (ArcPy) scripts, *csv2gdb.py*, *stripeeditor.py*, and *retrograder.py* are included in Appendix B and provided to Oregon DOT as part of an ArcGIS Toolbox (Figure 12.5). The *csv2gdb.py* script inputs the *csv* files output from the *RoME* software and converts them to feature classes in a new GIS geodatabase. The *stripeeditor.py* script provides a simple way to correct stripe coloring based on digitized yellow stripes. It also can screen any transverse markings. The *retrograder.py* script aggregates the retroreflectivity results into grades for larger sections. The GIS tool was developed using ArcGIS python (arcpy), which is the preferred scripting language for ArcGIS. Upon export of the *csv* files from the RoME tool, the GIS division would then run the python scripts in sequence to create a file geodatabase containing the results of each run (Table 12.9 and Figure 12.6). While each run will likely be an individual section of highway, the final results can then be merged with previous runs for inclusion in a statewide *TransGIS* layer using the "merge" geoprocessing tool available within ArcGIS, as necessary.

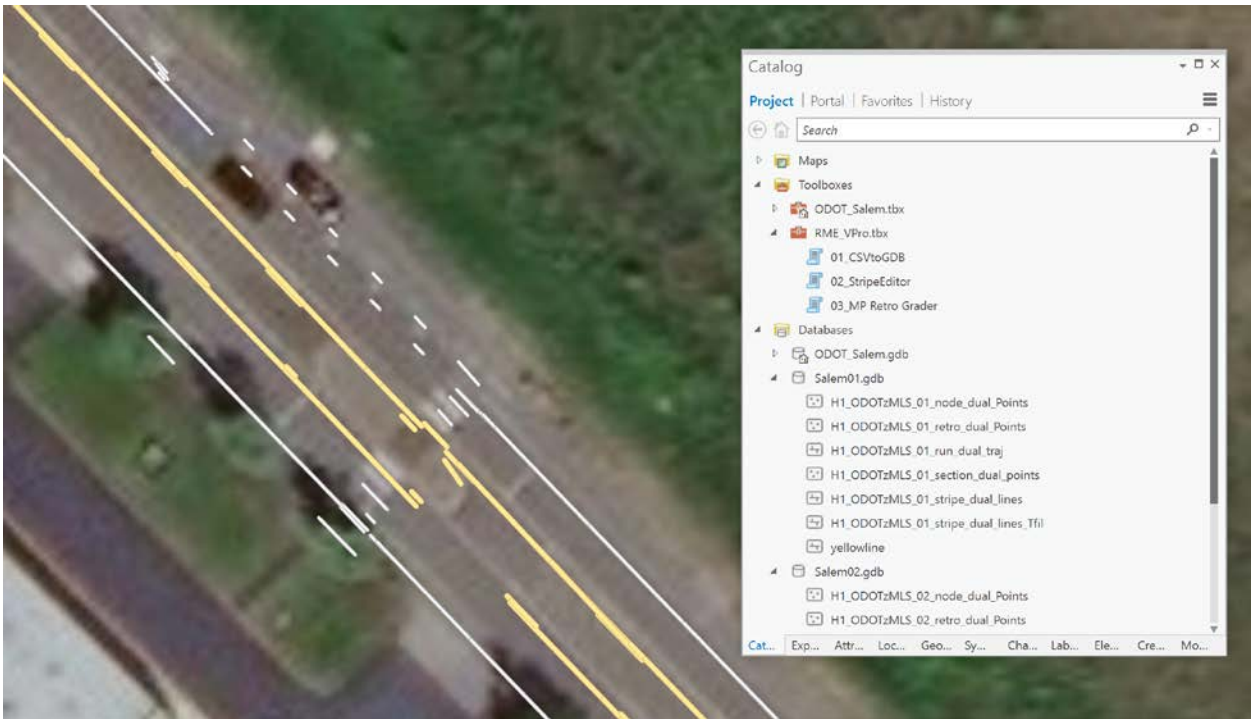

Figure 12.5: Screenshot of the RoME Toolbox and the associated scripts within *ArcCatalog*

Table 12.9: Description of data layers produced with the python script tool

Script#	Data Layer	Description
1	Run	Creates a polyline feature class with a single polyline for each run which represents an approximate version of the trajectory for each stripe
1	Stripe	Creates a polyline feature class with individual polylines for each extracted stripe (or segment of stripe). Contains quality control information on the stripe.
1	Node	Creates a point feature class with the start and end nodes for each stripe. The primary purpose of this table is simply for creation of the stripes.
1	Section	Creates a point feature class with points along the trajectory for each discretized section in the RoME tool. These sections are connected to create a polyline feature for the run feature class.
1	Retro	Creates a point feature class with simulated retro-reading samples every 3 ft (or other user specified increment) along each stripe. Contains various statistics related to the retro-reading from the lidar point cloud
2	Stripe_Tfil	Creates a new version of the Stripe Feature Class with transverse stripes removed and coloring corrected.
3	MP_Retro (user defined name)	Creates a polyline feature class that contains an aggregated condition score of the stripes located within the section of a certain increment (e.g., tenth of a mile) based on the Oregon DOT milepost layers. (Can use any mile increment provided the fields remain constant). This layer is meant to be used for regional or statewide asset management purposes.

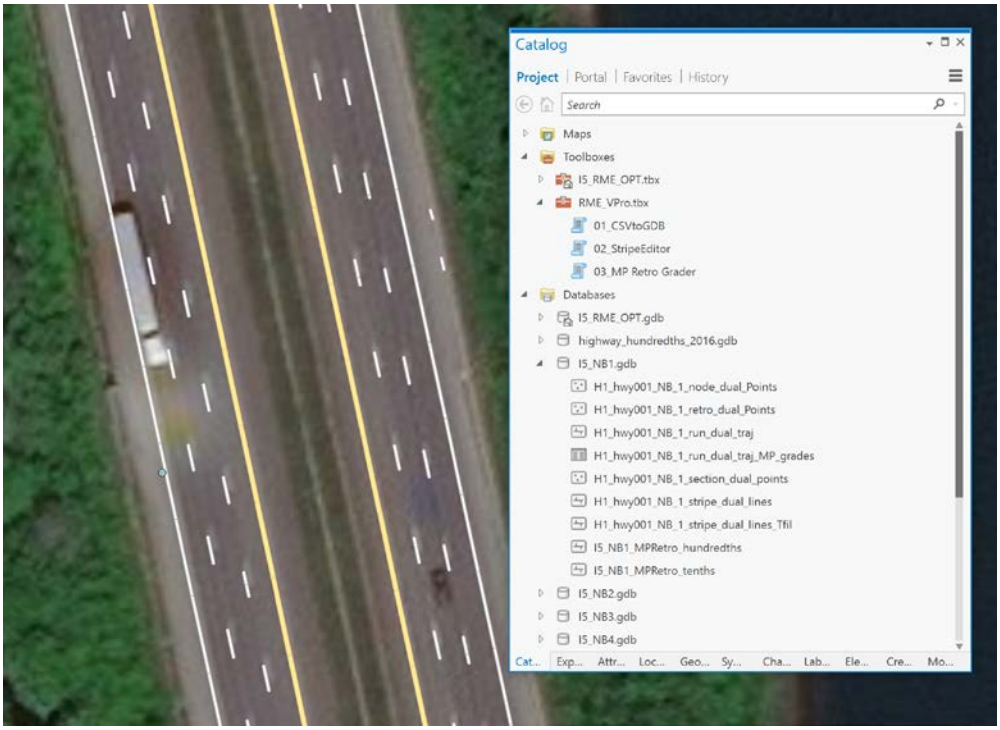

Figure 12.6: Screenshot of the output layers in a geodatabase in *ArcCatalog*

12.4.1 csv2gdb.py

The csv2gdb.py script (Figure 12.7) first imports the csv files into the geodatabase as tables. The tool creates a new geodatabase or can write to an existing geodatabase. It then creates point feature classes from the *Node*, *Section*, and *Retro* tables based on the *X, Y, Z* values in those tables. The tool then uses the information from the *Node* table to reconstruct the lines for the stripe table based on the ID links to represent the individual markings extracted from the RoME tool. It then reconstructs a polyline from the points in the section table to create a polyline feature class for the *Run* table. Note that the initial tables that are no longer needed are deleted to avoid confusion. (The csv files themselves are not affected by the script. It is recommended to archive them). The script takes approximately 30 seconds per mile of data, but will vary depending on the hardware used and if files are located on a network vs. the local machine).

In order to run this tool, the user must specify the following parameters:

1. An input folder for the *csv* files. (e.g., *C:\RetroData\hwy001\csv*)

2. An output folder for the geodatabase. (e.g., *C:\RetroData\hwy001*) – note that this folder should not be in the same folder as the *csv* files but can share the same root path.

3. A name for the output geodatabase (e.g., *hwy001retro*). Do not include the ".gdb" as the script will automatically add that.

4. The spatial reference of the data contained in the input *csv* files. (e.g., *OCRS_SALEM_NAD_1983_2011_TM_Meters*). This information should be provided by Geometronics based on the coordinate system used for exporting the LAS files.

Example outputs are shown on the following pages. Figure 12.8 shows the extracted stripes, nodes, trajectories and sections. Figure 12.9 shows the simulated retroreflectivity values on each stripe, colored by the retroreflectivity (Retro10). Figure 12.10 shows an example of the attributes available in the *Stripe* table.

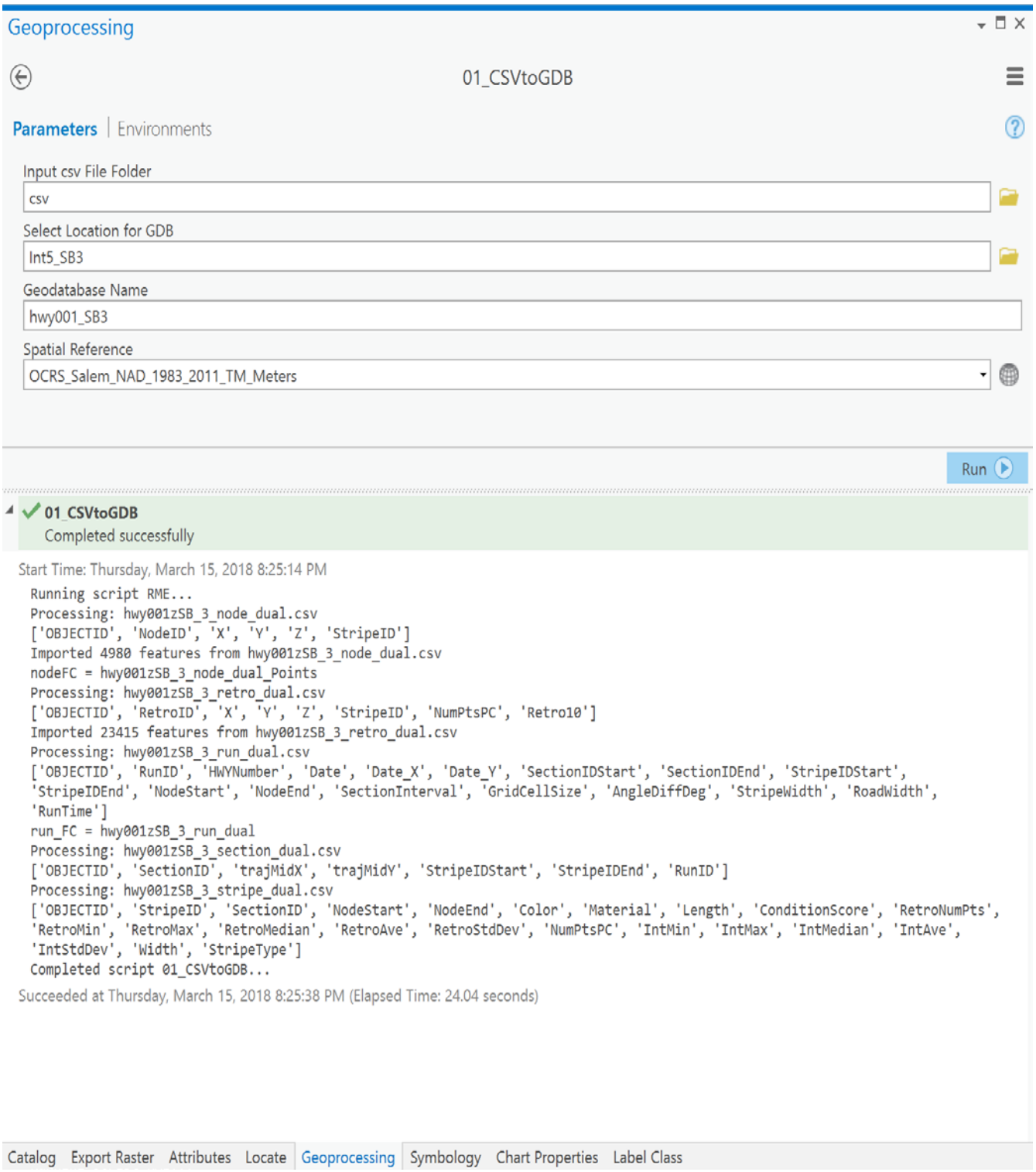

Figure 12.7: GUI for the csv2gdb.py tool in ArcGIS Pro showing input parameters as well as command line output.

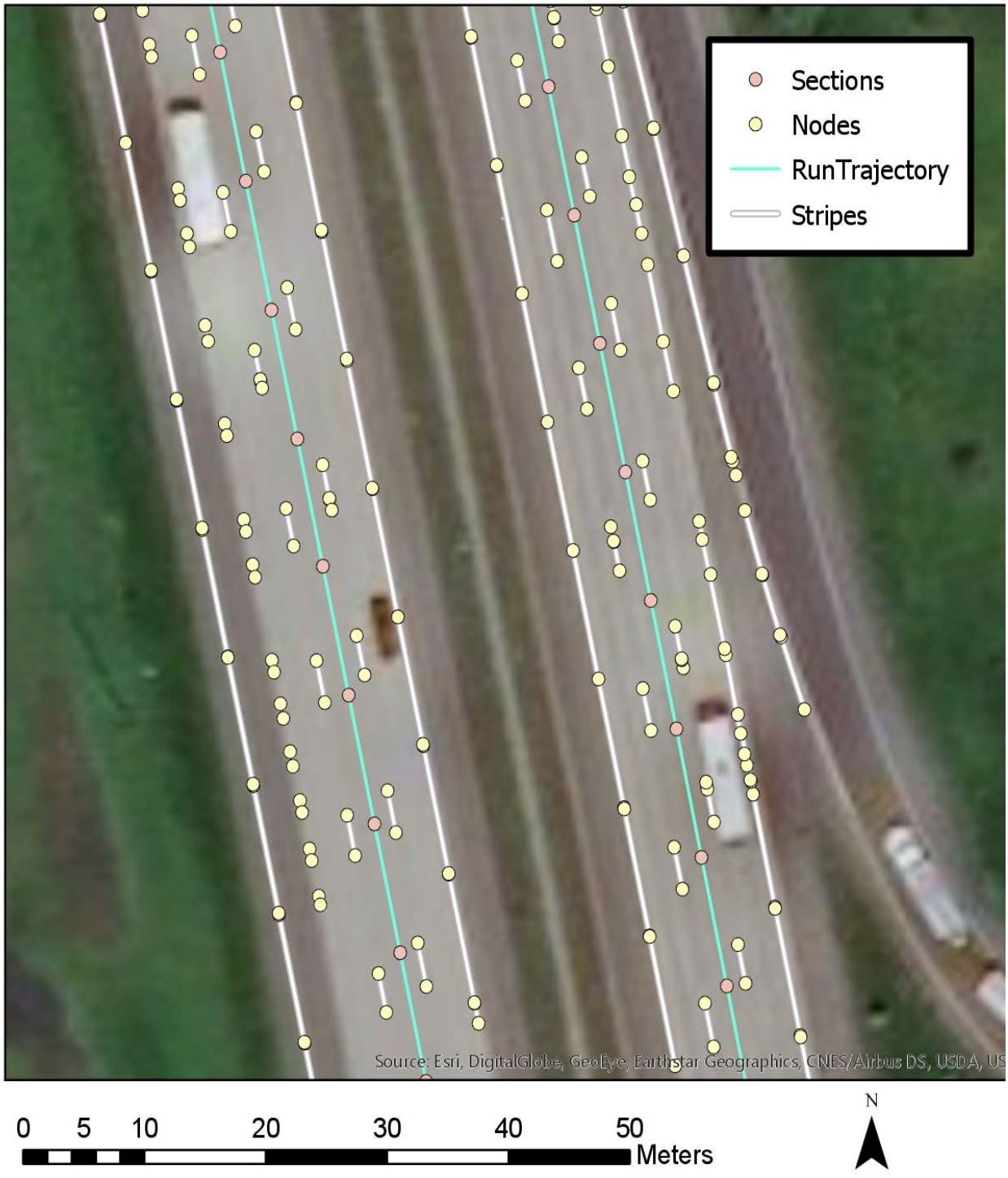

Figure 12.8: Example output of the csv2gdb script showing the nodes, stripes, run (trajectory), and section mid-points.

Figure 12.9: Example output of the csv2gdb.py script showing the retro feature class colored by retroreflectivity values.

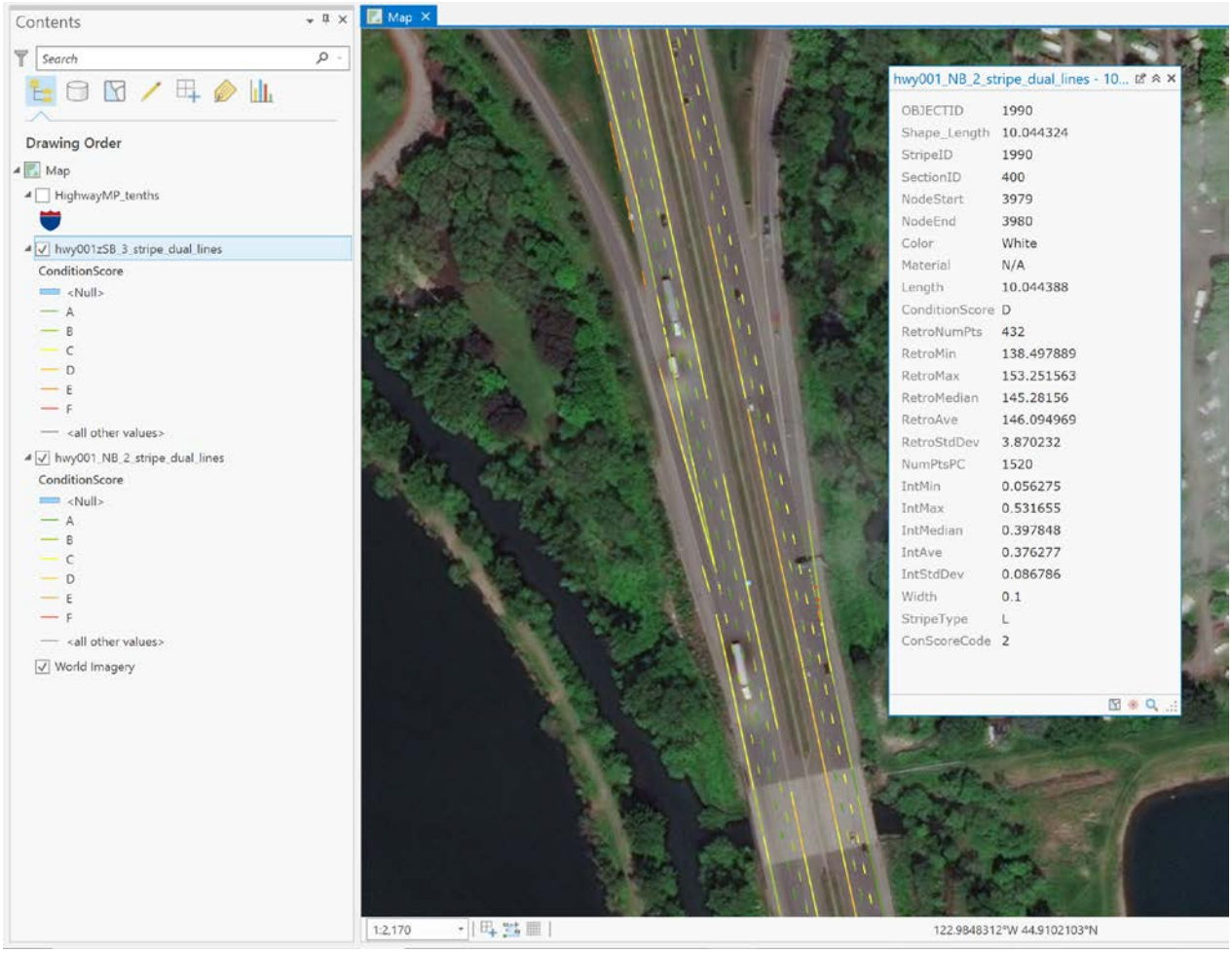

Figure 12.10: Example output of the *csv2gdb.py* script showing attributes available in the stripe table.

12.4.2 StripeEditor.py

A second (optional) python script inputs the stripe feature class as well as a feature class containing digitized lines of yellow stripes. The script changes the color of all lines within a user specified distance to be yellow and all others to be white. The assumption is that there are significantly fewer yellow lines, they are generally continuous, and thus can be quickly digitized. In cases where there are dashed yellow lines next to a solid yellow line, the user would still only need to digitize the main line since the dashed lines would be within the threshold distance. In the case of a single dashed yellow line to indicate passing, the user could simply digitize a continuous line to represent the yellow line since this is only used as a reference for coloring, but the dashed lines would be preserved in the stripe Feature Class. However, a limitation of this approach resides in the fact that erroneous results would occur with a white line in close proximity to a yellow line.

The script also has an option to remove transverse markings (which are the bulk of the false positives of the RoME tool). If that option is selected, it creates a new stripe feature class with "_Tfill" appended to its name.

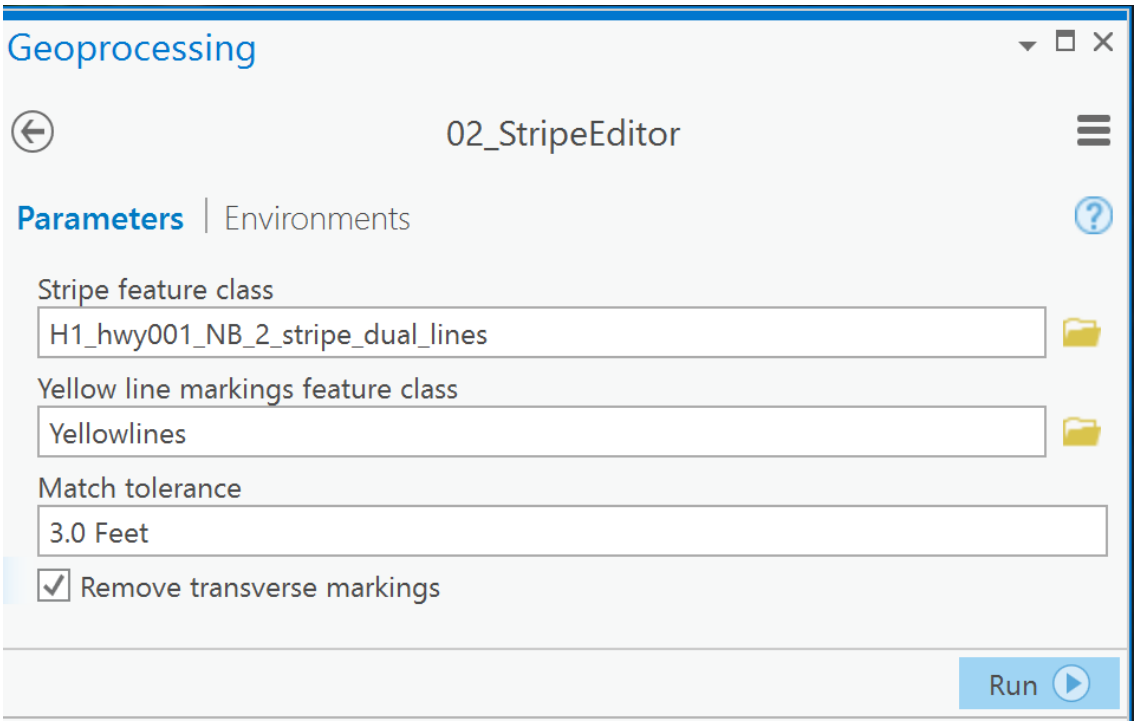

Figure 12.11: GUI for the *stripe.editor.py* script.

Figure 12.12: Example output of the stripeeditor.py script showing correct yellow and white stripes with transverse stripes removed. This data is the combination of 2 runs (clockwise and counter-clockwise) on the Oregon DOT Salem mobile lidar test course.

12.4.3 Manual Editing

To improve the data quality for asset management, it may be worthwhile to perform some manual cleanup of the data to remove erroneous stripes. The user may use some of the attributes such as stripe length, number of points, etc. as quality metrics to quickly select stripes that are likely false positives. They can then adjust the selection as appropriate and remove the false positives. They can also adjust the stripe color information by plotting the stripes with symbology in GIS and subsequently adjusting the color of the stripes to be correct. Note that the *retrograde.py* grades the stripes differently based on its color in accordance with specifications. As a shortcut, should a conservative result be desired for the aggregated asset management layer, one can change the color attribute field to be yellow for all stripes, which will result in a more conservative grading.

12.4.4 Retrograder.py

The *retrograder.py* script (Figure 12.13) inputs a mile marker feature class (e.g., the $1/10^{th}$ milepost layer on *transGIS*) and then provides a retroreflectivity quality score for each $1/10^{th}$ mile post section as an attribute field. The choice of the milepost layer depends on the resolution desired for asset management purposes.

The script reclassifies the condition score in the stripe table based on the median retroreflectivity value from all points in the retro feature class using the thresholds in Table 12.10. Although the RoME tool also performs this classification, the values are reclassified to account for any editing that may have occurred as outlined in Section 13.4.2 of this report. Next, the script creates a buffer (e.g., 200ft) on each side from the polyline in the *run* feature class. It then clips the mile marker feature class to include only those points that lie within the buffer. (Note that all attributes are preserved such that the results can be linked back to the milepost layer if desired). The script then reconstructs a polyline between each mile marker and stores it in a new feature class. Each polyline is buffered and all *stripe* polylines from the *stripe* feature class located within that buffer are analyzed to provide the overall score for that section. The grade for the section is assigned based on the thresholds in Table 12.10 depending on the color of the stripe (white or yellow). The script computes the mean retroreflectivity grade of all stripes within each MP section. (Note that for computation, the grades are converted to a numerical scale ranging from 0(F) to 5(A)). A value of Z represents no data.

Table 12.10: Grade (Condition Score) thresholds

Grade	White	Yellow
A	>350	>250
B	250-350	200-250
C	150-250	125-200
D	100-150	100-125
E	50-100	50-100
F	<50	<50

The script contains the following input parameters (Figure 12.13):

1. *Analysis Geodatabase* – The file path and name of the geodatabase output from the csv2gdb script.

2. *Stripe Feature Class* – The stripe feature class output from the csv2gdb script.

3. *Run Feature Class* – The run feature class output from the csv2gdb script

4. *Oregon DOT Tenth MilePost Feature Class* – The 1/10th milepost layer on *transGIS*. (Another layer could be used if finer (e.g., 1/100th mile) or coarser (e.g., 1 mile) aggregate results are desired. It should be noted that this table must have a field named "MP", which contains the milepost numbers of each marker. The program will reconstruct the polyline based on the order of the mileposts. The lower milepost is considered the start node of the section for the rating purposes). This ordering should be considered when field verifying the results since the direction of the mileposts may increase in the direction opposite the direction of travel.

5. *LRSKeyFilter* (optional) – A filter based on the LRS Key to filter the mileposts to a single route. This filter is useful for divided highways which have mileposts on different sides and areas where highways intersect to avoid misclassifying the results to the incorrect highway.

6. An *output name* for the output feature class providing retroreflectivity values at the milepost increments (e.g., hwy001_MP_Retro)

7. *Output layer spatial reference* (Optional) – *Note that the spatial reference for the milepost layers in TransGIS is Web Mercator. As a result, there can be a significant amount of distortion with geoprocessing tools such as Buffer in ArcGIS, which can lead to undesired results of stripes not being considered in the analysis.* The script allows the user to reproject the data layer to a low distortion coordinate system such as the appropriate zone in the Oregon Coordinate Reference System (which will likely be used for las files and RoME output files). However, an alternative to reprojecting the milepost data is to simply use a larger buffer should the output be desired in Web Mercator. If this parameter is left blank, the program will not reproject the data.

8. *Buffer Distance* – Enables the user to specify a buffer distance. The default is 100 ft. This buffer distance should ensure that all stripes of interest are within that distance of the line formulated between the mileposts. The buffer distance is also used

9. *Delete temporary files* – By default the program will delete the various geoprocessing layers created to produce the final results. However, the user can uncheck this box for troubleshooting purposes.

An example output for as section of Interstate-5 in Salem area is shown in Figure 12.14. This figure includes data from a single northbound and a single southbound pass from the center lane on each side.

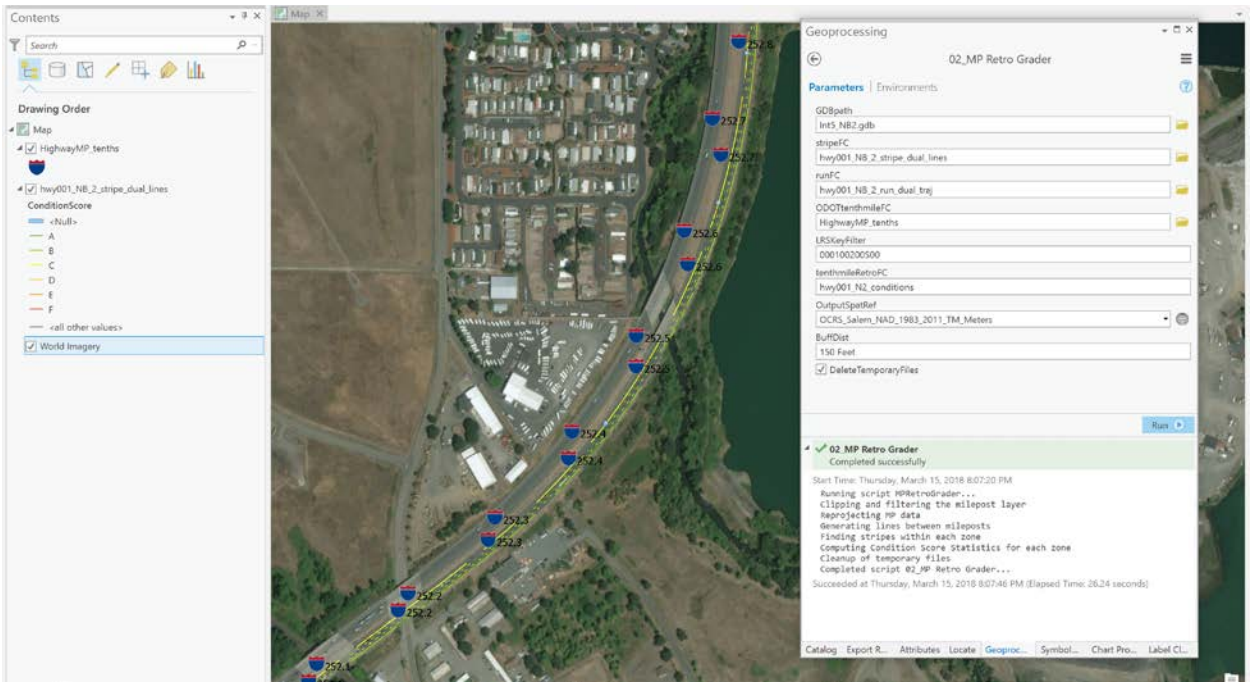

Figure 12.13: GUI for the retrograder.py script and associated inputs in ArcGIS Pro 1.5

Figure 12.14: Example output of the retrograder script showing the MP_retro results for a single northbound and single southbound pass colored by overall condition score.

12.5 TOOL LIMITATIONS

While the tool provides a great deal of functionality, below are some limitations that should be considered:

1. Not all stripes can be extracted. Some stripes are too faded to be distinguished by the mobile lidar unit from the pavement. In other cases, passing vehicles adjacent to the mobile lidar unit can block the view of the scanner, resulting in the stripes not being captured. The further the stripe is from the mobile lidar unit, the less sample points that will be available. Wider highways will require multiple passes to capture stripes from distant lanes.

2. The RoME tool is focused on extracting the linear or smoothly-curved markings such those used for as the centerline or lane boundaries. Highly-curved or complex markings (e.g., legend markings, arrows, bicycle symbols) are not currently considered.

3. Similarly, the tool does not capture small marking such as Stick-n-Stomp temporary reflectors and button markings.

4. The setting for the RoME tool is optimized for the current system being used by Oregon DOT. Should Oregon DOT purchase a new mobile lidar unit or change the scanners on the unit, they will need to perform several runs to select the appropriate parameters (including the internal ones).

5. Currently, the stripe width is an input parameter and is not calculated in the program. The stripes with the width exceeding the user input could not be properly extracted.

6. In the current implementation, the RoME tool uses the single profiler data to extract the stripes. Dual profiler mode requires both the dual profiler data and the single profiler data if the classification field in the point cloud data is not populated as required to distinguish each profiler.

7. Similarly, material type is an input that a user can apply to all stripes extracted within a single run. However, should the material type vary, the user needs to manually correct those. (GIS SQL query tools can help make this process more efficient).

8. The RoME tool will provide an estimate of color based on the RGB values mapped to the mobile lidar data. However, *at this time, these color estimates are of limited accuracy* due to variances in exposure, image quality, and offsets that occur when mapping the images to the point cloud.

9. Stripes will be split at each section boundary based on the selected interval, Δ. Additional GIS scripts could be developed to merge or link those segments, if desired.

12.6 IMPLEMENTATION PLAN\CONSIDERATIONS\FUTURE ENHANCEMENTS

Custom scripts to merge the results from various runs may be beneficial to Oregon DOT in implementation. In particular, using standard GIS layer merging techniques, the various links between the ID fields will not be maintained. A custom script could renumber the various ID fields such that those can be maintained when different runs are merged together, should that be desired. (The IDs are predominately used for the reconstruction process, although there may be some benefit to preserving the structure provided those IDs in future applications).

Another script could be developed to merge the results from different passes of the same section (e.g., different lanes) and appropriately compute new retroreflectivity statistics based on the overlapping data. Additional intuitive scripts that will help with identifying false positives will prove beneficial once Oregon DOT has gained more experience running the tool and implementing it on a series of mobile lidar data collections to help identify appropriate threshold values. Another helpful tool could identify if a stripe is missing because the stripe was not visible to the mobile lidar (e.g., blocked by a vehicle) or because the stripe is too worn to be detected.

As Oregon DOT compiles more data and has previous surveys available, that information can be used to correct inconsistencies in the new runs such as stripe color or other information much more efficiently. It can also be used to identify missing stripes that are not captured due to obstructing vehicles or nearly complete wear.

13.0 IMPLEMENTATION TEST (CASE STUDY)

13.1 TEST OVERVIEW

The final step in the analysis was to complete a full, end-to-end workflow test using both the RoME v1.2 software and Python scripts using a dataset obtained from Oregon DOT specifically for evaluation on approximately 3 miles of Interstate-5 in Salem. A total of 8 passes were completed (4 northbound, 4 southbound). This section of interstate alternates between 2 to 3 lanes in each direction. For each direction, one pass was completed in each lane (right, center, left) and the fourth pass was completed from the right lane.

Additional passes were completed at the same time for the Oregon DOT Geometronics mobile lidar test course in Salem, including passes in both the clockwise and counterclockwise direction. This test course is utilized by Geometronics for periodic evaluation and testing of the mobile lidar unit to ensure it is operating within specification and the calibration is still valid. This route has several curved section as well as a wide range of marking conditions. It generally has only one lane travelling each direction, but sometimes has a center turn lane. In some cases, the markings are located at the edge of pavement and sometimes overgrown with vegetation. Hence, this site represents a challenging location for validating the RoME tool. Note that the local roads on the test course are owned by the city and have different standards to update and maintain retroreflectivity than those used by Oregon DOT.

The objectives of these test were to:

1. Perform a rigorous test of the RoME software and scripts to identify and troubleshoot issues.

2. Evaluate the consistency of the detailed retroreflectivity analysis between different lanes and passes within the same lane.

3. Compare aggregated condition scores (grades) between each pass, and

4. Determine if any directivity effects exist.

The RoME tool was completed on a Dell Workstation with an Intel Xeon CPU E5620 Processor with 24 GB RAM. Each pass for Interstate-5 (approximately 3 miles) with dual profiler data was processed in approximately 1 hour in the RoME tool. User interaction to set up each run typically required 5 minutes. The Python scripts were tested in ArcGIS Pro 1.5 and took less than 30 minutes for all passes (including user interaction and browsing for data to add to GIS for display) to complete on a Microsoft Surface Book 2 with an Intel® Core™ I7 CPU and 16 GB RAM.

13.2 DETAILED REPEATABILITY EVALUATION

Before utilizing the RoME tool, in order to further evaluate the repeatability of the radiometric calibration approach on a three lane road, the research team selected two test sections about 100m located on Interstate-5 southbound and northbound, respectively (Figure 13.1). On each section, the point clouds were sampled with an interval of 1m for retroreflectivity estimates. By comparing the results of retroreflectivity estimation using dual profiler data (Figure 13.2), the proposed radiometric calibration shows reasonable robustness to the different lanes of operation. Note that because the data were collected at a speed of 55mph (approximately), the point density is much lower than the data used for the regression analysis as well as the validation in Chapter 11. As a result, there is likely more variance in the retroreflectivity analysis than would be observed on a slower road. Note that the white stripe (Figure 13.2a) in the southbound direction periodically reaches saturation (373 mcd/m^2/lux). Nearly identical results are achieved from the passes in the same lane, but differences up to 20% in retroreflectivity are observed between the different lanes. Similar results are seen for the yellow stripe (Figure 13.2b). For the yellow stripe, the left and middle lanes yield very similar results, but the data collected from the right lane shows a reduction of approximately 15%. The two right lane passes agree well with one another.

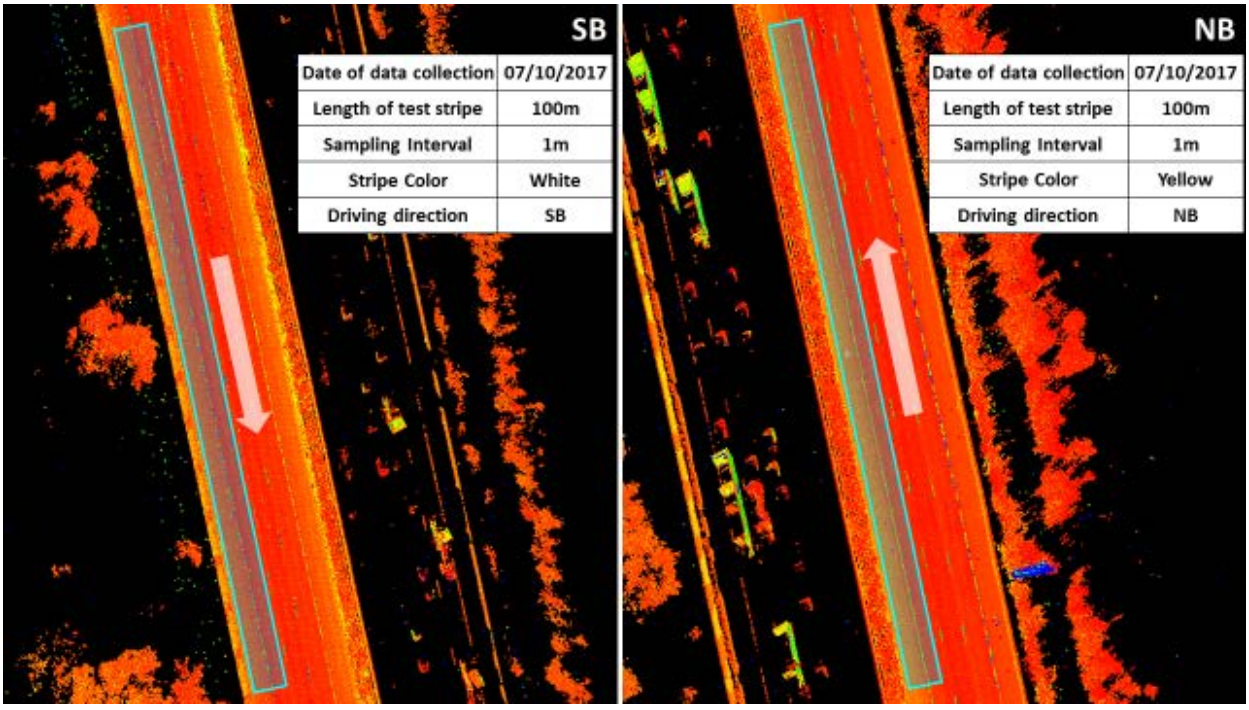

(a) (b)

Figure 13.1: Point cloud and details of the sections evaluated in detail for the repeatability test on Interstate-5 for (a) the Southbound edge line (white) and (b) the Northbound center line (yellow).

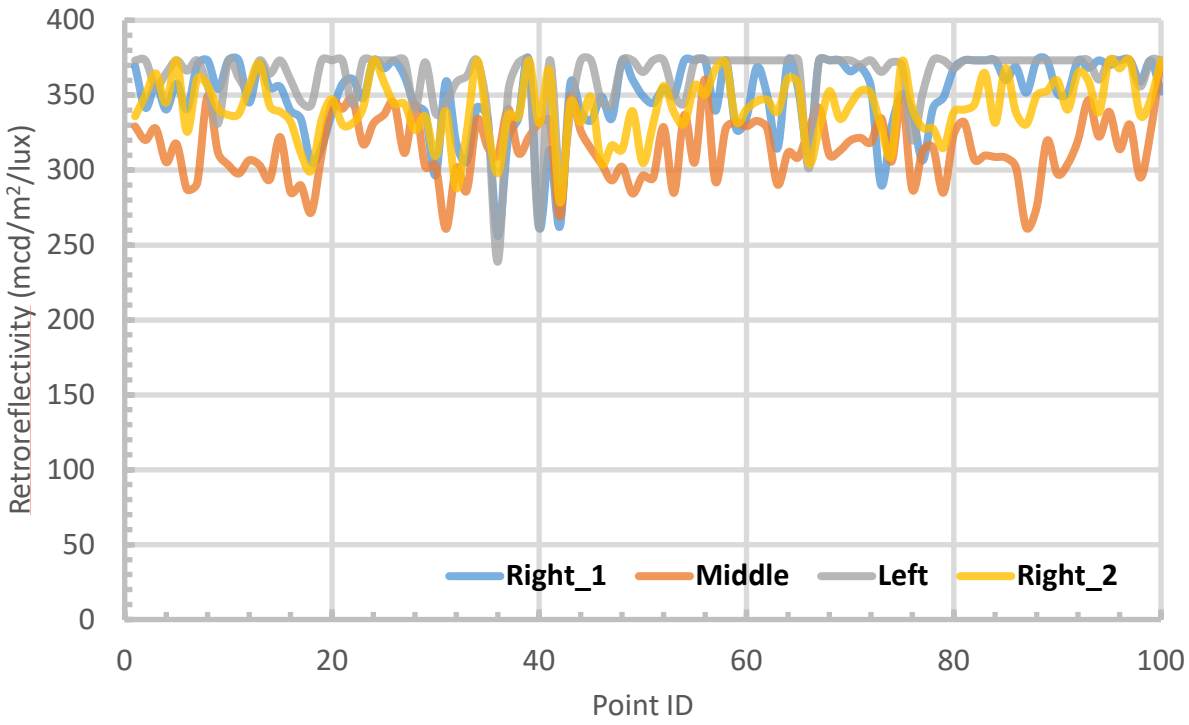

(a)

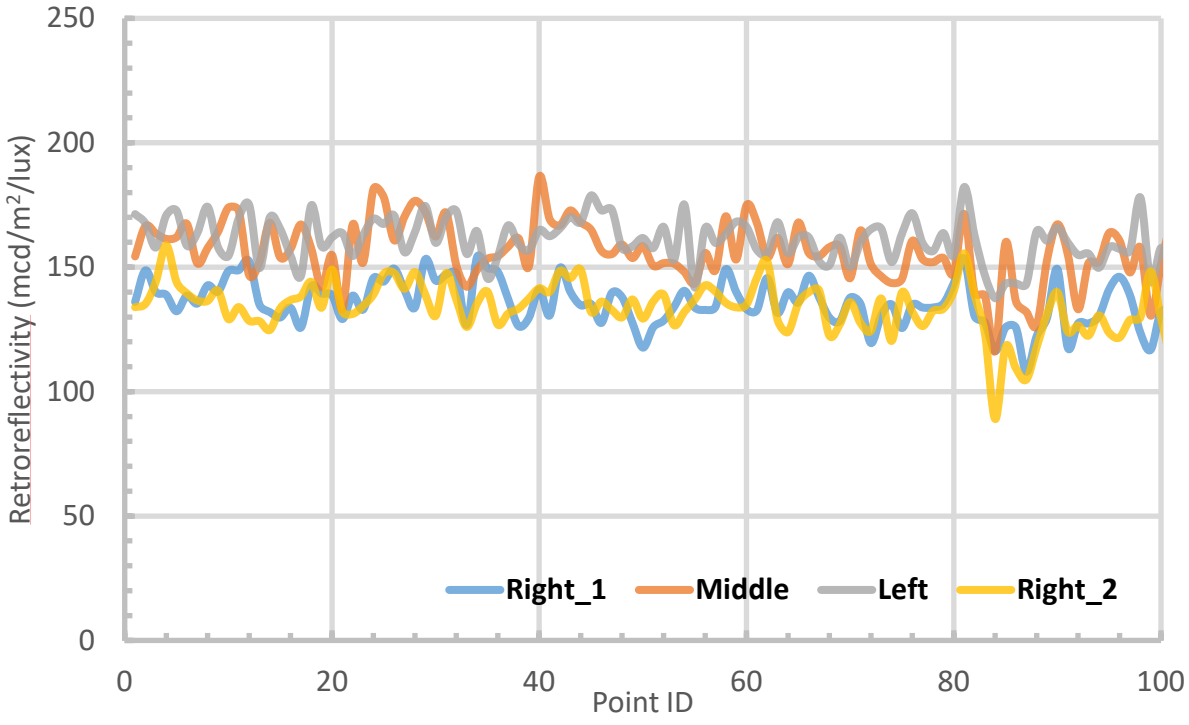

(b)

Figure 13.2: Comparison of retroreflectivity estimated from mobile lidar data collected from different lanes. (a) Right edge line (white) on Southbound of Interstate-5 (b) Left edge line (yellow) on Northbound of Interstate-5

Tables 13.1 and 13.2 provide additional statistical summaries between the different passes. In both cases, the differences are lowest for the passes completed from the same lane, as expected. The white line from Interstate-5 Southbound shows higher difference values given that it is highly retroreflective. As discussed in Chapter 9, the radiometric calibration model has less scatter at lower thresholds of retroreflectivity. Additionally, saturation effects lead to more erroneous measurements at these upper thresholds. Overall, the statistical results from Table 13.2 are very consistent with those from Chapter 11 (Philomath) for the highly worn white stripe.

Table 13.1: Summary statistics of differences between retroreflectivity estimated from mobile lidar data collected from different lanes for the right edge line (white) on Interstate-5 Southbound. (Unit: mcd/m^2/lux)

Statistic	Center-Right_1	Left-Right_1	Right_2-Right_1	Left-Center	Right_2-Center	Right_2-Left
RMS	47.8	34.6	31.9	60.3	36.2	36.6
Ave	-33.4	17.6	-5.0	50.9	28.3	-22.6
Std.Dev	34.5	30.0	31.7	32.5	22.6	29.0
Min	-112.6	-120.7	-63.0	-106.0	-13.7	-65.8
Max	60.6	100.3	91.7	111.7	92.5	145.0

Table 13.2: Summary statistics of differences between retroreflectivity estimated from mobile lidar data collected from different lanes for the left edge line (yellow) on Interstate-5 Northbound. (unit: mcd/m^2/lux)

Statistic	Center-Right_1	Left-Right_1	Right_2-Right_1	Left-Center	Right_2-Center	Right_2-Left
RMS	24.6	28.1	11.9	15.7	26.8	30.8
Ave	20.5	25.7	-2.3	5.2	-22.8	-28.1
Std.Dev	13.6	11.5	11.7	14.9	14.1	12.7
Min	-16.9	-6.5	-28.3	-28.8	-52.6	-53.9
Max	56.6	57.5	36.6	39.3	20.7	19.5

13.3 ROME TOOL EVALUATION

To further demonstrate the effectiveness and robustness of the proposed workflow including the RoME software and ArcGIS python scripts, the project team evaluated the aggregated retroreflectance condition scores at increments of 1/10th and 1/100th of a mile using the milepost layers available through Oregon DOT's TransGIS platform for the entire 3 mile segment of Interstate-5. For these results, the research team did not remove any of the false stripes. (However, these can be easily identified and removed from the GIS layer, if desired). Comparing the pavement marking condition maps generated using the data collected from different lanes (Figure 13.3), the results show the proposed workflow overall provides consistent results. By matching the milepost points (Figure 13.4), the evaluation results from different lanes follow the same trend and a reasonable repeatability can be achieved. To prove this statistically, the project team conducted the evaluation of the proposed results quantitatively (Table 13.3).

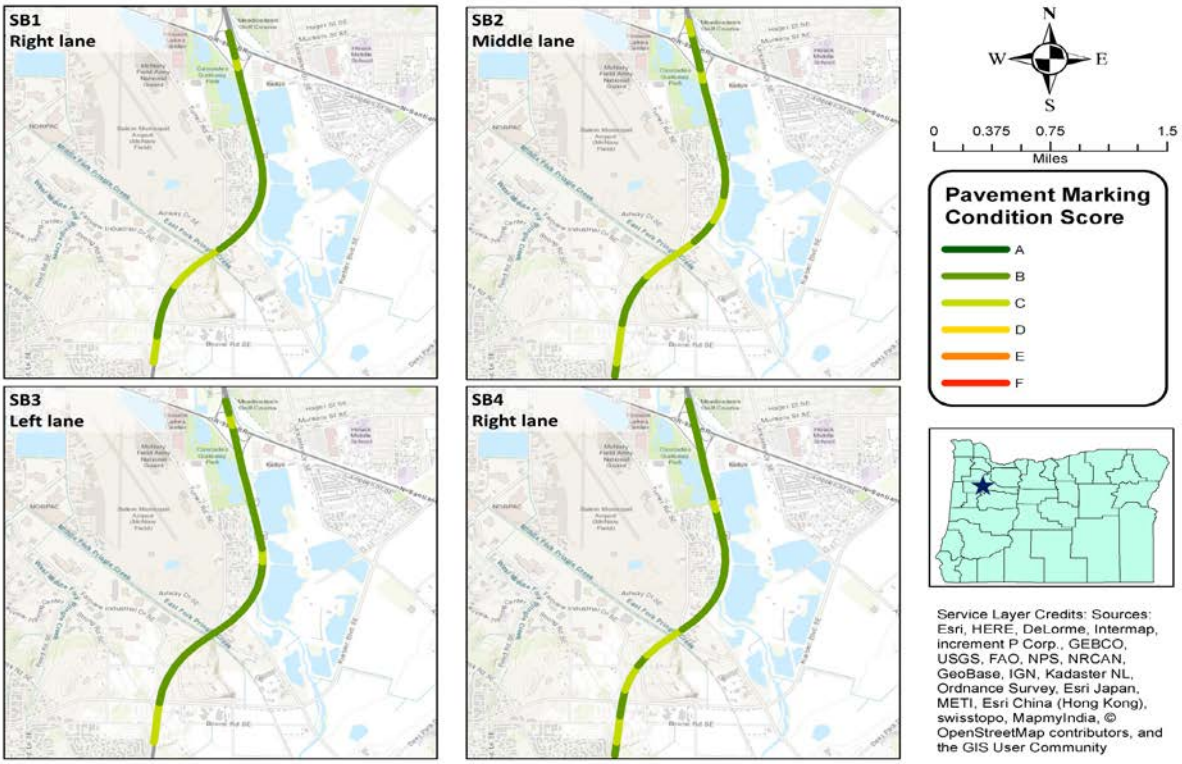

(a) Southbound at tenths of a mile.

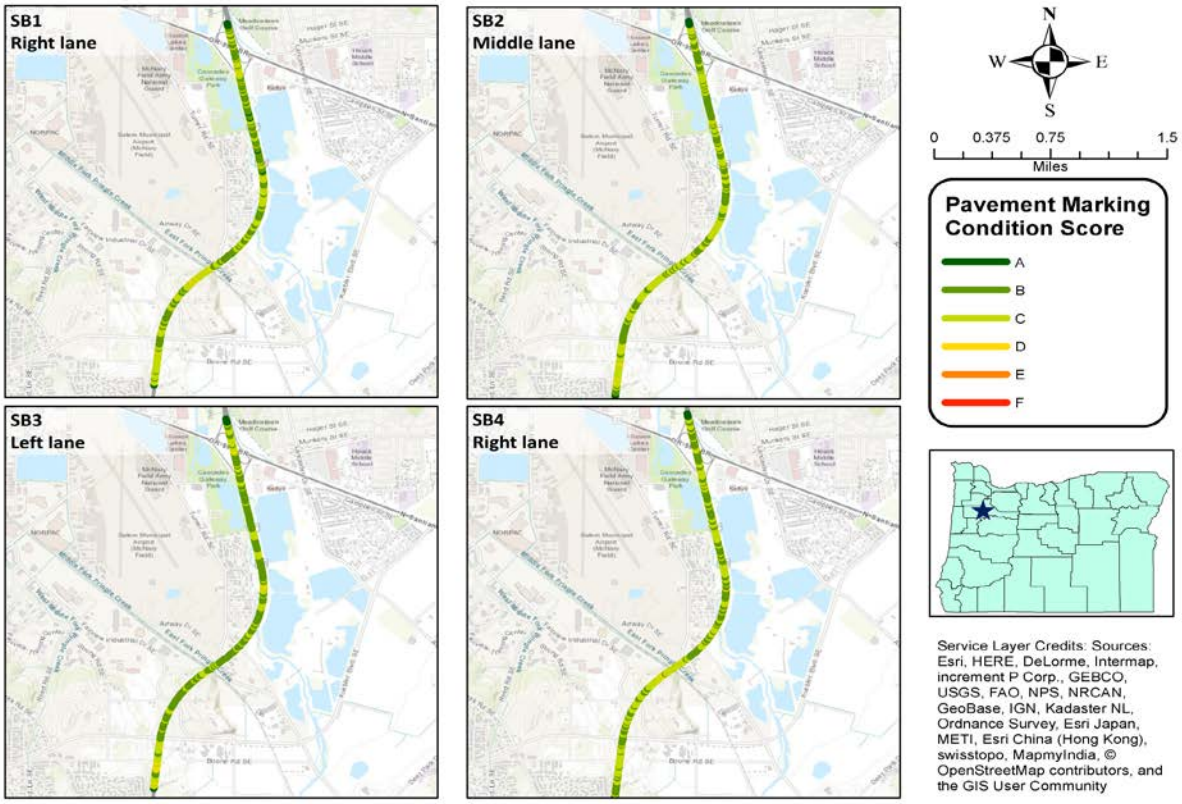

(b) Southbound at hundredths of a mile.

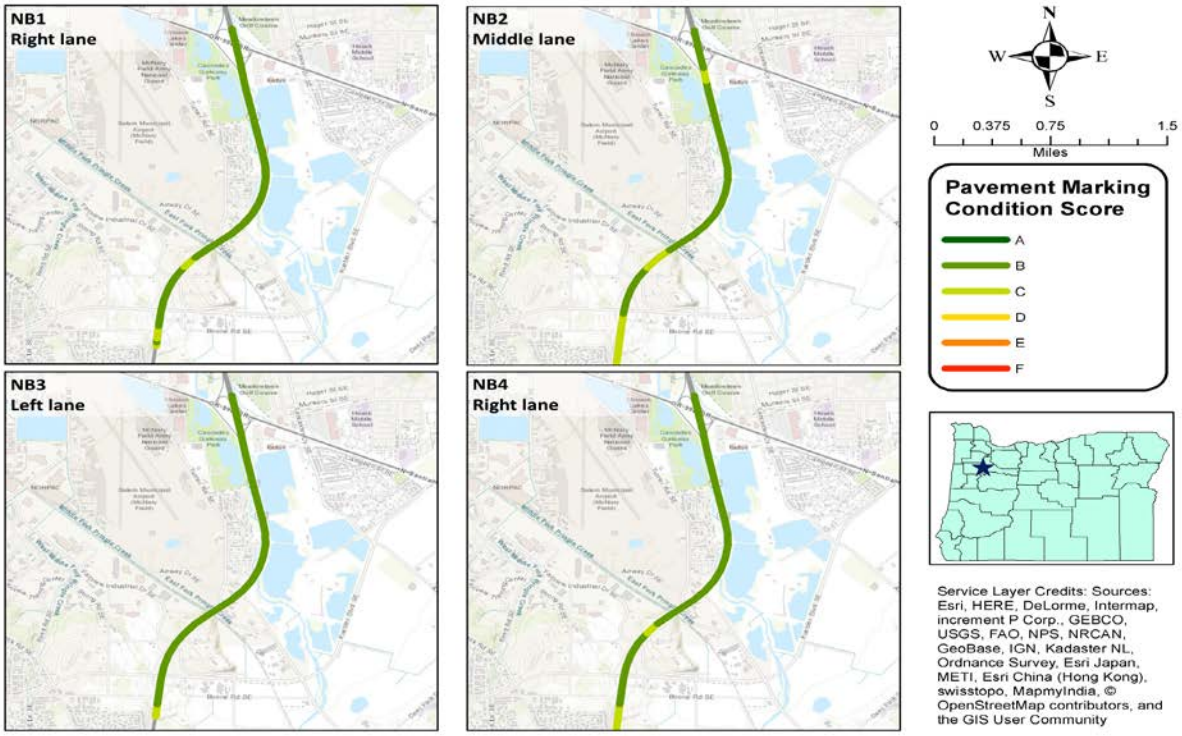

(c) Northbound at tenths of a mile.

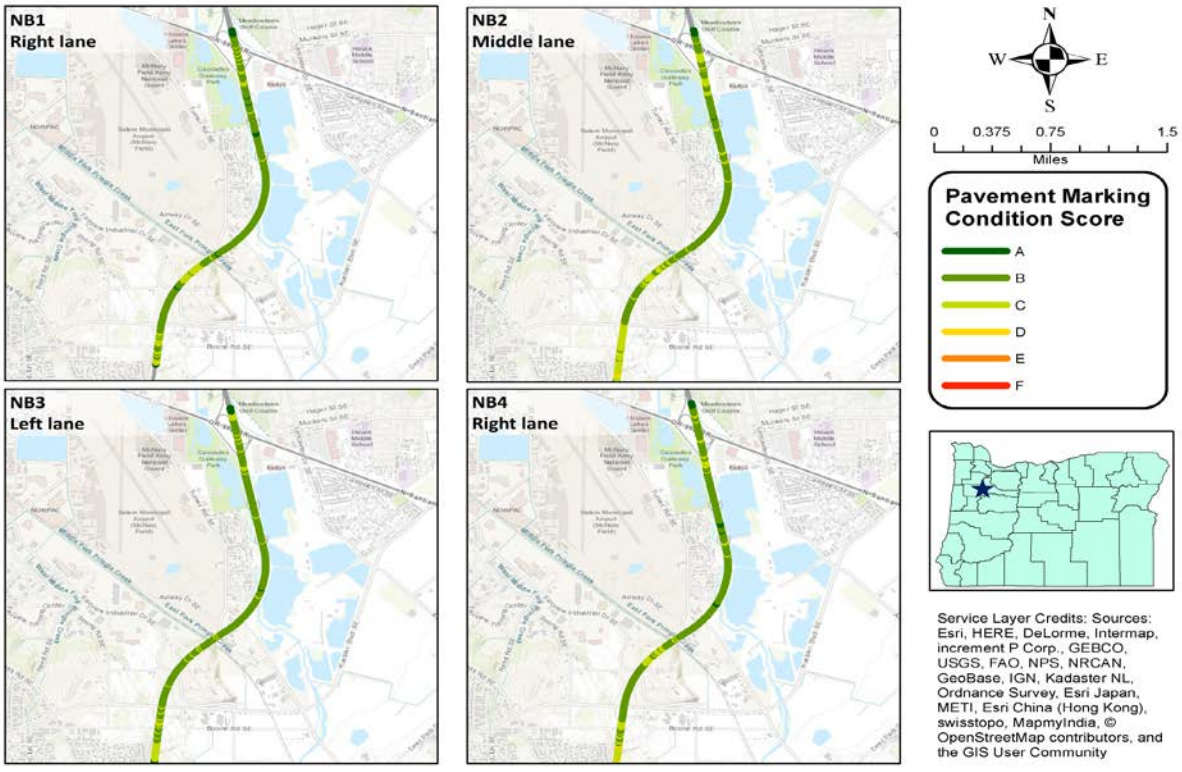

(d) Northbound at hundredths of a mile.

Figure 13.3: Pavement marking condition maps generated using mobile lidar data collected in different lanes on Interstate-5.

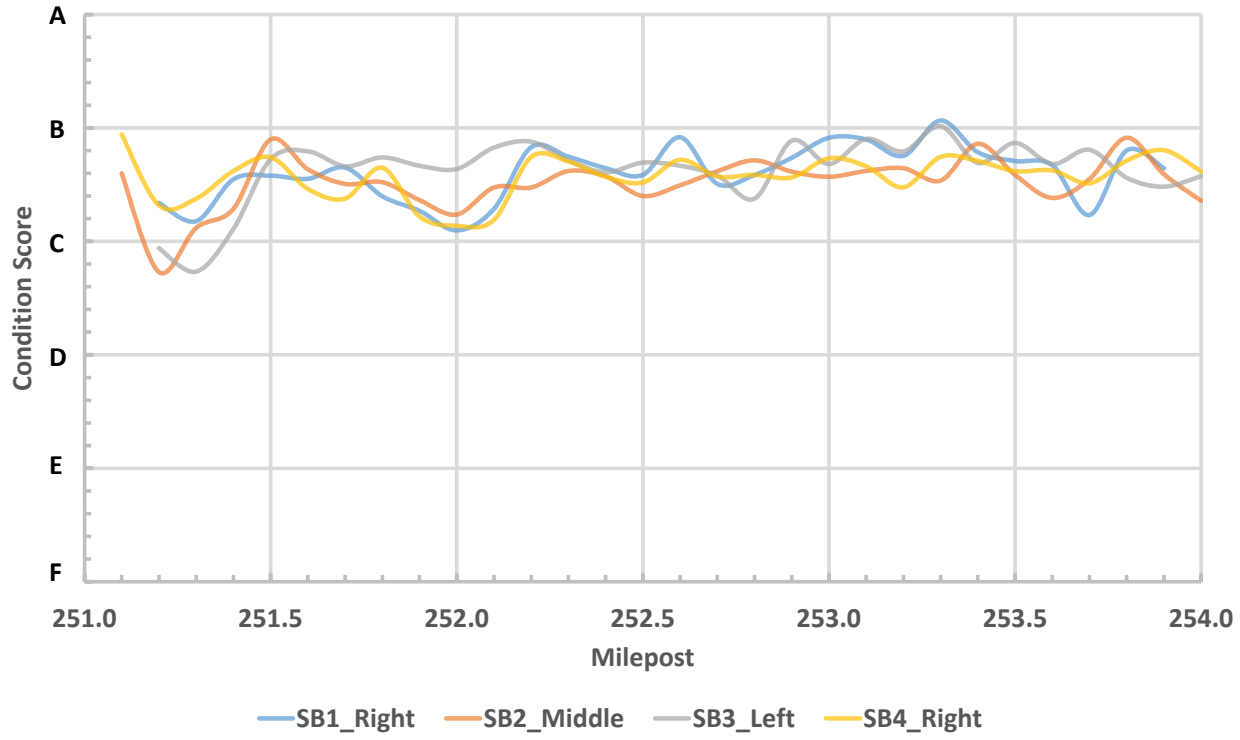

(a) Southbound at tenths of a mile

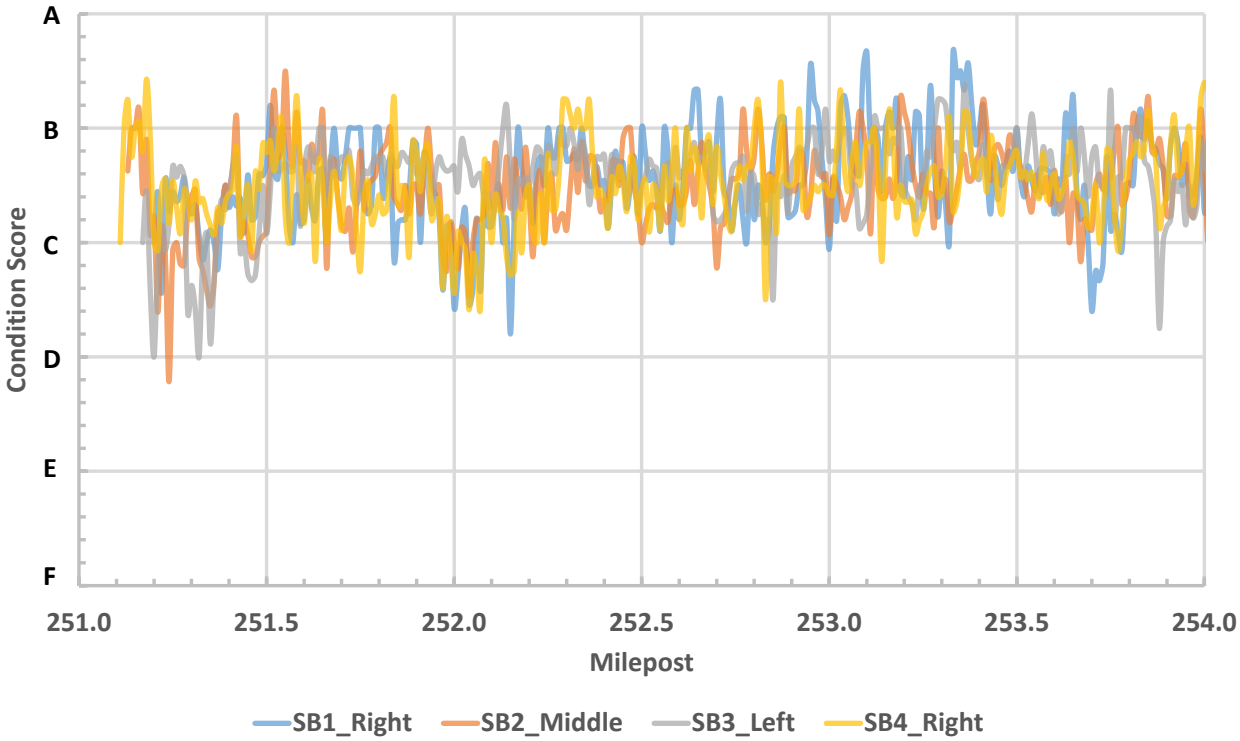

(b) Southbound at hundredths of a mile

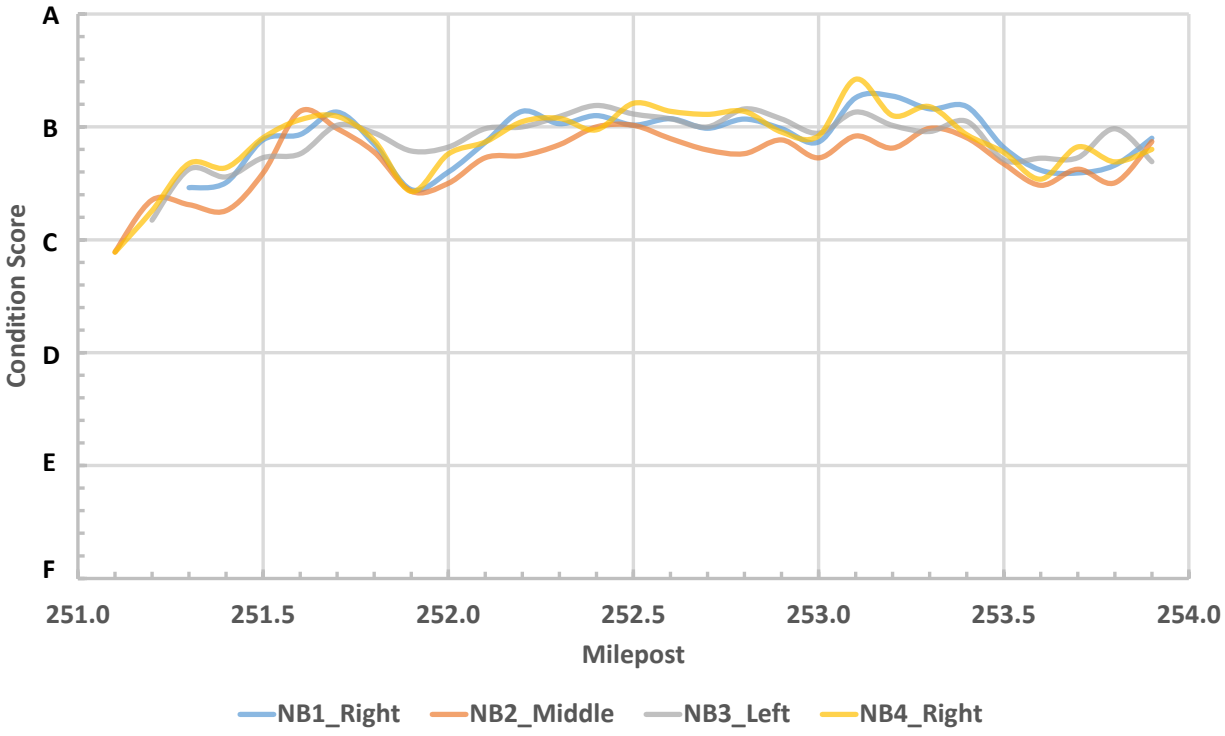

(c) Northbound at tenths of a mile

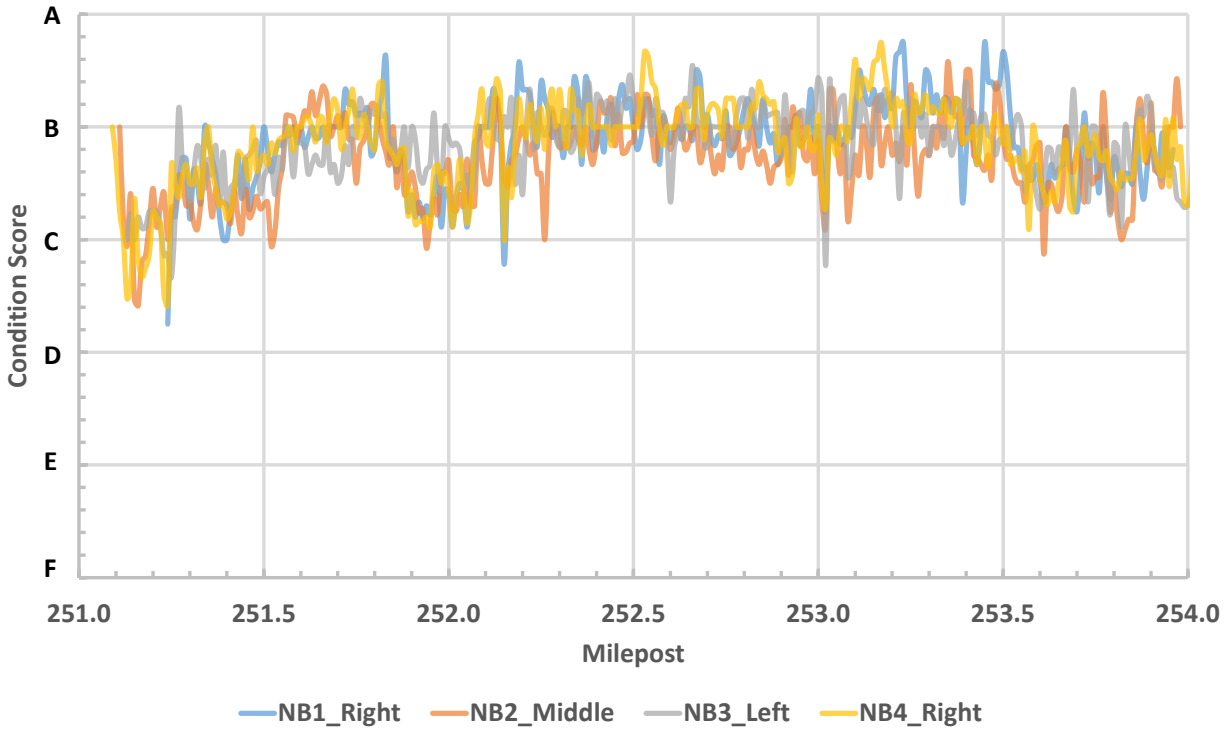

(d) Southbound at hundredths of a mile

Figure 13.4: Comparison of pavement marking condition evaluation from different passes.

Because no retroreflectometer measurements were acquired in this test area due to safety concerns and logistics, the project team did not conduct rigorous accuracy assessment for each pass as were done at other test sites (e.g., Testdeck, Philomath). Alternatively, to focus on the repeatability and robustness, the research team conservatively computed the difference between the maximum and minimum condition score from all the passes for each fraction of a milepost section. Then a statistics analysis was performed for both the southbound and northbound directions with different sampling intervals, respectively. The summary statistics in Table 13.3 show that the proposed evaluation method is averaging within approximately 1/2 of a letter grade (A through F) of condition scores and within 1.4 grades at a 95% confidence level based on the average and standard deviation for the 1/100th mile increment. For the 1/10th mile sections, the condition scores average to approximately 1/3 of a grade and are within 0.8 grades at a 95% confidence level. On one hand, the 1/10th mile layer, the evaluation results are more robust to different types of errors such as the missing stripes caused by occlusions, falsely detected stripes (which usually have a lower retroreflectivity), and the differences in retroreflectivity measurements with each lidar pass, and so forth. On the other hand, the results at 1/100th of a mile increments provide more details of the pavement marking condition. Hence, to minimize the requirement for manual editing, given the scale of interest, the 1/10th mile increment is recommended for the asset management purposes. When more detailed assessments are desired for localized sites, the stripe and retro feature classes can be used, as explained in Chapter 12.

Table 13.3: Summary statistics of the repeatability test for evaluating the aggregated pavement marking condition.

Sampling Interval	Direction	Average	Std. Dev.	Max.	Min.	Median
1/100th of a mile	SB	0.64	0.33	1.66	0.07	0.60
	NB	0.50	0.22	1.31	0.01	0.49
1/10th of a mile	SB	0.37	0.15	0.64	0.08	0.33
	NB	0.29	0.10	0.50	0.14	0.26

13.4 ACQUISITION DIRECTION EVALUATION

An additional dataset was collected on the Oregon DOT mobile lidar test course in Salem, OR. Loops around the course were completed in both the clockwise and counterclockwise directions. These data were used to evaluate the differences in retroreflectivity based on direction. This site includes a mix of major and minor roads. One particular challenge with this dataset is that the stripes in some locations are directly at the edge of pavement. Figures 13.5 and 13.6 show example maps of the simulated retroreflectivity values in the clockwise and counterclockwise directions. General patterns and observations of retroreflectivity trends in these figures are consistent with previous findings related to differences based on the lane of observation. However, in the closer views, additional limitations become more apparent. The first is that the stripe on the opposite side of the road can be difficult to detect at this site in some locations. This is particularly true in areas where the stripe is worn heavily or close to the edge of pavement and somewhat overgrown with vegetation. Another factor that the road is built with a cross slope for drainage. Although relatively small, this slope means that, in the direction of travel, the mobile lidar will be slightly tilted downward to the right while the stripe on the other side of the road will be tilted downward towards the left. The slight tilting results in a lower sampling of

points on a stripe on the left side of the road compared with one at an equal distance on the right. In some cases, this low point density results in the stripe not being able to be detected. In other cases, it results in an insufficient number of points for retroreflectivity evaluation.

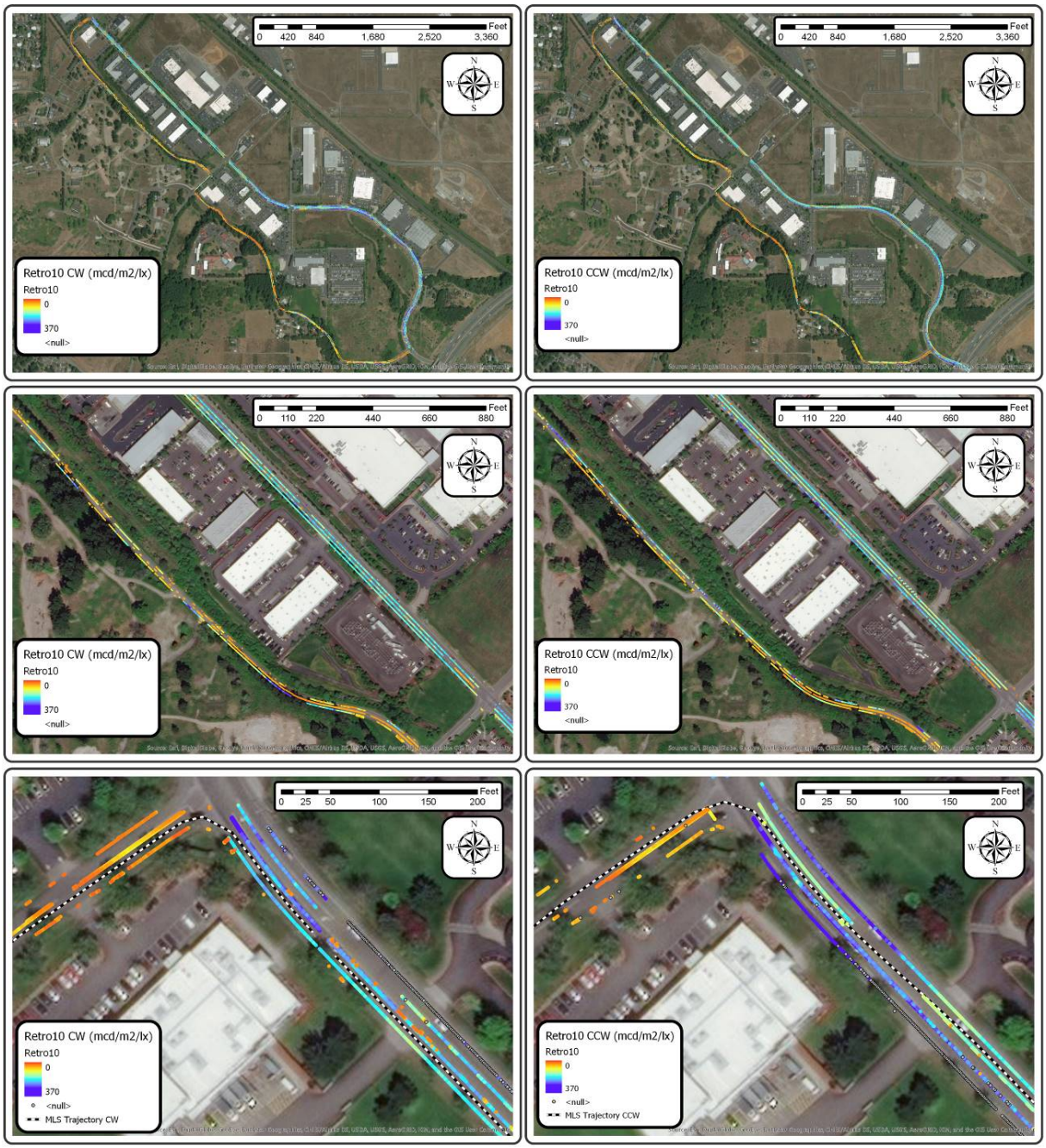

Figure 13.5: Detailed simulated retroreflectivity results for the clockwise (CW, left) and counterclockwise (CCW) loops. The top shows the main loop of the course, the middle shows a closer view of a section, and the bottom shows a detail of an intersection at the top of the loop. Stripes marked as null values were able to be extracted but did not have sufficient points to obtain retroreflectivity estimates.

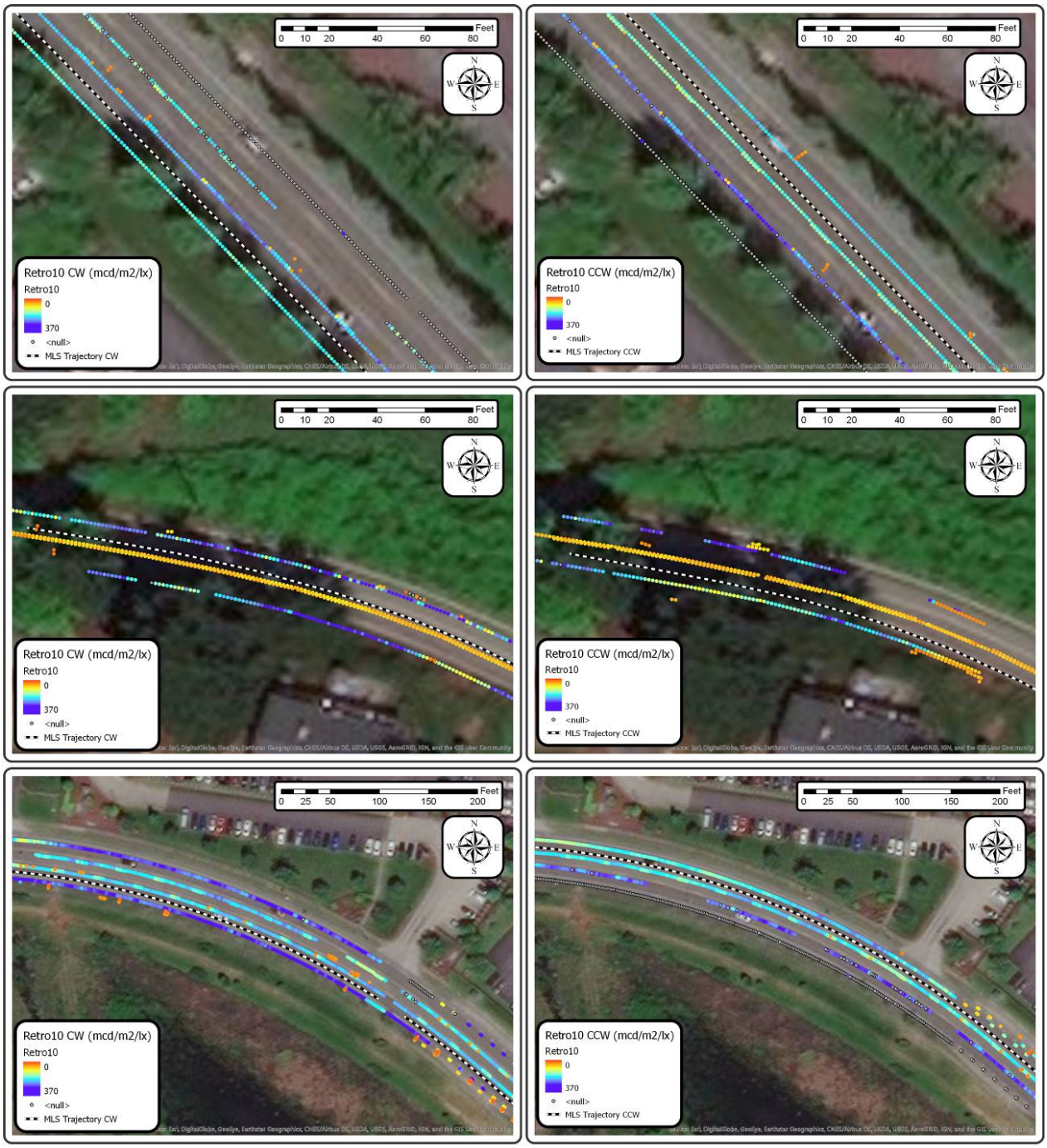

Figure 13.6: Detailed simulated retroreflectivity results from the Oregon DOT mobile lidar test course for the clockwise (CW, left) and counterclockwise (CCW, right) loops. This plot shows three additional close-up sections from those shown in Figure 13.5. Stripes marked as null values were able to be extracted but did not have sufficient points to obtain retroreflectivity estimates.

Simulated retroreflectivity readings were analyzed along an approximately 150 m (492 ft.) section of a yellow centerline stripe that was observed from approximately the same distance from the mobile lidar system in the counterclockwise and clockwise loops to evaluate the consistency between directions (Figure 13.7). The results generally agree well (RMS difference of 11.1 mcd/m^2/lux) and follow consistent patterns. Most differences are within the RMSE values (approximately 25 to 35 mcd/m^2/lux) reported within Table 9.6 for the radiometric calibration. Thus, they are unlikely substantially affected by the direction of travel. This finding would be expected given that the scanner operates in a dual profiler configuration with scanners pointed at -30° and +60°, which means that one laser looks forward while the other looks in reverse. Detailed views of two sections are provided in Figure 13.7 for additional clarity in comparison.

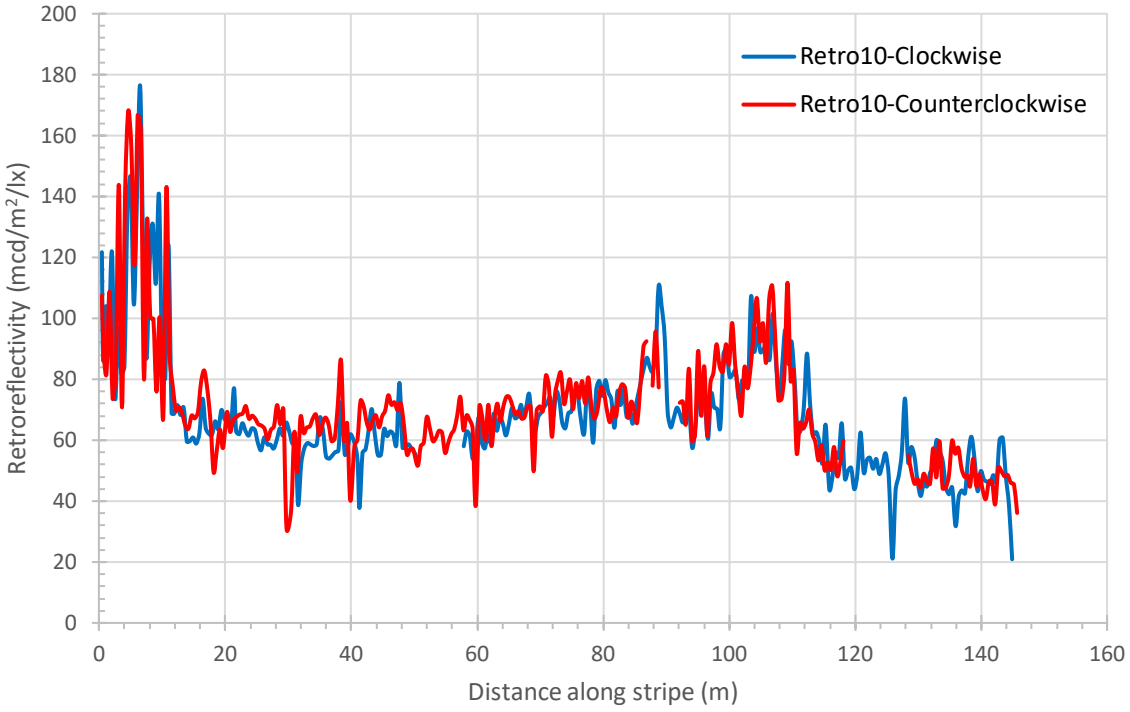

(a)

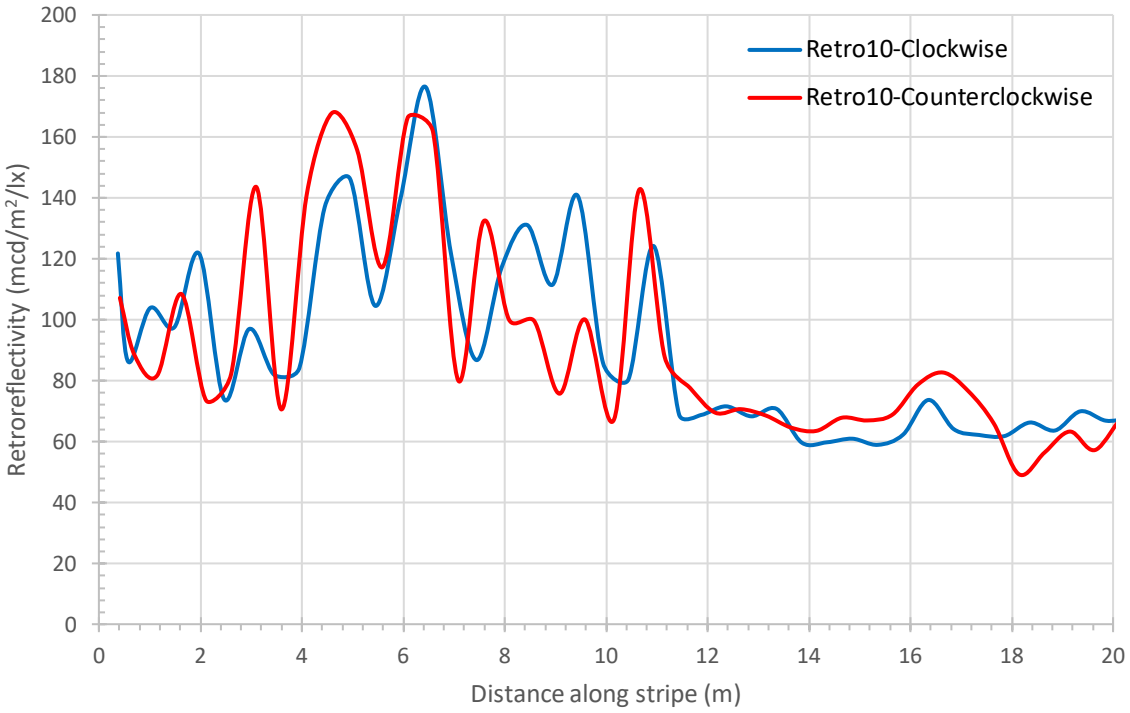

(b)

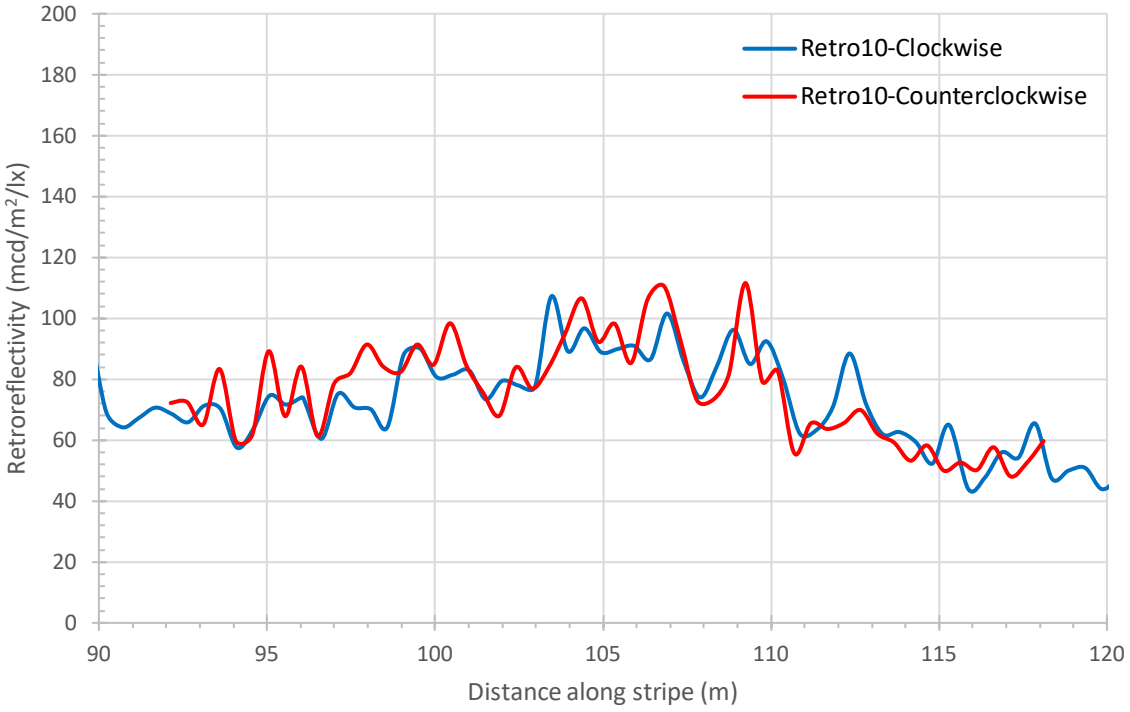

(c)

Figure 13.7: Retroreflectivity comparison for a portion of the yellow centerline on the Oregon DOT mobile lidar test course in Salem, OR. (a) shows the entire segment analyzed with more detailed close-ups shown from a distance of (b) 0-20 m (0-66 ft.) and (c) 90-120 m (295-394 ft.).

Figure 13.8 provides a quantitative analysis showing the agreement between the clockwise and counter clockwise data collections. When plotted against one another, the data follows a near 1:1 line, showing good agreement. The mean difference between datasets was 1.9 mcd/m^2/lux with a standard deviation of 11.0 mcd/m^2/lux. These values are consistent with the results observed from repeat passes in the same lane from Chapter 11.0 (Philomath) and Section 13.2 (Interstate-5), indicating that there is no distinguishable bias in terms of the direction of acquisition on the center stripe.

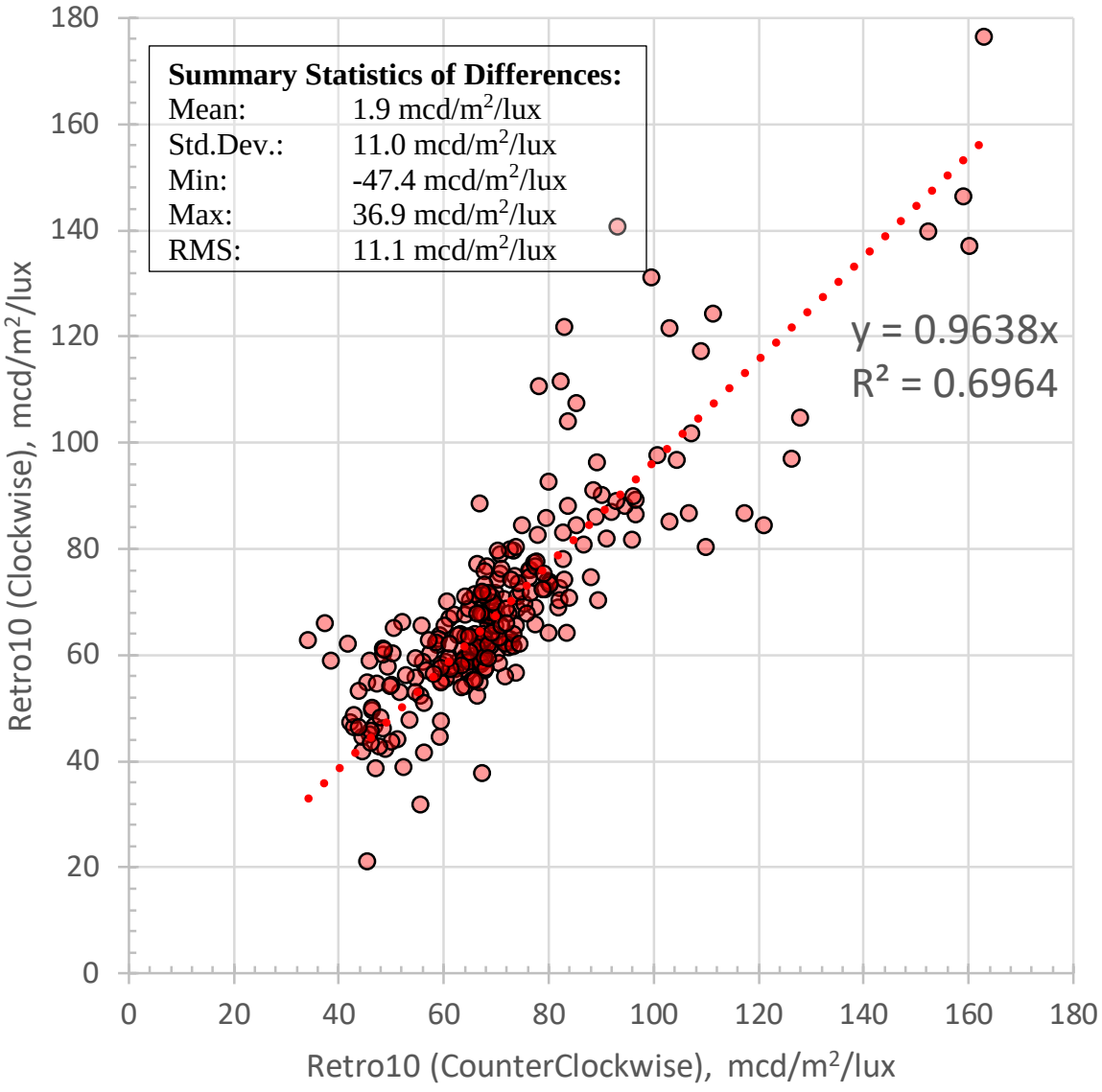

Figure 13.8: Quantitative retroreflectivity comparison for a portion of the yellow centerline on the Oregon DOT mobile lidar test course in Salem, OR with data collected in the clockwise and counterclockwise directions.

14.0 CONCLUSIONS AND RECOMMENDATIONS

14.1 CONCLUSIONS

This project developed an empirical model to perform radiometric calibration of mobile lidar intensity information from the Leica Pegasus:Two system owned by Oregon DOT so that data acquired by the system could be utilized for pavement marking evaluation. The model was developed using dense, handheld retroreflectometer measurements and mobile lidar data collected in a variety of geometric configurations at the Oregon DOT Testdeck site. This site consists of a variety of markings with varying degrees of wear. The model was then validated with additional datasets collected on US 20/34, Interstate-5, and local roads in Salem also containing pavement markings of variable degrees of wear. Note that the local roads are owned by the City of Salem and have different standards to update and maintain retroreflectivity than those used by Oregon DOT. A detailed evaluation of operational variables was performed including speed effects, the lane of travel, direction of travel, etc. to determine their influence on the retroreflectivity evaluations and identify limitations.

The project resulted in a number of important findings, products, and operational recommendations, which will be summarized in the following sections.

14.1.1 Effectiveness of mobile lidar for mapping evaluating pavement markings

- Data collected through normal operations (dry conditions) with the current dual profiler configuration by Oregon DOT Geometronics provides satisfactory data to use for evaluating pavement marking performance and for warranty claims for markings below 373 mcd/m^2/lux.

- Pavement markings extracted from mobile lidar data can be extracted, evaluated, and integrated into a GIS dataset. The software and supporting scripts developed in this research is capable of supporting detailed analyses as well as simpler, aggregated analyses to support asset management layers.

- With the system tested and procedures documented in this report, the retroreflectivity evaluation with mobile lidar worked successfully for pavement markings and is on par with results from handheld and mobile retroreflectometer units up to 373 mcd/m^2/lux. In fact, for lower ranges of retroreflectivity near the typical pass/fail ranges, the mobile lidar system outperforms the mobile retroreflectometer.

- The mobile lidar data enables a more efficient, higher resolution/detail, and more robust measurement compared with traditional approaches (e.g. visual assessment or handheld retroreflectometer). A key strength is that mobile lidar provides data along the entire stripe compared with relatively few, discrete measurements using a handheld retroreflectometer. Hence, it is not subject to user bias.

- Another key advantage of mobile lidar is its ability to capture retroreflectivity measurements on multiple stripes simultaneously from a single pass. Notably, on busy highways or freeways, some portions of the stripes can be blocked; however, performing multiple passes from different lanes can minimize this problem on busy highways (e.g., Interstate-5, Interstate-84). In the Interstate-5 tests with a 3 lane road, most stripes were successfully extracted from single passes.

- Relative consistency was observed in retroreflectivity condition assessment between different passes using the RoME tool and GIS scripts. This was observed in both the detailed stripe and aggregated milepost layers.

- The mobile lidar unit was effective in measuring the degradation of retroreflectivity and provided consistent results when compared with the handheld retroreflectometer.

- Retroreflectivity measurements as well as lidar data quality are significantly affected by wet surfaces, which degrade the laser intensity. Based on the analyses completed in this research, only relatively dry pavement marking evaluations using mobile lidar should be performed. Note that Oregon DOT Geometronics current practice is to collect mobile lidar data only under dry conditions to preserve the geometric accuracy and quality of the data. Nevertheless, future research could explore development of corrections for retroreflectivity in wet conditions if utilizing data collected under wet conditions be desirable or necessary.

- In its current implementation, the approach developed for the RoME tool can extract linear (or gently curved) markings, but it cannot handle complex markings such as legends, turn arrows, cross walks, and thick green bike boxes. The project team will be expanding those capabilities in future research through a small project recently accepted for funding through Pactrans.

- The direction of travel influenced the ability to extract certain stripes as well as obtain retroreflectivity estimates due lower point density, in part due to the geometric changes from the road cross slope.

14.1.2 Radiometric calibration

Several rigorous tests were conducted to develop a robust radiometric calibration for Oregon DOT's mobile laser scanner as well as to validate the accuracy, repeatability, and reproducibility of the results in different operational configurations.

- The radiometric calibration model developed in this study is specific to the Leica Pegasus:Two with its current sensors and configuration (as of the date of publication of this report). It should not be applied directly to another scanning system or if significant manufacturer upgrades (e.g., replacement of a scanner, change in sensor orientation, or calibration) are completed. The model can, however, serve as a reference for developing a radiometric calibration model for other systems if it is properly verified following a similar process to the testing completed in this report.

- Notably, the radiometric calibration does not include correctors for angle of incidence and range as are typically followed in most scientific literature (e.g., Kashani et al., 2015). Firstly, this research determined that these variables were highly correlated with the mobile lidar configuration. Secondly, the range of values for these parameters are quite limited given typical geometric configurations for acquisition. Other mobile lidar units may be oriented in different configurations that require correction for range and angle of incidence.

- For the system used in this study, retroreflectivity can only be estimated up to 373 $mcd/m^2/lux$ due to signal saturation such that any higher levels of retroreflectivity cannot be distinguished. Fortunately, this limitation does not significantly affect the ability to evaluate the condition of existing stripes or most newly placed stripes using current Oregon DOT requirements for retroreflectivity in conjunction with the different quality grades established in this research (e.g., $A > 350$ $mcd/m^2/lux$ for white stripes). The mobile lidar retroreflectivity data proved successful to evaluate lower levels of retroreflectivity well; however, the data were found to have higher variance at larger retroreflectivity values.

- Based on the experimental tests, the material and the color did not appear to affect the quality of the radiometric calibration significantly.

- The dual profiler configuration (the current configuration used by Oregon DOT) yielded more consistent results overall compared with the single profiler in a wide range of orientations.

- Best results were achieved using the dual profiler configuration operated from one lane over from the stripe of interest; however, reasonable results were still achieved on stripes adjacent to the lane of travel, particularly in the dual profiler configuration.

- In operation, it normally is recommended to limit the stripe extraction to a distance slightly larger than lane width from the mobile lidar unit to limit false positives.

- It is recommend to operate the mobile lidar unit from the center lane on highways with 3 lanes if only one pass is completed. However, unless a rolling slow down or other mechanism is utilized, there will be data gaps from passing vehicles and truck traffic.

- Different strategies may be necessary when trying to use a similar procedure for evaluating pavement markings on large freeways with more than three lanes in each direction (relatively rare in Oregon) . Nevertheless, in a practical sense, it would be difficult to have the necessary line of sight to acquire data on these markings given the wide range of obstructions from traffic that are likely in these large freeway systems without completing multiple passes from multiple lanes.

- The direction of travel did not significantly influence the retroreflectivity estimates aside from the differences that already occur from acquiring data from a different

lane. Large separations (e.g., medians) and roads with large cross slopes will affect the quality of extracting and analyzing the longitudinal stripe from the opposing lane.

14.2 RESEARCH PRODUCTS

A number of useful tools were developed from this research that are being integrated into Oregon DOT's workflows. Key products include:

1. A straightforward, radiometric calibration model to convert lidar intensity values to retroreflectivity estimates that is optimized for evaluating pavement markings closer to typical evaluation thresholds.

2. A novel and robust software tool called the *Road Marking Extractor (RoME)* Tool, which identifies and extracts the road markings from the lidar data, provides a lidar data file with points only, extracts useful attributes, and

3. ArcGIS python scripts to create data layers produced by the tool include both detailed layers with retroreflectivity evaluations every 2 feet along stripes to aid with detailed evaluation of specific sites well as simplified layers that link directly to Oregon DOT's milepost GIS layers to provide a retroreflectivity-based grade of pavement marking quality at the desire milepost increment for asset management purposes. This can be used to create a map product for Oregon DOT's preferred GIS software and directly produce a visual map layer (e.g., TransGIS) for maintenance crews to see pavement marking performance.

This process as well as the supporting software and scripts will require minor updates and hopefully be expanded in functionality as Oregon DOT continues to implement these research results into their workflows.

14.3 RECOMMENDATIONS FOR IMPLEMENTATION

The following are recommendations to Oregon DOT in the implementation process of this research:

- For freeways and major highways with three lanes travelling in the same direction, it is recommended that the mobile lidar unit be operated in the middle lane for best results in extracting stripes. On two lane roads, the left lane is recommended since the yellow stripe is of lower retroreflectivity and would be less affected by the increased scatter in the radiometric calibration model that occurs with increasing retro-reflectivity.

- For improved retroreflectivity degradation analysis and consistency, it is recommended to operate the mobile lidar unit from the same lane for each survey, whenever feasible. This will help maintain a more consistent scanning geometry (and retroreflectivity measurements) between epochs.

- The radiometric calibration equation and coefficients are only valid for the current system being used by Oregon DOT. Should Oregon DOT purchase a new mobile lidar unit or change the scanners on the unit, they will need to perform another calibration of the unit following the procedure outlined in this research.

- Should the sensor undergo calibration by the manufacturer, Oregon DOT should verify that the radiometric calibration remains valid by conducting some basic tests on the Testdeck or other site. Similarly,

- It is recommended that Oregon DOT perform periodic validation surveys similar to the Validation test in Philomath with a stripe with a broad range of retroreflectivity conditions to verify that there are no significant power\intensity readings changes in the system. However, for these validation surveys 20 retroreflective samples should be sufficient.

- The parameters used in the RoME code should be verified and adjusted as Oregon DOT gains more experience utilizing the software. Use of the RoME tool with a different mobile lidar unit may require some testing and modification of the default parameters.

- When GIS inventories expand and repeat evaluations are conducted, the earlier layers can be used to help screen false positive markings from the RoME tool for more efficient GIS cleanup. (e.g., a polygon could be formed between the two shoulder lane markings on each side of the road and slightly buffered to identify potentially false markings outside of this zone.

14.4 FUTURE CONSIDERATIONS

Oregon DOT may consider several enhancements to the RoME tool and GIS scripts as they develop more experience with implementing this research. In particular, additional research could help develop a similar tool to handle more complex road markings (e.g., letters and highly-curved ones). A discussion of current limitations and specific recommendations are made in Sections 12.5 and 12.6. Most notably, developing an approach to integrate pavement markings from different runs would be highly beneficial to improve the completeness before aggregating the results.

14.5 SUMMARY OF RESEARCH BENEFITS

Use of mobile lidar for pavement marking retroreflectivity provides significant benefits to Oregon DOT (and other agencies considering implanting a similar approach), including:

1. Safer data acquisition through reduction of roadside data collection.

2. Increased efficiency of data collection by leveraging existing, routine Oregon DOT mobile lidar acquisitions for other purposes, minimizing redundancy and adding additional value. The mobile lidar data acquisition has already shown solid performance, ROI, and many other benefits in Oregon DOT. Use of this system helps

reduce duplicative travel and field work, which can result in significant cost savings and efficiencies, particularly in remote areas.

3. A higher level of service of retroreflective markings for the public –retroreflectivity data from mobile lidar data can simultaneously be collected across the scales (detailed local measurements to broad, aggregated measurements) at highway speeds.

4. Improved QA/QC for markings by enabling spatially continuous measurements at more frequent time intervals, particularly in areas of concern. Markings deemed acceptable but close to the failing point could be surveyed more frequently with mobile lidar to determine the optimal time for reapplication of markings, essentially extending the life of the existing markings.

5. Enhanced asset management by improving user interaction with the data as well as improving the success of automated feature extraction algorithms.

6. Quantitative data to support warranty disputes.

7. Informative geospatial data layers that support informed decision making by supervisors within Oregon DOT management, and

8. Improve MAP-21 compliance through enabling performance-based procedures for evaluating pavement marking quality using the detailed information provided by mobile lidar and its ability to enable collection of retroreflectivity data on critical corridors throughout the state.

15.0 REFERENCES

Ahokas, E., Kaasalainen, S., Hyyppä, J. & Suomalainen, J. (2006). Calibration of the Optech ALTM 3100 laser scanner intensity data using brightness targets. *International Archives of Photogrammetry, Remote Sensing and Spatial Information Sciences, 36,* 14-20.

Ai, C. & Tsai, Y.J., (2016). An automated sign retroreflectivity condition evaluation methodology using mobile LIDAR and computer vision. *Transportation Research Part C: Emerging Technologies,63*, 96-113.

American Society for Testing and Materials. (2011). *Standard Test Method for Measurement of Retroreflective Pavement Marking Materials with CEN-Prescribed Geometry Using a Portable Retroreflectometer.* (ASTM E1710-11. DOI: 10.1520/E1710-11

American Society for Testing and Materials. (2012). *Standard Test Method for Measuring the Coefficient of Retroreflected Luminance of Pavement Markings in a Standard Condition of Continuous Wetting (R_L-2).* (ASTM E2832-12) DOI: 0.1520/E2832-12

American Society for Testing and Materials. (2015). *Standard Practice for Evaluating Retroreflective Pavement Markings Using Portable Hand-Operated Instruments.* (ASTM D7585M-10) DOI: 10.1520/D7585_D7585M-10R15

American Society for Testing and Materials. (2018). *Standard Test Method for Measuring the Coefficient of Retroreflected Luminance (R_L) of Pavement Markings in a Standard Condition of Wetness*. (ASTM E2177-18) DOI: 10.1520/E2177-18

Austin, R.L., & Schultz, R.J. (2009). *Guide to Retroreflection Safety Principles and Retroreflective Measurements.* San Diego, CA: RoadVista. Retrieved from www.gamma-sci.com/wp-content/uploads/2012/06/Retroreflectivity-Guide-RoadVista.pdf .

Balali, V., Sadeghi, M.A. & Golparvar-Fard, M., (2015). Image-based retroreflectivity measurement of traffic signs in day time. *Advanced Engineering Informatics, 29*(4), 1028-1040. DOI: 10.1016/j.aei.2015.08.003.

Baltsavias, E.P., (1999). Airborne laser scanning: Basic relations and formulas. *ISPRS Journal of Photogrammetry and Remote Sensing, 54*, 199-214.

Briese, C., Pfennigbauer, M., Lehner, H., Ullrich, A., Wagner, W., & Pfeifer, N., (2012). Radiometric Calibration of Multi-Wavelength Airborne Laser Scanning Data. *ISPRS Annals of the Photogrammetry, Remote Sensing and Spatial Information Sciences, 7,* 335–340.

Burns, D.M., Hedblom, T.P., & Miller, T.W. (2008). Modern Pavement Marking Systems: Relationship Between Optics and Nighttime Visibility. *Transportation Research Record: Journal of the Transportation Research Board*, 2056, 43-51.

Carlson, P.J., Hawkins Jr, H.G., Schertz, G.F., Mace, D.J., & Opiela, K.S. (2003). Developing updated minimum in-service retroreflectivity levels for traffic signs. *Transportation Research Record: Journal of the Transportation Research Board*, 1824, 133-143.

Carlson, P.J., & Hawkins Jr, H.G., (2003). *Updated minimum retroreflectivity levels for traffic signs. U.S. Department of Transportation* (Publication No. FHWA-RD-03-082). College Station, TX: Texas Transportation Institute. Retrieved from https://www.fhwa.dot.gov/publications/research/safety/03082/03082.pdf .

Carlson, P.J., Miles, J.D., Pike, A.M., & Park, E.S. (2007). *Evaluation of Wet-Weather and Contrast Pavement Marking Applications: Final Report* (Publication No. FHWA/TX-07/0-5008-2). College Station, TX: Texas Transportation Institute. Retrieved from https://static.tti.tamu.edu/tti.tamu.edu/documents/0-5008-2.pdf .

Carlson, P., & Picha, D. (2009). *Sign Retroreflectivity Manual: How to Meet the New National Standard for Small Agencies, Federal Land Management Agencies, and Tribal Governments* (Publication No. FHWA-CFL/TD-09-005). Washington, D.C.: Federal Highway Administration; U.S. Department of Transportation. Retrieved from https://d2dtl5nnlpfr0r.cloudfront.net/tti.tamu.edu/documents/FHWA-CFLTD-09-005.pdf.

Chen, X., Kohlmeyer, B., Stroila, M., Alwar, N., Wang, R. & Bach, J. (2009). Next generation map making: geo-referenced ground-level LIDAR point clouds for automatic retroreflective road feature extraction. *Geographic Information Systems*. DOI: 10.1145/1653771.1653851

Ceifetz, A. H., Yassin, J., Andridge, P., Kwigizile, V., Oh, J.-S., Burdick, B., Opus International Consultants., ... Michigan. (2017). *Evaluating road delineation practices in Michigan: Final report*. Retrieved from https://www.michigan.gov/documents/mdot/SPR1646_557606_7.pdf.

CTC & Associates LLC. (2016). *Use of Warranties and Retroreflectivity Values in Pavement Marking* (Publication). Madison, WI. Retrieved from www.dot.ca.gov/research/researchreports/preliminary_investigations/docs/use_of_warranties_and_retroreflectivity_values_in_pavement_marking_preliminary_investigation.pdf .

Gonzalez-Jorge, H., Riveiro, B., Armesto, J. & Arias, P., (2013). Evaluation of road signs using radiometric and geometric data from terrestrial LiDAR. *Optica Applicata*, *43*(3), 421-433.

Guan, H., Li, J., Yu, Y., & Wang, C. (2013). Rapid Update of Road Surface Databases Using Mobile LiDAR: Road-Markings. *2013 Fifth International Conference on Geo-Information Technologies for Natural Disaster Management*. doi:10.1109/git4ndm.2013.22

Guan, H., Li, J., Cao, S. & Yu, Y., (2016). Use of mobile LiDAR in road information inventory: A review. *International Journal of Image and Data Fusion, 7*(3), 219-242. DOI:10.1080/19479832.2016.1188860

Guan, H., Li, J., Yu, Y., Chapman, M., & Wang, C. (2015). Automated Road Information Extraction From Mobile Laser Scanning Data. *IEEE Transactions on Intelligent Transportation Systems, 16*(1), 194-205. DOI:10.1109/TITS.2014.2328589

Guan, H., Li, J., Yu, Y., Wang, C., Chapman, M., & Yang, B., (2014). Using mobile laser scanning data for automated extraction of road markings. *ISPRS Journal of Photogrammetry and Remote Sensing, 87*, 93-107. DOI: 10.1016/j.isprsjprs.2013.11.005

Guo, J., Tsai, M.J. & Han, J.Y. (2015). Automatic reconstruction of road surface features by using terrestrial mobile lidar. *Automation in Construction, 58*, 165-175. DOI: 10.1016/j.autcon.2015.07.017

Hadi, M. (2007). *Lane Marking/Striping to Improve Image Processing Lane Departure Warning Systems* (Tech. No. CA07-0529). Sacramento, CA: California Department of Transportation. Retrieved from www.dot.ca.gov/newtech/researchreports /reports/2007/ca07-0529.pdf

Hawkins, Jr., H. G., Pratt, M. P., & Carlson, P. J. (2008). *Preliminary Economic Impacts of Implementing Minimum Levels of Pavement Marking Retroreflectivity* (Rep. No. FHWA-SA-08-010). Washington, D.C.: Federal Highway Administration; U.S. Department of Transportation. Retrieved from https://safety.fhwa.dot.gov/roadway_dept/night_visib/ pavement_visib/fhwasa08010/fhwasa08010.pdf.

Hawkins, N., Smadi, O., Knickerbocker, S., & Carlson, P. (2016). *Rumble Stripe: Evaluation of Retroreflectivity and Installation Practices* (Publication No. MN/RC 2016-13). St. Paul, MN: Minnesota Department of Transportation. Retrieved from www.dot.state.mn.us/research/TS/2016/201613.pdf.

Höfle, B. & Pfeifer, N. (2007). Correction of laser scanning intensity data: Data and model-driven approaches. *ISPRS Journal of Photogrammetry and Remote Sensing*, *62*(6), 415-433. DOI:10.1016/j.isprsjprs.2007.05.008

Jaakkola, A., Hyyppä, J., Hyyppä, H., & Kukko, A., (2008). Retrieval algorithms for road surface modelling using laser-based mobile mapping. *Sensors*, *8*(9), 5238-5249. DOI: 10.3390/s8095238

Jelalian, A.V. (1992). *Laser radar systems*. Norwood, Massachusetts: Artech House, 292 pp.

Jensen, J.R. (2005). *Introductory digital image processing: a remote sensing perspective*, 3rd Ed., Pearson, Prentice Hall, Upper Saddle River, New Jersey, 526 pp.

Jutzi, B., & Gross, H. (2009). *Normalization of Lidar Intensity Data Based On Range and Surface Incidence Angle*. (Bretar, F. et al.: Laserscanning '09: ISPRS Workshop. 1.-2.

September 2009 Paris, France. (International archives of photogrammetry, remote sensing and spatial information sciences 38 Part 3 / W8).)

Kaasalainen, S.A., Krooks, A., Kukko, & Kaartinen, H. (2009). Radiometric calibration of terrestrial laser scanners with external reference targets. *Remote Sensing*, *1*(3), 144–158. DOI: 10.3390/rs1030144

Kaasalainen, S.A., Jaakkola, M. Kaasalainen, A., Krooks, A., & Kukko, A. (2011). Analysis of incidence angle and distance effects on terrestrial laser scanner intensity: search for correction methods. *Remote Sensing*, *3*(10), 2207-2221. DOI: 10.3390/rs3102207

Kashani, A.G., Olsen, M.J., Parrish, C.E., & Wilson, N. (2015). A Review of Lidar Radiometric Processing: from ad hoc Intensity Correction to Rigorous Radiometric Calibration. *Sensors*, *15*, 11, 28099-28128; DOI: 10.3390/s151128099

Khalilikhah, M., Heaslip, K. & Song, Z., (2015). Can daytime digital imaging be used for traffic sign retroreflectivity compliance? *Measurement*, *75*, 147-160.

Kirk, A. R., Hunt, E. A., Brooks, E. W., Transportation Development Division – Research Group, & Oregon Department of Transportation. (2001). *Factors Affecting Sign Retroreflectivity: Final Report* (Publication No. OR-RD-01-09). Salem, OR: Oregon Department of Transportation. Retrieved from https://www.oregon.gov/ODOT /Programs/ResearchDocuments/FactorsAffectSignRetroreflectivity.pdf .

Kopf, J. (2004). *Reflectivity of Pavement Markings: Analysis of Retroreflectivity Degradation Curves* (Publication No. WA-RD 592.1). Seattle, WA: Washington State Department of Transportation. Retrieved from https://www.wsdot.wa.gov/research/reports/fullreports /592.1.pdf .

Korpela, I., Ørka, H.O. Hyyppä, J., Heikkinen, V., & Tokola, T. (2010). Range and AGC normalization in airborne discrete-return LIDAR intensity data for forest canopies. *ISPRS Journal of Photogrammetry and Remote Sensing*, *65*, 4, 369-379.

Kumar, P., McElhinney, C.P., Lewis, P. & McCarthy, T., (2014). Automated road markings extraction from mobile laser scanning data. *International Journal of Applied Earth Observation and Geoinformation*, *32*, 125-137.

Lloyd, J., (2008). Understanding Retrorflectivity: A brief history of retroreflective sign face sheet materials. Retrieved from www.rema.org.uk/pub/pdf/history-retroreflective-materials.pdf .

Lundkvist, S.O. & Isacsson, U. (2007). Prediction of road marking performance. *Journal of Transportation Engineering*, *133*(6), 341-346.

Luzum, B., Starek, M. & Slatton, K.C., (2004). *Normalizing ALSM Intensities* (Publication No. Rep_2004-07-001). Gainesville, FL: University of Florida. Retrieved from www.aspl.ece.ufl.edu/reports/GEM_Rep_2004_07_001.pdf .

Mallet, C. & Bretar, F. (2009). Full-waveform topographic lidar: State-of-the-art. *ISPRS Journal of Photogrammetry and Remote Sensing, 64*(1), 1-16.

McGee, H.W., & Taori, S. (1998). Impacts of Maintaining Traffic Signs Within Minimum Retroreflectivity Guidelines. *Transportation Research Record: Journal of the Transportation Research Board, 1650*, 19-27. DOI:10.3141/1650-03

Migletz, J., Graham, J., Bauer, K., & Harwood, D. (1999). Field Surveys of Pavement-Marking Retroreflectivity. *Transportation Research Record: Journal of the Transportation Research Board, 1657*, 71-78. DOI:10.3141/1657-10

Olsen, M., V. Roe, G., Glennie, C., Persi, F., Reedy, M., Hurwitz, D., . . . Knodler, M. (2013). *Guidelines for the Use of Mobile LIDAR in Transportation Applications*. DOI: 10.13140/RG.2.1.2991.6884

Oregon Department of Transportation (n.d.). Mobile Lidar. Retrieved from https://www.oregon.gov/ODOT/ETA/Pages/LiDAR.aspx

Oregon Department of Transportation. (2002). *Desired Conditions of Maintenance Features on State Highways* (Publication). Salem, OR: Oregon Department of Transportation Office of Maintenance.

Oregon Department of Transportation (2015a). *Oregon standard specifications for construction*. Salem, OR: Oregon Department of Transportation

Oregon Department of Transportation (2015b). *Pavement markings design guidelines*. Retrieved from: https://www.oregon.gov/ODOT/Engineering/Documents_TrafficStandards/Pavement-Marking-Design-Guide.pdf

Oregon Department of Transportation (2018). *Traffic line manual*. Retrieved from: https://www.oregon.gov/ODOT/Engineering/Documents_TrafficStandards/Traffic-Line-Manual.pdf .

Oregon State Highway Division, Construction Section. (2015). *Manual of Field Test Procedures*. Salem, OR: Oregon Department of Transportation. Retrieved from https://www.oregon.gov/ODOT/Construction/Pages/Manual-of-Field-Test-Procedures.aspx .

Pike, A., Hawkins Jr, H. & Carlson, P.J. (2007). Evaluating the retroreflectivity of pavement marking materials under continuous wetting conditions. *Transportation Research Record: Journal of the Transportation Research Board*, 2015, 81-90.

Riveiro, B., González-Jorge, H., Martínez-Sánchez, J., Díaz-Vilariño, L. & Arias, P., (2015). Automatic detection of zebra crossings from mobile LiDAR data. *Optics & Laser Technology*, *70*, 63-70.

Saetern, L.T., Takigawa, S., California., California., & CTC & Associates,. (2016). *Commercial pavement marking management systems*. Retrieved from: www.dot.ca.gov/newtech

/researchreports/preliminary_investigations/docs/commercial_pavement_marking_management_systems_pi.pdf

Schaepman-Strub, G., Schaepman, M., Painter, T., Dangel, S., & Martonchik, J. (2006). Reflectance quantities in optical remote sensing—definitions and case studies. *Remote Sensing of Environment, 103*(1), 27-42. DOI:10.1016/j.rse.2006.03.002.

Schnell, T., Aktan, F. & Lee, Y.C. (2003). Nighttime visibility and retroreflectance of pavement markings in dry, wet, and rainy conditions. *Transportation Research Record: Journal of Transportation Research Board*, *1824*, 144-155. DOI:10.3141/1824-16

Smadja, L., Ninot, J., & Gavrilovic, T. (2010). Road extraction and environment interpretation from Lidar sensors. *International Society for Photogrammetry and Remote Sensing (ISPRS), 38*, part 3a, 281-286. Retrieved from www.isprs.org/proceedings/Xxxviii/part3/a/pdf/281_XXXVIII-part3A.pdf

Toth, C., Paska, E. & Brzezinska, D., (2008). Using road pavement markings as ground control for LiDAR data. *International Archives of Photogrammetry, Remote Sensing and Spatial Information Sciences*, *37*, 189-195.

Vain, A., Kaasalainen, S., Pyysalo, U., Krooks, A. & Litkey, P. (2009). Use of naturally available reference targets to calibrate airborne laser scanning intensity data. *Sensors*, *9*(4), 2780-2796. DOI: 10.3390/s90402780

van Schalkwyk, I., (2010). *Enhancements to pavement marking testing procedures* (Publication No. FHWA-OR-RD-11-02). Salem, OR: Oregon Department of Transportation. Retrieved from https://www.oregon.gov/ODOT/Programs/ResearchDocuments/Pavement_Marking_Testing.pdf.

Vosselman, G. (2009). Advanced point cloud processing. *Photogrammetric Week*, 9, 137-146. Retrieved from www.ifp.uni-stuttgart.de/publications/phowo09/160Vosselman.pdf

Wagner, W., Hyyppä, J., Ullrich, A., Lehner, H., Briese, C., & Kaasalainen, S. (2008). Radiometric calibration of full-waveform small-footprint airborne laser scanners. *International Archives of Photogrammetry Remote Sensing and Spatial Information Sciences, 37*, 1, 163-168.

Wen, C., Li, J., Luo, H., Yu, Y., Cai, Z., Wang, H. & Wang, C., (2016). Spatial-related traffic sign inspection for inventory purposes using mobile laser scanning data. *IEEE Transactions on Intelligent Transportation Systems*, *17*(1), 27-37.

Yan, L., Liu, H., Tan, J., Li, Z., Xie, H. & Chen, C., (2016). Scan line based road marking extraction from mobile LiDAR point clouds. *Sensors*, *16*(6), 903.

Yang, B., Fang, L., Li, Q. & Li, J., (2012). Automated extraction of road markings from mobile LiDAR point clouds. *Photogrammetric Engineering & Remote Sensing*, *78*(4), 331-338.

Yang, B., Liu, Y., Dong, Z., Liang, F., Li, B. & Peng, X., (2017). 3D local feature BKD to extract road information from mobile laser scanning point clouds. *ISPRS Journal of Photogrammetry and Remote Sensing, 130*, 329-343.

Yang, B., Dong, Z., Liu, Y., Liang, F. & Wang, Y., (2017). Computing multiple aggregation levels and contextual features for road facilities recognition using mobile laser scanning data. *ISPRS Journal of Photogrammetry and Remote Sensing, 126*, 180-194.

Yao, Y. & Hu, Q., (2014). Automatic extraction method study of road marking lines based on projection of point clouds. *2014 22nd International Conference on Geoinformatics*. DOI:10.1109/geoinformatics.2014.6950816

Yu, Y., Li, J., Guan, H., Jia, F. & Wang, C., (2015). Learning hierarchical features for automated extraction of road markings from 3-D mobile LIDAR point clouds. *IEEE Journal of Selected Topics in Applied Earth Observations and Remote Sensing, 8*(2), 709-726.

Zhang, H., Li, J., Cheng, M. & Wang, C., (2016). Rapid Inspection of Pavement Markings Using Mobile LIDAR Point Clouds. *The International Archives of the Photogrammetry, Remote Sensing and Spatial Information Sciences, 1*, 717-723.

APPENDIX A – SETTINGS FOR THE ROME TOOL (PARAMETER FILES – METRIC AND US CUSTOMARY UNITS)

parameters.txt - Notepad

File Edit Format View Help

```
%%%%%%%%%%%%%%%%% display and outcomes
fig=1;              % (1/2) display plots on the main interface(1) / display all plots(2)
savefig=0;          % (1/0 on/off) save intensity, marking, edges, and RGB images
savevid=0;          % (1/0 on/off) save video of marking and RGB images
speedvid=7;         % (7 default) video recording speed, the higher the value, the faster the recording speed
dtype=2;            % (1/2) display point cloud with intensity(1) / red&blue(2)
RR=5;               % (1 ~ ) point cloud reduction rate for display
RMEver=1.0;         % (1.0) Software version

%%%%%%%%%%%%%%%%% (1) road surface extraction
RoadLength=10;      % (10m or 32.808ft default) length of road setion
RoadWidth=10.8;     % (10.8m or 35.433ft default) width of road section

%%%%%%%%%%%%%%%%% (2) RANSAC
iteration=100;      % (100 default) RANSAC iteration
ths=0.05;           % (0.05m or 0.164ft default) RANSAC polyline threshold
increment=3;        % (3m or 9.842ft default) Searching space increments for dual segmentation

%%%%%%%%%%%%%%%%% (3) rasterization
pixelSize=0.05;     % (0.05m or 0.164ft default) pixel size
maskR=1;            % (1pixel default) dilation for infainting

%%%%%%%%%%%%%%%%% (4) image segmentation by Expectation Maximization
noc=2;              % (2 default) number of clusters

%%%%%%%%%%%%%%%%% (5) morphological filtering by opening operation
erode=0.1;          % (0.1m or 0.328ft default) erosion
dilate=0.15;        % (0.15m or 0.492ft default) dilation

%%%%%%%%%%%%%%%%% (6) line association
sa=15*pi/180;       % (15deg default) merging threshold of angular difference between lines
sr=0.1;             % (0.1m or 0.328ft default) merging threshold of ortho distance between lines
sd=1.5;             % (1.5m or 4.921ft default) merging threshold of distance between end points of lines

%%%%%%%%%%%%%%%%% (7) gap filling
gap=1;              % (1pixel default) dilation

%%%%%%%%%%%%%%%%% (8) noise filtering
sl=0.5;             % (0.5m or 1.640ft default) minimum length of line
stripeWidth=0.1;    % (0.1m or 0.328ft default) maximum width of line
p_value=0.05;       % (5% default) p-value to determine unimodality

%%%%%%%%%%%%%%%%% (9) retro evaluation
SW_length=0.20;     % (0.2m or 0.656ft default) Search window parameters
SW_width=0.045;     % (0.045m or 0.148ft default) Search window parameters
SW_minNPts=5;       % (5 default) Search window parameters
Interval=0.5;       % (0.5m or 1.640ft default)  Search window parameters
COEFF_1=1.19261;    % (1.19261 default) power function coefficient1
COEFF_2=373.28;     % (373.28 default) power function coefficient2
percentile=0.1;     % (10% default) percentile of intensity value use for power function
```

*Note that the advanced parameters are in metric units. For convenience, the default values are converted to feet in the comment portion of the parameter file. The program itself and the GUIs can work in either metric or US customary units depending on user preference.

APPENDIX B – ARCGIS PYTHON SCRIPTS

Note: This appendix contains 3 scripts: *csv2gdb.py, stripeeditor.py, and retrograder.py*. For clarity of readability in this appendix, a "…" has been inserted anywhere where the line is too long to fit on a single line in this document. These should be removed as well as the extra line break and extra spacing prior to using the code. Supplemental files have been delivered to Oregon DOT that do not require this editing.

csv2gdb.py

```
#Author: Joe Greenwood, Michael Olsen, Michael Bunn
#Funding Source: Oregon Department of Transportation SPR 799
#This program inputs the csv files from RoME, converts csv to feature class, creates point
feature classes, creates line feature classes

# Import system modules
import arcpy
import os
arcpy.env.overwriteOutput = True

#This function creates a feature class (out_fc) from an input table with its x,y,z field names.
#It also inputs the appropriate spatial reference.
def xy_table_to_fc(table, x, y, z, spatref, out_fc):
        lyr = str(arcpy.management.MakeXYEventLayer(table, x, y, "temp", spatref, …
                z).getOutput(0))
        arcpy.management.CopyFeatures(lyr, out_fc)
        #arcpy.Delete_management(table)

#This function determines the index of a field from its name.
def findindex(table,fieldname):
        return [i.name for i in arcpy.ListFields(table)].index(fieldname)

#set parameter 0 as a folder: "Input Folder with CSV files"
arcpy.env.workspace = arcpy.GetParameterAsText(0)
#set parameter 1 as a folder: "Outputfolder for Geodatabase"
OutLoc = arcpy.GetParameterAsText(1)
#set parameter 2 as Output Geodatabase Name: "Geodatabase name"
out_name = arcpy.GetParameterAsText(2)
#set parameter 3 as Spatial Reference: "Spatial Reference"
SpatRef = arcpy.GetParameterAsText(3)

#Set variables
dataBasePath = OutLoc + "/" + out_name + ".gdb"
stripeTable = ""
node_FC = ""

#Check to see if database exists, if not, create it!
if arcpy.Exists(dataBasePath) == 0:
        arcpy.CreateFileGDB_management(OutLoc, out_name)

# Execute TableToTable, create point layer files, create point to lines
for csv_file in arcpy.ListFiles("*.csv"):
        arcpy.AddMessage("Processing: " + csv_file)
        inTable = os.path.basename(csv_file)
```

```
        outTable = os.path.splitext(inTable)[0]
        arcpy.TableToTable_conversion(inTable, dataBasePath, outTable)
        fields = arcpy.ListFields(dataBasePath + "/" + outTable)
        field_names = []
        for field in fields:
                field_names.append(field.name)
        arcpy.AddMessage(field_names)
        if ("X" in field_names) & ("Y" in field_names) & ("Z" in field_names):
                #arcpy.env.workspace = dataBasePath
                out_FC = outTable + "_Points"
                xy_table_to_fc(dataBasePath + "/" + outTable, "X", "Y", "Z", SpatRef,     …
                                dataBasePath + "/" + out_FC)
                arcpy.AddMessage("Imported "+arcpy.GetCount_management(dataBasePath+ …
                                        "/" + out_FC).getOutput(0) + " features from " + inTable)
                arcpy.Delete_management(dataBasePath + "/" + outTable)

                if ("NodeID" in field_names):
                        node_FC = out_FC
                        arcpy.AddMessage("nodeFC = " + node_FC)

        if ("HWYNumber" in field_names):
                run_FC = outTable
                arcpy.AddMessage("run_FC = " + run_FC)

        if ("trajMidX" in field_names) & ("trajMidY" in field_names):
                #arcpy.env.workspace = dataBasePath
                section_FC = outTable + "_points"
                xy_table_to_fc(dataBasePath + "/" + outTable, "trajMidX", "TrajMidY", "", …
                                SpatRef, dataBasePath + "/" + section_FC)
                arcpy.Delete_management(dataBasePath + "/" + outTable)

        if ("Material" in field_names) & ("Color" in field_names):
                stripeTable =  outTable

# Creates lines from Node Table
# Joins the Stripe Table with the new Stripe FC.  Deletes the extra stripe ID Field from the join.
# Deletes the unnecessary tables
arcpy.env.workspace = dataBasePath
line_FC = stripeTable + "_lines"
traj_FC = run_FC + "_traj"
arcpy.PointsToLine_management(dataBasePath + "/" + node_FC, dataBasePath + "/" + …
                                        line_FC, "StripeID")
arcpy.JoinField_management(dataBasePath + "/" + line_FC, "StripeID", dataBasePath + "/" + …
                                stripeTable, "StripeID")
arcpy.DeleteField_management(dataBasePath + "/" + line_FC, "StripeID" + "_1")
arcpy.Delete_management(dataBasePath + "/" + stripeTable)
```

```
arcpy.PointsToLine_management(dataBasePath + "/" + section_FC, dataBasePath + "/" + …
                                                    traj_FC , "RunID", "SectionID")
arcpy.JoinField_management(dataBasePath + "/" +traj_FC, "RunID", dataBasePath + "/" +  …
                                                  run_FC, "RunID")
arcpy.DeleteField_management(dataBasePath + "/" + line_FC, "RunID" + "_1")
arcpy.Delete_management(dataBasePath + "/" + run_FC)
```

stripeeditor.py

```
#Authors: Michael Olsen, Joe Greenwood, Ezra Che
#Funding Source: Oregon Department of Transportation SPR 799
#This script modifies the color values of the stripe based on lines that are
#close to lines in a feature class that represent yellow markings.
#It also can filter out transverse markings, if desired.
#
# Import system modules
import arcpy
import os
arcpy.env.overwriteOutput = True

# Get product name
Arcpy_Info = arcpy.GetInstallInfo()

if Arcpy_Info['ProductName'] == u'Desktop':
        EXP_TYPE = "PYTHON_9.3"
elif Arcpy_Info['ProductName'] == u'ArcGISPro':
        EXP_TYPE = "PYTHON3"
else:
        arcpy.AddMessage("Failed to detect the product name!")


#INPUTS
# Set the workspace (to avoid having to type in the full path to the data every time)
stripeFC = arcpy.GetParameterAsText(0) #feature class
yellowFC = arcpy.GetParameterAsText(1)#feature class
yellowTOL = arcpy.GetParameterAsText(2)#string set default value to "3.0 Feet"
deleteTstripes = arcpy.GetParameterAsText(3) #boolean - set default value to True

#Create FileNames
stripeFC_Tfil = os.path.basename(stripeFC) + "_Tfil"

GDBpath = os.path.dirname(stripeFC);
arcpy.AddMessage(GDBpath)
arcpy.env.workspace = GDBpath

#Select stripes within threshold distance from yellow lines and change color field to yellow
stripeFClyr = stripeFC + "_lyr"
arcpy.MakeFeatureLayer_management(stripeFC, stripeFClyr)

arcpy.AddMessage("Coloring Stripes within " + yellowTOL + " of Yellow Lines")
arcpy.SelectLayerByLocation_management (stripeFClyr, "WITHIN_A_DISTANCE",  …
                                        yellowFC, yellowTOL, "NEW_SELECTION", "NOT_INVERT")
arcpy.CalculateField_management(stripeFClyr, "Color", "'Yellow'")
```

```
#Select stripes farther than threshold distance from yellow lines and change color to white
arcpy.AddMessage("Coloring all others white")
arcpy.SelectLayerByLocation_management (stripeFClyr, "WITHIN_A_DISTANCE",  …
                                        yellowFC, yellowTOL, "NEW_SELECTION", "INVERT")
arcpy.CalculateField_management(stripeFClyr, "Color", "'White'")

#Cleanup of tranverse stripes, if selected.
if deleteTstripes:
    arcpy.AddMessage("Removing Transverse Stripes")
    Tquery = "StripeType = 'L'"
    arcpy.FeatureClassToFeatureClass_conversion(stripeFC, GDBpath, stripeFC_Tfil, Tquery)
```

retrograder.py

```
#Authors: Michael Olsen, Joe Greenwood, Michael Bunn
#Funding Source: Oregon Department of Transportation SPR 799
#This program calculates retroreflectivity condition scores per MP section.
#Meant to work with Tenths MP layer from TransGIS by Oregon DOT but could be used with
other milepost layers.
#Requires a field "MP" with the MilePost numbers.  Connects them based on the milepost order.
# Import system modules
import arcpy
import os
arcpy.env.overwriteOutput = True

#CHANGE DEPENDING ON THE ARCGIS VERSION (ARCGIS 10+ = "PYTHON_9.3",
ArcGIS Pro = PYTHON3 but can use 9.3
EXP_TYPE = "PYTHON_9.3"

#INPUTS
# Set the workspace (to avoid having to type in the full path to the data every time)
stripeFC = arcpy.GetParameterAsText(0) #feature class
runFC = arcpy.GetParameterAsText(1)#feature class
ODOTtenthmileFC = arcpy.GetParameterAsText(2) #feature class
LRSKeyFilter = arcpy.GetParameterAsText(3)  #string, make optional
tenthmileRetroFCname = arcpy.GetParameterAsText(4) #string output name
spatRef = arcpy.GetParameterAsText(5) #spatial Reference - optional
bufferDist = arcpy.GetParameterAsText(6) #string - set default value to 30 m or 100 Feet
deleteTempFiles = arcpy.GetParameterAsText(7) #boolean - set default value to True

GDBpath = os.path.dirname(stripeFC);
arcpy.AddMessage(GDBpath)
arcpy.env.workspace = GDBpath
tenthmileRetroFC = GDBpath +"/" + tenthmileRetroFCname

#python code blocks for reclassification of fields based on values.
codeblock = """
def RetroGrade(color, retroval):
   if color == 'Yellow':
      if (retroval >250):
         return 'A'
      elif (retroval>200):
         return 'B'
      elif (retroval>125):
         return 'C'
      elif (retroval>100):
         return 'D'
      elif (retroval>50):
```

```
            return 'E'
        elif (retroval >0):
            return 'F'
        else:
            return 'Z'
    else:
        if (retroval >350):
            return 'A'
        elif (retroval>250):
            return 'B'
        elif (retroval>150):
            return 'C'
        elif (retroval>100):
            return 'D'
        elif (retroval>50):
            return 'E'
        elif (retroval >0):
            return 'F'
        else:
            return 'Z"""'

gradetonum = """
def RetroGradetoNum(grade):
    if grade == 'A':
        return 5
    elif grade == 'B':
        return 4
    elif grade == 'C':
        return 3
    elif grade == 'D':
        return 2
    elif grade == 'E':
        return 1
    elif grade == 'F':
        return 0
    else:
        return """

numtograde = """
def RetroNumtoGrade(num):
    if num > 4.5:
        return  'A'
    elif num > 3.5:
        return 'B'
    elif num > 2.5:
        return 'C'
```

```
    elif num > 1.5:
        return 'D'
    elif num > 0.5:
        return 'E'
    elif num > -0.5:
        return 'F'
    else:
        return 'Z'"""

#Calculate Condition Scores for each stripe
expression = "RetroGrade(!Color!, !RetroMedian!)"
arcpy.CalculateField_management(stripeFC, "ConditionScore", expression, EXP_TYPE,
codeblock)
fields = arcpy.ListFields(stripeFC, "ConScoreCode")
if len(fields) != 1:
        arcpy.AddField_management(stripeFC, "ConScoreCode","SHORT")
expression2 = "RetroGradetoNum(!ConditionScore!)"
arcpy.CalculateField_management(stripeFC, "ConScoreCode", expression2, "PYTHON3", …
                                        gradetonum)

# Process: Buffer all retro single points by input distance
bufferOutputFC = runFC + "_buff"
arcpy.Buffer_analysis(runFC, bufferOutputFC, bufferDist,"", "ROUND")

# Create names for temporary output layers
MPclip_PointsFC = runFC + "_MP_pts"
MPclipLRS_PointsFC = "MP_LRS_pts"
MPclipLRSRP_PointsFC = "MP_LRS_RPRJ_pts"
MPclip_LineFC = runFC + "_MP_line"
MPclip_LinkFC = runFC + "_MP_link"
MPclip_StartNodeFC = runFC + "_MP_linesSN"
MPclip_MidNodeFC = runFC + "_MP_linesMidPt"
MPclip_Lines_BuffFC = tenthmileRetroFC + "_buff"
MPclip_StripesinBuff_FC = stripeFC + "_MP"
MP_clipLines_ThePoly = tenthmileRetroFC + "_ThPoly"
#create summary statistic table
MPclip_gradesTBL = runFC + "_MP_grades"

arcpy.AddMessage("Clipping and filtering the milepost layer")
# Process: Clip the milepost feature class to the run trajectory
arcpy.Clip_analysis(ODOTtenthmileFC, bufferOutputFC, MPclip_PointsFC)

LRSquery = ""
if LRSKeyFilter != "":
      LRSquery = "LRS_KEY = '" + LRSKeyFilter + "'"
arcpy.FeatureClassToFeatureClass_conversion(MPclip_PointsFC, GDBpath, …
```

```
                                                MPclipLRS_PointsFC, LRSquery)

#REPROJECT data if desired.
if spatRef != "":
      arcpy.AddMessage("Reprojecting MP data")
      arcpy.Project_management(MPclipLRS_PointsFC, MPclipLRSRP_PointsFC, spatRef)
else:
      MPclipLRSRP_PointsFC = MPclipLRS_PointsFC

arcpy.AddMessage("Generating lines between mileposts")
arcpy.PointsToLine_management(MPclipLRSRP_PointsFC, MPclip_LineFC,"","MP")
arcpy.SplitLine_management(MPclip_LineFC, tenthmileRetroFC)
arcpy.FeatureVerticesToPoints_management (tenthmileRetroFC, MPclip_StartNodeFC, …
                                                "START")
arcpy.Intersect_analysis ([MPclip_StartNodeFC, MPclipLRS_PointsFC], MPclip_LinkFC, …
                          "ALL", "1 Meters")
arcpy.JoinField_management(tenthmileRetroFC, "ObjectID", MPclip_LinkFC, "ORIG_FID")

arcpy.AddMessage("Finding stripes within each zone")
#uses Thessien polygons for the mid point of each MP segment.
arcpy.FeatureVerticesToPoints_management (tenthmileRetroFC, MPclip_MidNodeFC, "MID")
arcpy.CreateThiessenPolygons_analysis (MPclip_MidNodeFC, MP_clipLines_ThePoly, "ALL")
arcpy.Intersect_analysis ([stripeFC, MP_clipLines_ThePoly], MPclip_StripesinBuff_FC, "")

arcpy.AddMessage("Computing Condition Score Statistics for each zone")
#compute summary statistics of retro grade for each section.
summaryField = ["ORIG_FID"]
summaryStatistics = [["ConScoreCode", "MEAN"]]
arcpy.Statistics_analysis (MPclip_StripesinBuff_FC, MPclip_gradesTBL, summaryStatistics, …
                          summaryField)

#Update outputFC with condition score
fields2 = arcpy.ListFields(MPclip_gradesTBL, "ConditionScore")
if len(fields2) != 1:
         arcpy.AddField_management(MPclip_gradesTBL, "ConditionScore","TEXT", "", "", …
                                                1, "", "NULLABLE")
expression3 = "RetroNumtoGrade(!MEAN_ConScoreCode!)"
arcpy.CalculateField_management(MPclip_gradesTBL, "ConditionScore", expression3, …
                                              "PYTHON3", numtograde)
arcpy.JoinField_management(tenthmileRetroFC, "ObjectID", MPclip_gradesTBL,"ORIG_FID")

#cleanup
if deleteTempFiles == "true":
      arcpy.AddMessage("Cleanup of temporary files")
      arcpy.Delete_management(MPclip_PointsFC)
      arcpy.Delete_management(MPclipLRS_PointsFC)
```

```
arcpy.Delete_management(MPclip_LineFC)
arcpy.Delete_management(MPclip_LinkFC)
arcpy.Delete_management(MPclip_StartNodeFC)
arcpy.Delete_management(MPclip_Lines_BuffFC)
arcpy.Delete_management(MPclip_StripesinBuff_FC)
arcpy.Delete_management(bufferOutputFC)
arcpy.Delete_management(MPclipLRSRP_PointsFC)
arcpy.Delete_management(MP_clipLines_ThePoly)
arcpy.Delete_management(MPclip_MidNodeFC)
```